UNIVERSITY OF SOUTHAMPTON

FACULTY OF ENGINEERING, SCIENCE & MATHEMATICS

School of Civil Engineering and the Environment

PROTECTIVE DESIGN AGAINST DISPROPORTIONATE COLLAPSE OF RC AND STEEL FRAMED BUILDINGS

by

Sakthivel Paramasivam

A thesis submitted in fulfilment of the degree of Doctor of Philosophy in the School of Civil Engineering and the Environment of the University of Southampton

December 2008

ABSTRACT

To avoid disproportionate collapses in steel framed buildings the British standards provide the tying force method. This work investigates the reliability of this method for redistributing loads away from damaged columns and the results indicate that the factor of safety against collapse is less than 0.2 if low ductility nominally pinned connections are used. This is shown to be as a result of industry standard nominally pinned joints possessing the ductility required to redistribute column loads using catenary action. A simple method has been used to estimate this factor of safety; it is unlikely that a more complex analysis would change the overall conclusion. This work then move on to estimate the likelihood of column fracture due to blast loading from high explosives. The column response to this loading is then analysed using both single degree of freedom (SDOF) and multi-degree of freedom solutions to the equations of motion. Response charts were developed considering both systems and then compared. The deflection and bending moment obtained using SDOF system are comparable with those from MDOF models. However, the SDOF system is shown to significantly underestimate shear force when the ratio of the duration of blast load to the natural vibration period is less than 0.1 ($T_d/T_n<0.1$). It is concluded that the design shear force should be increased by 50% if SDOF system predictions of behaviour are used. A method for simplifying the blast loading on columns with clearing is developed. The method provides a simplification of the complex blast load profile in case of clearing whereby the same reflected pressure is adopted but the time duration load is adjusted to give an equivalent impulse. The simplification is assessed using a parametric study which showed that the results provide a conservatism of less than 10%. This technique for estimating column response to blast loading is compared against the real life behaviour as observed from the forensic investigation of the Murrah Building. The blast analysis predicts two columns to fail in shear and an existing method presented by McVay predicts a third column failure in brisance. This failure modes correspond to those found in the forensic investigation. The Murrah building was subsequently reanalysed by replacing the transfer girders with a conventional beam column arrangement and the blast analysis suggests that a substantial progressive failure would still have occurred because of widespread column shear and brisance failures. Thus is was concluded that even if the Murrah Building had been as per GSA guidelines for federal buildings which were revised following the Murrah event, it could not have survived. Subsequently, the methodology to estimate the safe stand off distance for a particular RC column and a charge weight is proposed and the design charts are prepared through nonlinear regression analysis. The safe scaled distance of 2.0 m/kg$^{1/3}$ is estimated for the Murrah Building. The recommendation suggested by US DoD (4.46 m/kg$^{1/3}$) is much higher than the actual value.

Keywords: blast load, disproportionate collapse, dynamic analysis, protective design, safe stand off distance

Contents

List of Figures

List of Tables

Nomenclature

A, B, C and D – integration constant

A_c - Area of concrete section

A_n - Amplitude of n^{th} mode

A_s - Area of tension reinforcement

A_v - Total cross-sectional area of lateral ties at a section

B - Breadth of column

D - Depth of column

d - Diameter of shear studs, Effective depth

E - Modulus of elasticity of concrete

f_{ck} - Characteristic compressive strength of concrete

f_y - Yield stress of steel reinforcement

f_{yv} -Yield stress of lateral ties

g_k - Self-weight of the structure

H - Horizontal reactions

h - Span

I - Moment of inertia about bending axis

I_c - Cracked moment of inertia

I_{eff} - Effective moment of inertia

I_g - Gross moment of inertia

I_t - Moment of inertia of transformed section

K_e - Stiffness factor for SDOF system

K - Flexural stiffness of column

K_L - Load factor for SDOF system

K_m - Mass factor for SDOF system, Flexural strength factor

K_s - Shear strength factor

L - Length of column

m - Mass of column per metre

M_{max} - Maximum bending moment at mid span of column

M - Ultimate moment capacity of column section.

M_e - Equivalent mass of SDOF system

M_n - Ultimate moment capacity at mid span region

M_p - Ultimate moment capacity at support

N - Number of shear studs used to connect an edge of profiled sheet/m

N - Applied axial load

n - Mode number

P_{oA} - Incident pressure on the front face

P_{oB} - Incident pressure on the rear face

P_{rA} - Reflected pressure on the front face

P - Peak blast load and total load on column

$P[t]$ - Blast load on column per metre length at time, 't'

p_b - Bearing strength of profiled sheet

$P_e[t]$ - Equivalent blast load of SDOF system

p_r - Reflected pressure

p_s - Static over pressure

P_{up} - Upward reactive force caused by slab tying capacity per metre

q_A - Dynamic pressure on the front face;

$q[t]$ - Time function

q - UDL acting directly onto the beam

Q_{CE} - Expected ultimate, un-factored capacity of the component or connection/joint

q_k - Live load of the structure

q_s - Dynamic pressure

Q_{UD} - Acting force (demand) determined in the component or connection/joint

$r(x)$ - Resistance function

r_u - Ultimate resistance

S - Clearing distance, equal to half the width of the face which experience the blast pressure

s_v - Spacing of lateral ties along the member

S_{max} - Maximum shear force at support of column

SSD_{chart} - Safe stand off distance of a column considering length of 3 m, concrete strength of 25 N/mm^2, shear strength factor of 0.4, flexural strength factor of 0.2, gross moment of inertia and a charge weight of 1000 kg

t_c - Clearing time for the front face

t_{dA} - Duration of incident pressure on the front face

t_{dB} - Duration of incident pressure on the rear face;

t_r - Rising time for the rear face

t - Thickness of profiled sheet.

T - Tying force

t_d - Duration of blast load

T_{slab} - Tying capacity of slab

U_A - Blast wave front velocity for the front face

U_B - Blast wave front velocity for the rear face

u_{max} - Maximum displacement at mid span of column

u - Displacement

V - Vertical reactions, Shear force

V_c - Shear strength offered by concrete

v_c - Design concrete shear stress

V_s - Shear strength offered by lateral ties

V_u - Ultimate shear strength of column section

w - Uniformly distributed load on column

W_1 - Reaction from the secondary beam

W_2 - Reaction from the main beam plus the weight of column for that storey

w_k - Design lateral wind load

x_e - Elastic displacement

x_{eq} - Equivalent stiffness of elasto plastic system

x_u - Total displacement

Y_o - Maximum displacement at time, 't'

$\alpha_1, \alpha_2, \alpha_3$ and α_4 - - Modification factor for charge weight

α_d - Deflection coefficient

α_f - Modification factor for concrete strength

α_i - - Modification factor for moment of inertia

α_L - - Modification factor for length of the column

α_m - - Modification factor for flexural strength

α_m - Bending moment coefficient

α_s - - Modification factor for shear strength

α_s - Shear force coefficient

α_w - Modification factor for charge weight

γ - Unit weight of concrete

ρ_s - Density of air molecules

ω_n - Natural frequency of n^{th} mode

ω - Natural frequency of the column

$\phi_n[x]$ - Spatial function of mode shape

Acknowledgements

I have benefited greatly from the advice and guidance of my supervisor, Dr. Mike Byfield. I am very grateful to Mike for his love and kindness on me. I would like to express my thanks to the school of Civil Engineering and the Environment at the University of Southampton that provided the studentship for pursuing this research. I would also like to express my gratitude to other members of staff in school of civil engineering, especially Dr. A. C. Lock, Mrs. Jacqui Holmes and Mrs. Barbara Hudson. I would like to thank my friends Ram, Chandra, Arun, Tesmi, and Praveen for their help in various ways. I would like to acknowledge all my colleagues. Finally, I would like to express my sincere gratitude to my wife, mother, father and brother, especially my wife as she supported and motivated me all along the way.

Chapter 1

Introduction

1.1. Introduction

In recent years commercial and government office buildings have an increased risk of experiencing abnormal loads from blast or impact. Large amount of explosives can be exploded at close range, sometimes with the use of suicide bombers. As a result the building can be subjected to huge pressures, which leads to the possible failure of one or more primary load bearing elements. The loss of the elements can cause either major structural instability and/or over load the adjacent members, resulting in a chain reaction of failure of building members to an extent disproportionate to the original localized damage. This is called as disproportionate collapse. Unlike other abnormal loads, such as earthquake loads which can lead to the global failure of the building, the blast load causes localized damage as the blast pressure attenuates with the cube root of the distance.

This chapter reviews some relevant historical cases studies of disproportionate collapses and moves on to introduce the main design methods available to mitigate the effects of localised damage. Finally, the aims and objectives of this dissertation are presented.

1.2. Disproportionate collapse

In the UK high-rise steel framed buildings are designed with low-cost simple joints such as fin plate, flexible end plate and double angle web cleat connections, as the country is subjected to neither extreme wind loads nor seismic activity. However, these structures can be relatively fragile, compared with those designed to survive

extreme loads such as typhoons and earthquakes. This fragility was famously demonstrated at Ronan Point, when a domestic gas explosion knocked out load bearing pre-cast concrete panels near the corner of the 18th floor of the tower block, leading to the now famous collapse. During the subsequent forensic investigation it was estimated that the peak over pressure from the gas explosion was 34kN/m^2 and this led to the requirement for all members key to stability to resist this statically applied load. The post Ronan Point revision to the Building Regulations also required all floor members to be effectively tied together in order to enhance robustness. In practice this means providing beam connections with a tensile strength at least equal to the design shear strength – a method known as the tie force method for ensuring robustness.

The Murrah Federal Office Building in Oklahoma City was damaged by a bomb in April 1995. In this incident the direct blast pressure destroyed one column by brisance and another two by shear. The loss of these three columns led to a collapse that consumed ½ of the floor area of this nine storey building. This apparently strong building typifies modern office developments, in that it was glazed and used open plan architecture. Although it was correctly designed to the code requirements of that time it was unable to redistribute the column loads. Lacking the strong internal partition walls or cladding, the building had no emergency means for redistributing loads.

More recently were the attacks on the World Trade Centre. Both towers remained globally stable immediately after the impacts, despite the severing of up to 36 perimeter columns in the face of each tower. The towers were highly redundant, comprising a rigid perimeter frame and a gravity load bearing central core, together with a system of deep outrigger (hat) trusses installed between the 106th and 110th floors. The gravity loads from the damaged perimeter columns were partially transferred to adjacent undamaged columns via vierendeel action, see Fig. 1.1. In addition, perimeter columns were also believed to have become suspended from these outrigger trusses. Fire damage eventually led to the complete collapse of both towers.

1.3. Design methodologies

The risk of progressive collapse can be reduced in three ways: the safe stand off distance approach, indirect design, and direct design. In safe stand off distance approach, the structure is designed to resist a given threat for a given stand off distance. In case of indirect design, the load, carried by the removed load bearing elements are redistributed through the structure through minimum strength, continuity and ductility. In direct design, the safety of the building is ensured by two methods: the specific local resistance method and the alternate load path method. The alternate load paths could be achieved for example through: arching, beam and catenary actions in the frame system and out-trigger trusses installed in higher floors.

During arching action, the accidental load from the removed column is transferred to the adjacent columns through compression struts which may be formed in the beam webs either side of the damaged column; see Fig. 1.2(a). Such a mechanism is possible but only for very short span beams. In the case of infilled steel frames, load can be transferred by a compression strut formed in the masonry infill as shown in Fig. 1.2(b). This approach is restricted by US practise (DoD, 2005), because if the infill walls do not fully connect the frame members, diagonal compression strut action will not develop. Furthermore, the debris created by these infilled walls can endanger lives, for example in the Oklahoma City bombing several persons lost their lives after being struck by structural debris generated by infill walls of a concrete frame building in the Water Resources Building across the street from the Murrah building (FEMA 427, 2003). US practice recommends double span beam action in which the load is transferred through bending as shown in Fig. 1.2(c). It also suggests an accidental load of dead load plus 25% of imposed load, with a dynamic amplification factor of 2 (GSA, 2003). This method can be expensive as full moment joints are required.

The catenary action mechanism upon which the tying method relies (indirect design) is illustrated in Fig. 1.2(d). This method was introduced into the UK regulations after the Ronan Point collapse and it has subsequently been incorporated in a modified form into the Eurocodes. In this approach, all floor members are required to be effectively tied together. The tying force approach assumes the accidental load, at the time of damage, is equal to $1/3^{rd}$ of the imposed load plus 1.05 of the dead load.

When support to a column is removed, adjacent beams on either side support the accidental load through catenary action.

In case of the removal of internal columns, the force equilibrium can be maintained by the radial tensile and compressive forces, created as a result of the dishing action, and compressive hoop stress as shown in Fig 1.2(e).

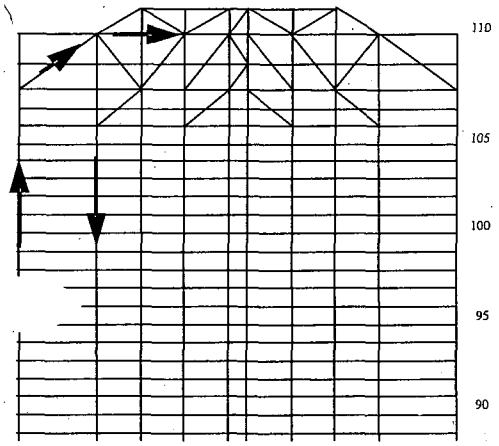

Fig. 1. 1 Example of an alternative load path route in WTC1

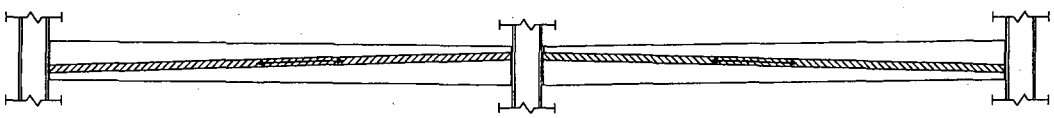

(a) Arching action in steel beam

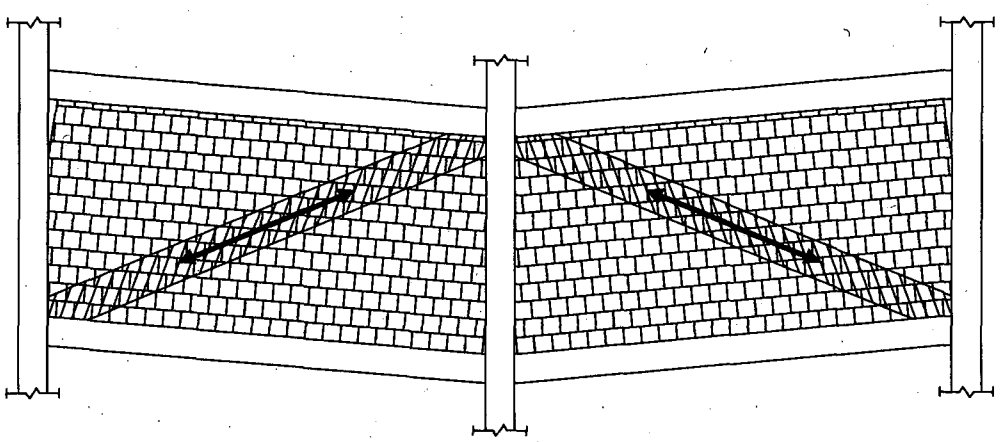

(b) Arching action in masonry panels

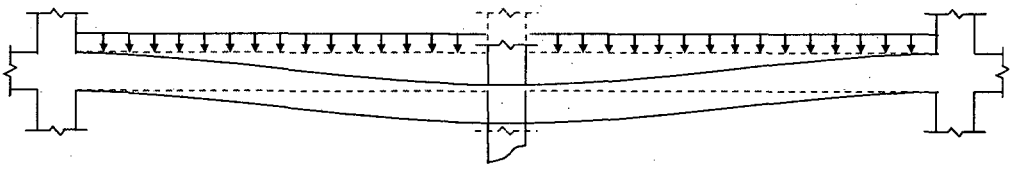

(c) Double span beam action

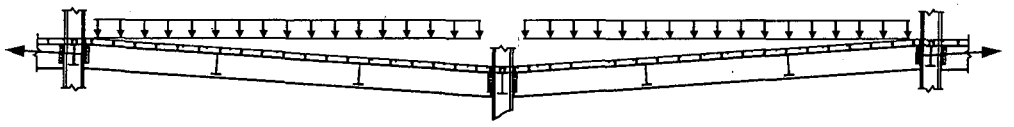

(d) Catenary action

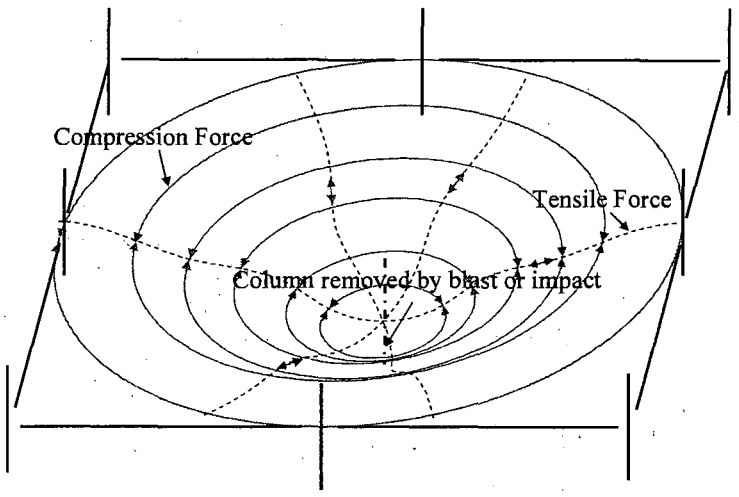

(e) Diaphragm action

Fig. 1. 2 Mechanism of transferring the accidental load

1.4. Observations of the behaviour of damaged structures

During WWII, the general purpose bombs, typically weighing between 50 and 250 kg were dropped on London (weights inclusive of shell casing). These charge sizes are smaller than those often by terrorist organisation with the vehicle borne improvised explosive device. Such device can deliver a charge equivalent ranging from 100 kg up to over 2000 kg of TNT using home made explosives. Despite this, the behaviour of multi-storey buildings subjected to blast during that time is of interest because such a large number of events were documented and available for inspection in archives such as the Walley Collection, which is housed in the archive section of the Institution of Civil Engineers Library.

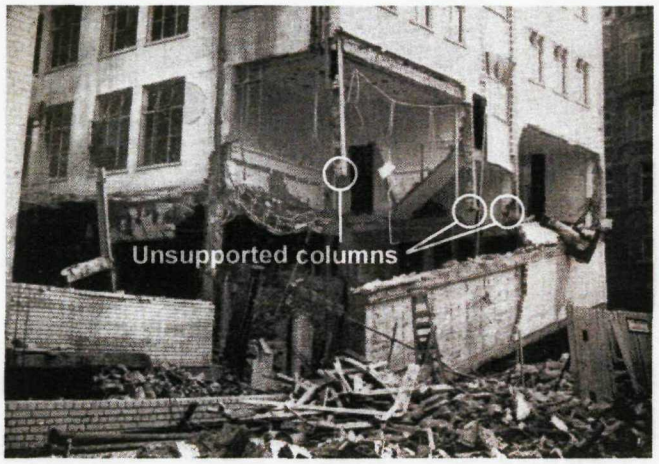

Fig. 1. 3 Bracing from panel walling (Baker, 1948)

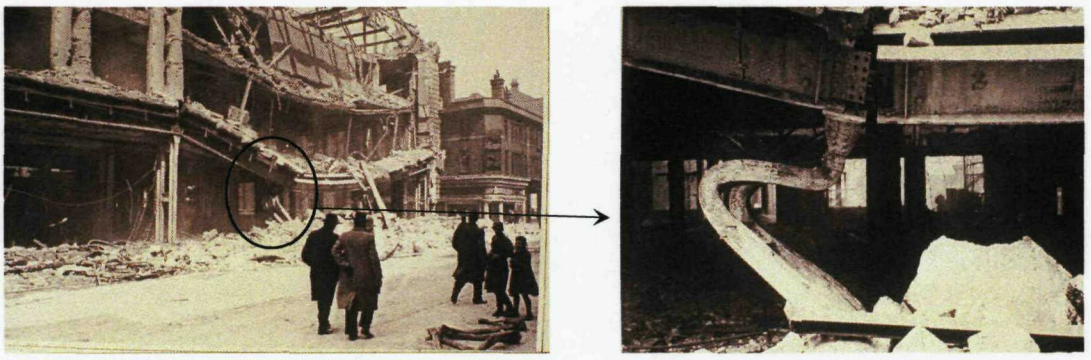

Fig. 1. 4 Building illustrating the failure of catenary action in resisting the load following a bomb attack together with column ductility and connection failure, (Gibbons, 2003)

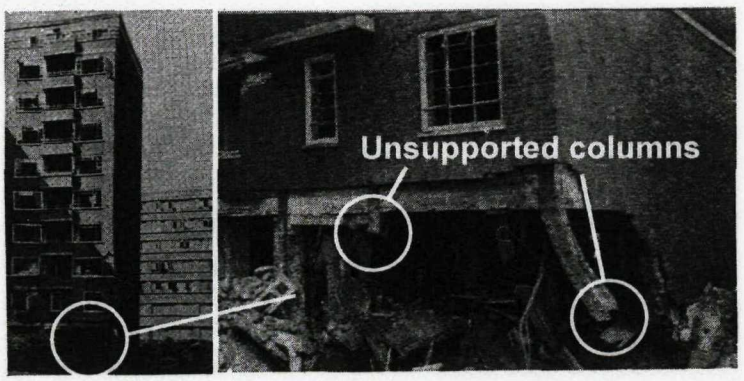

Fig. 1. 5 Bracing from panel walling (Baker, 1948)

The behaviour of building shown in Fig. 1.4 seems to indicate tying mechanism in which the accidental load is transferred through catenary action, but the inspection of records has not revealed any possibility of catenary action as the fracture can be seen at the joint. However, the collapse was prevented by massive deformation of the column. Another interesting response of the building during that time is shown in Fig. 1.3 (Baker, 1948), in which an entire perimeter wall remains apparently unsupported due to the unseating of the main girder. Another good example of the behaviour of buildings is shown in Fig. 1.5 (Baker, 1948). This shows a 10 storey building which seems to have no difficulty in redistributing loads from two damaged corner columns.

Progressive collapse in these buildings was prevented by the shear strength of the 4½ inch and 9 inch thick masonry walling and cladding. Investigators concluded that these panels were primarily responsible for preventing progressive collapses during that time, J.F. Baker (1948). Importantly, glass cladding modern office buildings lack these alternative load paths, and it is perhaps for this reason that the Murrah Building collapsed with the loss of 168 lives. This apparently strong building typifies modern office developments in that it was glazed and used open plan architecture. Although it was correctly designed to the requirements of that time, it lacked strong internal partition walls and it was fully glazed along the front face. Unlike the WWII buildings described, it possessed no emergency means for redistributing loads and lost half of the floor area of the building following damage to three perimeter columns.

Many buildings in the UK lack both of these emergency load paths. Vierendeel action cannot be expected to play a significant stabilising role because beam-column connections are usually nominally pinned, with the low cost fin-plate connection proving particularly popular. Outrigger trusses are also not incorporated and market considerations in office buildings require that the number of columns be kept to a minimum. In these conditions heavy reliance is placed on catenary action to support widely spaced columns.

1.5. Aim, objective and scope of this research

Aim:

1. To study the feasibility of tying approach in the preventive design of steel frame building against disproportionate collapse.

2. To develop response charts for a column, subjected to blast load, based on single degree of freedom (SDOF) and multi degree of freedom (MDOF) systems and explore the exactness of the SDOF system response, as the higher modes significantly contribute in the shear response (because of the short duration of blast load).

3. To estimate blast load on the column and carry out the case study on the Murrah building incidents, considering with and without transfer girder.

4. To develop design charts for preventive design of RC framed building against blast using a safe stand off distance approach.

In this research, multi-storey commercial or office buildings with glass cladding and open plan architect are considered. This form of building is considered because alternative load paths from masonry walls and or cladding are not available. Therefore emergency load paths in the frame must be utilised to prevent collapse of the floor area previously supported by the damaged column. This form of building is therefore relatively simple to assess the vulnerability to progressive collapse. As the blast load causes localised damage, the blast damage analysis is carried out on an idealized column which is either pinned at both ends, or fixed at both ends, or pinned at one end and fixed at other end.

Objective:

These aims are achieved through the following objectives.

1. Review previous progressive collapses and methods of mitigating such events. [Chapter 2]

A review of previous research includes the case studies on the collapses of Ronan Point, the Murrah Building and the Khobar Towers, the blast loading and the available codal recommendations to mitigate disproportionate collapse. In addition to this, a review of the behaviour of RC and steel structures, especially after the removal of column support is included.

2. Examination of the capability of the tying force method to prevent progressive collapse following loss of column support for steel framed buildings with simple connections [Chapter 3]

   A methodology is proposed to determine the factor of safety against disproportionate collapse, considering load redistribution from a damaged column through catenary action. Using this method, the safety of steel framed buildings with fin plate, double angle web cleat and flexible end plate connections are examined against disproportionate collapse.

3. Single and multi-degree of freedom dynamic analysis of columns subjected to blast loads [Chapter 4]

   A dynamic analysis for an idealized column is discussed considering both systems: an equivalent lumped mass single degree of freedom system and a distributed mass continuous system. The results obtained from both systems are compared and contrasted. Finally, the response charts are developed to obtain the deflection, shear force and bending moment coefficients for an idealized column.

4. Estimation of blast loads on columns [Chapter 5]

   A method is proposed to calculate the blast load on a column. Using this method, a case study of the Murrah building incident is carried out to examine the method as well as to understand the behaviour of building subjected to blast.

5. Development of a method for estimating the safe stand off distance for reinforced concrete columns [Chapter 6]

A method is proposed to obtain the safe stand off distance for a particular RC column and a charge weight. Design charts are developed for an idealised RC column to obtain the safe stand off distance for a given charge weight.

Chapter 2

Literature Review

2.1 Introduction

Structural behaviour under the blast loading is complex as the duration of the loading very short, often much shorter even than the natural period of vibration of the member. In the analysis, dynamic effects, material and geometric nonlinearities and instability need to be considered. Several analysis methods are developed to predict the potential against progressive collapse. The issues related to these analyses are discussed in this chapter. In addition, the protective design methods, mentioned in chapter 1, for steel and reinforced concrete structures are reviewed and presented in this chapter.

2.2 Case studies

New York's World Trade Centre (WTC) collapsed on September 11, 2001 and subsequently the Pentagon building was attacked on the same day. In these attacks almost 3,000 people were killed. The US embassy bombings in Tanzania and Kenya on August 7, 1998 killed 225 people. Prior to this, the Murrah Building collapsed following the Okalahoma City bombing in April 19, 1995 killed 168 people. Numerous investigations have been conducted and several interesting findings were reported after these attacks. In order to avoid these catastrophes in the future, it is important to study and learn from these events. Such attacks remind structural engineers of the importance of providing a minimum level of structural robustness to buildings for minimizing the number and the severity of causalities. Previous studies reveal that collapse can be lessened or be avoided by incorporating redundancy into frames that can provide multiple load paths and help transfer the loads away from damaged columns.

2.2.1 Ronan Point (Pugsley, 1968)

The 22 storey Ronan Point flats collapsed in progressive manner in 1968 due to the natural gas explosion in the 18th floor (Fig. 2.1). This explosion knocked out the corner walls of the apartment. As there was no structural support for the walls directly above, the floor 19 collapsed, then floor 20 and so on, propagating upward. The main reason for the collapse was that the walls were not tied sufficiently together and reinforced. The above floors fell onto level 18 with sudden-impact causing the collapse progressively from floor 18 to the ground. The Ronan Point Collapse led directly to the current regulations for robustness namely the tying force method and specific resistance design for the load of 34 kN/m^2.

Fig. 2. 1 Ronan Point collapse

2.2.2 The Murrah Building (FEMA-227, 1996)

The nine storey Murrah building was designed as an ordinary moment frame. Its overall dimensions were approximately 67 m in the east-west direction and 30.5 m in the north-south direction. The building consisted of ten 6.1 m bays in the east-west

direction, two 10.7 m bays in the north-south direction. Transfer girders were introduced along column line G at the third floor to enhance aesthetic and to facilitate ground floor more access (see Fig. 2.2). This girder supported intermediate columns, thereby providing 12.2 m column spacing at the ground floor. The typical floor-to-floor height was 3.96 m for the third through eight floors. There was a massive explosion in front of the building. From the produced crater size, soil condition and the carrier vehicle, the bomb size was estimated and it was equivalent to 1800 kg of TNT. The centre of the explosives was 1.4 m above the ground surface and located about 2.1 m east and 4.3 m north of column G20 (Fig. 2.3) (Mlakar, 1998).

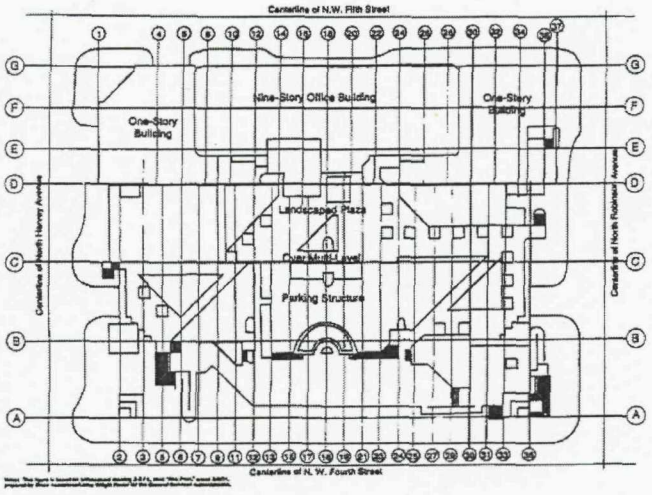

Fig. 2. 2 Site plan for Murrah Building (FEMA 227, 1996)

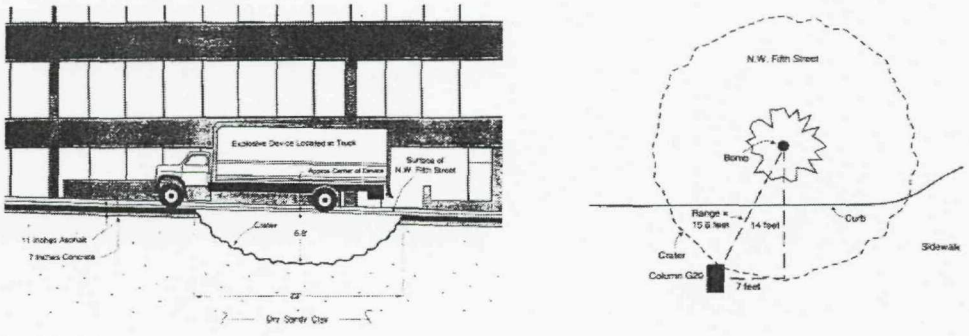

Fig. 2. 3 Location of bomb and dimensions of crater (Mlakar, 1998)

In the incident one column was destroyed by brisance and another two by shear, however because of the use of transfer girders this cause removal of support to a further 4 perimeter columns, see Fig. 2.4. It is interesting to note that even if the building were designed as per GSA guidelines, it would have been unlikely to survive in tact because GSA require the removal of only one column on either the short or long direction in the analysis for progressive collapse (Mlakar, 1998). The behaviour of this building is considered in more detail in Chapter 5.

Fig. 2. 4 The Murrah Building after collapsed (FEMA 427, 2003)

2.2.3 The Khobar Towers

Khobar Towers was a housing complex built in the Saudi Arabia in 1979 near the city of Dahran. This was essentially unoccupied until the first Gulf War in 1990. During and following the war the coalition forces occupied the Towers which comprised of a living quarters (high-rise apartments up to eight stories tall), office space and administrative facilities. The perimeter of the US, French, and British area was surrounded by a fence and a row of Jersey Barriers, Fig. 2.5. There is a parking

lot outside the northern perimeter which is adjacent to a park and a small group of houses. A terrorist truck bomb exploded outside the northern perimeter of Khobar Towers on June 25, 1996.

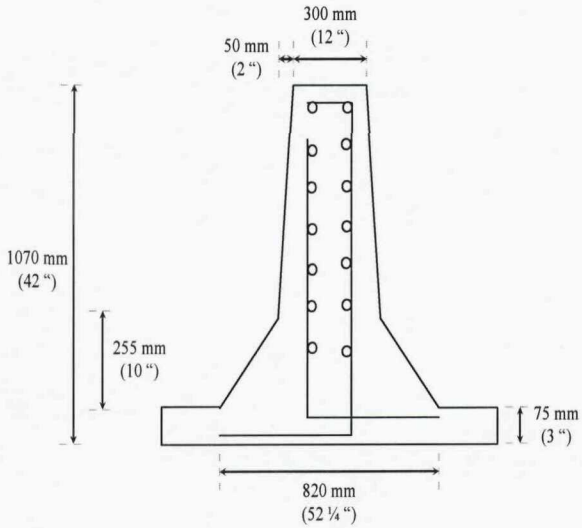

Fig. 2. 5 Typical Jersey barrier

The Defence Special Weapons Agency concluded that the truck bomb exploded with the force close to 9,000 kg (20,000 pounds) of TNT (House Armed Services Committee, 1996). There is no information publically available about the type of explosive used. The effect of an air burst was more dangerous because of the truck used formed a crude form of shape charge and the high clearance between the ground and the truck (Grant, 1998). Stand off distance of this blast was 32 m (105 feet) as shown in Fig. 2.6 (Grant, 1998).

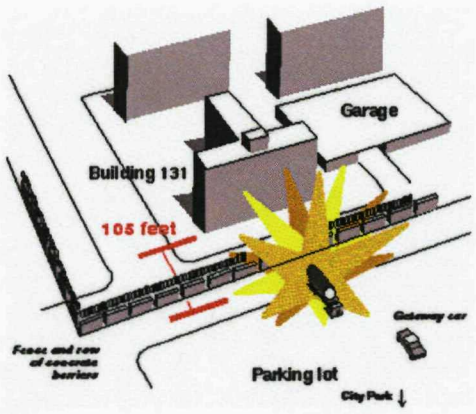

Fig. 2. 6 Truck bomb exploded on Khobar Towers (Grant, 1998)

(a) Crater resulting from the bomb (b) North face of the building

Fig. 2. 7 Khobar Tower after the blast (House Armed Services Committee, 1996)

Nineteen American service personnel were killed and more than 200 were injured along with hundreds of Saudi citizens and Third Country Nationals that were injured, although arguably the casualties were light given the scale of the attack. The blast blew out windows throughout the compound and created a crater of 26 m (85 feet) wide and 10.6 m (35 feet) deep (Fig. 2.7.a). As the blast waves hit building 131, they propelled pieces of the Jersey Barrier into the first four floors. The outer walls of the bottom floors were blown into rooms. As there was no structural support below, the facades of the top three floors sheared off as shown in Fig. 2.7.b and fell into a pile of rubble (House Armed Services Committee, 1996). The sequence of the damage in the building is shown in Fig. 2.8.

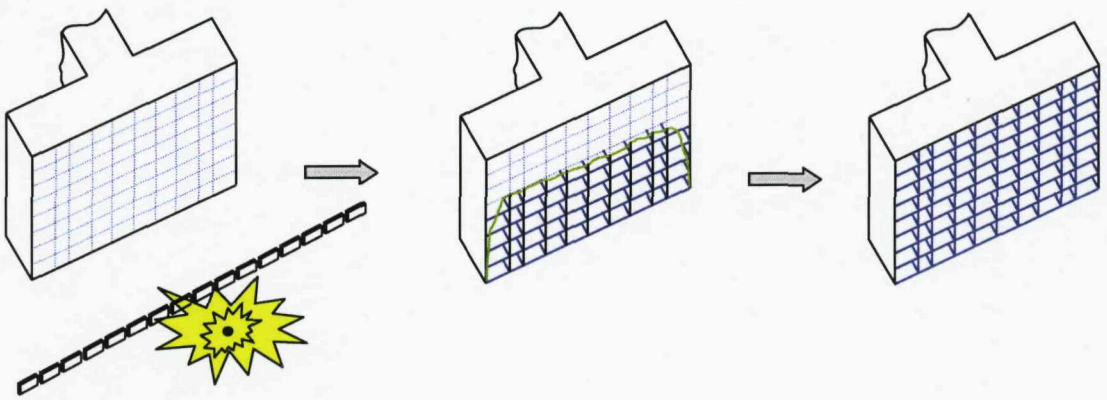

(a) (b) (c)

Fig. 2. 8 Sequence of damages in the Khobar Towers (a) Truck bomb explodes near to the northern face, (b) Jersey walls propell in to the first four floors of facade, (c) top three floors of façade are sheared off

FEMA - 427 (2003) states the reasons for the survival of buildings that 'The building was an all-precast, reinforced concrete structure with robust connections between the slabs and walls. The numerous lines of vertical support along with the ample lateral stability provided by the "egg crate" configuration of the structural system prevented collapse'. In other words, the building survived because of the closely spaced walls that provided ample alternate load paths, and the precast panels which reduced the prorogation of blast and high velocity fragmentation and reduced the loads transmitted onto connections. The building was designed to BS8110 and the minimum tying force provided is believed to have helped contribute to the robustness as it kept the precast units tied together maintaining structural integrity

2.3 Codes and standards

2.3.1 United Kingdom

The Building Regulations (2004) classify buildings into 4 categories (1, 2A, 2B and 3), see Fig. 2.9. Class 1 structures are expected to have a low risk of experiencing severe blast or impact, therefore additional measures are not required to avoid

disproportionate collapse. Class 2A, 2B and 3 structures need to be designed to prevent such a collapse. In class 2A, beams and their connections are designed as horizontal ties and anchorage of floors to walls must be ensured. Similarly, beams and their connections of Class 2B structures are designed as horizontal ties (Fig 2.10) and one of the following designs is carried out: (i) columns and their splices are designed as vertical ties, (ii) alternate load paths are ensured by considering the removal of columns, (iii) load bearing members, key to stability are designed as key elements. Class 3 structures are designed considering all the design issues given in Class 2B. In addition to this, a risk assessment on the structure needs to be undertaken for normal and abnormal hazards.

BS5950 suggest three ways to avoid disproportionate collapse: *minimum tying forces, designing as key elements or localizing the damage.* The tying approach suggests the tying capacity of the connection to be at least equal to the ULS shear force (i.e. using 1.4 dead + 1.6 imposed) or 75 kN which ever is less. It is very simple to adopt in practice and most of the industrial connections meet this requirement without any problem. It assumes that the load at the time of damage is equal to dead load plus $1/3^{rd}$ of imposed load. This assumption allows columns to redistribute the load from the removed column comfortably, as the design shear force is higher than that of accidental load. The provision did not have any scientific base (Menzies and Nethercot, 1998). To transfer the accidental load, the beam-column joints need to have sufficient rotation ductility. This approach is salient about the requirements for the joint ductility and does not consider the dynamic effect due to sudden removal of column.

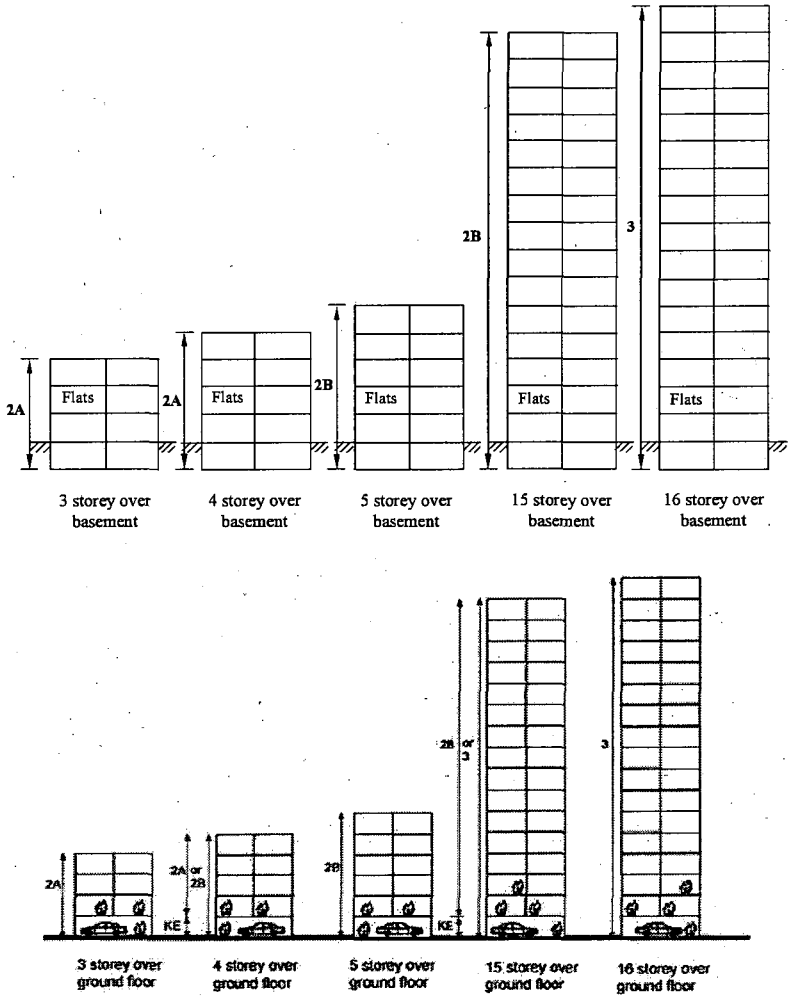

Fig. 2. 9 Classification of buildings adopted in UK (Building Regulations, 2000)

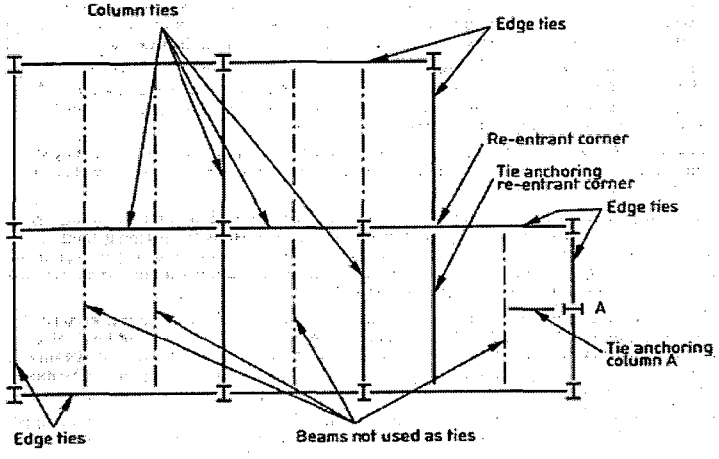

Fig. 2. 10 Members, designed as ties

If the building frames are unable to satisfy the above provision, BS 5950 clause 2.4.5.3 recommends not more than 15% of the floor or roof area or 70 m^2 (100 m^2 in EN 1991-1-7) whichever is less at the relevant level and at one immediately adjoining floor or roof level, either above or below it. However, even if the corner bay satisfies the requirements for tying force method, it will certainly fail because of no alternate load path. In this situation, this clause allows the limited and localised damage. If the area at risk of collapse exceeds the above limits due to removal of support to a column or to an element of a system, that column or element should be designed as key elements for the accidental load of 34 kN/m^2 specified in BS 6399-1 (clause 12). The value of 34kN/m^2 was adopted with reference to the pressure of gas explosion which led to failure of load bearing wall at Ronan Point. This load may not be appropriate now, as the buildings have a high risk of experiencing vehicle-borne improvised explosives which produces huge pressure.

2.3.2 European Union Regulations

The provision, adopted in the Eurocodes is same as that of UK, except the factored tensile loads for internal and external ties, and the area of localised damage which is equal to 15% of the floor or roof area or 100 m^2 whichever is less. The tying capacity of the connection is at least equal to the ULS shear force (i.e. using 1.6 dead + 0.8 imposed) or 75 kN which ever is less. The partial load factor for imposed load, adopted in Eurocode (EN 1990, 2002) is half of that of BS. Similar to BS, Eurocode does not have any provisions for the joint ductility and dynamic amplification due to sudden removal of column.

2.3.3 United States of America

General Service Administration (GSA) – Progressive Collapse Analysis and Design Guidelines for New Federal Office Buildings and Major Modernization Projects (2003):

GSA is an organisation which provides the guidelines to be followed by federal offices in order to improve public services. It sets out some guidelines to check whether the building needs to be analyzed for the progressive collapse, through a set

of flow charts on the basis of occupancy and functional use. It also suggests three progressive collapse analysis methods: linear elastic static, linear elastic dynamic, and nonlinear dynamic. For nonlinear analysis, it provides acceptance criteria such as the maximum ductility ratio which is defined as the ratio of yield to ultimate strains and end rotation for steel and reinforced concrete structures.

For linear elastic static analysis of a structure, GSA suggests the following vertical load to be applied in the downward direction:

$$\text{Load} = 2(g_k + 0.25q_k) \quad (2.1)$$

where g_k = self-weight of the structure; and q_k = live load of the structure.

As the work done by suddenly applied load will be twice that of gradually applied load, a dynamic amplification factor of 2 is used. This factor is arrived without considering any damping effects (i.e., energy dissipation due to yielding of reinforcement and concrete cracking), hence it is conservative.

For linear elastic dynamic and nonlinear dynamic analysis, GSA suggests same load without dynamic amplification factor, as the dynamic analysis incorporates the amplifications of response due to sudden removal of column.

The following cases of column removal should be considered for framed or flat plate structures (excluding soft storey buildings in which the ground floor does not have any partitions. The ground floor is used for car parking, hence the removal of interior column needs to be considered) as shown in Fig. 2.11.

1. Removal of a 1st storey column near or at the middle of the short side of the building
2. Removal of a 1st storey column near or at the middle of the long side of the building
3. Removal of a 1st storey column at the corner of the building

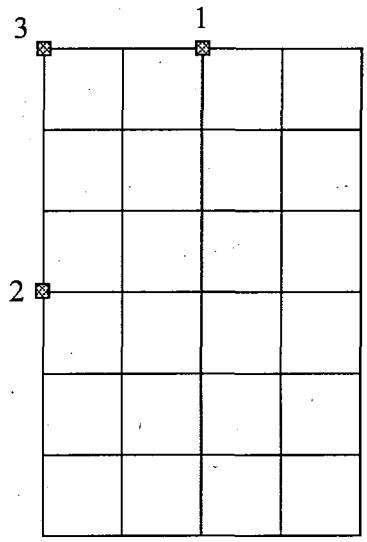

Fig. 2. 11 Analysis case – Top view

The GSA also recommends the localization of damage. The damage should not be more than the structural bays directly associated with the removed column or 167 m^2 in the case of the removal of an exterior column or 334 m^2 for an interior column (at the floor level directly above the instantaneously removed column) whichever is less. This value is high in comparison with British Standards (70 m^2).

In linear elastic analysis, the failure of members or their connections can be assessed by using a method termed Demand-Capacity Ratios (DCR), where:

$$DCR = \frac{Q_{UD}}{Q_{CE}} \qquad (2.2)$$

Where

Q_{UD} = Acting force (demand) determined in the component or connection/joint (moment, axial force, shear, and possible combined forces)

Q_{CE} = Expected ultimate, un-factored capacity of the component or connection/joint (moment, axial force, shear, and possible combined forces)

Basically, the DCR is a reverse of factor of safety. The linear elastic analysis ignores the energy absorption due to yielding of members and joints. The absorbed energy reduces the effects of accidental load. This benefit is taken into account indirectly by allowing the DCR value more than 1. The DCR values for steel and concrete buildings are arrived from the experiments. For reinforced concrete structures, the DCR should be less than or equal to 2.0 in the case of typical structural

configurations and 1.5 in the case of atypical structural configurations. For steel frame buildings, the DCR depends on the member and its failure criteria (GSA-Table 5.1). To determine the capacities, the expected material strength, calculated by multiplying the design strength of the materials with the strength increase factor (ratio of dynamic strength to static strength of material) can be used, as the load is applied suddenly. The strength increase factor for both concrete and reinforcing steel is considered as 1.25. In dynamic analysis, the duration for the removal column has significant impact on the response of the structure. Normally, blast produces load associated with strain rates in the range of 10^2-10^4 s^{-1} (Ngo, et. al., 2007). This high strain rate causes sudden failure of column, for example, the time taken to reach the concrete strain of 0.0035 is around 0.035 mSec (considering the strain rate of 10^2 s^{-1}). In other word, time period for the removal of column is less than 1/200 of the natural time period (say 10 mSec). It is very difficult to carry out the progressive collapse analysis for this impulsive load. Hence, the GSA recommends that the time period for the removal of column should not be more 1/10 of that of the natural time period of vibration. This assumption provides less than 2 percent error in the results. This is explained in Fig. 2.12. In this figure, P is the column reaction; T_r is time duration for the removal of column and T_N is the natural time period of the removed column. For $T_r/T_N = 0.1$, the dynamic load factor (DLF) is 1.98 with 2 % error. For $T_r/T_N = 0.25$, the DLF is 1.9 with 5% error.

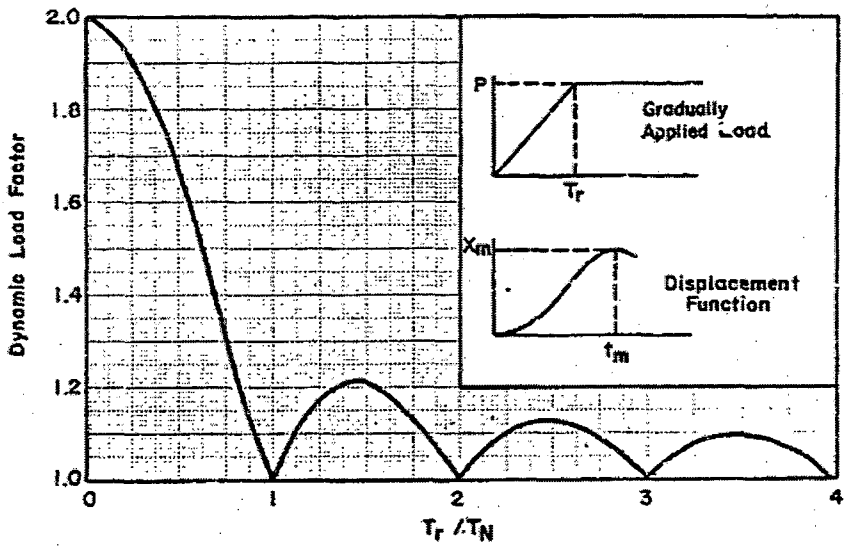

Fig. 2. 12 Maximum response of SDF system for gradually applied load

US Department of Defence (2001) Progressive Collapse Design Guidance:

The main objective of this document is to provide guidelines for minimizing the casualties from terrorist attacks. This document considers two-or three-dimensional static or dynamic linear elastic or nonlinear analysis methods and provides detailed guidelines for the procedures. In the analysis, one column or one beam is removed at any level within the structure in the case of moment resisting frame systems. The possibility of progressive collapse can be determined through an iterative analysis for linear elastic methods. In the iterative analysis, the members whose fixed moments exceed ultimate moment capacities, are removed and replaced with fixed moments equal to their corresponding ultimate moment capacities, and then the structure is reanalyzed. If the member fails by shear or compression, then the member is considered to have fallen on the element below it and the dynamic impact of the debris should also be included in the analysis. For linear elastic dynamic and nonlinear analysis, the DoD guidance suggests the following load:

$$\text{Load}=g_k+0.5q_k+0.2w_k \qquad (2.3)$$

where w_k=design lateral wind load.

When the static analysis is carried out to assess the building against progressive collapse, the DLF of 2.0 is used to account for deceleration effects. Due to the importance of defence building, the partial load factor of 0.5 is used for imposed load (instead of 0.25). It also suggests that all floors should be designed to withstand load reversals with a net uplift load equal to the dead load plus one-half of the live load. It recommends acceptance criteria for nonlinear analysis such as maximum ductility and rotation for steel and reinforced concrete members, in common with GSA guidance. It also recommends the localizing of damage through damage criteria. For framed systems, the damaged area should not be greater than one bay in any direction from a column. For other framed systems, the damage area should not be greater than 70 m^2 or 15% of the floor area. This provision is similar to British Standards. The DoD provisions are same as GSA except the partial load factor of imposed load.

2.3.4 Canada

The National building code of Canada (1995) covers structural integrity under the design requirements of section 4 and explained preventive design considerations in Commentary C. This Commentary includes a statement that buildings designed in accordance with Canadian Standards Association (CSA) design standards encompass a sufficient degree of structural integrity, generally through the detailing requirements for connections between components. Nevertheless, it suggests that special attention needs to be paid to medium/high rise buildings, made up of components of different materials, whose interconnection is not covered by CSA design standards, and for the buildings exposed to severe accidental loads such as vehicle impact or explosion. It is more general and does not suggest specifically about the control of accidental events, the design of key elements to resist accidental loads, the design of ties, the possibility of alternate paths for support, and the localization of damage to avoid the spread of collapse. The protective design against progressive collapse is not directly addressed in the code.

2.4 Progressive collapse

If the removal of load bearing members causes a failure which propagates laterally as well as vertically for substantial distances from the triggering local failure, then the failure is termed a progressive collapse. As the collapse is not proportionate with the effects caused by the accidental load, the collapse is also termed as a disproportionate collapse. After the Ronan Point incident, Countries like the UK, USA and Canada proposed guidelines to avoid progressive/disproportionate collapses. For the past three decades, research has been focussed on how to economically avoid progressive collapse, and whether the codal provisions are adequate to safe guard structures. The provisions regarding tying, made by British Standards do not have a scientific basis, although the quality of structural robustness can often be recognised (Menzies and Nethercot, 1998). This is explained with an example of 3 storey building by Liu (2001). The author performed a non-linear analysis on the building, designed as per BS 5950: Part 1:2000, for the removal of a column using LS-DYNA and concluded that the minimum tying capacity required as per BS 5950-1:2000 is not adequate to safeguard the building against progressive

collapse. Similarly, to evaluate the competence of USA codes, such as ASCE 7-02, ACI 318-02, facilities standards for the public building services and progressive collapse guidelines of GSA, in providing the robustness against progressive collapse, Nair (2004) carried out a case study on buildings which collapsed progressively earlier. Those buildings were designed based on the above standards and analysed to estimate their possibility of survival. The results could not consistently provide assurance against progressive collapse of those buildings (Table 2.1). These studies necessitate the revision in the code/standard provision.

Table 2. 1 Results obtained from case studies (Nair, 2004)

Would use of these codes and standards in their design have improved the performance of Ronan Point, Murrah and WTC?	Redundancy	Local Resistance	Interconnection	Threat-dependent analysis	Ronan Point	Murrah Building	WTC 1 & 2
ASCE 7-02	•				?	N	N
ACI 318-02			•		Y	?	N
GSA...PBS, 2000	•				?	N	N
GSA...PBS, 2003				•	N	Y	N
GSA PC Guidelines	•				N	N	N

2.4.1 Analysis to predict potential for progressive collapse

Following the 1995 bombing at Oklahoma City several methods have evolved for assessing the potential of buildings to resist progressive collapse. Gilmour and Virdi (1998) developed a computer code to carry out the collapse analysis of reinforced concrete plane frames using the quasi-state finite element approach. This programme was divided into three parts: namely local damage analysis, alternate load path analysis and debris load analysis. They carried out local damage analysis using the single degree of freedom approach. Alternative load path analysis was carried with 50 % of end moments and shears, obtained from the previous analysis, which were then applied to the rest of the structure and then these loads were incremented up until they reached 100% of their original value. At the end of each iteration, the failed member was eliminated and the frame was re-analysed. Once the alternative analysis was completed, the debris load analysis was carried out with the additional factored debris load (1.25 times debris weight).

Guo and Gilsanz (1999) carried out progressive collapse analysis in accordance with GSA guidelines for a flat slab and rigid frame structure designed for basic

requirements, using the FLEX code. This is an explicit, nonlinear, large deformation transient analysis finite element code for the analysis of structures subjected to air blast, fragment and ground shock loadings. In the modelling of flat slab structures, each slab-column joint modelled using two non-linear rotational springs rotated about two horizontal axes. Similarly, in the modelling of rigid frame structures, non-linear rotational springs were used in each beam-column connection/joint. The spring was defined by rotational stiffness, ultimate bending moment and maximum rotation of the joint as shown in Fig 2.13. The strain energy due to strain hardening was neglected since the effects were negligible on the end results. The authors concluded that the structure which satisfied only basic requirements was very vulnerable to progressive collapse. The reanalysis was carried out for the flat slab structures considering the continuous reinforcing steel detailing. The results indicated a high potential for progressive collapse. Similarly the reanalysis was done for the rigid frame structure in which the capacity of joints and spandrel columns were increased by a factor of about 2.0 and the results still showed a high potential for progressive collapse. In all the analyses, the damage was limited to bays supported by the damaged columns. In the analysis, they considered ultimate bending moment, rotation capacity and indirectly shear force as damage parameters and did not consider the catenary action of beams.

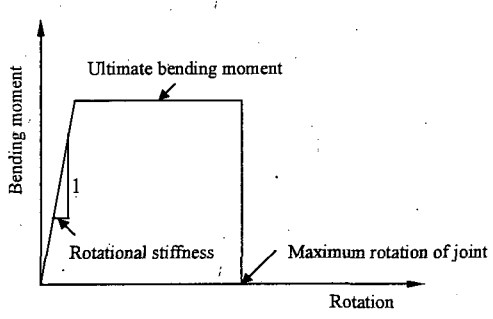

Fig. 2. 13 Definition of spring

Kaewkulchai (2003) developed the software to simulate the dynamic behaviour of planar frames up to, and through to collapse. This software considered geometric and material nonlinearity, and strength and stiffness degradation using damage index concepts. The author carried out progressive collapse analysis of planar frames using the alternative load path method. He analysed the planar frame both in deformed and

un-deformed configuration and reported that the difference in the response was much reduced. He also showed that the damage appears only to the collapsing bays.

Guo and Gilsanz (2004) proposed the procedure for nonlinear static analysis with an example of a six storey concrete building. In this analysis, a load, proportional to the reaction of the removed column was applied, and then increased gradually to characterise the pushover curve of the structure. The area below the pushover curve is the energy that the structure can absorb, and this energy is divided by the corresponding displacement to obtain the capacity curve. The load curve was drawn straight equal to the reaction of removed column (Fig. 2.14). The load and capacity curves were used to measure the vulnerability to progressive collapse. The authors considered that, (i) if the reaction was less than half of the yield strength of the pushover curve, then the structure was categorized as having a low potential for progressive collapse and (ii) if the reaction was greater than the maximum strength of the pushover curve, then the structure was categorized as having a high potential for progressive collapse. The potential energy lost when the equivalent reaction was applied to the removed column is more than that of when the gravity load was applied. Hence, this is a conservative approach for predicting the potential for progressive collapse. This kind of push over/down analysis is more useful is case of seismic analysis, as the locations of formation of plastic hinges in the frame are not possible to predict. In case of progressive collapse analysis, the failure mostly occurs on either side of the removed column; hence the detailed analysis can be done using nonlinear dynamic analysis.

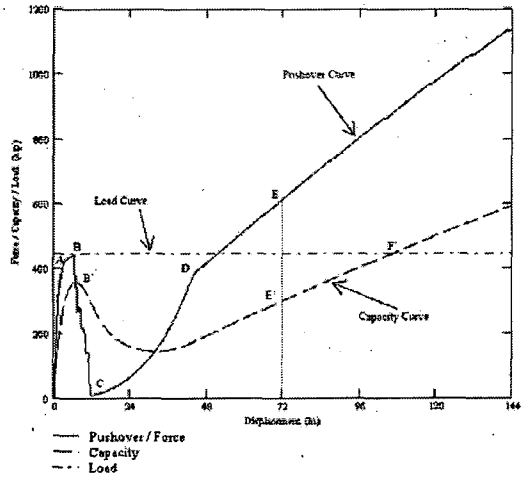

Fig. 2. 14 Pushover, capacity and load curves

Marjanishvilli (2004) presented an effective analysis procedure for progressive collapse. The response of the structure was evaluated starting with a simple static linear analysis and proceeding increasingly to complex methods until results make sure that the possibility of progressive collapse was low. The progressive collapse analysis consisting of linear and nonlinear static analysis, linear and nonlinear dynamic analysis was shown in Fig. 2.15.

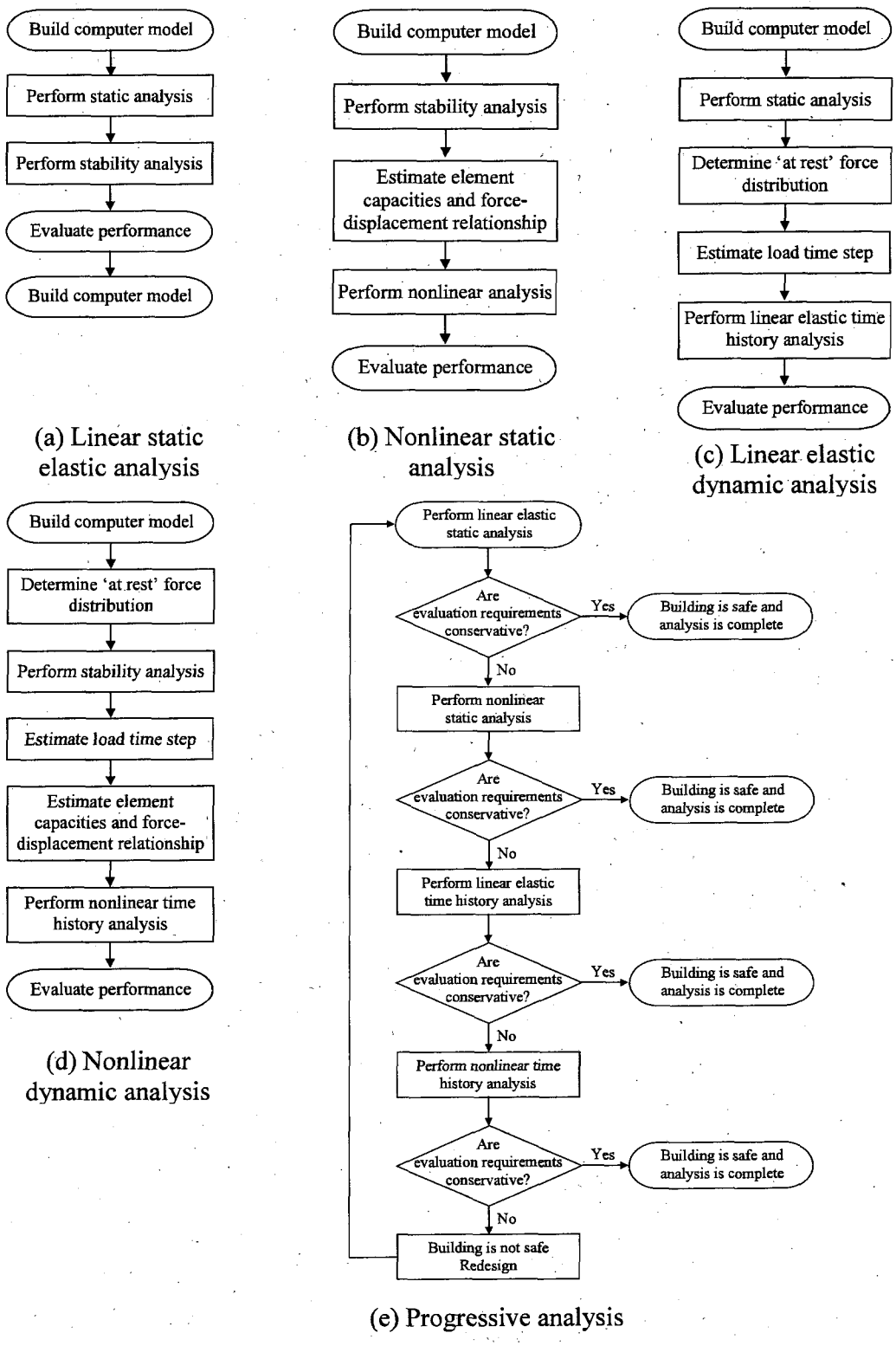

Fig. 2. 15 A methodology for progressive collapse analysis

Rahimian and Moazami (2004) proposed a new method for enhancement of the structural integrity requirement based on 3D computer analysis, incorporating geometric and material non-linearity and the membrane forces generated by diaphragm action. They studied three dimensional behaviour of a frame with slab using "LARSA", which is an integrated linear and non-linear finite element analysis and design program. The tensile capacities of concrete and metal deck were ignored and a maximum strain limit of 5% was adopted. Finally, they concluded that the system did not depend on the tying capacity of the connection, and force equilibrium was maintained after removal of the column by the radial tensile forces, created as a result of the dishing action, and compressive hoop stress as shown in Fig 2.16. They did not discuss the tensile and compressive strengths of the floor slab, and how much reinforcement was provided to resist the tensile force, since the stress pattern changes with the amount and distribution of reinforcement and cracks in the slab. Importantly, they also concluded that beams need to have full plastic moment connections throughout the span to behave successfully as members in a catenary.

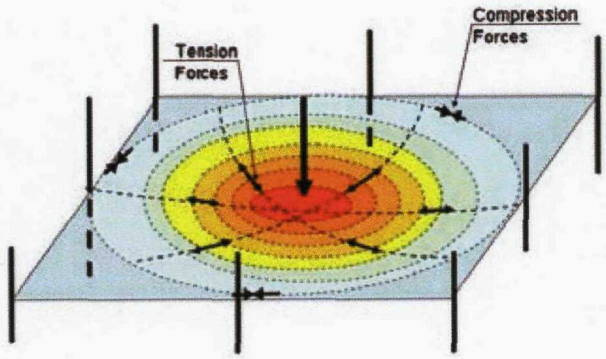

Fig. 2. 16 3D catenary action of the composite floor system (Rahimian, 2004)

2.4.2 Protective design for mitigation of progressive collapse

In the preventative design for mitigation of progressive collapse, the load from the removed column is transferred through one or more of the following methods: catenary action, beam action and diaphragm action. The design, using only beam action is very expensive and straight forward. British Standards suggest catenary action indirectly through the specification for structural integrity. Astaneh-Asl, et al (2001) carried out an investigation to study (i) the potential of typical steel structures

to the prevent progressive collapse by redistributing the removed column load through catenary action and; (ii) the performance of connections when subjected to large deformations and large catenary forces. The test frame had four bays, consisting of two 3.05 m (10 ft) exterior bays and two 6.1 m (20 ft) interior bays, in the longitudinal direction and one bay in the transfer direction with a width of 5.5 m (18 ft). The steel frame, shear connections and a concrete slab were designed to satisfy the US code requirement. The 20 gauge steel deck was connected to the beams with welds and shear studs. Hence, the ripping and tearing failures of deck slab were isolated. As a result, the strength of the system was not influenced by the steel deck. The thickness of the floor slab was 160 mm. Extra cables were provided in addition to reinforcement mesh in the plane of the removed column. The beam-column joint designed with the bolted seat angles plus a bolted single angle on the web. Similarly, the beam to beam connection was designed with standard shear tabs. In the experiments, the author found that the catenary action of the beams and steel appeared to be adequate provided that the connection has sufficient ductility. However, they did not carry out any parametric study to propose design guidelines based on the catenary action. This experimental result provides an opportunity in research to validate finite element model of catenary action.

Kuhlmann et al. (2008) carried out an experiment to study the robustness of an office building under the removal of column. The test frame, adopted from the composite building, was composed of two 1.5 m exterior bays and two 4 m interior bays. It was designed as per Eurocode 4 (EN 1994-1, 2005). The composite beam-column connection is shown in Fig. 2.17. In the experiment, the vertical load was applied to the central column until collapse. The maximum load of 114 kN was reached for a maximum vertical displacement of 775 mm and the ultimate rotation of the joint was 10.89°. Finally they have concluded that the progressive collapse can be prevented by robust design. They have not mentioned how far the robustness was realized. The conclusion may not be valid for all the cases due the following reasons:

1. ***Safety of frame:*** The failure load of 114 kN is equivalent to 7.13 kN/m^2 approximately. The dead load and super imposed load (ceiling and finishing) from the slab were 3 kN/m^2 and 1.5 kN/m^2 respectively. The imposed load

for an office building as per Eurocode 1 (EN 1991-1, 2002) is 2.5 kN/m^2. From these loads, the accidental load is calculated as per British Standards (BS 6399-1) which is equal to 5.33 kN/m^2. The frame is safe with a factor of safety of 1.34. At the same time, the dynamic effect due to sudden removal of column is ignored. If the dynamic amplification factor of 2.0 is considered as per GSA (2003), the frame will certainly fail.

2. ***Ductility of frame:*** In case of simple and semi rigid connections, the rotation ductility is roughly estimated as a ratio of the displacement of extreme bolt row to lever arm (distance of the extreme bolt row to beam bottom flange). The displacement of extreme bolt row mainly depends on bending of end plate and column flange. For most of the connections, the thickness of end plate and gauge distance for bolts are same. The displacement of extreme bolts can be reasonably assumed to be 20 mm. As per above definition of joint ductility, the rotation capacity of the connection is equal to 10.30° (lever arm = 110 mm; joint rotation = $\tan^{-1}(20/110)$ = 10.30°), resembling that of experimental result. In most of the office buildings, the width of bay will be 9 m and more. In that case size of the beam is huge and low ductility will result. For example, for UB533 beam, the lever arm is 430 mm, resulting in the rotation capacity of 2.67°, inducing premature fracture attributed to low ductility.

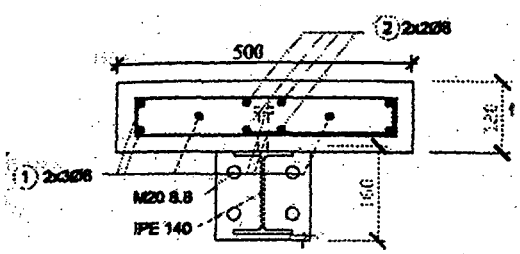

Fig. 2. 17 Cross section of the composite joint (Kuhlmann et. al., 2008)

More literatures have been reviewed about the estimation of blast load, the dynamic analysis of column and catenary action in the steel framed building, and presented in subsequent chapters.

Chapter 3.

Direct Design Methods: Protective Design for Steel Framed Structures

3.1. Catenary action in simple connection frames

After the removal of support to an intermediate column, the accidental load may be redistributed through the catenary action. In catenary action, beam and beam-column connections are under tension; hence sufficient tensile strength (tying capacity) for the connection needs to be maintained to redistribute the load to the column. The phenomenon of maintaining the connection without failure termed as structural integrity. The British Standard BS5950 proposes the requirement for structural integrity based on the shear capacity of the connection.

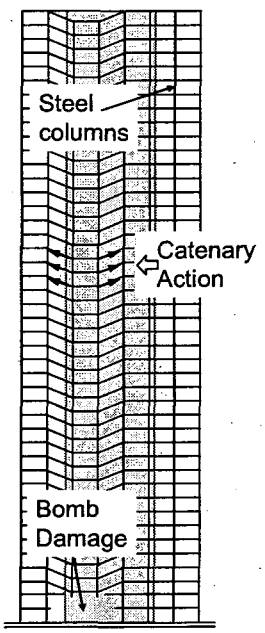

Fig. 3. 1 Catenary Action

The rationale behind the provision of tying between members (the tying force approach) is that by providing beam joints with sufficient tensile strength, floors should be able to span between undamaged columns by catenary action, a process which is sketched in Fig. 3.1. This approach assumes fairly that the loading on a structure at the time of damage will be significantly less than the ultimate limit state(ULS) load , with the load at the time of damage assumed to be equal to $^{1}/3^{rd}$ of the imposed load plus 1.05 of the dead load. Since it is a requirement that the tying capacity of the connection be at least equal to the ULS shear force (i.e. using 1.4 dead + 1.6 imposed), then the tying force substantially exceeds the shear force at the connection. Floor beams therefore will need to rotate by 20 to 30 degrees to the horizontal in order to achieve equilibrium under the applied loads.

These simple calculations ignore the dynamic amplification of the tying force. These amplification of forces occur as a result of the additional tying force needed to absorb the kinetic energy generated by the downwards movement of a heavy object such as a subsection of a building. Since the tying force method assumes large displacements, these additional loads will be significant, because any movement will generate significant momentum in the building. Therefore, static calculations provide only a lower bound estimate of the tying force needed to arrest the fall. If a more complicated dynamic analysis is carried out, then one must assume a time for removing the support from a column or columns. US guidance (GSA, 2003) recommends that the time period for this event should not be more $1/10^{th}$ of that of the natural time period of the column. Shock waves from high explosives are capable of destroying columns almost instantaneously by a fracture process called brisance. Since rapid column removal leads to rapid accelerations, the additional force needed to decelerate the structure results in the dynamic amplification of tying forces. This process is illustrated in Fig. 3.4. The University of Sheffield have published research carried out for a PhD project into catenary action (Liu *et al,* 2005). This has shown that the forces generated during catenary action substantially exceed those currently assumed in design.

Progressive collapse analysis has been rapidly evolving in the USA and guidelines for New Federal Office Buildings in the USA (GSA, 2003) provide useful information on the treatment of the dynamic amplification of loads. In their approach

the loading during a damage scenario should be doubled to account for deceleration effects, if a static (linear elastic) analysis is carried out. By omitting this effect the UK approach could in certain circumstances underestimate tying forces.

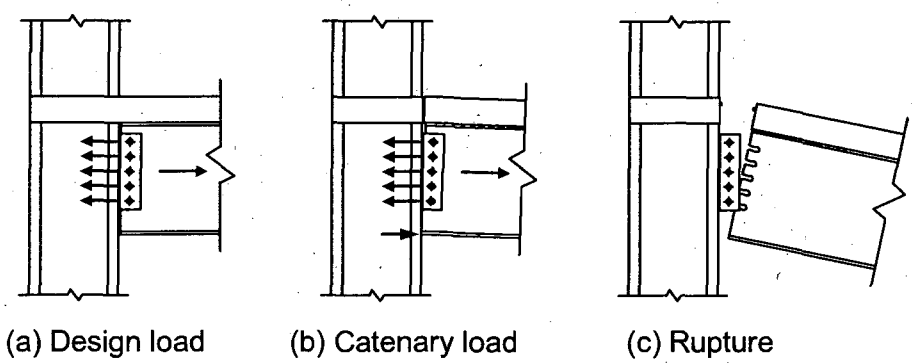

Fig. 3. 2 Prying and catenary action

Connection Ductility. The Building Regulations place no requirement for joints to have sufficient ductility (rotation capacity) in order to tolerate the rotations necessary to generate catenary action. The result of this regulatory freedom is that the tensile (tying) capacity of industry standard connections, such as those presented in the design guide of Steel Construction Institute (SCI, 2002) are calculated in the absence of any rotation, see Fig. 3.2(a). However, only a small amount of rotation is necessary to cause the prying sketched in Fig. 3.2(b). Horizontal equilibrium of the joint dictates that the reaction generated between the beam and column flanges must reduce the tying force capacity of the joint, leading to fracture at a fraction of design tying force.

Inspection of the catenary action approach quickly reveals other unresolved questions. For example it is not clear how catenary action is to generate the required anchorage to support columns located next to corner columns in buildings. Corner columns cannot provide anchorage, although diaphragm action in the slabs may provide the lateral restraint needed to support a catenary. Moreover, tying could conceivably widen progressive collapses as the additional weight of the unsupported frame could lead to the buckling of previously undamaged columns in a process known as drag down.

3.2. Methodology used to determine the factor of safety against collapse

An analysis of catenary action is presented herein, in an attempt to quantify factors of safety against collapse. Ideally this would be carried out using a fully non-linear dynamic finite element analysis of a building. Such a method has the potential to yield accurate results, but would take a great deal of time and resource. Instead a relatively simple analysis is presented, with the aim of bounding the likely factors of safety against collapse. Thus, a best case and a worst case scenario are considered, with the real solution laying somewhere between these values.

The basic assumptions in the analysis can be summarised as follows:

Assumption 1: Accidental limit state loading

During the member sizing fully glazed cladding was assumed. This load was removed during the accidental limit state because it was assumed that blast would have destroyed the glazing. During the accidental limit state 1.05 dead load + $1/3^{rd}$ of imposed load was assumed.

Assumption 2: Columns remain in line

The composite metal deck slabs are stiffened throughout the building by the arrangement of secondary and primary beams bonded together by shear studs. It is believed that this relatively stiff composite arrangement of elements will create a floor plate with a great resistance to the relatively small shear forces that are introduced into the system by the tying force imposed during catenary action. Therefore it is assumed that the columns will not translate sideways following the removal of column.

Assumption 3: Slab tensile strength, T_{slab}

The tensile strength of the slab has been included in the analysis of catenary action, in order to mobilise all available strength. The slab strength, $T_{slab} = T_{deck} + T_{mesh}$, where T_{deck} is the strength of the profiled metal decking and T_{mesh} is the strength of the mesh reinforcement embedded in the slab. The failure of profiled sheet subjected to tension occurs because of insufficient end distance, box shear failure or bearing failure. The minimum centre-to-centre spacing of stud shear connectors should be

five times nominal shank diameter along the beam (BS 5950 – 3.1:1990, clause 5.4.8.4.1). Furthermore, the end distance for profiled sheet measured to the centre line of the studs should not be less than 1.7 times the stud diameter (BS 5950-4:1994, clause 6.4.3). Because of these provisions the critical failure mode is in bearing, as shown in Fig. 3.3. Hence, the maximum tying force carried by profiled sheet per metre in this example was 42 kN, which was calculated using the following:

$$T_{deck} = N.d.t.p_b \qquad (3.1)$$

Where,

N is the number of shear studs used to connect an edge of profiled sheet on beam normal to sag per metre.

d is the diameter of shear studs.

t is the thickness of profiled sheet.

p_b is the bearing strength of profiled sheet.

T_{mesh} be calculated by multiplying the area of reinforcement per metre with the yield strength of reinforcement, which equals 65 kN/m run. These provide a total tensile capacity of the slab, T_s equal to 107 kN/m run.

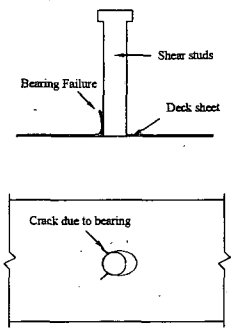

Fig. 3. 3 Failure of Profiled Sheet

Assumption 4: Dynamic load amplification

As stated earlier when support to the the column is removed, potential energy is converted into the kinetic energy as well as strain energy. The frame will then vibrate until all the kinetic energy is absorbed. The maximum tying force generated during this process can be represented by the final at rest tying force, multiplied by the dynamic amplification factor (DAF), see Fig. 3.4. The magnitude of the DAF will depend on the amount of damping present in the system, as well as the time duration of column removal. Fire would let a column down slowly and produce a

DAF of 1.0. At the other extreme, a brisance failure in the column would represent an instantaneous column removal. The extent of damping is very difficult to estimate without full scale experimental tests. If the system were undamped, then the DAF could be in the region of 2.0.

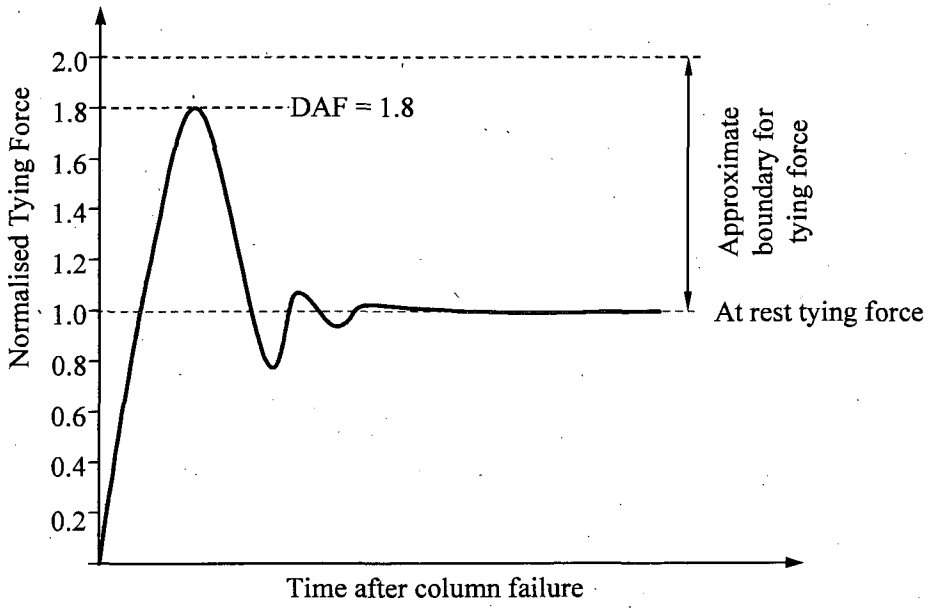

Fig. 3. 4 Illustration of the dynamic amplification for tying force

Method for estimating Factor of Safety against collapse

After removal of the support to column C, the beams ACB shown in Fig. 3.5 act like an inverted three hinged arch as shown in Fig. 3.6. This is a determinate structure, with the horizontal thrust at the support (H) given by:

$$H = \frac{1}{L\tan\theta}\left[W_1 L + \frac{W_2 L}{2} + \frac{qL^2}{2}\right] \qquad (3.2)$$

Where

W_1 is the reaction from the secondary beam

W_2 is the reaction from the main beam C-C_1 plus the weight of column for that storey

q is the UDL acting directly onto the beam 'ACB'

Resolving vertically provides the vertical reactions:

$$V = 0.5\left[4W_1 + W_2 + 2qL\right] \qquad (3.3)$$

And the tying force is given by:

$$T = \sqrt{H^2 + V^2} \qquad (3.4)$$

The factor of safety against collapse is provided by dividing T by the tensile capacity of the joint. These calculations are relatively simple, with the load W_1 easily determined by multiplying the accidental limit state load by half the area supported by the beam. Calculating the load W_2 is more complex because catenary action in the slab provides a route by which load from beam CC_1 can be removed directly from the system before it emerges into beam ACB.

After the removal of support to the column, the slab deflects downward and experience diaphragm action. The diaphragm action depends on the anchorage of slab, i.e. a robust connection of profiled sheet with transverse beam and the continuous reinforcement mesh across the beam. The slope in the slab varies from zero at the support where both the columns remain undamaged, to maximum at the mid-section where removal of column support occurs as shown in Fig 3.5 This changes in slope causes the upward reactive force. To find the upward reactive force due to catenary action of reinforcement mesh and profiled sheet, the panels are divided into one metre strips along AA_1 from $A_1C_1B_1$. Let us consider the one metre strip XZY (Fig. 3.7), located at distance 'x' from the beam $A_1C_1B_1$. The tying capacity of XZ and YZ causes upward reactive force at Z which is calculated using Eq. 3.5. Similarly, the upward resisting force caused by tying capacity of the slab is calculated for each one metre strip and applied on the beam CC_1. It reduces the accidental load acting on the beam CC_1 (Fig. 3.8). At the same time, there will not be any reduction in the accidental load on the secondary beam as no change in angles of tying force occurs on either side.

$$P_{up} = 2\, T_{slab} \sin\left(\frac{\theta x}{L}\right) \qquad (3.5)$$

Where,

P_{up} = Upward reactive force caused by slab tying capacity per metre

T_{slab} = Tying capacity of slab

$\left(\frac{\theta x}{L}\right)$ = inclination of tying capacity of XZ or YZ, shown in Fig. 3.7.

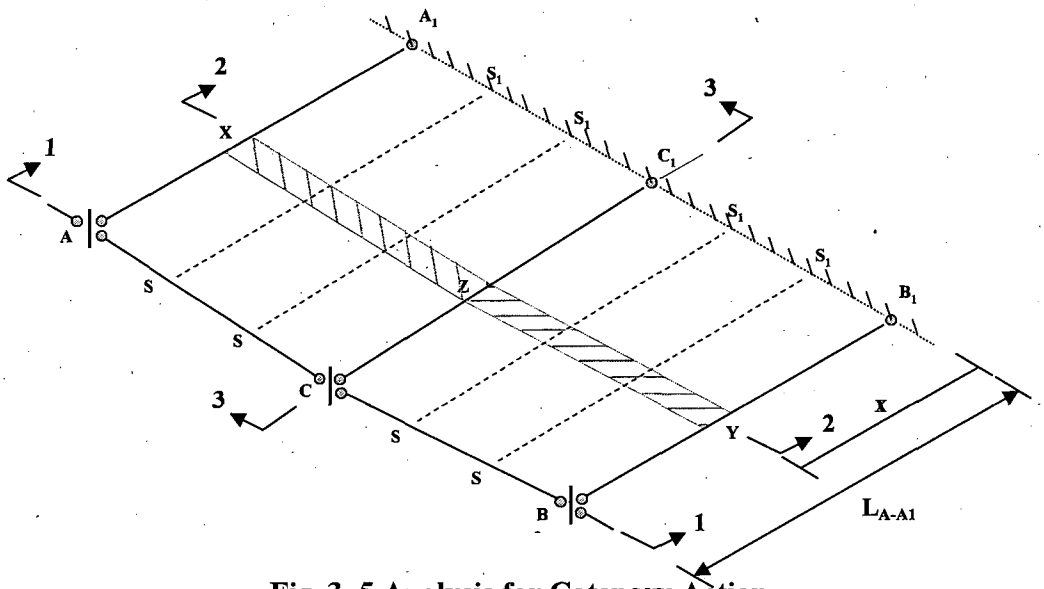

Fig. 3. 5 Analysis for Catenary Action

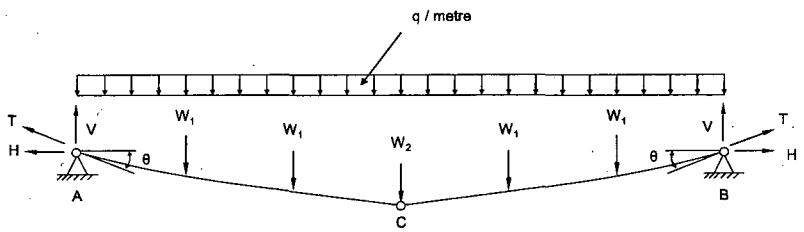

Fig. 3. 6 Analysis for Catenary Action - Section at 1-1

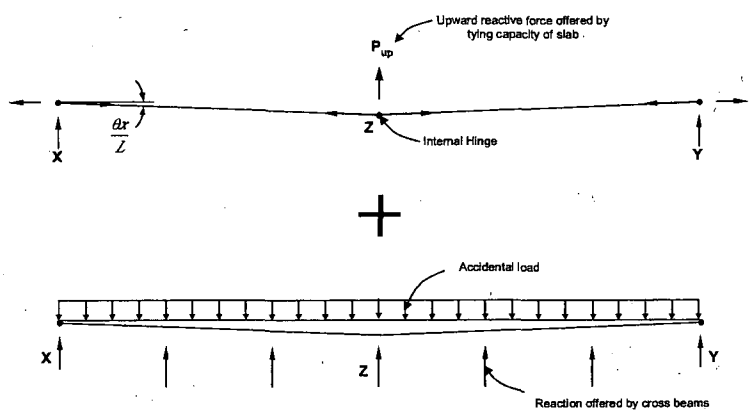

Fig. 3. 7 Analysis for Catenary Action - Section at 2-2

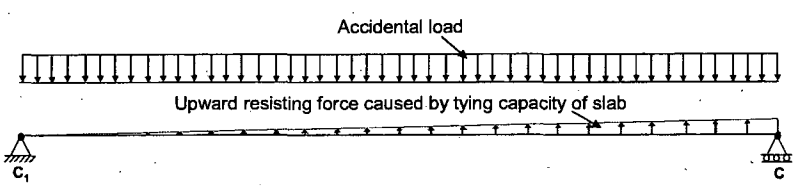

Fig. 3. 8 Analysis for Catenary Action - Section at 3-3

Factor of safety for the joint is defined as the ratio between tying capacity of the joint and tying force acting in the joint. If the tensile strength of slab is mobilised, the factor of safety depends on the rotation capacity of the joint implicitly. Hence, the required rotation capacity is calculated by trial and error procedure. On the other hand, if the tensile strength of slab is ignored, the factor of safety is an explicit function of the required rotation capacity.

3.2.1. Case study

Typical Steel Frame

To study the potential for the tying force method to mitigate disproportionate collapse via catenary action the multi-storey framed building shown in Fig. 3. 9 is considered as a case study. This frame reasonably resembles many commercial medium rise office developments. The components of steel frame, including the connections, metal decking and sections, is designed using industry standard design guides as presented in the Steel Construction Institute Design Guides, and British Standards (BS 5950 (2000), SCI (2002) and SCI (1989)). The floor comprises a 125mm thick composite slab, reinforced with A142 fabric reinforcement and formed on 1.2 mm gauge decking. Composite action between the beams and slab is achieved with 19 mm diameter, 100 mm high headed studs, spaced at 300 mm centres, i.e., 40 studs in each half span of the secondary beams. For the main beams, the studs are provided at 450 mm centres, i.e., 22 studs in each half span. The floor slab is extended by 0.5 m beyond the edge beams to support a curtain wall system. The total dead and imposed loads are 5.1kN/m^2 and 6.0kN/m^2 (inc. partitions) respectively and this provides an accidental limit state load of 7.1kN/m^2. All steel is S355 grade except the end plates which is S275 and all concrete is C35 normal weight. Bolts of M20 grade 8.8 are used in the beam to column joints. To study the feasibility of simple connections in resisting accidental load through catenary action the frame is designed with fin plate, flexible end plate and double angle web cleat connections. The member and connection details of the frame are shown in Figs. 3.10 to 3.13.

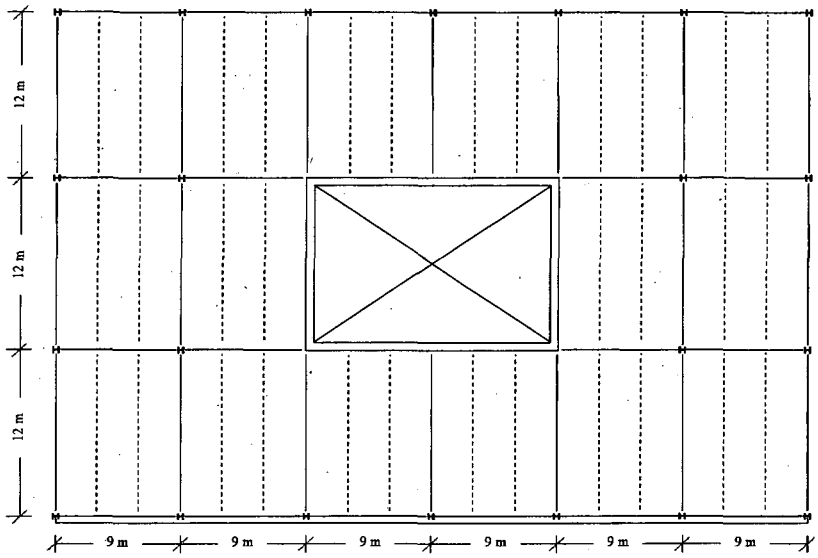

Fig. 3. 9 Plan of the building

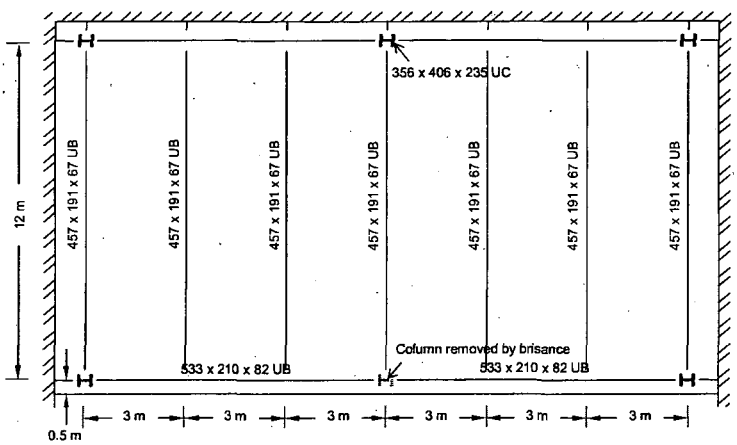

Notes:
All columns – 356 x 406 x 235 UC
All main beams – 533 x 210 x 82 UB
All secondary beam – 457 x 191 x 67 UB
Steel grade – S355
Concrete grade – C35
Imposed load – 5 kN/m^2
Partition load – 1 kN/m^2

Fig. 3. 10 Idealised frame for the analysis

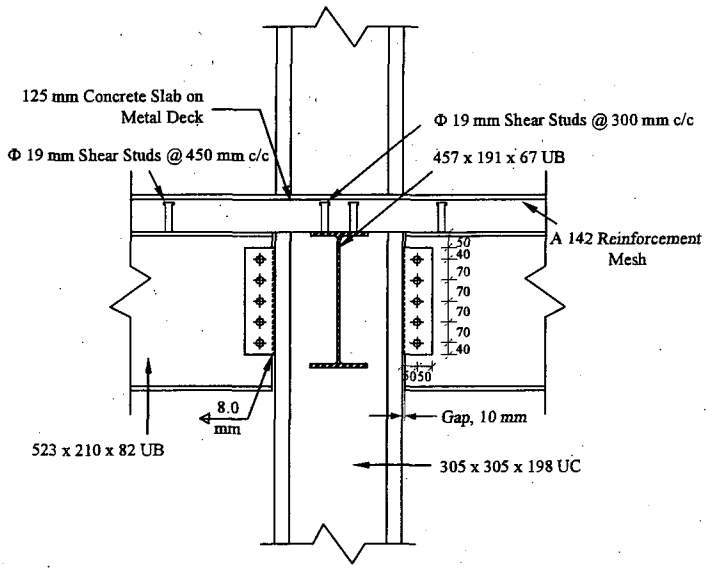

Fig. 3. 11 Beam – column joint details connections between 533UB and columns, see Fig. 3. 10

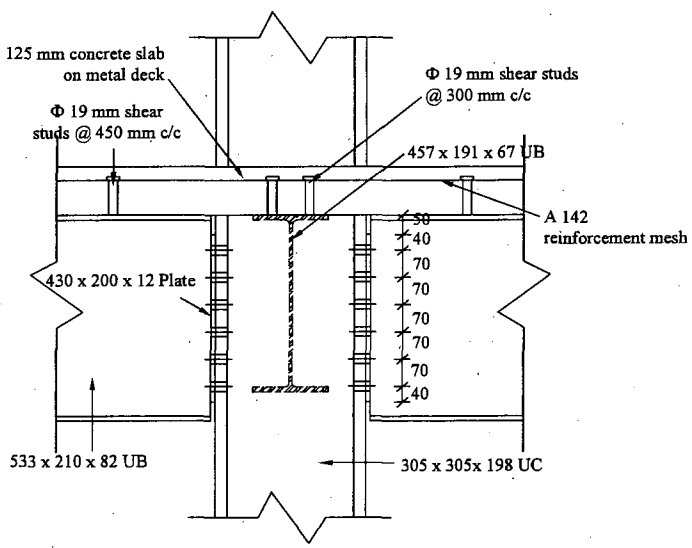

Fig. 3. 12 Details of end plate connection

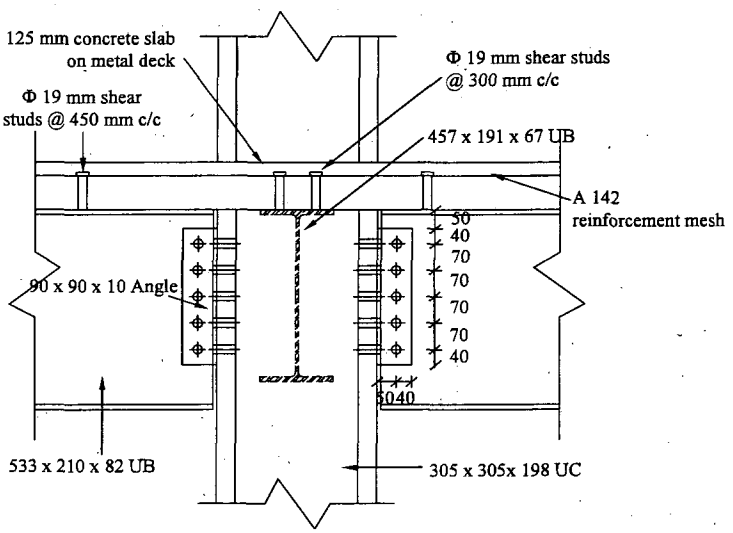

Fig. 3. 13 Details of double angle web cleat connection

3.2.2. Joints Behaviour

3.2.2.1 Simple Fin Plate Connection

Liu *et al* (2004) have developed a design method for quantifying the rotation capacity of fin-plate connections as part of investigations related to seismic design. Their method assumes beam rotation is centred about the centroid of the bolt group and it produces a maximum rotation capacity of 2° for the joint considered in this study, Fig. 3.11. This limit is perhaps too restrictive for this study; therefore it has been assumed that rotation occurs about the centroid of the beam, with a total plastic deformation of the upper bolt hole in the fin-plate of 10mm (corresponding to half a bolt diameter). Beyond this it is highly likely that the plate will begin to rupture, initiating fracture due to prying. Using this approach the rotation capacity of the joint in this design example was equal to 4 degrees, with the resulting deformation of the bolt group shown in 3.14.

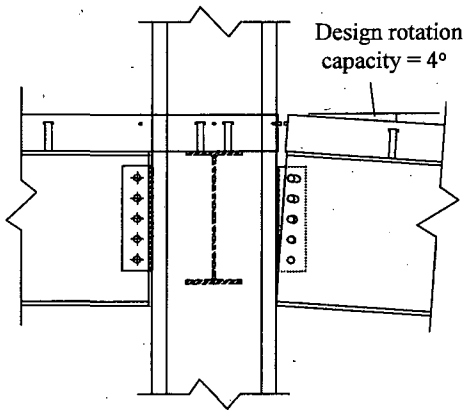

Fig. 3. 14 Beam-column joint at maximum rotation capacity

The tensile (tying) capacity of the connection between the primary beams and perimeter columns shown in Fig. 3.11 were determined using the SCI design guide (SCI, 2002). The calculations underpinning this capacity assume zero beam rotation, therefore the tensile capacity holds true only at low values of beam rotation. As discussed in chapter 1, the prying action will create a reduction in the tying capacity of the joint. The extent of this decline in strength can be easily gauged by comparing the design tying force with a rough estimate of the prying force:

The design tying force of the joint = 528 kN
Estimate of prying force = bottom flange area x flange yield stress = 978 kN

Since the prying force is greater than the tensile capacity of the bolt group, prying will cause the tensile capacity of the joint to fall to approximately zero, to be replaced by a joint moment. These simple calculations ignore the possibility that flange buckling will cause a reduction in the prying force and they also ignore the tensile strength of the slab mesh. However, incorporation of these other factors would not change the overall conclusion – that prying will substantially damage the tying force capacity of the joint. In view of this conclusion this study assumes that the design tying force is maintained only until the rotation capacity is exceeded. Joint moments are ignored up to this stage of the analysis.

The approximate bending moment that would be developed owing to prying action in the joint shown in Fig. 3.14 is 166 kN m. A joint moment capacity of 1064 kN m would, however, be required to support the column damaged in this design example. Since the moments generated during prying are much less than those needed to

redistribute loads away from the damaged columns, collapse is assumed after the limit on rotation capacity is exceeded.

3.2.2.2 Flexible End Plate Connection

The analysis of the beam, after removal of column mainly depends on the response of the connection which includes the interaction of tensile force, bending moment and rotation. The behaviour of connection is modelled using the component method (Yee and Melchers (1986) and Faella et al. (1996)). In the component method, the joint behaviour is divided into the following components (Fig. 3.15):

- Column web panel in shear
- Column web in compression
- Column flange in bending
- End plate in bending
- Bolts in tension
- Column web in tension
- Beam flange and web in compression
- Beam web in tension

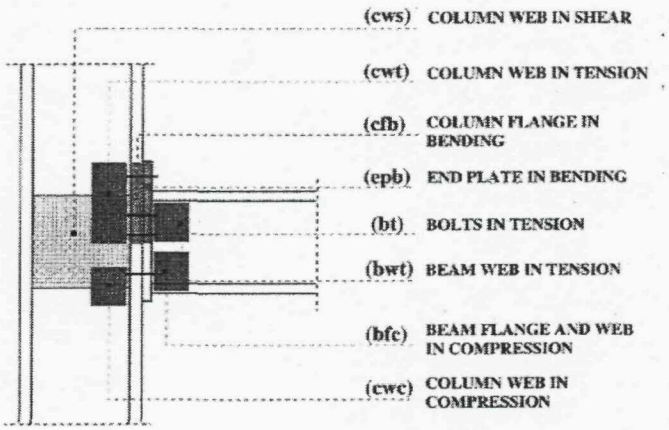

Fig. 3. 15 Components of end plate connections, Source Faella *et al*(2000)

The beam flange and web contributes only in the estimation of the joint strength. The rest of the components contribute both in the estimation of the joint strength and rotational stiffness. This method is well explained in the book, "Structural Steel Semi-rigid Connections" by Faella, et al., (2000). The equations to estimate the strength and stiffness of joint components are presented in Appendix A1.1.

The strength and stiffness of end plate and column flange in bending is estimated using an equivalent T stub (i.e., two T-elements connected through the flanges by means of one bolt rows), presented by Yee and Melchers (1986). Fig. 3.16 shows the identification of T stubs which is used to estimate the deformations due to the bending of the column flange and end plate/double web cleats. The T stubs fail in the following modes: (a) flange yielding; (b) flange yielding with bolt failure and (c) bolt failure (Fig. 3.17). The failure mode is governed by a parameter (β_u), defined as the ratio between the flexural strength of the flanges and the axial strength of the bolts. The resistance and deflection for each failure mode is provided in Yee and Melchers (1986) and presented in Appendix A1.2. The strength and deformation of the stub is calculated at different points, such as yielding, strain hardening and ultimate or fracture points using the method specified by Faella et al (2000). Finally, the rotation capacity is calculated based on the plastic deformation of T-stubs.

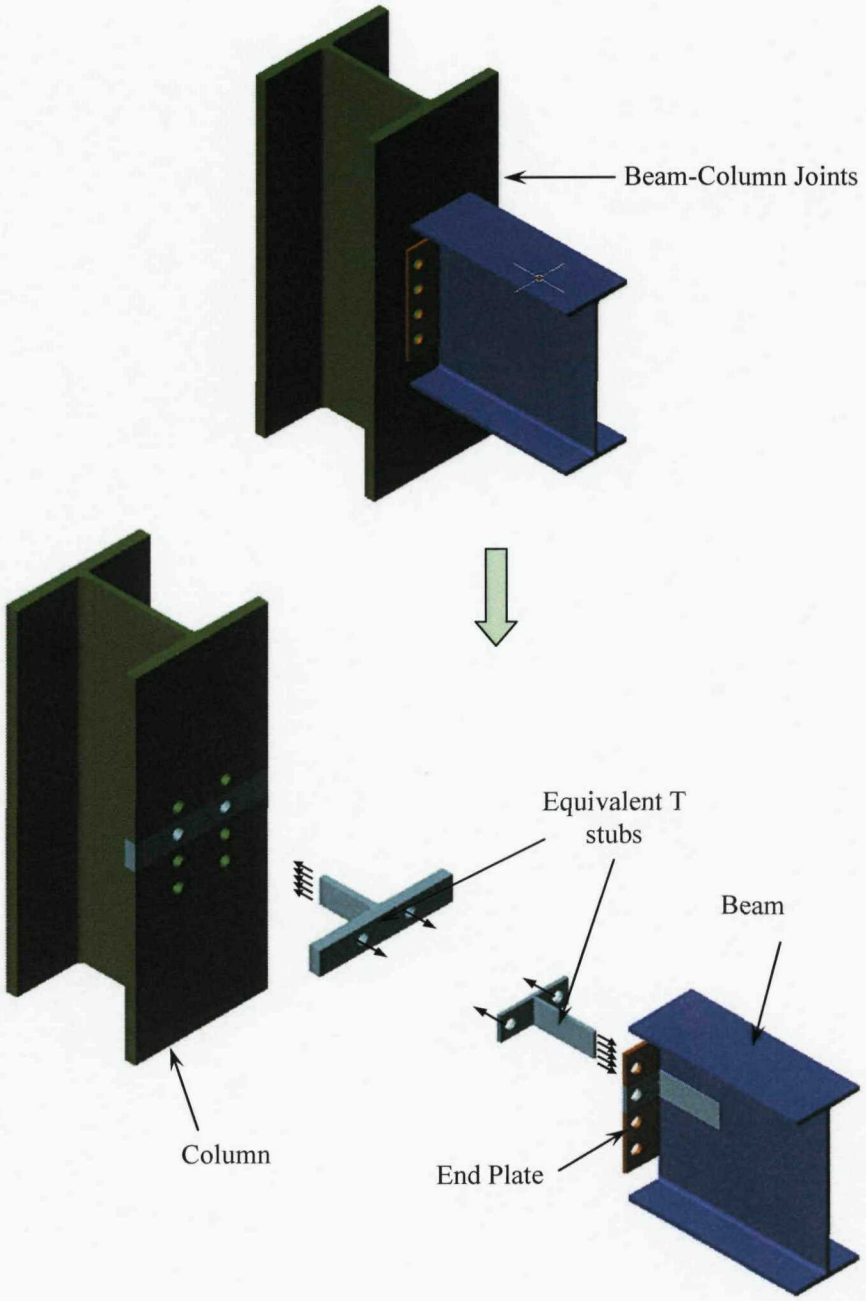

Fig. 3. 16 End Plate Connection and its T stubs

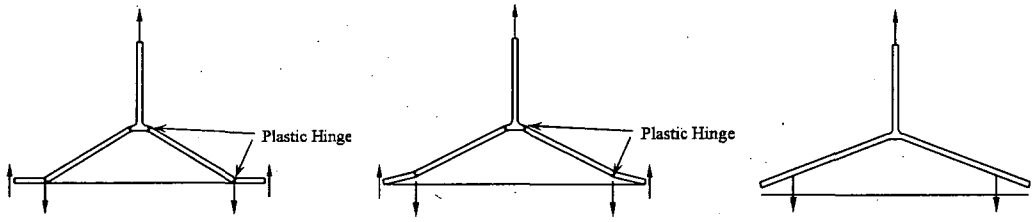

(a) Flange yielding (b) Flange yielding with bolt failure (c) bolt failure

Fig. 3. 17 Failure modes of T stub

In this analysis, the end plate connection shown in Fig. 3.12 is divided into T stubs. The force displacement curves (Fig. 3.19) of each component including bolts, 2 T-stubs and column web, up to failure are modelled based on the stress – strain curve sketched in Fig. 3.18 (Kato et al., 1990). As the ultimate strength of the T stub of end plate (116.3 kN) is the lowest among the connection components, it is considered as the weakest joint component. The contribution in the ultimate plastic deformation from the compression of column web is low and is therefore ignored. The detailed calculation of resistance and deformation of the joint component is explained in Appendix A1.3. The deformation of other components is obtained corresponding to this axial force. The sum of the deformations (corresponding to 116.3 kN) of the joint components is the ultimate deformation capacity of one bolt row which is equal to 29.55 mm. After the removal of support, the columns starts to drop down and the beams on either side rotate about the joints. The joints are assumed to rotate about the bottom of end plate. The lateral movement of columns is assumed to be arrested by the composite slab, as the stiff arrangement of secondary and primary beams bonded together by shear studs can resist the tying loads without buckling. The rotation capacity of the connection is 4.33° which is calculated by dividing the ultimate deformation of the top most T-stub (29.55 mm) by its distance from bottom end plate (390 mm).

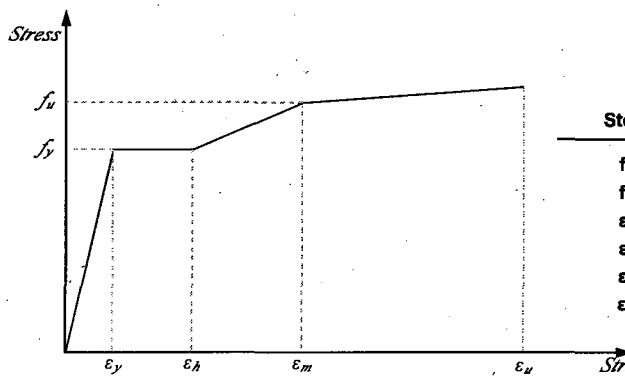

Steel	S275	S355
f_y	275	355
f_u	430	510
ε_y	0.13%	0.17%
ε_y	0.13%	0.17%
ε_h	1.43%	1.67%
ε_u	55%	80%

Fig. 3. 18 True Stress-Strain Curve (Kato et al., 1990).

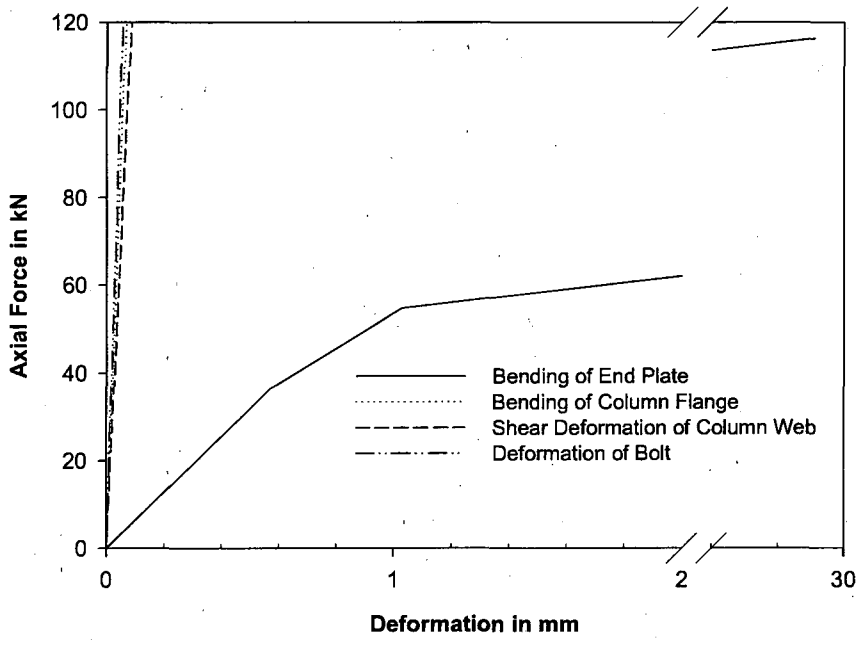

Fig. 3. 19 Axial Deformation of Flexible End Plate Joint Components

Beyond this rotation the connection will fail in a prying type action. Small moments are generated in the connection at this limit of rotation, however they have little effect on the redistribution of loads and have therefore been ignored, hence flexural strength of the connection (188 kN-m) is much lower than the bending moment required to support the damaged column (1060 kN-m). Hence, the load from the removed column is transferred to the extreme columns only through catenary action, with the tensile strength of the joint limited to 587 kN and the rotation capacity limited to 4.33°.

3.2.2.3 Double Angle Web Cleat Connection

The above component method is used to estimate the rotation capacity of the double angle web cleat connection. The detailed calculation of resistance and deformation of the components is explained in Appendix A1.4. As the ultimate strength of the double angles (211.68 kN) is the lowest among the connection components, it is considered as the weakest joint component (Fig. 3.20). The deformation of other components is obtained corresponding to this axial force. The sum of the deformations (corresponding to 211.68 kN) of the joint components is the ultimate deformation capacity of one bolt row which is equal to 17 mm. The rotation capacity of the connection is 2.5° which is calculated by dividing the ultimate deformation of top most T-stub (17 mm) by its distance from bottom end plate (390 mm). Similar to other joints (fin plate and flexible end plate connections), this joint fails by prying beyond the rotation capacity, as flexural strength of the connection (321 kN-m) is much lower than the bending moment required to support the damaged column (1060 kN-m)

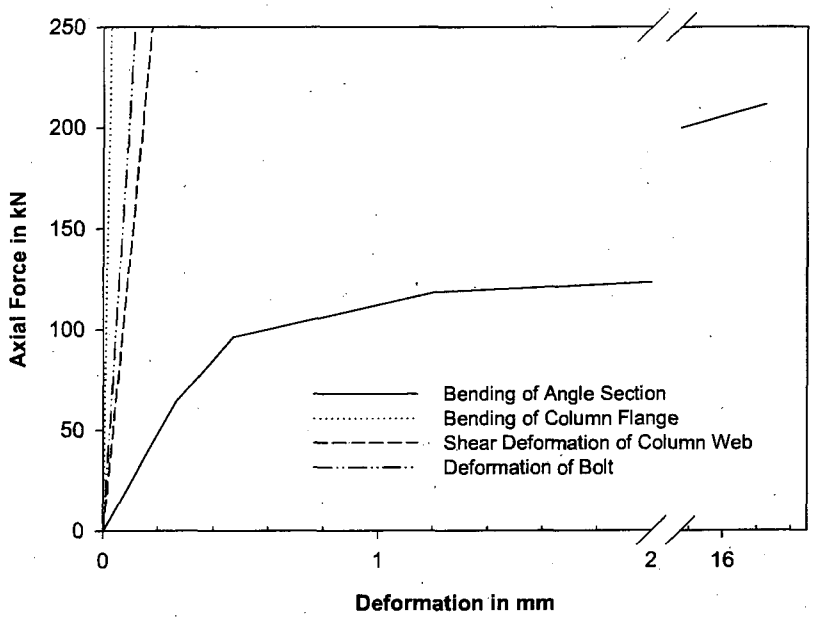

Fig. 3. 20 Axial Deformation of Joint Components

3.2.2.4 Summary of joint strengths and rotation limits

The tensile strengths and rotation limits of three connection types have been estimated and is summarised in Table 3.1.

Table 3. 1 Summary of joint strengths and rotation capacity

Type of connection	Tying capacity (kN)	Rotation capacity
Fin plate connection	528	4°
Flexible end plate connection	587	4.33°
Double angle web cleat connection	1058	2.5°

Beyond the rotation capacity, the joints are assumed to rupture because of,

1. Prying force, caused by beam bottom flange, is likely to be greater than the tensile capacity of bolt group.
2. Joints have limited flexural strength, caused by prying action to distribute the accidental load through beam action

3.2.3 Estimation of factors of safety against collapse

The factor of safety against collapse has been determined for the three scenarios listed below (Fig. 3.21). Appendix A1.5 contains all of the basic design parameters, the accidental limit state loads on the catenary and the tying forces necessary to achieve equilibrium under these loads.

Best case scenario. In this case, the full tensile strength of the slab is considered to be mobilised and the dynamic effect on the system due to sudden removal of column is not considered, as these assumptions yield upper bound values for factor of safety. These assumptions provided the factor of safety of 0.19 in case of fin plate connection and this can be regarded as an upper bound estimate.

Worst case scenario. It can be argued that the tensile strength of the slab cannot be relied upon to generate catenary action because it is likely to fracture under large deformations. It has therefore been ignored in this scenario. In addition, the DAF has

been taken as equal to 2.0, in accordance with US practice (GSA, 2003). This provides a factor of safety of 0.08 in case of fin plate connection.

Best guess scenario. In this case, catenary action in the slab is included and a DAF of 1.5 was assumed, producing a factor of safety of 0.12 in case of the fin plate connection.

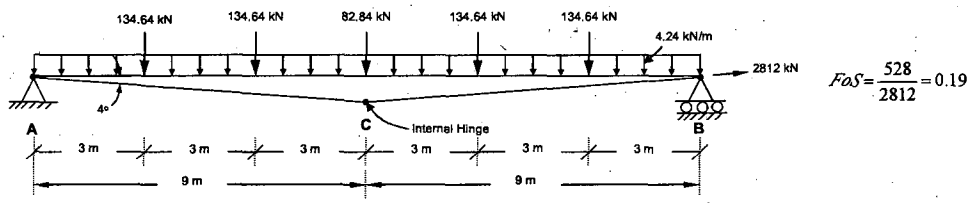

(a) Best case scenario

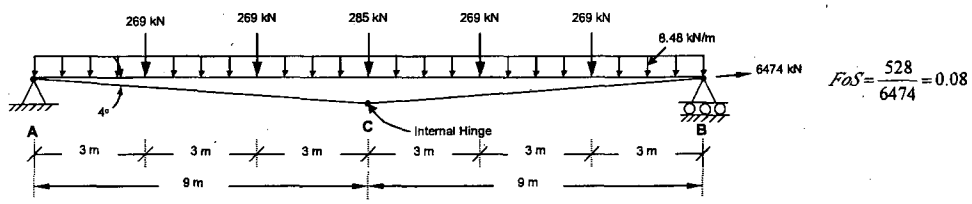

(b) Worst case scenario

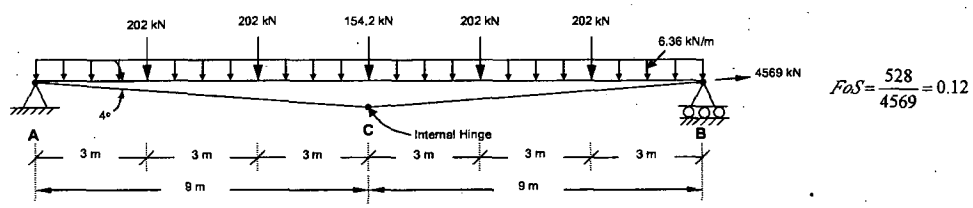

(c) Best guess scenario

Fig. 3. 21 Accidental loads on main beam 'ACB' in case of fin plate connection

Using an iterative procedure it is possible to define what deformation is necessary in the example considered herein, in order to support the damaged column via catenary action. Assuming that the beam-column joints remain able to transfer their design tying force (regardless of the rotation), the connections would need to rotate by 24 degrees to the horizontal in order to support the damaged column by catenary action (assuming full tensile capacity of the slab was mobilised and assuming a dynamic amplification factor of 1.5), see Fig. 3.22. This would produce the deflected shape described in Fig 3.23 (a) and would require a downwards movement of 3.84 m. The resulting joint deformation is shown in Figs. 3.23 (b) and (c). Such deformations are not possible without fracturing the joints and the reinforcement in the slab. The slab

is unlikely to possess the ductility required to withstand such a high degree of deflection because the tensile capacity of the concrete is approximately 245kN/m, whereas the tensile capacity of the mesh and profile metal deck is only 107kN/m. Since the concrete strength is high in comparison with the mesh, plastic strains in the mesh would be concentrated into a few widely spaced cracks, such as the crack shown in Fig 3.23 (a) and Fig. 3.24. This would lead to an early fracture of the slab during a progressive collapse.

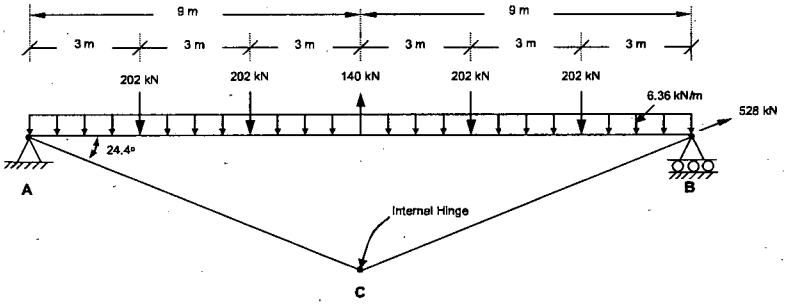

Fig. 3. 22 Accidental loads on main beam 'ACB' for the calculation of required rotation capacity

Flexible end plate connection: This connection yields low factor of safety of 0.23, 0.10 and 0.14 for best, worst and best guess scenarios. Its factor of safety is nearly same as that of fin plate, since tying capacity and the limiting rotation of both connections are approximately same.

Double angle web cleat connection: This connection also yields low factor of safety of 0.24, 0.10 and 0.15 for best, worst and best guess scenarios. Although, it has twice the tying capacity of fin plate connection, its factor of safety is nearly same as that of fin plate because of low ductility.

3.2.3. Discussions

Insufficient ductility is the primary reason for these low factors of safety, although it should be noted that this analysis assumed 4 degrees of maximum rotation in the joints, whereas ductility predictions based on the Liu *et al* (2004) method show a limit of 2.17 degrees on rotation. The results therefore suggest that fracture of a column would lead to subsequent fracture of the primary beam to column joints. Since the tensile strength of the composite decking is insufficient to bridge the damaged column, failure would progress to a tensile failure of the slab, leading to a collapse of the area of building previously supported by the damaged column.

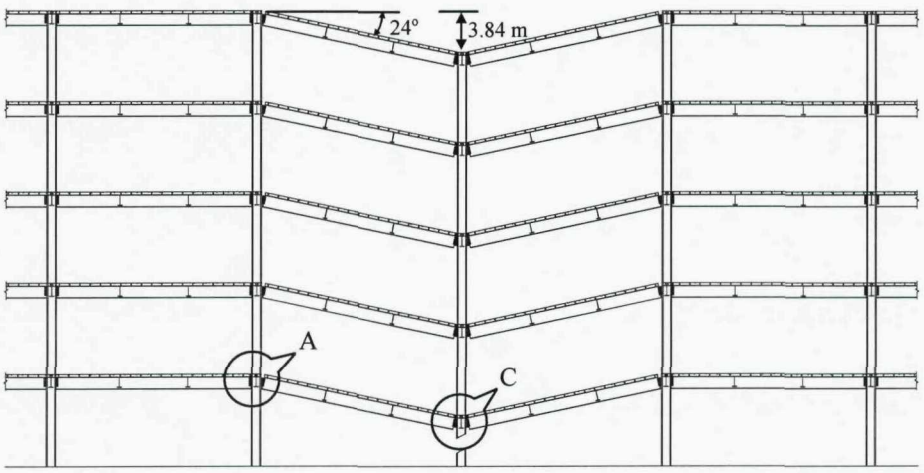

(a) Deflected shape of frame

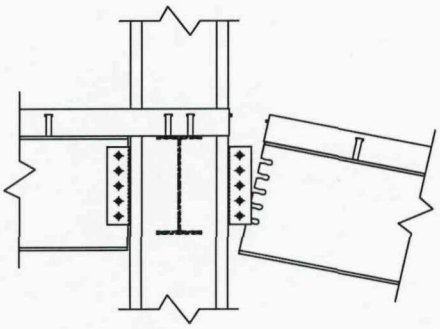

(b) Joint

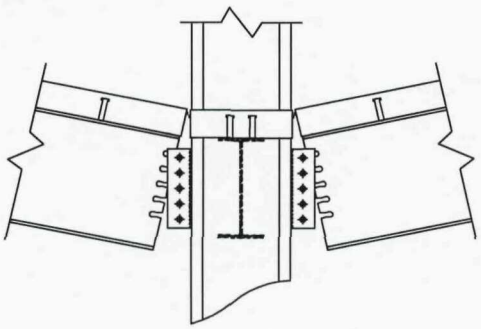

(c) Joint 'C'

Fig. 3. 23 Frame at failure

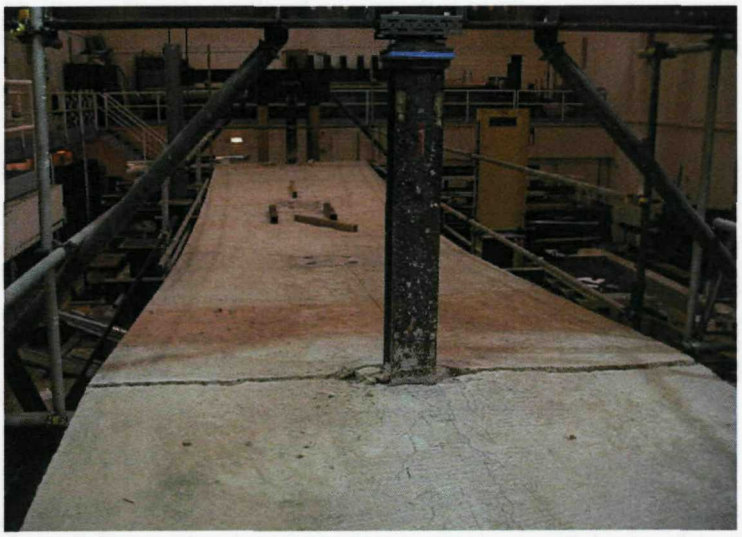

Fig. 3. 24 Crack in composite slab that led to fracture of mesh reinforcement (Byfield, 2004)

Since the factors of safety against collapse are less than 0.2 any changes to the frame layout are unlikely to alter the main finding from this investigation: that *catenary action alone will not prevent progressive collapse.* Equally, a more rigorous analysis, involving the use of dynamic FE analysis combined with full-scale testing would also not alter this finding. If catenary action is to be used to provide robustness, then joints would need to be significantly strengthened and provided with improved ductility.

The ability of other connections such as flexible end plate and double angle web cleat connections, to transfer load through catenary action was quantified in terms of factor of safety using the method presented in section 3. The factor of safety for these connections was calculated considering a DAF of 1.5 and the full tensile capacity of slab. In both the connections, the factor of safety was less than 0.1.

A response to this problem could be to improve both the strength and robustness of beam column connections. However, this may not provide the optimum solution because high strength connections increase risks from drag down. This is a process in which collapse progresses sideways as catenary forces drag down undamaged columns. This is a particular problem with the tying force method, because it is impossible to predict exactly how many columns would be destroyed by blast or impact. Therefore it is difficult to assess the design catenary forces. This problem of drag down also exists if nominally pinned connections were replaced with full-moment connections.

Whilst the provision of horizontal tying is an essential component of any good design, it should not be relied upon to provide support to damaged columns. Structures that are at high risk from blast or impact should be provided with proven emergency load paths. These could be out-rigger trusses, as used at the top of the World Trade Centre Towers, and also used in other iconic structures, such as the 2nd International Financial Centre in Hong Kong. These fail-safe systems have a proven ability to redistribute loads from damaged columns. Importantly they do not require the frame to deform significantly and therefore do not introduce dynamic amplification to the loads. They are also relatively free from the risks presented by drag-down. For these reasons procurers of high-rise buildings should be encouraged to adopt these systems.

3.3. Beam and catenary actions in semi-rigid connection frames

In multi-storey framed buildings, composite floor construction has become the dominant structural form due to its strength and stiffness, in comparison with non-composite construction. In semi-rigid frames, the flexural strength of the connections is significantly less than that of beams. In order to utilize the full strength of the beams, the redistribution from support to span is necessary which demands a significant requirement on the rotation capacity of the connections. Practical design carried out based on connection strength and ductility, as well as beam strength and the end rotation required to generate that strength. The required end rotation is necessary to achieve the design moment of 0.85 M_p. If the available rotation capacity is greater than the required rotation, the flexural strength of the beam can be increased between 0.85 and 1.0 M_p. However, it is usual to restrict the design sagging moment to $0.85M_p$ because of known problems regarding the ability of composite connections to accommodate the rotations required to achieve the full $1.0M_p$ in the span (Byfield, 2004).

When the construction is unpropped, the steel section supports the dead load alone. As a result, the beam undergoes greater strains, leading to plastification at lower imposed loads. Consequently, the beam deflects more, and imposes greater demands for end rotation. The available rotation capacity for industry standard composite connections are limited at only 32 mrad (1.80°) for S355 beams and 25 mrad (1.43°) for S275 beams (Byfield, 2004). As there is a limitation on the available rotation capacity in the design of unpropped composite beams, the maximum design sagging moment in the beam must be no greater 0.85 M_p and the ratio between the support and span moments must not be less than 0.3 (Byfield, 2004). Due to the limitation in available rotation capacity and the insufficient reserved strength for redistribution (0.85 to 1.0M_p), the semi-rigid connection cannot be able to redistribute the accidental load through beam action.

3.4. Beam and catenary actions in rigid connection frames

Unlike semi-rigid connections, rigid connections have sufficient ductility to accommodate catenary actions, as the plastic hinges form in the beam, providing the

strength of the connection exceeds that of the beam. The joint ductility helps in redistributing the support moment to the span moment. In the double span approach, the failure takes place at either column core tension field or weak panel zone as shown in Fig. 3.26. The failure at column core tension field can be avoided by maintaining discrete beam-to-beam continuity. The beam-to-beam continuity is ensured by connecting the top and bottom flange of the beams by means of plates. The dimensions of plates are mainly decided by the design sagging moment of the beam. The failure at weak panel zone is due to in-plane shear. This can be avoided by providing the diagonal plate across the zone. Due to the huge joint ductility, the frame can be able to redistribute the accidental load, after the removal of the column, provided that the column webs are strong enough against the failures which take place at core tension field and weak panel zone.

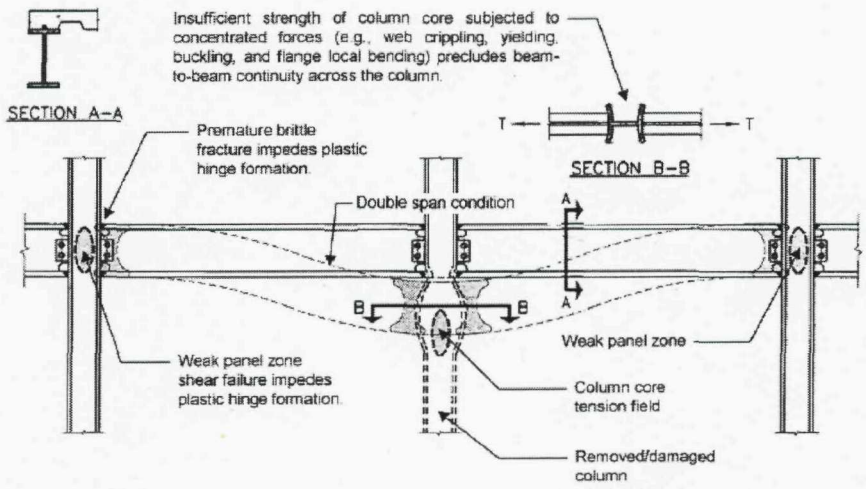

Fig. 3. 25 Double Span Approach (GSA, 2003)

3.5. Conclusions

The tying force method is a popular low cost means by which to comply with the Building Regulations concerning robustness. The tying capacity of connections is generally determined in the absence of beam rotations. When subject to the rotations required for catenary action, connections can develop a prying action that leads to rapid failure. If low ductility connections are used with the tying force method the factor of safety against collapse is estimated at less than 0.2. It is concluded that the

method will not prevent progressive collapse in steel framed buildings with simple and semi-rigid connections. In case of frames with rigid connections, the survival of the steel frame can be increased by designing the beam and beam-to-beam continuity plate for low design sagging moment (<0.85 M_p), show that the reserved strength can be utilized to overcome the loss of intermediate column.

The review of bomb damaged buildings indicates that the provision of emergency bracing is the most effective means of redistributing loads away from damaged columns. During WWII emergency bracing was provided by stiff masonry panel walling and cladding. The World Trade Centres were able to survive the immediate aftermath of the impacts partly because damaged columns were able to hang from the outrigger truss installed in the top floors. Conversely, the Murrah Building featured neither of these alternative load paths and lost approximately half of the floor area following removal by blast of three perimeter columns. It is concluded that multi-storey buildings that could pose a target for malicious actions should be provided with emergency bracing in order to redistribute column loads following localised damage, rather than relying upon catenary action as the sole means for ensuring robustness.

Chapter 4.
Dynamic Analysis for Columns subjected to Blast Load

4.1. Introduction

For medium rise multi-storey buildings, the natural period of vibration will typically be more than 1 Sec which is very high compared with the duration of a typical blast from high explosive (1-3 mSec). Hence, blast initially causes localized damage, which can lead to progressive failure in certain circumstances. As the load duration is often short in comparison with the natural period, it may be impulsive in which case a large part of the applied load is resisted by the inertia of the structure, and the stresses produced are smaller than those of similar peak pressure but longer loading duration loads. Hence, most of the response of the column occurs after the net load had diminished to zero as shown in Fig. 4.1. This illustrates the importance of dynamic analysis of the member. Beams are of secondary interest because i) failure of columns may trigger a progressive collapse and (ii) beams are often more robust in comparison with columns. The column is the main critical member for the direct blast load, as the removal of column support may result in progressive collapse. Columns can be failed by the brisance effect or shear or by bending. In RC columns, shear or compression dominated failures lead to brittle modes of failure and the flexural failure leads to a ductile mode of failure. Hence, the linear dynamic analysis may be carried out to check column shear strength and the nonlinear dynamic analysis may be appropriate for assessing the flexural strength of the column against blast load. During the dynamic analysis of blast it is usual to ignore the damping when solving the equations of motion. This assumption is considered valid because load duration is very short, whereas damping systems require time to absorb energy.
In this chapter the dynamic analysis for columns will be explained and response charts will be developed for an idealized column with a range of end support

conditions, namely (i) pinned at both ends, (ii) fixed at both ends (iii) pinned at one end and fixed at other end and (iv) fixed at one end and freed at other end (cantilever).

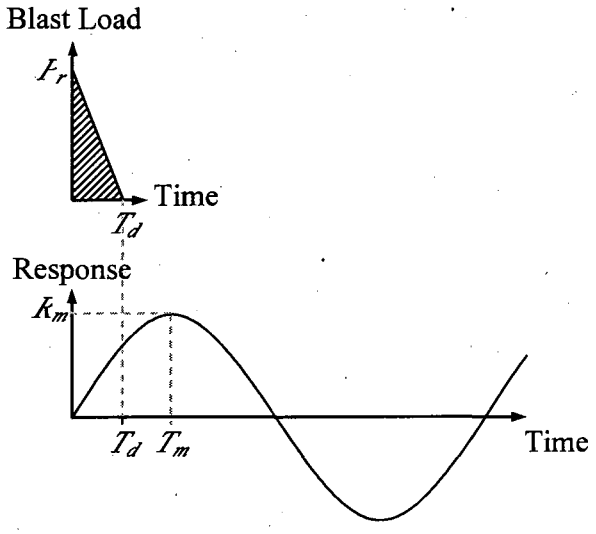

Fig. 4. 1 A typical response of column for blast load

4.2. Comparisons between linear dynamic analysis using either SDOF and MDOF systems

As the dynamic analysis of columns with axial compression is complex in nature, it can be idealized as a beam with a certain degree of end fixity depending on the beam-column stiffness. Analysis using multi degree of freedom (MDOF) and single degree of freedom (SDOF) systems is compared herein.

4.2.1. Single degree of freedom system modelling of columns

In this method, only the first mode of vibration is considered and then the equivalent SDOF system is identified by equating respective energy such as kinetic energy, potential energy and work done by the load (explained in section 4.3). For example, for a simply supported beam, the equivalent load ($P_e[t]$) is calculated by comparing the work done by two systems (Fig. 4.2) which is equal to $0.64\,P[t]$; the equivalent stiffness (K_e) is calculated by comparing the strain energy of the systems which is equal to 0.64 K; and the equivalent mass (M_e) is calculated by comparing the kinetic

energy of the systems which is equal to 0.50 M. This approximate method is explained in the book, "Introduction to Structural Dynamics" by Biggs (1964). The equations of motion are expressed for the equivalent lumped-mass single degree of freedom systems as shown in Eq. 4. 1. The response (u) of the system is obtained by solving this differential equation. If the duration of the blast is large enough i.e., $t_d > 0.371 t_n$ (Craig, 1981), the maximum response occurs before the load diminishes and the maximum response is calculated using Eq. 4.2. If the duration of the blast is very small compared with the natural vibration period, the maximum response occurs after the load diminishes and the maximum response is calculated using Eq. 4.3. Shear force and bending moments are evaluated from the free body diagram which includes inertia force also.

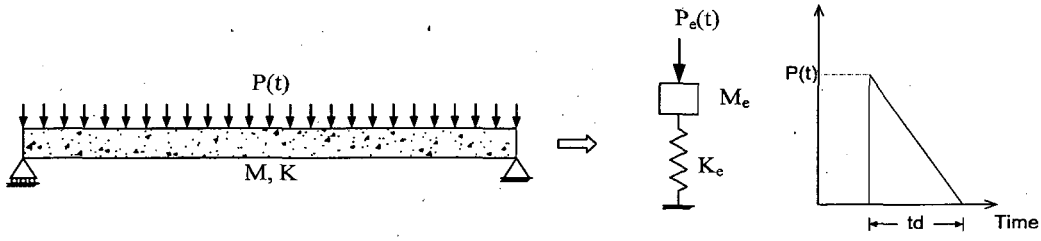

Fig. 4. 2 Single Degree of Freedom System

$$M_e \ddot{u} + K_e u = P_e[t] \tag{4.1}$$

$$u[t] = \frac{P_e[t]}{K_e}\left((1-\cos\omega t) + \frac{\sin\omega t}{\omega t_d} - \frac{t}{t_d}\right) \tag{4.2}$$

$$u[t] = \frac{P_e[t]}{K_e}\left(\frac{\sin\omega t_d}{\omega t_d} - \frac{\sin\omega(t-t_d)}{\omega t_d} - \cos\omega t\right) \tag{4.3}$$

Where,

K - Stiffness of the column

K_e - Equivalent stiffness of SDOF system

L - Length of the column

m - Mass per unit length

M_e - Equivalent mass of SDOF system

P - Peak blast load

$P[t]$ - Blast load on column per metre length at time, 't'

$P_e[t]$ - Equivalent blast load of SDOF system

t_d - Duration of blast load

u - Displacement

ω - Natural frequency of the column

Based on 'equivalent lumped-mass single degree of freedom' systems, TM 5 – 1300 provides a set of curves (based on the approximate method of Biggs (1964)) to calculate the response of real distributed mass structural elements for different loading profiles. In most dynamic structural analysis, especially earthquake analysis, the contribution of the first mode is around 80 percent of the total; hence the contribution from other modes is often neglected.

4.2.2. Multi-degree of freedom system modelling

The idealised column is a continuous system where every mass particle has its own equation of motion. This structural dynamics problem can be solved in two ways: using either the lumped mass method or the distributed mass method. In lumped mass systems, the column is discritized, typically with lumped masses; the system of ordinary differential equations governing the motion of such a system is assembled and solved. This method is ideal for computer implementations but the accuracy depends on the number of dynamic degrees of freedom of the system. In the distributed mass method, the system has an infinite number of DOF, the partial differential equation (Eq. 4.4) is developed using force equilibrium, shown in Fig. 4.3. The response $u(x,t)$ is expressed as the superposition of the response of individual modes as shown in Eq. 4.5.

$$m\frac{\partial^2 u}{\partial t^2} + EI\frac{\partial^4 u}{\partial x^4} = P[x,t] \tag{4.4}$$

$$u[x,t] = \sum_{n=1}^{\alpha} \phi_n[x]_n q[t] \tag{4.5}$$

By substituting Eqs. 4.5 in 4.4 two separate ordinary differential equations, shown in Eqs. 4.6 and 4.7 can be obtained in which one yields the spatial function (Eq. 4.8) and the other yields time function. By substituting the boundary conditions of the beam into the spatial function, the natural frequencies and mode shapes for different beams are obtained and are shown in Fig. 4.4 and Table 4.1.

$$\phi_n^{iv}[x] - \beta_n^4 \phi[x] = 0 \tag{4.6}$$

$$M_n \frac{\partial^2 [q_n[t]]}{\partial t^2} + K_n q_n[t] = P_n[t] \tag{4.7}$$

Where,

$$\beta_n^2 = \frac{\omega_n^2 m}{EI}$$

$$M_n = \int_0^L m[\phi_n[x]]^2 dx$$

$$K_n = EI \int_0^L \phi_n[x](\phi_n''[x])'' dx$$

$$P_n[t] = \int_0^L P[t]\phi_n[x] dx$$

$$\phi[x] = A\sin\beta x + B\cos\beta x + C\sinh\beta x + D\cosh\beta x \tag{4.8}$$

This standard derivation is available in many textbooks, such as Chopra (2001), Craig (1981), Clough (1995) and Biggs (1964). If we consider the simple form of a simply supported beam, the natural frequency (Eq. 4.9) and mode shapes (Eq. 4.10) are obtained by substituting the boundary conditions such as zero bending moment at both ends and zero deflections at both ends.

$$\omega_n = \frac{n^2\pi^2}{L^2}\sqrt{\frac{EI}{m}} \tag{4.9}$$

$$\phi_n[x] = A_n \sin\frac{n\pi x}{L} \tag{4.10}$$

Where,

A, B, C and D – integration constant

A_n - Amplitude of n^{th} mode

E - Modulus of elasticity of concrete

I - Moment of inertia about bending axis

L - Length of the column

m - Mass per unit length

n - Mode number

$P[t]$ - Blast load on column per metre length at time, 't'

$q[t]$ - Time function

t_d - Duration of blast load

u - Displacement

ω_n - Natural frequency of n^{th} mode

$\phi_n[x]$ - Spatial function of mode shape

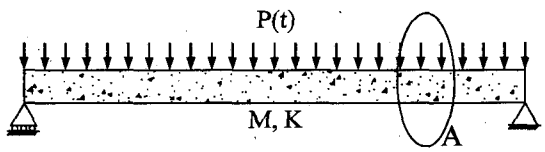

(a) Simply supported beam

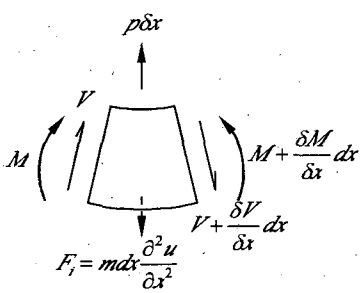

(b) Section at A

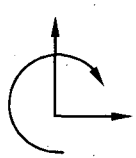

(c) Sign conversion (positive)

Fig. 4. 3 Multi-degree of freedom system

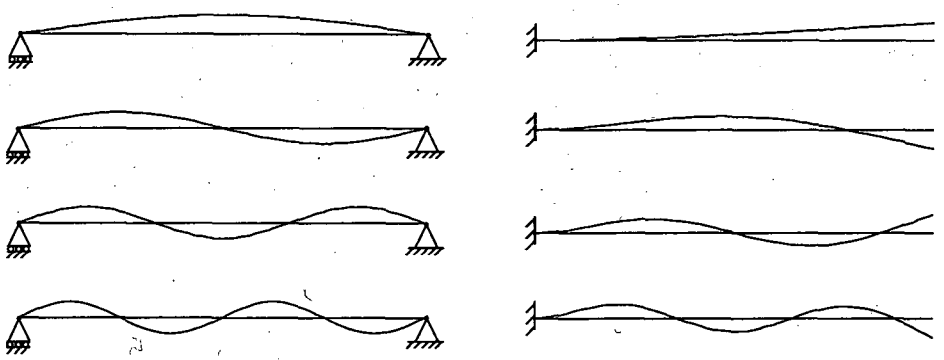

(a) Simply Supported Beam (b) Cantilever Beam

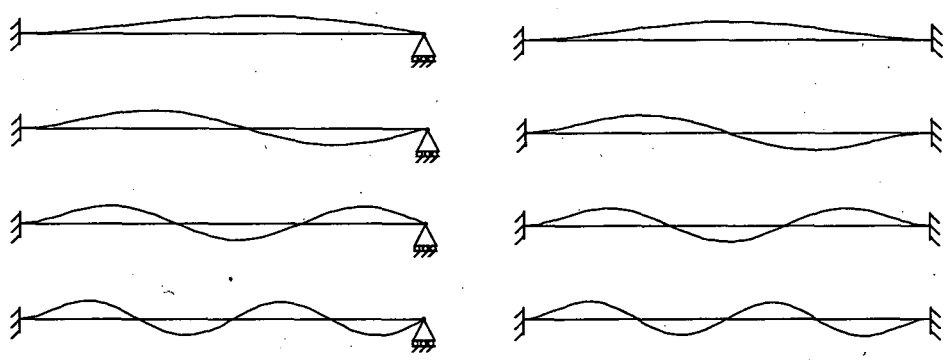

(c) Propped Beam (d) Fixed Beam

Fig. 4. 4 First 4 mode shapes for different beams

Table 4. 1 Natural Frequency and mode shape

Type of Beam	Natural Frequency (ω_n)	Mode shape (φ_n)
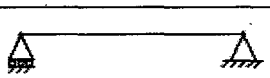	$\frac{\pi^2 n^2}{L^2}\sqrt{\frac{EI}{m}}$	$\phi_n[x] = \sin\left[\frac{n\pi x}{L}\right]$
	$\frac{\pi^2(4n+1)^2}{16L^2}\sqrt{\frac{EI}{m}}$	$\phi_n[x] = \cos[\beta_n x] - \cosh[\beta_n x] + k_n(\sinh[\beta_n x] - \sin[\beta_n x])$ *where,* $k_n = \frac{\cos[\beta_n L] - \cosh[\beta_n L]}{\sin[\beta_n L] - \sinh[\beta_n L]}$ $\beta_n = \frac{\pi(4n+1)}{4L}$
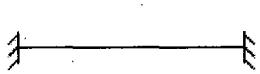	$\frac{\pi^2(2n+1)^2}{4L^2}\sqrt{\frac{EI}{m}}$	$\phi_n[x] = \cos[\beta_n x] - \cosh[\beta_n x] - k_n(\sin[\beta_n x] - \sinh[\beta_n x])$ *where,* $k_n = \frac{\cos[\beta_n L] - \cosh[\beta_n L]}{\sin[\beta_n L] - \sinh[\beta_n L]}$ $\beta_n = \frac{\pi(2n+1)}{2L}$

	$\frac{3.516}{L^2}\sqrt{\frac{EI}{m}}$ $n=1$ $\frac{22.03}{L^2}\sqrt{\frac{EI}{m}}$ $n=2$ $\frac{61.70}{L^2}\sqrt{\frac{EI}{m}}$ $n=3$ $\frac{120.9}{L^2}\sqrt{\frac{EI}{m}}$ $n=4$ $\frac{\pi^2(2n-1)^2}{4L^2}\sqrt{\frac{EI}{m}}$ $n\geq 4$	$\phi_n[x]=\cosh[\beta_n x]-\cos[\beta_n x]-k_n(\sinh[\beta_n x]-\sin[\beta_n x])$ *where,* $k_n=\frac{\cosh[\beta_n L]+\cos[\beta_n L]}{\sinh[\beta_n L]+\sin[\beta_n L]}$ $\beta_n=\frac{\pi(2n-1)}{2L}$

The response (u) is obtained by combining the time and spatial functions. As mentioned earlier, if the duration of the blast is large enough, the maximum response occurs before the load diminishes and the maximum response of an idealized column which is pinned at both ends is calculated using Eq. 4.11. If the duration of the blast is very small compared with the natural vibration period, the maximum response occurs after the load diminishes and the maximum response of idealized column which is pinned at both ends is calculated using Eq. 4.12. These equations were solved using the programme called Mathematica, a tool that has been used for the analysis presented throughout this thesis.

$$u[x,t]=\frac{-4PL^2}{\pi^5 EI}\sum_{n=1,3,5,\ldots}^{\alpha}\frac{1}{n^5}\left(\frac{\sin[\omega_n t]}{\omega_n t_d}-\cos[\omega_n t]+\frac{t_d-t}{t_d}\right)\sin\left[\frac{n\pi x}{L}\right] \qquad (4.11)$$

$$u[x,t]=\sum_{n=1,3,5,\ldots}^{\alpha}\left(\frac{u_n[t_d]}{\omega_n}\sin[\omega_n(t-t_d)]+u_n[t_d]\cos[\omega_n(t-t_d)]\right)\sin\left[\frac{n\pi x}{L}\right] \qquad (4.12)$$

Where,

$$u_n[t=t_d]=\frac{2P}{mL\omega_n^2\pi}\frac{\left((-1)^n-1\right)}{n}\left[\frac{\sin[\omega_n t_d]}{\omega_n t_d}-\cos[\omega_n t_d]\right]$$

$$\dot{u}_n[t=t_d]=\frac{2P}{mL\omega_n\pi}\frac{\left((-1)^n-1\right)}{n}\left[\frac{\cos[\omega_n t_d]}{\omega_n t_d}-\sin[\omega_n t_d]-\frac{1}{\omega_n t_d}\right]$$

Shear forces and moments are calculated from the displacement function by solving the governing differential equations (beam equations). The maximum responses are expressed as follows.

$$u_{\max}=\alpha_d\frac{P}{K} \qquad (4.13)$$

$$M_{max} = \alpha_m (PL) \quad (4.14)$$

$$S_{max} = \alpha_s (P) \quad (4.15)$$

Where,

u_{max} - Maximum displacement at mid span of column

M_{max} - Maximum bending moment at mid span of column

S_{max} - Maximum shear force at support of column

K - Flexural stiffness of column

L - Length of column

P - Total load on column

α_d - Deflection coefficient

α_m - Bending moment coefficient

α_s - Shear force coefficient

4.2.3. Comparison of SDOF and MDOF systems

The above responses are the function of the ratio of the duration of load (T_d) to the natural vibration period (T_n). Considering both systems, the responses for the idealized column with different end conditions are calculated for different T_d/T_n values using Mathematica and the response charts are prepared and compared. The response charts for an idealized column, pinned at both ends are shown in Figs. 4.5 to 4.7. Fig 4.5 shows very little variation in the deflection predictions between SDOF and MDOF systems (i.e., the deflection contributions from higher modes are negligible), since the equations (Eq. 4.11 and 4.12) governing deflection converge very fast as it has n^5 in the denominator. Contrary, the SDOF system model underestimates bending moment and shear force as shown in Figs 4.6 and 4.7 (i.e., the contributions from higher modes are significant), as the equations governing shear force and bending moment converge slowly compared with the equations governing deflection (n^5 in the denominator) as they have only n^2 and n^3 in the denominator respectively. Therefore, the range of T_d/T_n for columns is explored for blast, located at safe stand off distance (defined as the minimum stand off distance required to save the column from the blast) such that it loads the columns just close

to failure. The safe stand off distances for different columns and charge weights are calculated using the method, presented in chapter 6. The blast load for these columns is estimated using the method, presented in chapter 5 and T_d/T_n is estimated (Table 4.2). The results show that T_d/T_n widely varies from 0.03 to 0.16. The error in the response of SDOF system is plotted against T_d/T_n and shown in Fig. 4.8. The plot shows that the SDOF system underestimate shear by 20 to 50% and moment by 10 to 20%, therefore one might consider increasing shear force, calculated using such SDOF methods, by 50% to account for the higher modes. This approximation is crude but likely to be safe. At the same time, the SDOF system model can be used to estimate the dynamic bending moment.

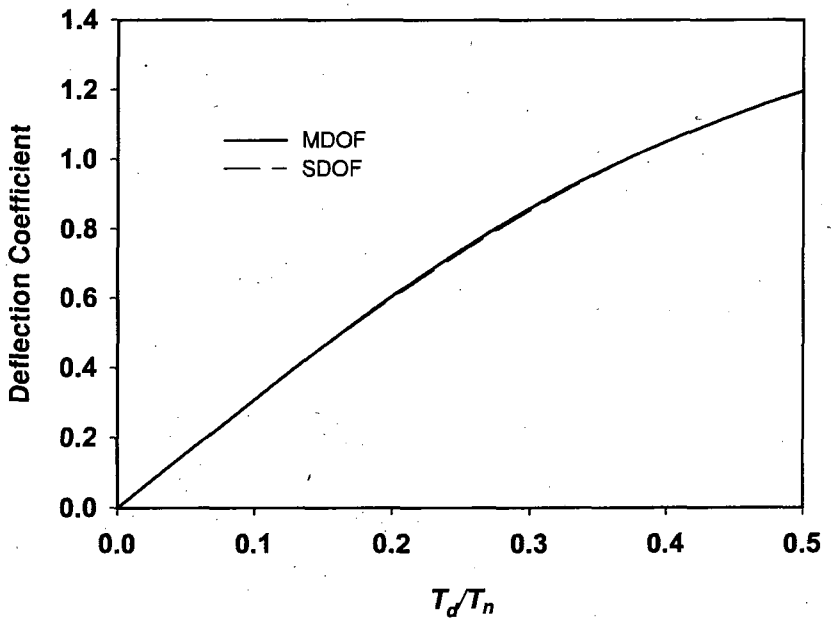

Fig. 4. 5 Maximum deflection of idealized column, pinned at both ends

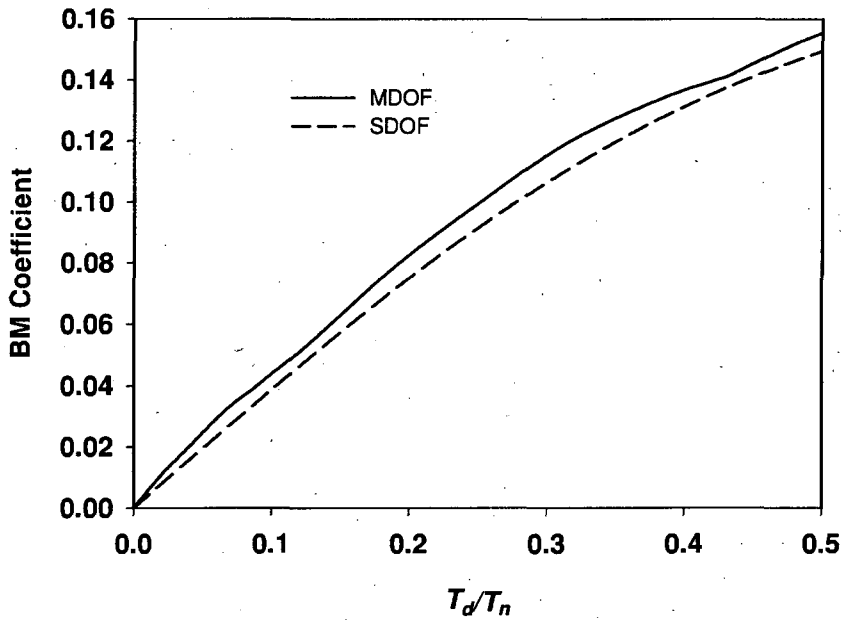

Fig. 4. 6 Maximum bending moment of idealized column, pinned at both ends

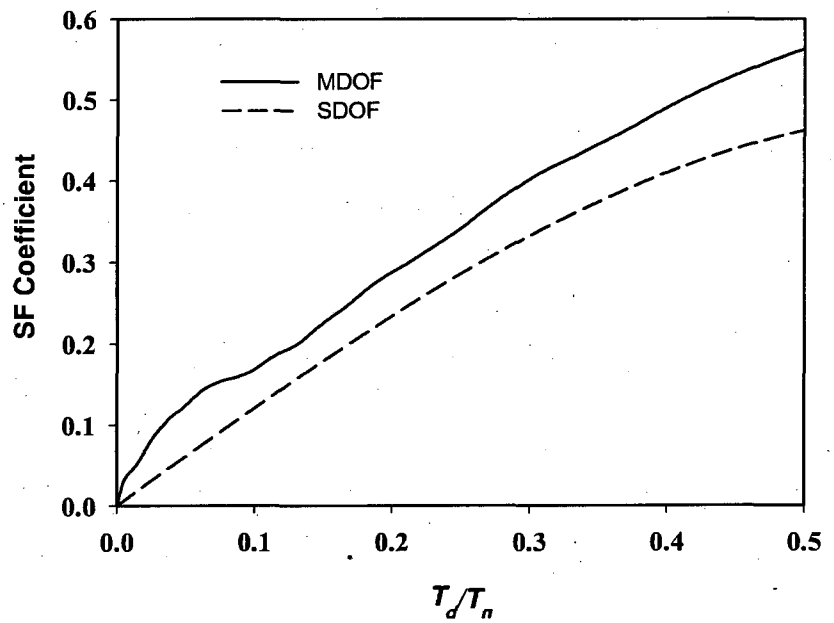

Fig. 4. 7 Maximum shear force of idealized column, pinned at both ends

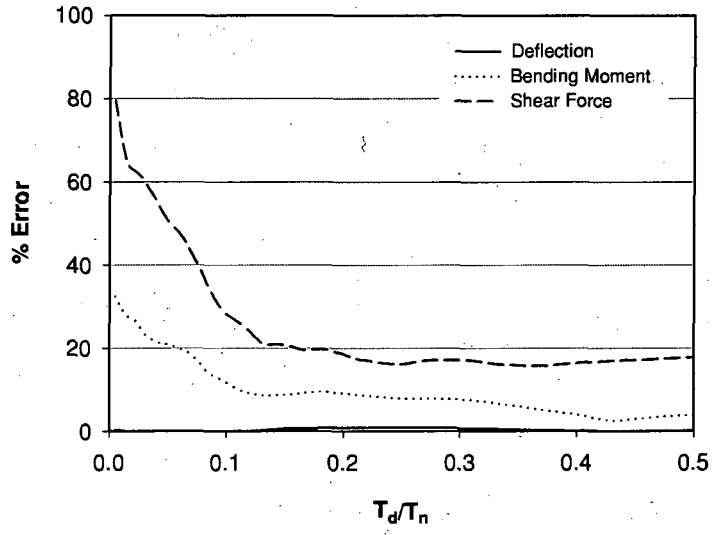

Fig. 4. 8 Percentage error in SDF system's responses of idealized column, pinned at both ends

Table 4. 2 T_d/T_n for different columns and blast

Column ID	Charge weight (kg)	Stand off distance (m)	Breadth (mm)	Depth (mm)	Length (m)	Duration of blast load, t_d (mSec)	Natural time period, t_n (mSec)	t_d/t_n
1	998	21.9	406	406	4.27	2.90	0.09	0.09
2	1814	26.8	406	406	4.27	3.33	0.11	0.11
3	1814	23.0	457	457	4.27	3.12	0.11	0.11
4	454	14.8	610	610	4.27	2.68	0.13	0.13
5	454	14.0	610	610	4.27	2.56	0.12	0.12
6	408	19.5	305	305	5.49	2.37	0.03	0.03
7	1814	23.8	813	813	5.49	3.96	0.16	0.16
8	998	20.7	356	356	4.83	2.69	0.07	0.07

The Mathematica programmes for dynamic analysis and the response charts for idealized column with different boundary conditions are given in the appendix A2.1 to A2.3. The MDOF curve (Fig. 4.7) in this range is observed to be markedly kinked. The reason for this is interesting and is explained by way of figures 4.9 and 4.10. When T_d/T_n is equal to 0.025 there is no phase difference between the maximum shear response of the system and the 1st mode (Fig. 4.9(a)). In contrary, when T_d/T_n is equal to 0.10, there is a phase difference between the maximum shear response of the system and 1st mode (Fig. 4.9(b)). The reason is that the maximum response occurs after t_d time even for higher modes, when T_d/T_n is less than 0.05. This phase lacking in the maximum shear response of the 1st mode creates kinks in the shear response after T_d/T_n=0.05, as explained in Fig. 4.10.

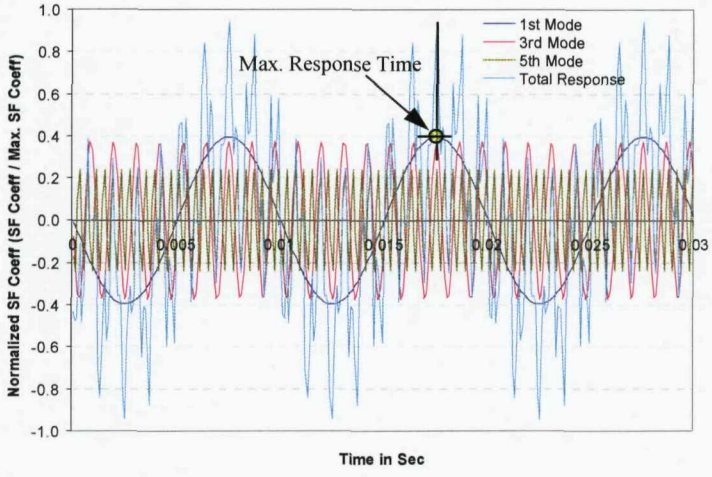

(a) $T_d/T_n = 0.025$

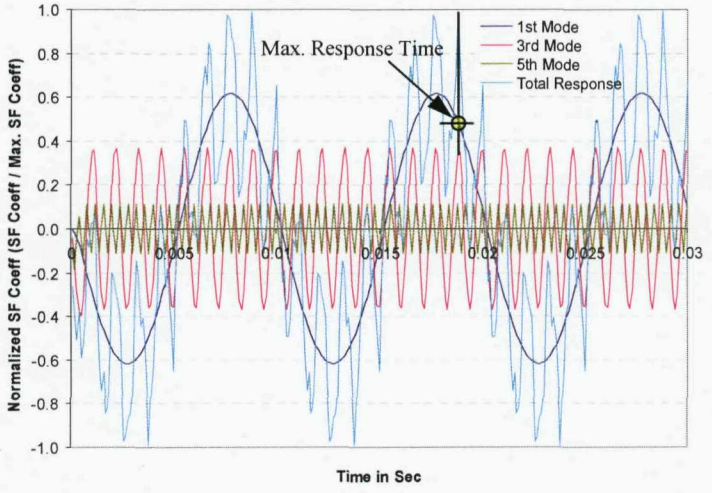

(b) $T_d/T_n = 0.10$

Fig. 4. 9 Shear contribution of modes Vs Time

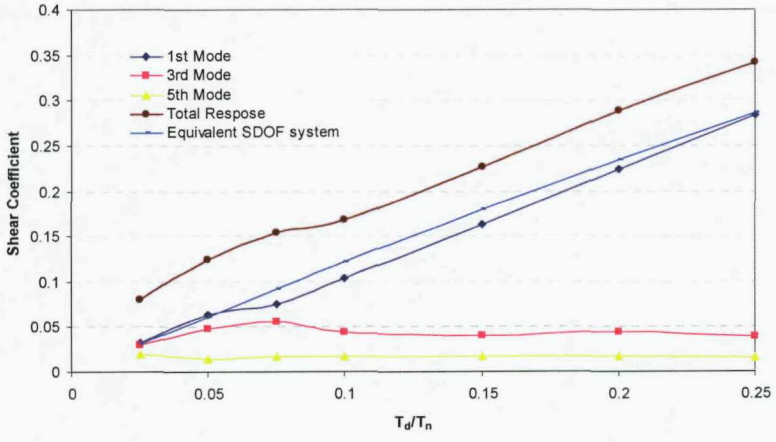

Fig. 4. 10 Mode's shear contribution in total shear response of the system

It is clear from the analysis that the SDOF system model is capable of accurately modelling deflection but is less accurate with moments and less accurate still with

shear. This is well explained through Figs 4.13 and 4.14. The normalized shear force of higher modes is comparable with that of first mode (4.13 (c)) and can not be neglected. Contrary, the normalized deflection of higher modes is negligible, compared with that of first mode, as shown in Figs 4.13 and 4.14. This is the main reason SDOF models can significantly underestimate shear force and bending moment, where little error is present for (maximum) deflection. Therefore, the contribution from higher modes cannot be neglected in the case of blast loading in which $T_n >> T_d$. For example, when $T_d/T_n = 0.025$, the shear contribution from the 1st and 2nd modes is almost equal (Fig. 4.11). Hence the shear force from the SDF system model is 60 percent less than that from the MDF system. However as T_d approaches T_n the shear contribution from the higher modes become less important. For example, Fig. 4.12 shows $T_d/T_n = 0.5$, in which high modes of vibration produce little effect on shear force and bending moment In conclusion, if T_d/T_n is less than 0.1, the SDF system will significantly underestimate shear force and bending moment.

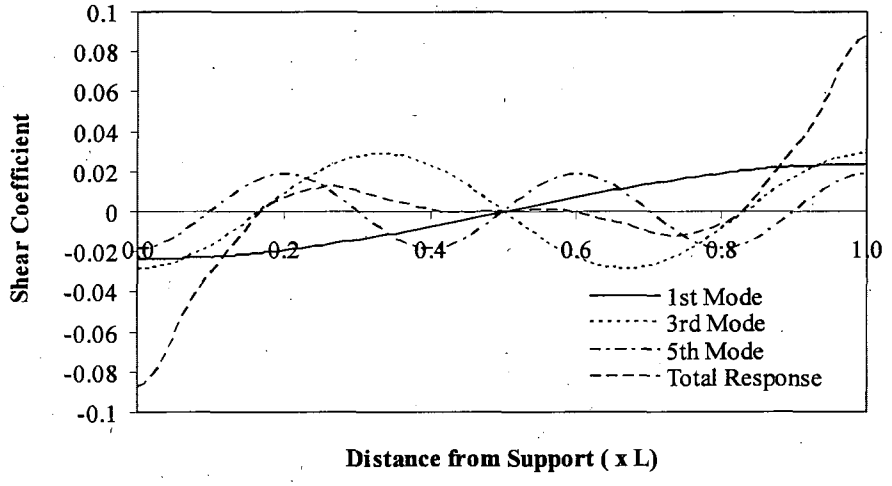

Fig. 4. 11 Maximum Shear Response at $T_d/T_n = 0.025$

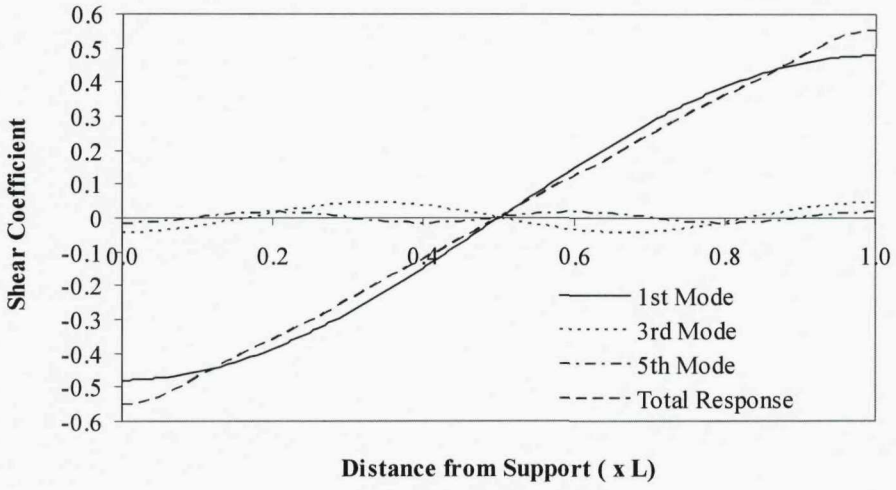

Fig. 4. 12 Maximum Shear Response at T_d/T_n = 0.50

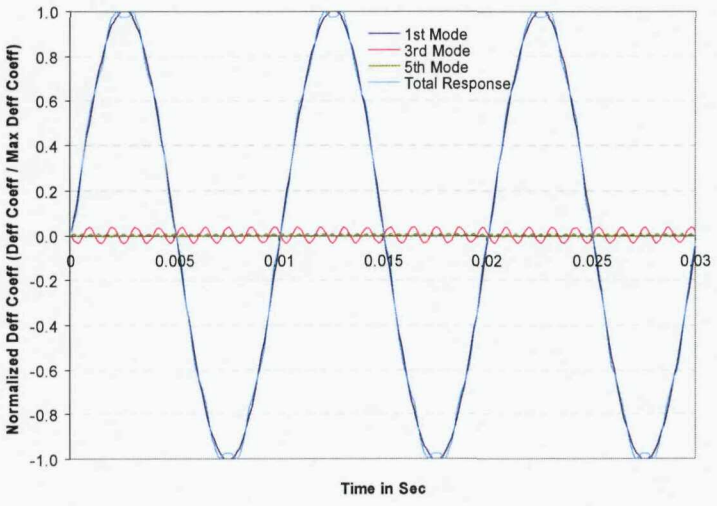

(a) Deflection Coefficient

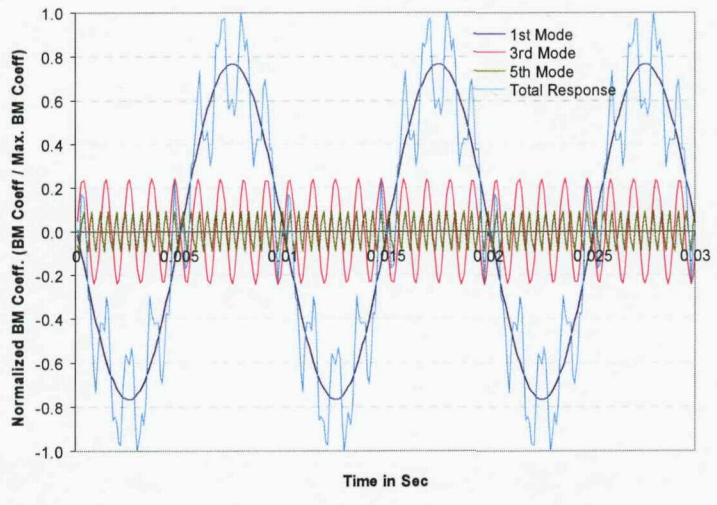

(b) Bending Moment Coefficient

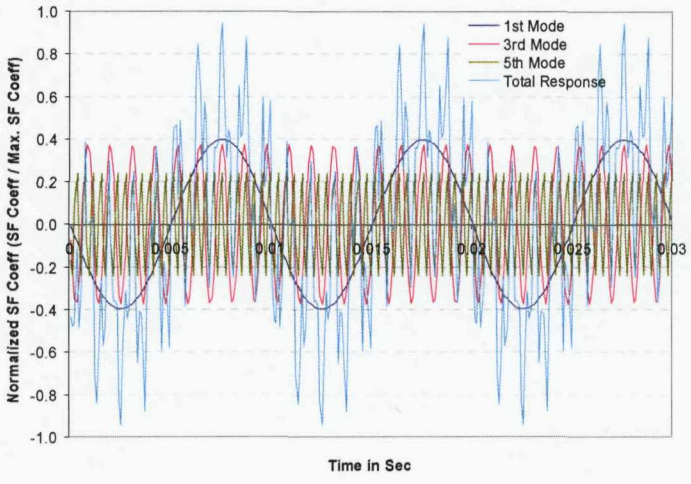

(c) Shear Force Coefficient

Fig. 4. 13 Response of idealized column, pinned at both ends at $T_d/T_n = 0.025$

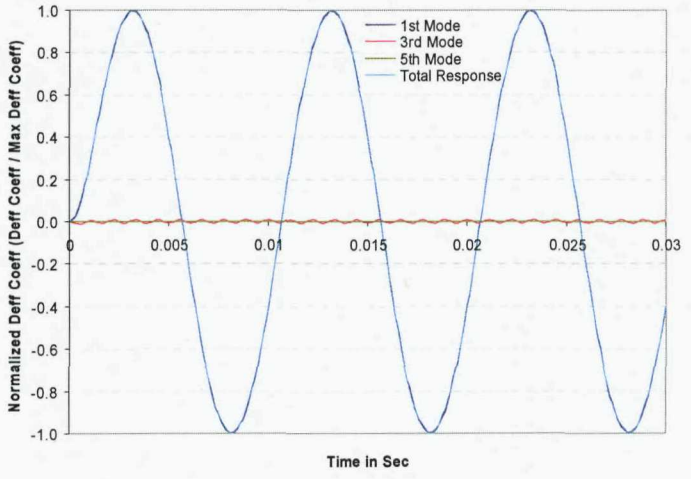

(a) Deflection Coefficient

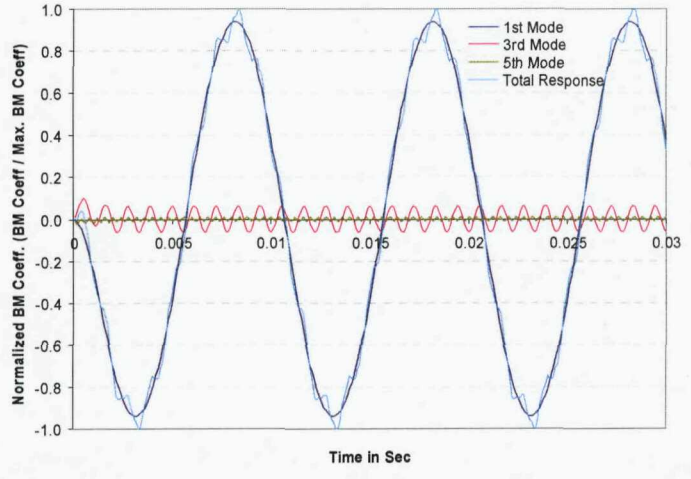

(b) Bending Moment Coefficient

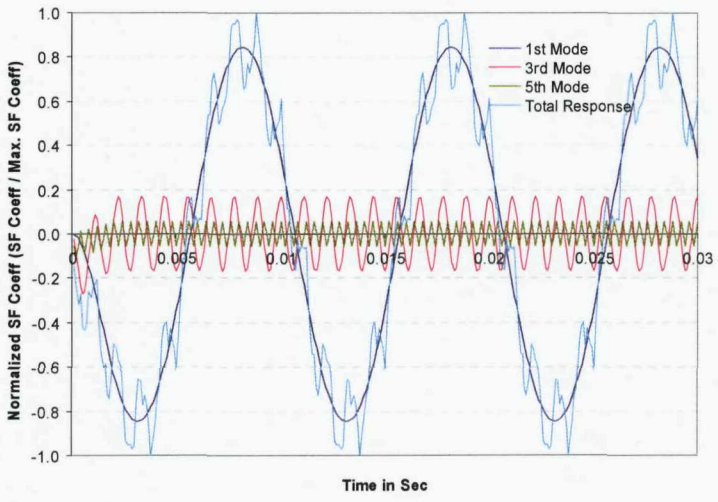

(c) Shear Force Coefficient

Fig. 4. 14 Response of idealized column, pinned at both ends at $T_d/T_n = 0.20$

4.3. Nonlinear dynamic analysis considering SDOF

Ductility of columns

Ductility is the capacity of members to undergo considerable plastic deformation without loss of strength capacity and is also a measure of the energy absorption capacity. The best way to quantify ductility is through either deformation, or deflection, or rotation. Here, the ductility is defined as the ratio of total deflection to elastic deflection, i.e., $\left(x_p / x_e \right)$. The concept of ductility is linked to the moment redistribution capacity and, consequently, the safety of the structure. The typical force-displacement curve for a column is shown in Fig. 4.15. In reality, the column deforms beyond its elastic limit, until the plastic collapse mechanism is formed. The region, OA represents the elastic behaviour. At point-A, the plastic hinge is formed in the support. After this point, the support moment is redistributed to the mid-span due to free rotation at support. In the region AB, the complete span is elastic apart from support. At point B, the plastic hinge is formed in the mid-span in the case of fixed supports and 0.58 L from support in the case of propped cantilever column as shown in Figs. 4.16 and 4.17. After point B, the small increment of force leads to plastic deformation, represented by region BC.

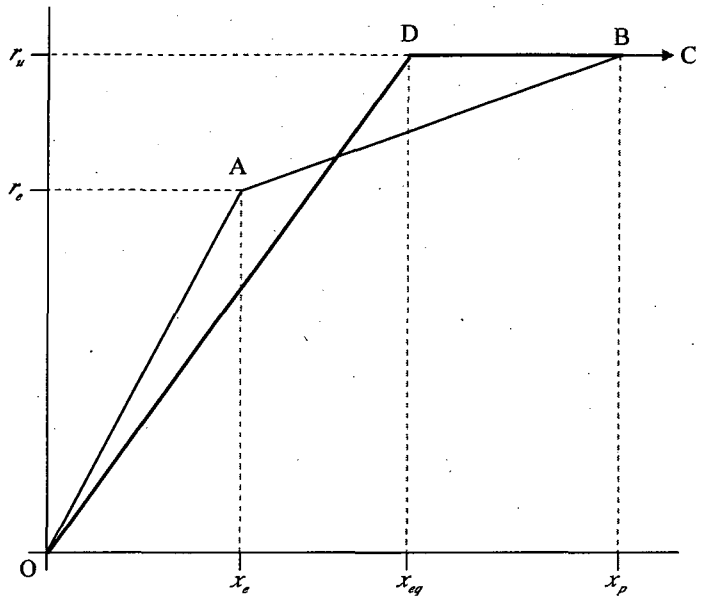

Fig. 4. 15 Resistance-deflection function

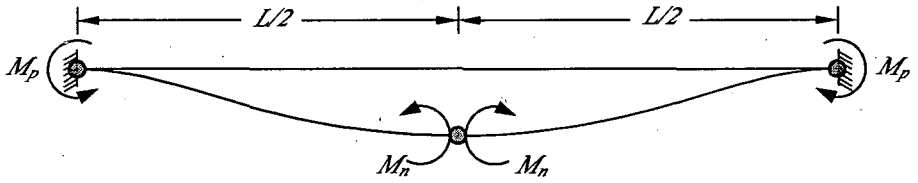

Fig. 4. 16 Plastic analysis of column, fixed at both ends

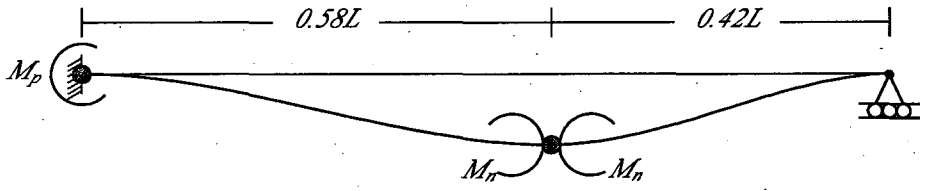

Fig. 4. 17 Plastic analysis of column, fixed at one end and pinned at other end

In the nonlinear analysis, the plastic region (the region after B) is ignored and the resistance function is considered until the elasto-plastic phase (upto point B). In case of pinned columns, there is no way redistributing the mid span moment, hence the elastic analysis is used to estimate safe stand off distance (Chapter 6). In the case of the columns, fixed at both ends and fixed at one end and pinned at other end, the detailed elasto-plastic analysis is carried out and the response charts are prepared. These charts will be used to estimate the safe stand off distance considering flexural failure of these columns (Chapter 6). The resistance-deflection function can be replaced by the bilinear function, ODB, so that the area under this curve is equal to

the area under the curve OAB (Smith, P. D., 2003)). The slope of line, OD is termed as equivalent elastic stiffness.

The elastic resistance (i.e. force) and deflection is calculated from simple structural analysis. As the support rotates freely after the formation of plastic hinge at the supports, the increment in deflection, due to increment in load after the elastic phase is calculated considering the column, pinned at both ends from simple structural analysis. In columns the flexural capacity of mid and end sections is same i.e., $M_n = M_p = M$. Tables 4.3 and 4.4 shows the key points of resistance-deflection function for the column with different boundary conditions.

Table 4. 3 Resistance-deflection function for column, fixed at both ends

Phase	Resistance	Deflection
Elastic (Point, A)	$r_e = \frac{12M}{L^2}$	$x_e = \frac{r_e L^4}{384EI}$
Plastic (Point, B)	$r_u = \frac{16M}{L^2}$	$x_p = \frac{5(r_u - r_e)L^4}{384EI} + x_e$
Equivalent Elastic (Point, D)	$r_u = \frac{16M}{L^2}$	$x_{eq} = \frac{r_{eq} L^4}{307EI}$

Table 4. 4 Resistance-deflection function for column, fixed at one end and pinned at other end

Phase	Resistance	Deflection
Elastic (Point, A)	$r_e = \frac{8M}{L^2}$	$x_e = \frac{r_e L^4}{185EI}$
Plastic (Point, B)	$r_u = \frac{12M}{L^2}$	$x_p = \frac{5(r_u - r_e)L^4}{384EI} + x_e$
Equivalent Elastic (Point, D)	$r_u = \frac{12M}{L^2}$	$x_{eq} = \frac{r_{eq} L^4}{160EI}$

The ductility of 1.6 and 1.27 is estimated for the columns, fixed at both ends and fixed at one end and pinned at other end respectively. TM 5-1300 suggests the maximum ductility columns should not exceed 3, hence the estimated ductility is within this working limit.

Equivalent SDOF system

As there is little difference in the bending moments obtained from MDOF and SDOF systems (Fig. 4.6), the SDOF system is used to estimate the elasto-plastic responses. The first step in the analysis is, identifying the equivalent SDOF system for columns with different boundary condition. As mentioned in Section 4.2.1, mass, load and stiffness factors $(K_m, K_L \text{ and } K_s \text{ respectively})$ are calculated by comparing kinetic energy, work done and strain energy of the two systems. In the first step of the calculation, the suitable displacement function is obtained depending on boundary conditions of the column. For example, the displacement function for pinned columns subjected to uniformly distributed load can be expressed as $\frac{16w}{384EI}\left(L^3x-2Lx^3+x^4\right)$ with central displacement of $Y_o=\frac{5wL^4}{384EI}$. This function is rewritten in terms of central displacement, i.e., $\frac{16}{5L^4}\left(L^3x-2Lx^3+x^4\right)Y_o$, because the maximum displacement of the column is considered to be equal to the displacement of the SDOF system (Y_o). Similarly, the displacement functions for other columns with different boundary conditions are given in Table 4.4. After obtaining the displacement function, $K_m, K_L \text{ and } K_m$ are estimated by equating kinetic energy, work done and strain energy (the equations to estimate these quantities given in Table 4.4) of two systems respectively. The method to estimate these factors is explained comprehensively in TM 5-1300 and it is summarized in Table 4.5 and 4.6.

Table 4. 5 Transformation of MDOF system to SDOF system

Description	MDOF system	SDOF system
Deflection (elastic analysis):		
Pinned at both ends	$\frac{16}{5L^4}\left(L^3x-2Lx^3+x^4\right)Y_o$	Y_o
Fixed at both ends	$\frac{16}{L^4}x^2\left(L-x\right)^2Y_o$	Y_o
One end fixed and other end pinned	$\frac{185}{48L^4}x^2\left(3L^2-5Lx+2x^2\right)Y_o$	Y_o
Deflection (elasto-plastic analysis): Fixed at both ends & One end fixed and other end pinned	$\frac{16}{5L^4}\left(L^3x-2Lx^3+x^4\right)Y_o$	Y_o
Deflection (plastic analysis):		
Pinned at both ends & Fixed at both ends	$\begin{cases}\frac{x}{L/2}Y_o & x\le L/2\\ \frac{(x-L)}{L/2}Y_o & x\ge L/2\end{cases}$	Y_o
One end fixed and other end. pinned	$\begin{cases}\frac{x}{0.58L}Y_o & x\le 0.58L\\ \frac{(x-L)}{0.42L}Y_o & x\ge 0.58L\end{cases}$	Y_o
Work done	$\int_0^L p(t)y(x)\,dx$	$K_L p(t) Y_o$
Strain Energy	$\frac{EI}{2}\int_0^L\left(\frac{d^2y}{dx^2}\right)^2 dx$	$\frac{1}{2}K_s K Y_o^2$
Kinetic Energy	$\frac{1}{2}\int_0^L m\left(\frac{dy}{dt}\right)^2 dx$	$\frac{1}{2}K_m mL\left(\frac{dY_o}{dt}\right)^2$

Table 4. 6 Transformation factor

Boundary Condition	Mass factor K_m	Stiffness factor K_s	Load factor K_L
Pinned at both ends			
elastic	0.50	0.64	0.64
plastic	0.33	0.50	0.50
Fixed at both ends			
elastic	0.41	0.53	0.53
elasto-plastic	0.50	0.64	0.64
plastic	0.33	0.50	0.50
One end fixed and other end pinned			
elastic	0.45	0.58	0.58
elasto-plastic	0.50	0.64	0.64
plastic	0.33	0.50	0.50

Where,

K_e - Stiffness factor for SDOF system

K_L - Load factor for SDOF system

K_m - Mass factor for SDOF system

M - Ultimate moment capacity of column section.

M_n - Ultimate moment capacity at mid span region

M_p - Ultimate moment capacity at support

$r(x)$ - Resistance function

r_u - Ultimate resistance

w - Uniformly distributed load on column

x_e - Elastic displacement

x_u - Total displacement

x_{eq} - Equivalent stiffness of elasto plastic system

Y_o - Maximum displacement at time, '*t*'

Nonlinear Dynamic Analysis

The linear dynamic analysis of SDOF systems is explained in section 4.2.1. In the dynamic equation for SDOF systems (Eq. 4.1), $K_e\mu$ represents resistance and can be replaced by the function $r(x)$. Eq. 4.1 becomes,

$$K_m M\ddot{x} + K_e r(x) = K_L P[t] \tag{4.16}$$

$r(x)$ represents the bilinear resistance deflection curve (ODB), shown in Fig. 4.15 and can be mathematically formulated as follows,

$$r(x) = \begin{cases} \dfrac{r_u}{x_{eq}} x & x \le x_{eq} \\ r_u & x > x_{eq} \end{cases} \tag{4.17}$$

Eq. 4.16 is solved using mathematica and the response curves, (i) T_d/T_n vs ductility (x_p/x_{eq}) and (ii) T_d/T_n vs (r_u/P) are plotted (Fig 4.18 and 4.19).

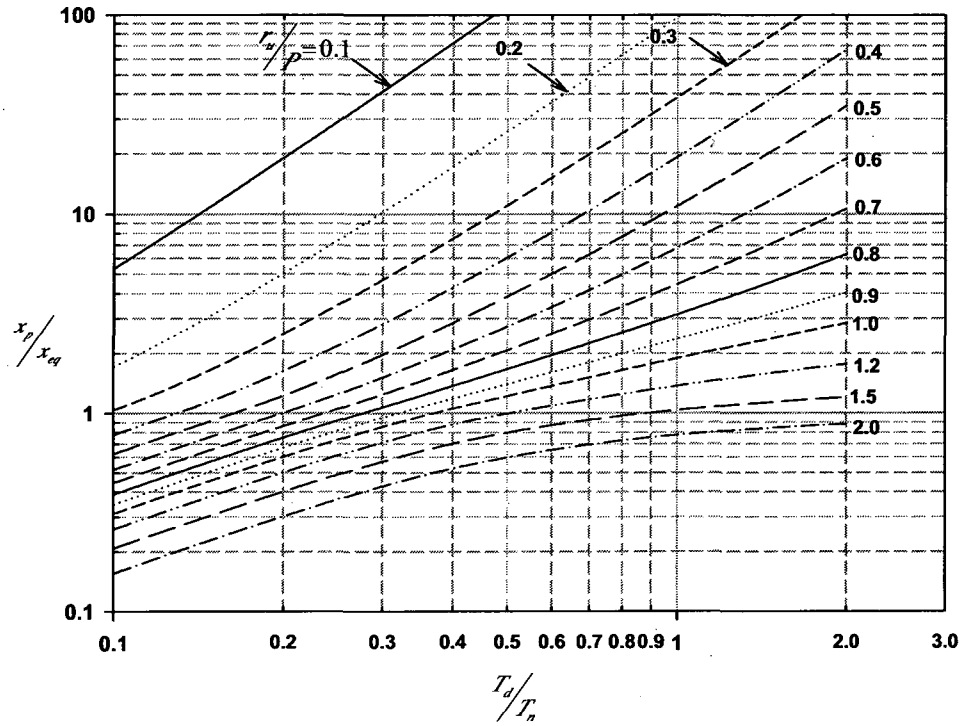

Fig. 4. 18 T_d/T_n vs ductility (x_p/x_{eq})

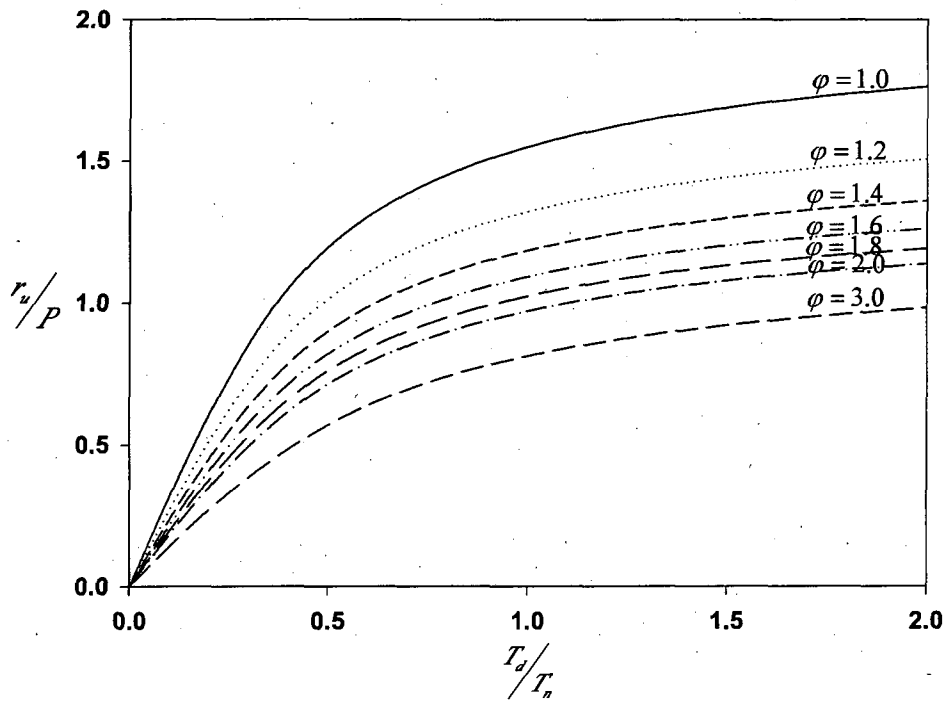

Fig. 4. 19 T_d/T_n vs (r_u/P)

From Fig. 4.19, the resistance of the columns is estimated for its ductility and the ratio of the blast duration and its natural time period.

4.4. Conclusions

The response of columns subjected to blast has been compared between SDOF and MDOF models. This showed that when the ratio of the duration of blast load (T_d) to the natural vibration period (T_n) is greater than 0.1, the contribution from the higher modes can be neglected to simplify the analysis, hence SDOF models are sufficiently accurate. However, when T_d/T_n is less than 0.1, the SDOF systems were shown to underestimate shear force by approximately 50%. Whilst deflections and moments were comparable with those from MDOF solutions for most columns when blast occurs at a distance close to that required for failure, T_d/T_n will be in the 0.05 to 0.15 region. For example T_d/T_n for the failed columns, G16 and G24 of the Murrah Buildings are 0.07 and 0.11 respectively. Therefore, this lack of conservation inherent in SDOF analysis does have design implications, with most of the design guidelines such as TM 5-1300 based on SDOF system analysis. Therefore one might

consider increasing shear force, calculated using such SDOF methods, by 50 % to account for the higher modes. This approximation is crude but likely to be safe.

Chapter 5.

Protective Design for RC Framed Structures with a Case Study of the Murrah Building

5.1. Introduction

Disproportionate collapse can be avoided through either: provision of a safe stand off distance, indirect design or direct design. A description and the limitation of these methods are explained below, with the level of protection against malicious use of high explosives indicated by the use of the ***** system, 5* being highest and * lowest:

Table 5. 1 Level of protection

Level of Protection against Progressive Collapse	Description	Pros & Cons
(1) Safe Stand off Distance (5*)	Possible threat is measured and the safe stand off distance is maintained	**Pros:** highest level of protection. **Cons:** It may not be possible to maintain the safe stand off distance due to either uneconomic or constrained land.
(2) Direct Design (i) Alternate Load Path method (a) Outrigger	Localised damage to the	**Pros:** highest level of

Truss Method (5*)	frame is accepted. The columns above the damaged frames suspended from the outrigger trusses. In the case of WTC 1 and 2, the outrigger trusses installed between the 105^{th} and 110^{th} floors provided the alternate load path.	protection. **Cons:** All the column joints such as splicing or lapping need must be designed to transfer tensile forces from the damaged columns. The out-rigger system is redundant except in an emergency.
(b) Double Span Method (4*)	Localised damage to the frame is accepted. The load from the damaged frames is transferred to the adjacent columns through beam and/or catenary actions. US General Service Administration (2003) advocates this method.	**Pros:** Simple method and the level of protection are satisfactory. **Cons:** Severe problems could be encountered if support to more than one column removed, as it was the case in the Murrah Building. Such an incident could cause collapse of floor area supported by the damaged columns. The full moment joints could cause drag-down of undamaged columns. Reliance on full moment joints is costly.
(ii) Key Element Method (3*)	In this approach, the key elements are designed for the uniformly distributed load of $34kN/m^2$. This load is applicable in any direction (BS 6399 – 1 and BS-EN 1991-1:2006).	**Cons:** This load is arrived from the gas explosion. Now days, the buildings have high risk of experiencing vehicle bomb, hence this approach may not be applicable in the present situation.

(iii) Specific local resistance method (5*)	The load bearing members are designed to resist specific blast load.	**Pros:** highest level of protection. **Cons:** It may not be economic in certain situation where the scaled distance is very less. The method is complex and iterative, involving the estimation of blast load, its dynamic effect on the member, and dynamic strength of the member.
(3) Indirect Design (1*)	Load carried by the removed load bearing elements are transferred to the rest of the structure through minimum strength, continuity and ductility. In the case of steel framed buildings, the continuity helps maintain structural integrity, although as has been demonstrated in Chapter 3, support to a damaged column via catenary action is probably not feasible. In the case of reinforced concrete columns, the ductility (as provision in ductile design for seismic loads) can help to limit extent of localised damage and continuity in	**Pros:** Inexpensive. Experience from blast damaged buildings shows that ensuring structural elements are properly tied together is important for avoiding collapses. **Cons:** In most cases the method is incapable of redistributing column loads.

the reinforcement can help
to redistribute column loads
through beam action.

The importance of alternate load paths and maintenance of a safe scaled distance were demonstrated in the incident of the Khobar Towers as explained in chapter 2. The stand off distance saved the buildings from a massive explosion. If the stand off distance had not been maintained, then it is likely that the internal structure of the building would have been destroyed at the ground level resulting in a progressive collapse. The façade was completely destroyed. Despite the destruction of these load bearing elements, the provision of adequate tying between members helped maintain structural integrity and would have helped avoid progressive collapse. The dangers of not maintaining a safe scaled stand off distance was also realized in the Murrah building incident. The truck bomb, equivalent to 1800 kg of TNT, exploded very close to the building. In this incident, the direct blast pressure destroyed one column by brisance and another two columns by shear. The loss of these three columns led to a collapse that consumed ½ of the floor area of this nine storey building. The use of current codes/standards could not consistently provide assurance against progressive collapse (Nair, 2004). For this reason, some specifications, such as US DoD guidelines, specify safe scaled distances for structural safety from air blast loads. It recommends a safe stand off distance of 4.46 $m/kg^{1/3}$ for unstrengthened buildings (US DoD, 1999). This recommendation was arrived at without considering the type of structure, the configurations, and the behaviour of structural elements. It necessitates further studies on the behaviour of structures, subjected to blast load. This chapter explains the blast load for a column with a case study of the Murrah building incidents.

5.2. Blast loading

High explosive detonation converts explosive material into a gas at high pressure and temperature which forms a shock wave front travelling radially with high velocity into the atmosphere by compressing the air in its path. This produces the ambient overpressure or the incident pressure which finally hits the building and gets reflected with amplified over pressure, called reflected pressure. A typical pressure-

time profile for a blast wave in free air is shown in Fig. 5.1. The over pressure depends on the stand off distance and charge weight. The stand off distance is defined as the distance from the bomb to the target; and the charge weight is represented by the equivalent weight of TNT. The charge weight can be roughly estimated based on the carrier (truck and briefcase etc.). Federal Emergency Management Agency Guidelines (2003) provide typical charge sizes for design purposes (Table 5.2).

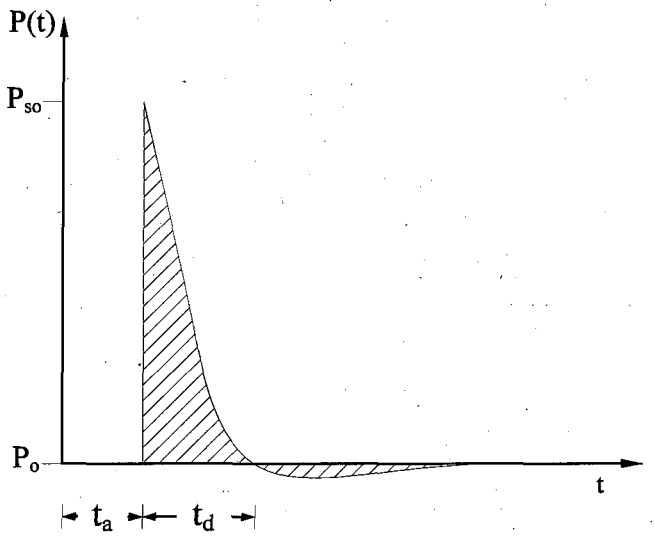

Fig. 5. 1 Blast wave pressure-time profile

Table 5. 2 Typical size of Improvised Explosive Devices (FEMA, 2003)

Type of bombs	Size in TNT equivalent (kg)
Truck bomb	4500
Vehicle bomb (Van)	1800
Vehicle bomb (Car)	230
Briefcase bomb	25
Pipe bomb	2

Various graphs (TM5-1300 based on Kingery, 1984) and formulae (Brode, 1955 and Henrych, 1870) are available to estimate air blast loads. TM5 – 1300 (US Army, 1991) provide a set of design curves to determine blast wave parameters such as peak incident and normal reflected pressures, incident and normal reflected impulses,

time of arrival of the blast wave, duration and shock front velocity for different scaled distances. It also provides a set of curves to estimate reflected pressure with the orientation, i.e. where the structural face is not normal to the direction of blast wave. Apart from this, the computer programmes such as CONWEP and AT-Blast are available to estimate blast wave parameters. Using this programme, the over and reflected pressures were calculated herein for the above mentioned explosive devices and the different stand off distances, and the graphs, shown in Figs. 5.2 and 5.3 are plotted. The dynamic pressure is calculated based on static over and reflected pressure using Eq. 5.1 (Rankine, 1870).

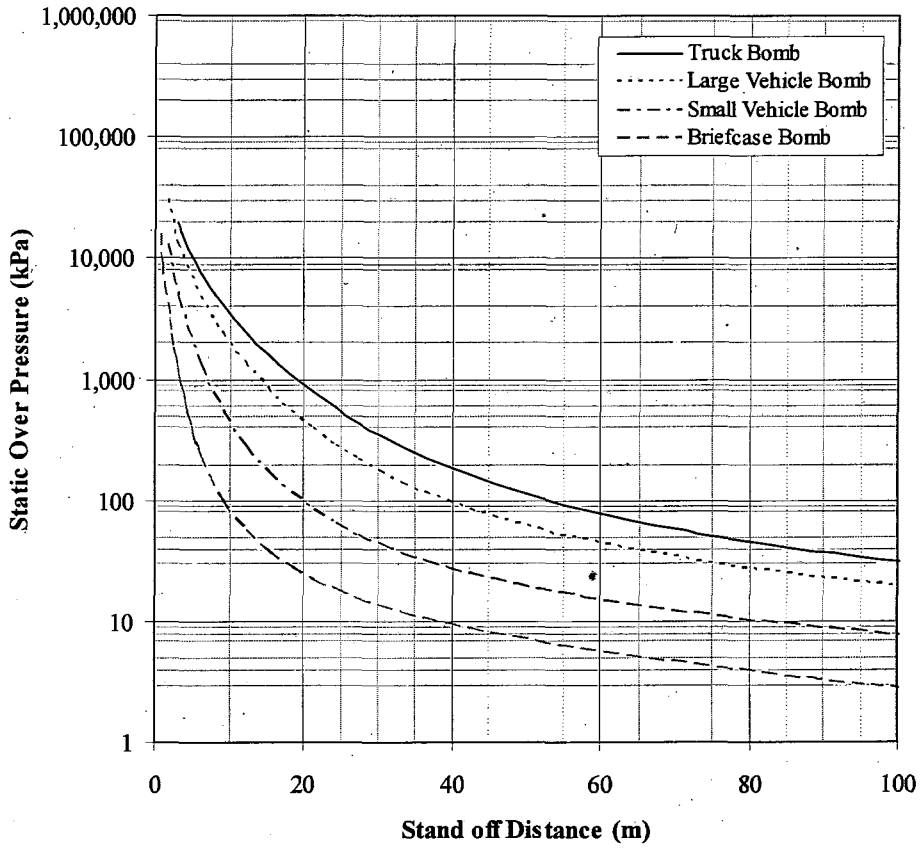

Fig. 5. 2 Static over pressure for different explosive devices

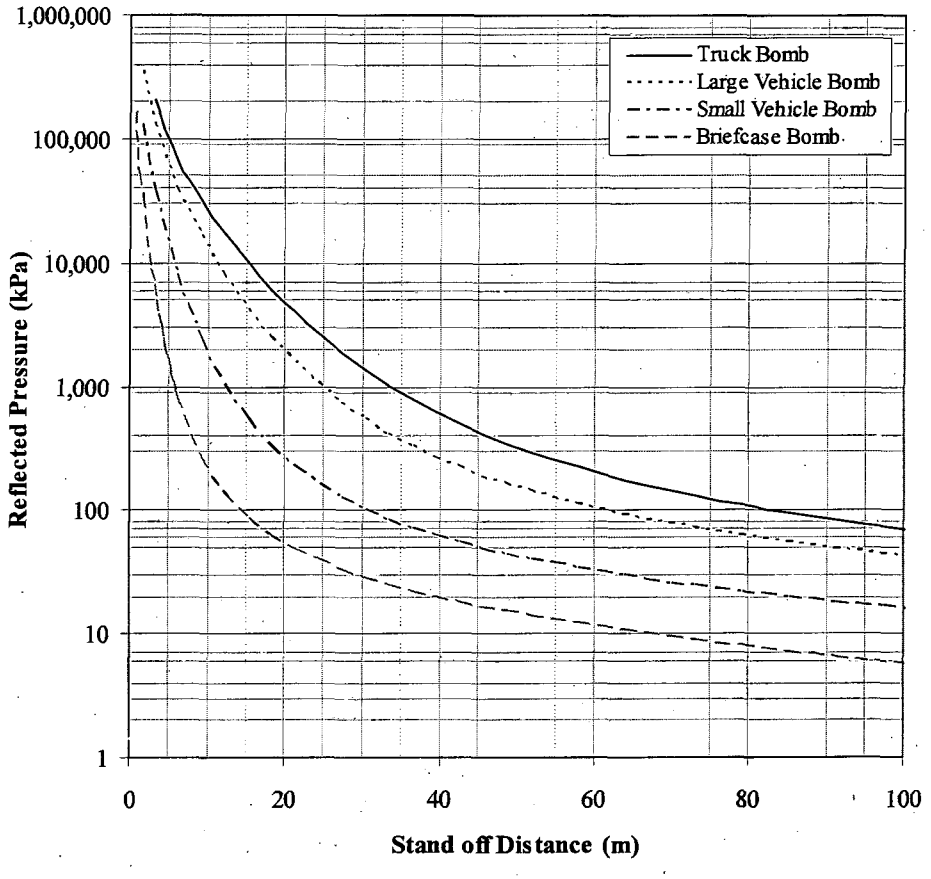

Fig. 5. 3 Reflected pressure for different explosive devices

$$p_r = 2p_s + (\gamma + 1)q_s \tag{5.1}$$

Where,

p_r - Reflected pressure

p_s - Static over pressure

ρ_s - Density of air molecules

q_s - Dynamic pressure

γ - Gas constant, normally 1.4 for air.

When the over pressure is much less than the ambient pressure, the velocity of air molecules reduces nearly to zero, resulting in low dynamic pressure. As a result, the reflected pressure is two times the static over pressure. Shock waves from blasts can break this simple relationship between static over pressure and reflected pressure as shown in Fig 5.4. For example, for objects located at close range to detonations the reflective pressure can be typically 8 times the static over pressure. In extreme cases the reflective pressure can be up to 20 times the static over pressure due to

dissociation effects, which is a chemical process in which complex molecules split into smaller molecules.

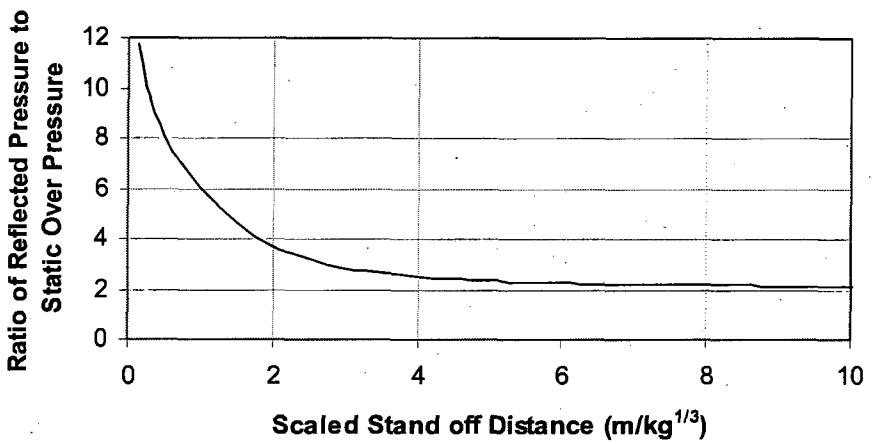

Fig. 5. 4 Scaled distance Vs Ratio of reflected pressure to static over pressure

The calculation of blast load duration for columns differ from that of walls. In the case of walls, the duration is governed by reflective impulse and reflected pressure, as the blast wave takes more time to clear. In the case of columns, the duration is governed by the velocity of the wave front and the clearance distance, as the blast wave clears quickly due to small width. This blast wave clearance is possible only if the blast wave is free to wrap around the column. When the shock front wave strikes the front face, the pressure immediately rises from zero to the reflected pressure (P_{rA}). The reflected pressure clears in clearing time, (t_c) which is calculated using Eq. 5.2. This equation was proposed by Glasstone and Dolan (1977). At clearing time, the pressure reaches the stagnation pressure, $P_s(t_c)$ equal to the sum of incident pressure, (P_{oA}) and the drag pressure, $(C_D q_A)$. The sum of incident and drag pressures decays to zero within (t_{dA}) time after striking the target. The coefficient of drag, C_D is considered to be equal to 1 for the front face. At the same time, the pressure wave reaches the rear side at time $\left(L/U_A\right)$ and suddenly rises from zero to the incident pressure (P_{oB}) at rising time, (t_r) which is calculated using Eq. 5.3 (Glasstone and Dolan, 1977). This pressure decays to zero within (t_{dB}) time

after reaching the rear face (Fig. 5.5). As the movement of air molecules will be restricted by the walls and floors, etc, the effect of dynamic pressure on rear face can be safely neglected. The blast pressure-time history, acting on the column is shown in Fig 5.5.

$$t_c = 3S/U_A \tag{5.2}$$

$$t_r = \frac{4S}{U_B} \tag{5.3}$$

Where,

P_{rA} - The reflected pressure on the front face

P_{oA} - The incident pressure on the front face

q_A - The dynamic pressure on the front face;

t_{dA} - The duration of incident pressure on the front face

U_A - The blast wave front velocity for the front face

P_{oB} - The incident pressure on the rear face

t_{dB} - The duration of incident pressure on the rear face;

U_B - The blast wave front velocity for the rear face

t_c - The clearing time for the front face

t_r - The rising time for the rear face

S - clearing distance, equal to half the width of the face which experience the blast pressure

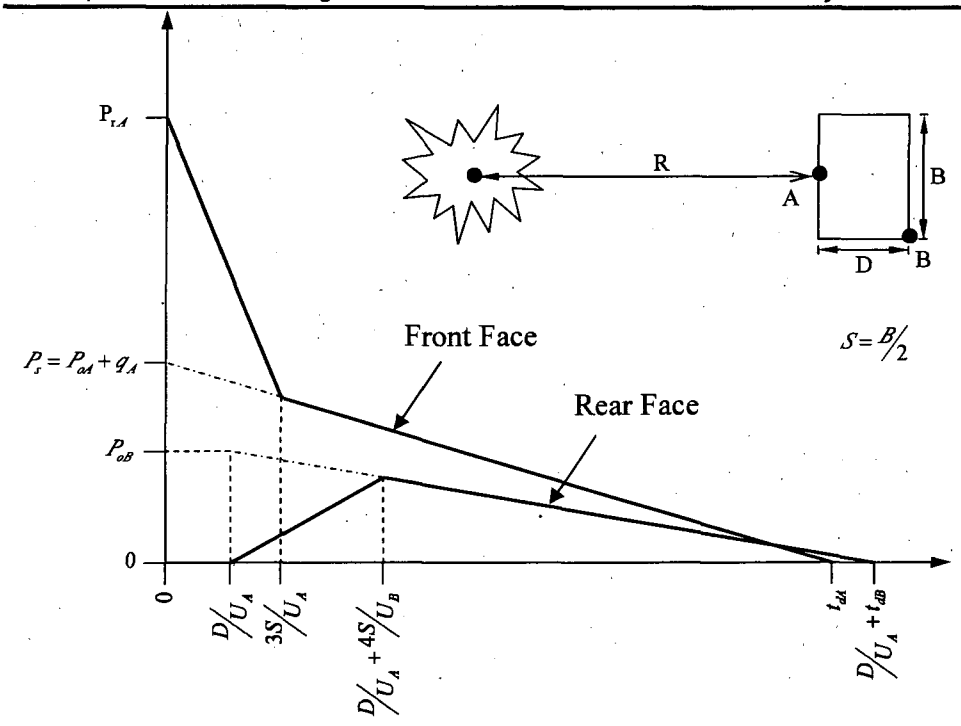

Fig. 5. 5 Blast pressure on front and rear side of column

The net load on the column is the front side load (Point, A) minus the rear side load (Point, B). The estimation of column response for this net pressure-time history can be more difficult, hence the complex pressure-time history is converted into a simple triangular pulse of equivalent area (impulse). The time duration for the triangular pulse is calculated by dividing the impulsive force (net area under pressure-time curve) by the peak reflected pressure. A parametric study is carried out herein to assess the scale of the inaccuracy introduced by this simplification. The column response for the complex pressure-time profile is estimated using a SDOF system as explained in chapter 4.

5.2.1 Comparison of column responses obtained using complex pressure-time profile and simplified triangular impulse

The complex pressure-time history is divided into several phases as shown in Fig. 5.6. For a system without damping, starting from rest, the response during the phase-I is determined by evaluating Duhamel's integral (Eq. 5.5). At the end of phase-I, the system has velocity and displacement. The response of the system during phase-II is calculated considering the velocity, $\dot{u}[t_c]$ and displacement, $u[t_c]$ as initial

conditions and by evaluating Duhamel's integral of phase-II (Eq. 5.7). Similarly, the response of the column is determined for all the phases and given below. The flowchart, given in Appendix A3.1 explains the calculation followed to estimate the response of the columns for complex pressure time-history profiles.

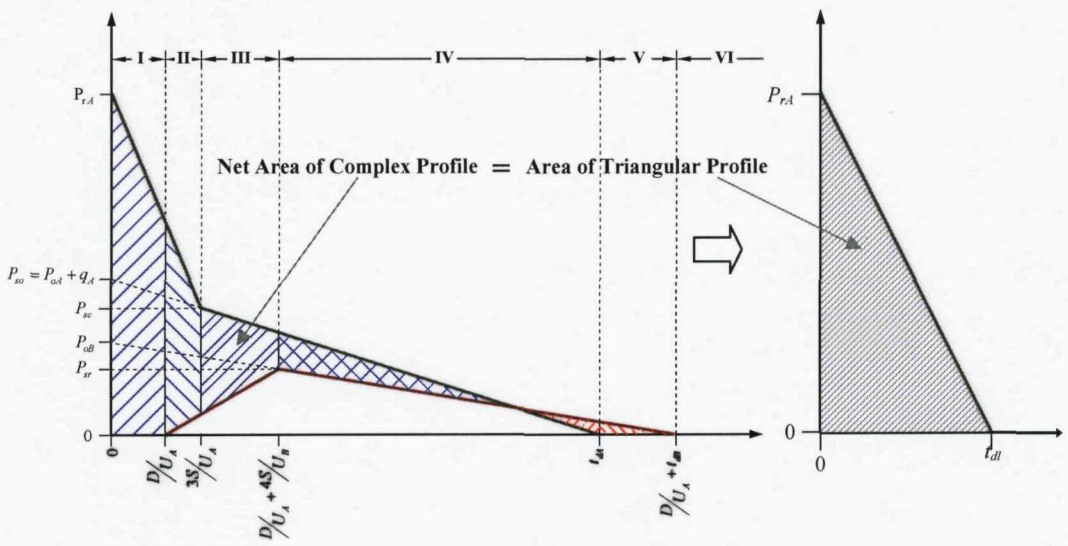

Fig. 5. 6 Complex pressure time profile and simplified triangular impulse

Phase-I:

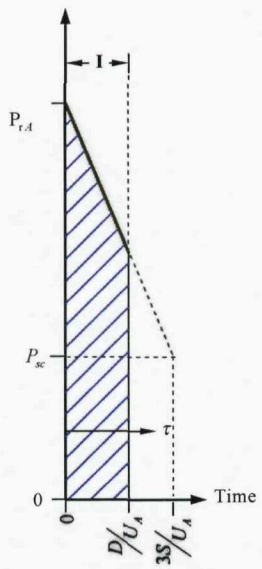

Fig. 5. 7 Phase-I of pressure time profile - 1

$$P[\tau] = P_{rA} - \frac{(P_{rA} - P_{sc})}{t_c}\tau \tag{5.4}$$

$$u_1[t] = \frac{(P_{rA}BL)L^3}{384EIm\omega_n}\int_0^t P_1[\tau]\sin\left[\omega_n(t-\tau)\right]d\tau \tag{5.5}$$

Phase-II:

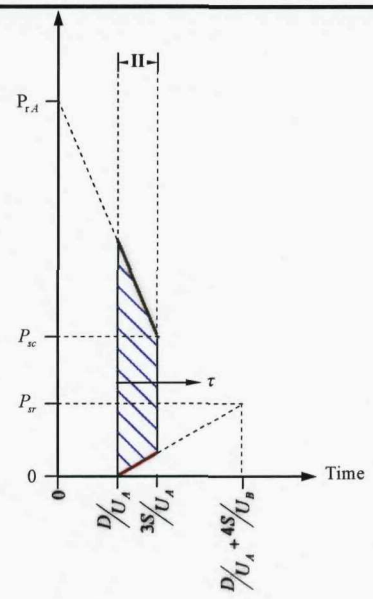

Fig. 5. 8 Phase-II of pressure time profile - 1

$$P_2[\tau] = P_{rA} - \frac{(P_{rA} - P_{sc})}{t_c}(t_l + \tau) - \frac{P_{sr}}{t_r}\tau \tag{5.6}$$

$$DI_2[t] = \frac{(P_{rA}BL)L^3}{384EIm\omega_n}\int_0^t P_2[\tau]\sin[\omega_n(t-\tau)]d\tau \tag{5.7}$$

$$u_2[t] = u_1\left[D/U_A\right]\cos[\omega_n(t-t_l)] + \frac{u_1'\left[D/U_A\right]}{\omega_n}\sin[\omega_n(t-t_l)] + DI_2[t-t_l] \tag{5.8}$$

Phase-III:

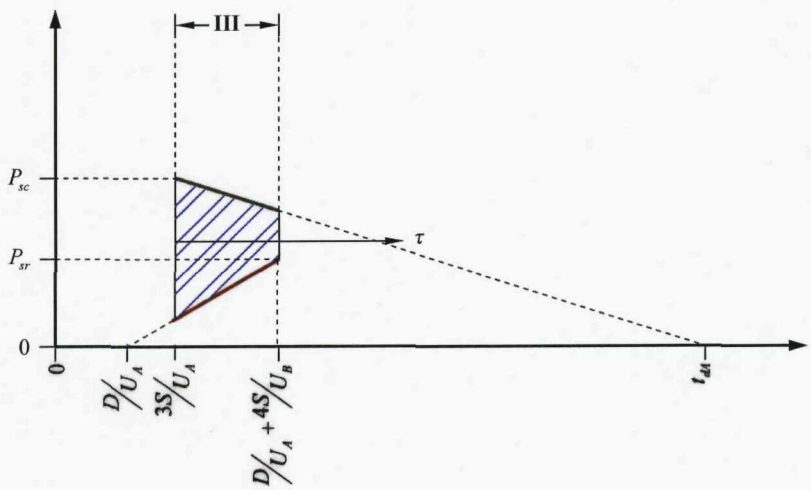

Fig. 5. 9 Phase-III of pressure time profile - 1

$$P_3[\tau]=\frac{P_{sc}}{(t_c-t_{dA})}\left(\tau+(t_c-t_{dA})\right)-\frac{P_{sr}}{t_r}(t_c-t_l+\tau) \tag{5.9}$$

$$DI_3[t]=\frac{(P_{rA}BL)L^3}{384EIm\omega_n}\int_0^t P_3[\tau]\sin\left[\omega_n(t-\tau)\right]d\tau \tag{5.10}$$

$$u_3[t]=u_2[t_c]\cos\left[\omega_n(t-t_c)\right]+\frac{u_2'[t_c]}{\omega_n}\sin\left[\omega_n(t-t_c)\right]+DI_3[t-t_c] \tag{5.11}$$

Phase-IV:

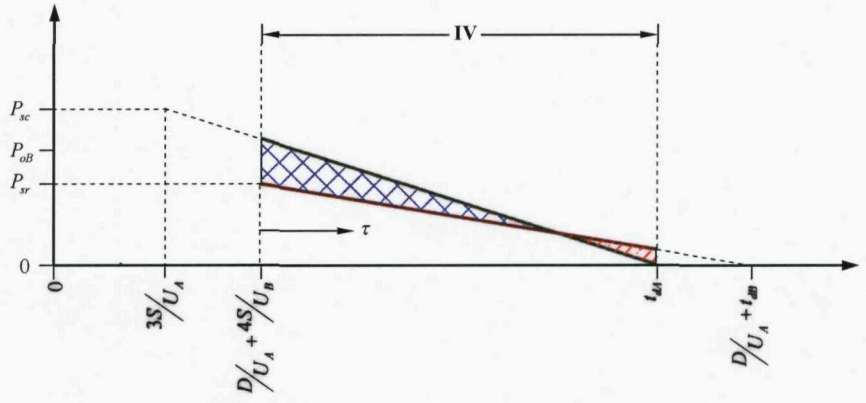

Fig. 5. 10 Phase-IV of pressure time profile - 1

$$P_4[\tau]=\frac{P_{sc}}{(t_c-t_{dA})}\left(\tau+(t_l+t_r-t_{dA})\right)-\frac{P_{sr}}{(t_r-t_{dB})}\left(\tau-(t_{dB}-t_r)\right) \tag{5.12}$$

$$DI_4[t]=\frac{(P_{rA}BL)L^3}{384EIm\omega_n}\int_0^t P_4[\tau]\sin\left[\omega_n(t-\tau)\right]d\tau \tag{5.13}$$

$$u_4[t]=u_3[t_l+t_r]\cos\left[\omega_n\left(t-\left(D/U_A+t_r\right)\right)\right]+\frac{u_3'[t_l+t_r]}{\omega_n}\sin\left[\omega_n\left(t-\left(D/U_A+t_r\right)\right)\right] \tag{5.14}$$
$$+DI_4\left[t-\left(D/U_A+t_r\right)\right]$$

Phase-V:

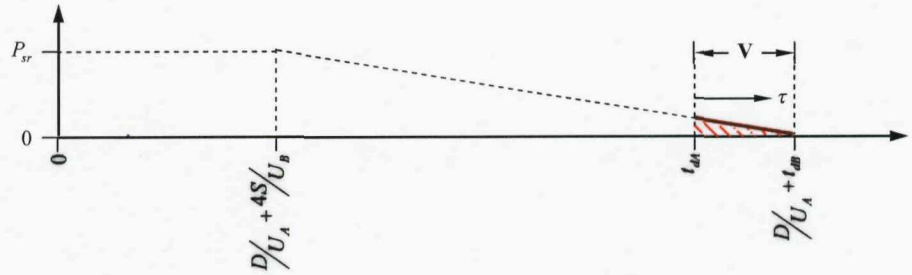

Fig. 5. 11 Phase-V of pressure time profile - 1

$$P_5[\tau]=\frac{-P_{sr}}{(t_r-t_{dB})}\left(\tau+t_{dA}-(t_{dB}+t_l)\right) \tag{5.15}$$

$$DI_5[t] = \frac{(P_{rA}BL)\hat{E}}{384EIm\omega_n}\int_0^t P_5[\tau]\sin\left[\omega_n(t-\tau)\right]d\tau \tag{5.16}$$

$$u_5[t] = u_4[t_{dA}]\cos\left[\omega_n(t-t_{dA})\right] + \frac{u_4'[t_{dA}]}{\omega_n}\sin\left[\omega_n(t-t_{dA})\right] + DI_5[t-t_{dA}] \tag{5.17}$$

Phase-VI:

$$u_6[t] = u_5\left[t_{dB}+D/U_A\right]\cos\left[\omega_n\left(t-\left(t_{dB}+D/U_A\right)\right)\right] + \frac{u_5'\left[t_{dB}+D/U_A\right]}{\omega_n}\sin\left[\omega_n\left(t-\left(t_{dB}+D/U_A\right)\right)\right] \tag{5.18}$$

In the parametric study, the columns of 300 x 300, 450 x 300 and 600 x 300 mm cross section are considered. They are assumed to be subjected to an explosion of 230, 1000, 1800 kg of TNT. The stand off distances for the charges are adopted based on the minimum stand off distance required to avoid spall damage. The blast load for the charge weight and stand off distance is estimated and shown in Table 5. 3. The deflections of the typical columns are calculated considering the complex pressure-time history and simple triangular impulse. The results are shown in Fig. 5.12. The error in column response for triangular impulse (Fig. 5.13) is less than ten percent and the response is conservative, hence the column is hereafter analyzed this triangular impulse.

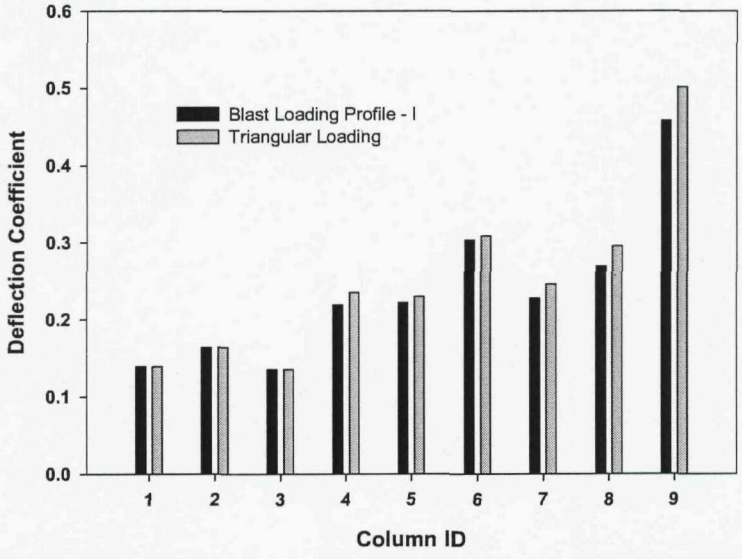

Fig. 5. 12 Comparison of responses, obtained considering complex pressure-time history and triangular impulse

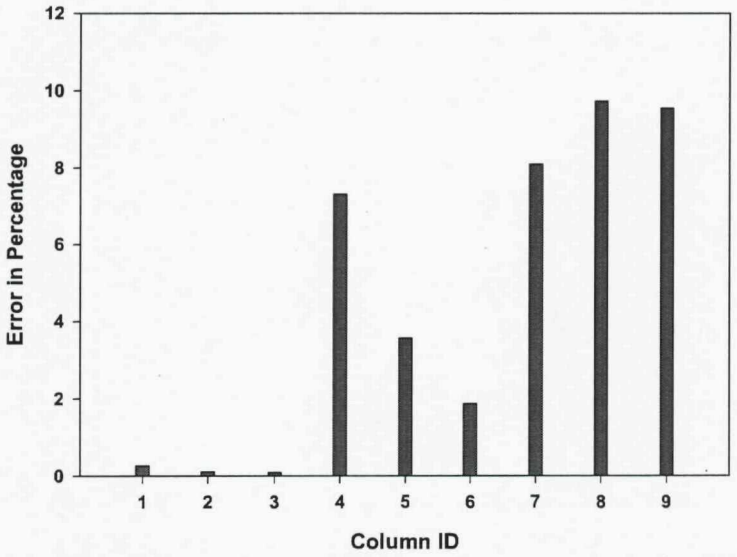

Fig. 5. 13 Percentage error in the response for triangular impulse

Table 5. 3 Blast load on different columns

Column ID	Charge Weight	Breadth	Depth	Stand off distance	Scaled distance	Front face loading				Rear face loading			Net Impulse	Duration of Blast Load
						Pressure		Time		Pressure	Time			
						P_r	$P_s(t_c)$	t_c	t_d	$P_s(t_r)$	t_r	t_d	I	t_{dl}
	(kg)	(mm)	(mm)	(m)	($m/kg^{1/3}$)	(kN/m^2)	(kN/m^2)	(mSec)	(mSec)	(kN/m^2)	(mSec)	(mSec)	(kN/m^2-mSec)	(mSec)
1	230	300	300	12	1.96	1125.09	453.54	0.71	5.65	235.07	0.96	5.83	991.74	1.76
2	230	450	300	12	1.96	1125.09	421.10	1.06	5.65	211.92	1.44	5.83	1166.42	2.07
3	230	600	450	6	0.98	8608.66	2450.11	0.74	2.06	666.58	1.06	2.34	4916.90	1.14
4	1000	300	300	30	3.00	330.74	147.88	0.94	16.03	104.48	1.26	16.23	493.08	2.98
5	1000	450	300	21	2.10	912.59	375.83	1.12	10.12	209.87	1.51	10.31	1329.76	2.91
6	1000	600	450	16	1.60	2080.56	786.19	1.19	7.02	346.27	1.62	7.29	2730.64	2.62
7	1800	300	300	73	6.00	71.29	33.93	1.17	38.54	30.24	1.56	38.65	111.26	3.12
8	1800	450	300	73	6.00	71.29	33.40	1.76	38.54	29.60	2.34	38.65	134.20	3.76
9	1800	600	450	36	2.96	342.95	146.88	1.87	19.19	101.04	2.51	19.48	745.72	4.35

5.3. Material properties for concrete and steel

Dynamic strength of concrete and steel

Normally, blast produces load associated with strain rates in the range of 10^2-10^4 s^{-1} (Ngo, et. al., 2007). This high straining rate increases the static compressive strength of the concrete as shown in Fig. 5.14. TM 5-1300 introduces the dynamic increase factors (DIF) for steel and concrete to account the effect of high strain rate. The DIF is defined as a ratio of the dynamic to static strengths and it mainly depends on strain rate, increasing with strain rate. Recognising the difficulty in estimating strain rate TM 5-1300 (1990) proposes a conservative DIF for the design purposes. Table 5.4 presents the DIF's for steel and concrete, considering both shear and flexure. To avoid brittle failure a more conservative value of DIF is used for shear.

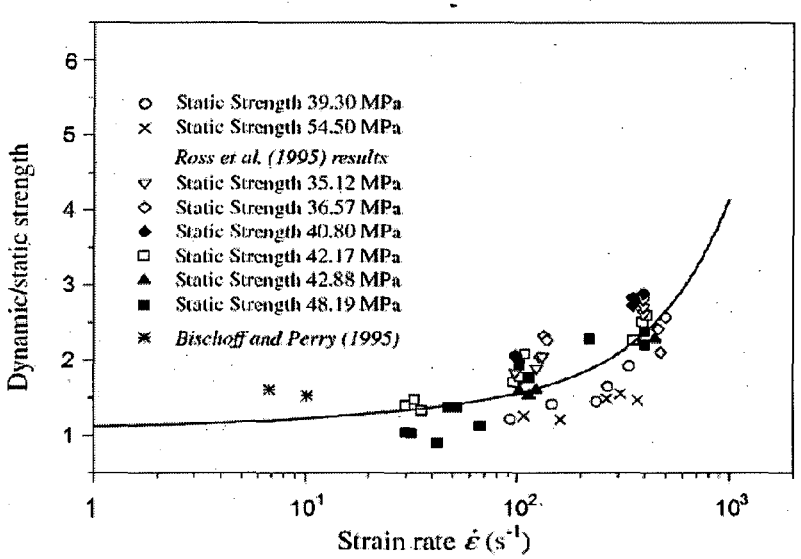

Fig. 5. 14 Normalized concrete compressive strength vs strain rate (Source: Lu, et. al, 2004)

Table 5. 4 Dynamic Increase factor for reinforced concrete members

Type of stresses	Reinforcement Steel	Concrete
	f_{dy}/f_y	f_{dck}/f_{ck}
Bending	1.23	1.25
Shear	1.10	1.10

Where,

f_y - Static yield stress of reinforcing steel

f_{dy} - Dynamic yield stress of reinforcing steel

f_{ck} - Static cube strength of concrete

f_{dck} - Dynamic cube strength of concrete

Modulus of elasticity of concrete and steel

The modulus of elasticity is mainly dependent on the concrete materials, such as aggregates, cement and their proportions. Several studies have been carried out to quantify the elastic modulus of concrete (E_c) and established empirical equations. ACI 318-2002 provides Eq. 5.19 to estimate E_c,

$$E_c = 33 w_c^{1.5} \sqrt{f_c'} \qquad (\text{lbs/ft}^2) \qquad (5.19)$$

Where,

E_c - Modulus of elasticity in lbs/ft^2

f_c' - Cylindrical strength of concrete in lbs/ft^2

w_c - Unit weight of concrete in lbs/ft^3 (150 lbs/ft^3 for normal weight concrete

For normal weight concrete, Eq. 5.19 is simplified to,

$$E_c = 4490\sqrt{f_{ck}} \qquad (\text{N/mm}^2) \qquad (5.20)$$

Where,

f_{ck} - Cube strength of concrete in N/mm^2

The British standards suggest Eq. 5.21 to estimate the modulus of elasticity

$$E_c = K_o + 0.2 f_{ck} \qquad (\text{kN/mm}^2) \qquad (5.21)$$

K_o - Constant related to the modulus of elasticity of the aggregate (taken as 20 kN/mm^2)

f_{ck} - Cube strength of concrete in N/mm^2

Eq. 5.20 is used in the estimation of safe stand of distance for a column because of simplicity. The typical stress-strain curves for concrete and steel are shown in Fig. 5.15 and 5.16. Due to high strain rates slight increments in elastic modulus are

observed and are shown Fig 5.15. This enhancement is incorporated in the present work by replacing f_{ck} by f_{dck} in Eq. 5.15. At the same time there is no change in young's modulus of steel (Fig. 5.16) due to high strain rate and it is taken as 200000 N/mm^2.

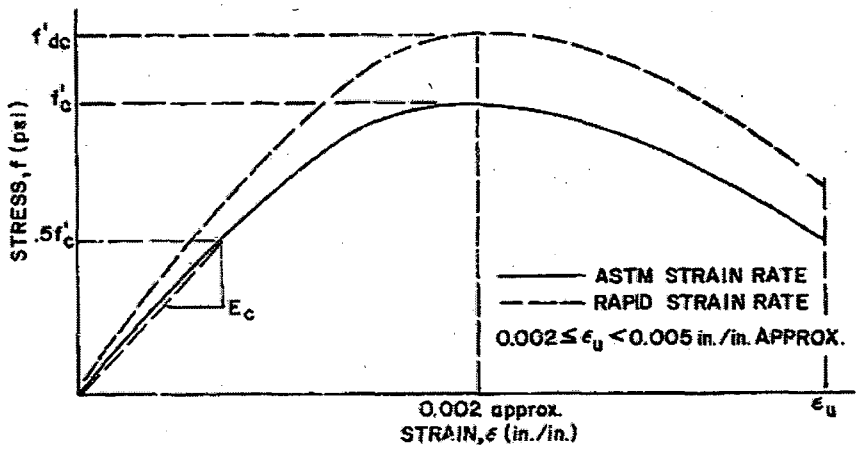

Fig. 5. 15 Typical stress-strain curve for concrete under compression (Source: TM 5-1300, 1990)

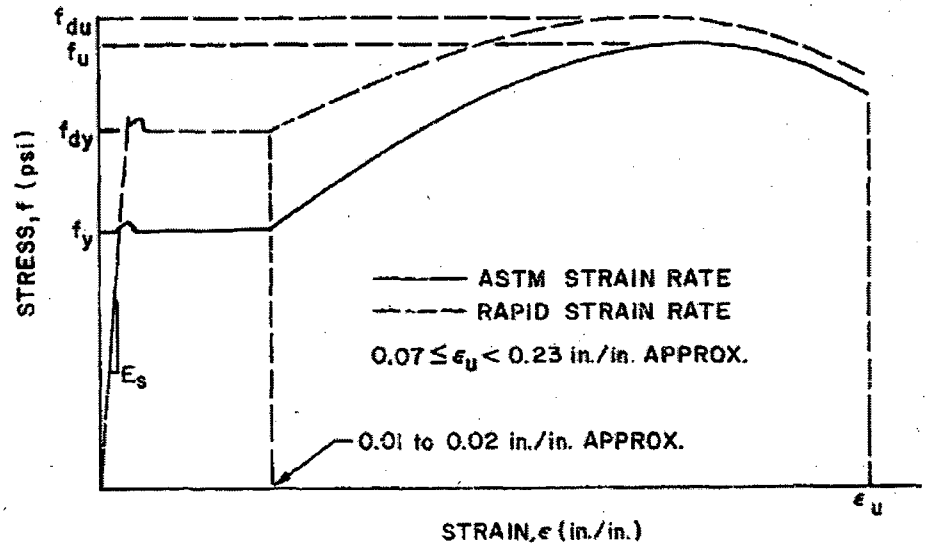

Fig. 5. 16 Typical stress-strain curve for steel under tension (Source: TM 5-1300, 1990)

5.4. Flexural strength of RC columns

The flexural strength of RC columns is estimated using the pure bending theory in which the section is assumed to be plane before and after bending. The basic assumptions, made in the estimation of flexural strength are:

1. Strains in the concrete and reinforcement are derived assuming that plane sections remain plane.
2. The tensile strength of the concrete is ignored.
3. A perfect bond exists between the reinforcement and the concrete such that the strain in the reinforcement is equal to the strain in the concrete at the same level.

Reinforced concrete analysis for axial force and bending moment is usually performed by assuming a given strain value at the extreme compression fibre with a linear strain distribution over the depth of the section. When the section is partly in tension, the strain in the extreme compression fibre is limited to 0.0035 (Fig. 5.17). When the section is in compression, the compressive strain at a point $3/7^{th}$ of height from the extreme compression fibre is assumed to be 0.002 (Fig. 5.18). The stress distribution is typically assumed as a rectangular stress block with a depth equal to 0.9 times the neutral axis depth and a magnitude equal to 0.667 times the concrete compressive strength (Fig. 5.17 and 5.18). Here 0.667 takes account of the relation between the cube strength and the bending strength in a flexural member (BS 8110-1:1990, clause 2.6.2) and the factor of safety on concrete has been taken out.

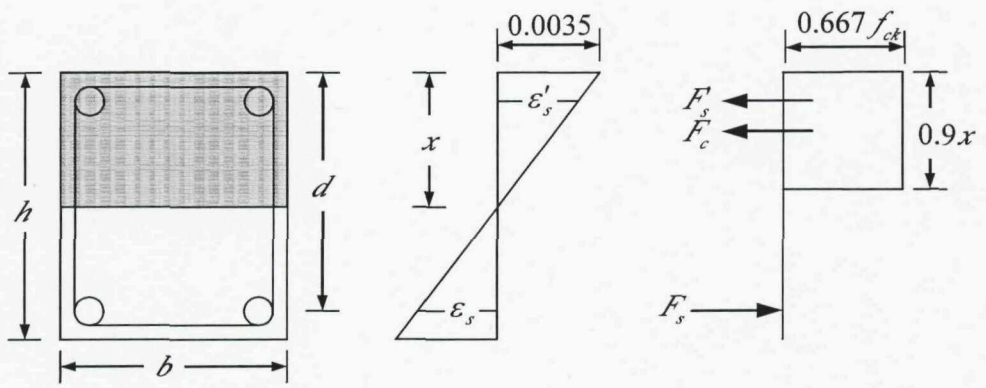

Fig. 5. 17 Stress and strain profiles for concrete column (neutral axis lies within the section)

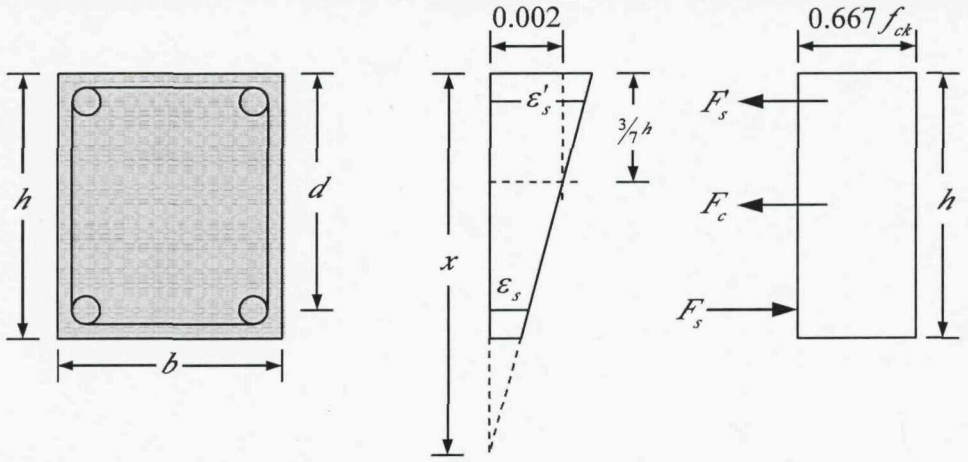

Fig. 5. 18 Stress and strain profiles for concrete column (neutral axis lies outside the section)

A static analysis of the building frame is carried out for the accidental load and the axial force in the column is estimated. For the given axial force, column dimensions and reinforcement details, the flexural strength is calculated as follows:

1. Estimate the dynamic strength of concrete and steel by multiplying the allowable static stresses with the dynamic increase factor, explained in section 5.3.
2. Obtain axial force from the static analysis of the building (analysed for accidental loads).
3. Assume a value for the depth of neutral axis
4. Estimate strains at extreme fibre and at the level of reinforcements, using Eq. 5.22 and 5.23.

$$\varepsilon_s = \begin{cases} \dfrac{0.0035}{x}(d-x) & x \le h \\ \dfrac{0.002}{x-\frac{3}{7}h}(x-d') & x > h \end{cases} \tag{5.22}$$

$$\varepsilon'_s = \begin{cases} \dfrac{0.0035}{x}(x-d') & x \le h \\ \dfrac{0.002}{x-\frac{3}{7}h}(x-d') & x > h \end{cases} \tag{5.23}$$

Where,

d - Effective depth for tension steel

d' - Effective depth for compression steel

h - Overall depth of column

x - Neutral axis depth

ε_s - Strain in tension steel

ε'_s - Strain in compression steel

5. Estimate stresses in rebars using Eq. 5.24 and 5.25.

$$f_s = \begin{cases} -f_y & \varepsilon_s < -\dfrac{f_y}{E_s} \\ \varepsilon_s E_s & -\dfrac{f_y}{E_s} \le \varepsilon_s \le \dfrac{f_y}{E_s} \\ f_y & \varepsilon_s > \dfrac{f_y}{E_s} \end{cases} \tag{5.24}$$

$$f_{sc} = \begin{cases} -f_y & \varepsilon'_s < -\dfrac{f_y}{E_s} \\ \varepsilon'_s E_s & -\dfrac{f_y}{E_s} \le \varepsilon'_s \le \dfrac{f_y}{E_s} \\ f_y & \varepsilon'_s > \dfrac{f_y}{E_s} \end{cases} \tag{5.25}$$

Where,

f_s - Stress in tension steel

f_{sc} - Stress in compression steel

f_y - Yield stress of steel reinforcement

f_{ck} - Characteristic compressive strength of concrete

E_s - Young's modulus of steel

6. Estimate the axial compression using Eq. 5.26. In this equation, the partial safety factors for concrete and steel are not considered, so that the maximum flexural strength of the section can be estimated as the low probability of occurrence of the blast event.

$$P_u = 0.67 f_{ck}(bx) + f_s A_s + f_{sc} A_{sc} \tag{5.26}$$

Where,

A_s - Cross sectional area of tension steel

A_{sc} - Cross sectional area of compression steel

P_u - Axial compression

7. Repeat step 4 to 5 for other values of neutral axis until the axial compression is equal to the axial force.
8. Estimate the flexural strength of the section using Eq. 5.27.

$$M_u = 0.67 f_{ck}(bx)\left(h/2 - x\right) + f_s A_s\left(d - h/2\right) + f_{sc} A_{sc}\left(h/2 - d'\right) \quad (5.27)$$

Where, M_u - Flexural strength

This flexural strength is compared with the dynamic bending moment, produced by lateral blast load. To assess the flexural strength of column section quickly, the design charts are developed (without considering the material partial safety factor) and are presented in Fig 5.19 for C25 concrete and the reinforcement on two opposite faces. The design charts for other grades of concrete and arrangement of reinforcement are given in Appendix A3.2.

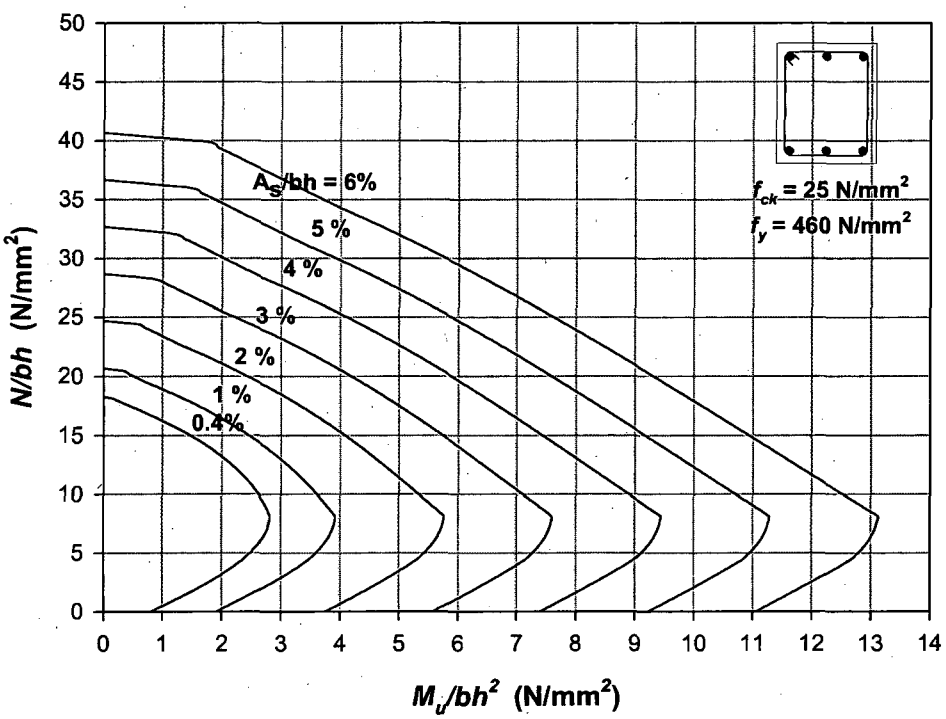

Fig. 5. 19 Design charts for C25 concrete column with reinforcement on two opposite faces

5.5. Shear Strength

The shear strength of the section is achieved from the contributions of concrete and transverse steel. The shear contribution of concrete is offered by the aggregate interlocking, dowel action in the aggregate and shear resistance from the uncracked concrete. This shear strength of concrete is again enhanced by the presence of axial compression. Shear resistance of lateral ties yielding across the diagonal tension cracks is also included. Due to the complexity in the prediction of shear strength several models have been developed based on: (i) fitting the experimental data, (ii) simple structural mechanics such as the strut and tie model (STM) and (iii) advanced mechanics such as the modified compression field theory (MCFT). Most of the codes estimate the shear strength of concrete using empirical equations developed with extensive experimental data. The shear contribution from the tie is estimated using either the STM or the MCFT model. The STM was developed by Ritter and Morsch (1902) based on truss mechanism. In this model, the concrete strut is assumed to be inclined at 45°. Most of the codes use the strut and tie model to estimate shear strength except the Canadian code that uses the MCFT model (Entz and Collins, 2006). The MCFT model was first presented by Collins and Vecchio (1986) as an extension of compression field theory (Mitchell & Collins, 1974). In most of the codes the shear strength of reinforced concrete members is considered to be the sum of the shear resistance of the concrete and steel. The various codal provisions adopted to estimate shear strength are given below.

British Standards Institution (BSI 8110-1:1997):

$$v_c = 0.79\left(\frac{100A_s}{bd}\right)^{1/3}\left(\frac{400}{d}\right)^{1/4}\left(\frac{f_{ck}}{25}\right)^{1/3} \tag{5.28}$$

$$V_c = \left(v_c + 0.6\frac{NVh}{A_cM}\right)bd \tag{5.29}$$

$$V_s = \frac{A_w f_{yw} d}{s} \tag{5.30}$$

$$V_u = V_c + V_s \tag{5.31}$$

Where,

A_c - Area of concrete section

A_s - Area of tension reinforcement

A_v - Total cross-sectional area of lateral ties at a section

b - Breadth of section

d - Effective depth

f_{ck} - Characteristic compressive strength of concrete in MPa

f_{yv} -Yield stress of lateral ties

h - Span

M - Moment

N - Applied axial load

s - Spacing of lateral ties along the member.

v_c - Design concrete shear stress

V - Shear force

V_c - Shear strength offered by concrete

V_s - Shear strength offered by lateral ties

V_u - Ultimate shear strength of column section

Note:

$\left(\frac{100A_s}{bd}\right)$ should not be taken as greater than 3;

$\left(\frac{400}{d}\right)^{1/3}$ should not be taken as less than 1

$\frac{Vh}{M}$ should be taken as not greater than 1

Euro code – 2 (EN 1992-1-1:2004)

$$V_{Rd,c} = \left(C_{Rd,c}k\left(100\rho_1 f_{ck}\right)^{1/3} + k_1\sigma_{cp}\right)b_w d \text{ with a minimum of} \quad (5.32)$$

$$V_{Rd,c} = \left(v_{\min} + k_1\sigma_{cp}\right)b_w d \quad (5.33)$$

$$V_{Rd,s} = \frac{A_w f_{yv} d}{s} \quad (5.34)$$

$$V_u = V_{Rd,c} + V_{Rd,s} \quad (5.35)$$

Where,

$C_{Rd,c} = 0.18$

$$v_{\min} = 0.035 k^{3/2} f_{ck}^{1/2}$$

$$k = 1 + \sqrt{\frac{200}{d}} \leq 2.0 \text{ with d in mm}$$

$$k_1 = 0.15$$

$$\sigma_{cp} = \frac{N_{Ed}}{A_c} < 0.2 f_{cd}$$

A_c - Area of concrete section

A_v - Total cross-sectional area of lateral ties at a section

b_w - Breadth of section

d - Effective depth

f_{ck} - Characteristic compressive strength of concrete in MPa

f_{yw} - Yield stress of lateral ties

N_{Ed} - Applied axial load

s - Spacing of lateral ties along the member.

$V_{Rd,c}$ - Shear strength offered by concrete

$V_{Rd,s}$ - Shear strength offered by lateral ties

V_u - Ultimate shear strength of column section

ρ_1 - Percentage of tension reinforcement

American Concrete Institute (ACI 318-2002)

$$V_c = 0.166\left(1 + \frac{P}{13.8A_g}\right)\sqrt{f_c'}bd \tag{5.36}$$

$$V_s = \frac{A_v f_{yw} d}{s} \tag{5.37}$$

$$V_u = V_c + V_s \tag{5.38}$$

Where,

A_g - Area of concrete section

A_v - Total cross-sectional area of lateral ties at a section

b - Breadth of section

d - Effective depth

f_c' - Cylindrical compressive strength of concrete in MPa

f_{yv} - Yield stress of lateral ties

P - Applied axial load

s - Spacing of lateral ties along the member

V_c - Shear strength offered by concrete

V_s - Shear strength offered by lateral ties

V_u - Ultimate shear strength of column section

Canadian Standards Association (CSA A23.3-04)

$$\varepsilon_x = \frac{M_f / d_v + V_f + 0.5N_f}{2A_sE_s} \tag{5.39}$$

$$V_r = \left(\varphi_c \beta \sqrt{f_c'} + \frac{A_v \phi_s f_y}{b_w s} \cot\theta \right) b_w d_v \tag{5.40}$$

$$V_r \le 0.25 \varphi_c f_c' \tag{5.41}$$

$$\beta = \frac{0.4}{1+1500\varepsilon_x} \left(\frac{1300}{1000 + s_{ze}} \right) \tag{5.42}$$

$$\theta = 29^o + 7000\varepsilon_x \tag{5.43}$$

Where,

A_s - Area of main flexural reinforcement

A_v - Total cross-sectional area of lateral ties at a section

b_w - Breadth of section

d - Effective depth

d_v - Flexural lever arm ($d_v = 0.9d$)

E_s - Young's modulus of the reinforcement

f_c' - Cylindrical compressive strength of concrete in MPa

f_y - Yield stress of lateral ties

M_f - Factored applied moment

N_f - Factored applied axial force (tension positive)

s_{ze} - Crack spacing (= 300 mm)

s - Spacing of lateral ties along the member

V_f - Factored applied shear force

V_r - Shear strength of the member

β - Factor to account for aggregate interlock in concrete members

ε_x - Longitudinal strain

θ - Angle of average principle compression in member with respect to longitudinal axis

ϕ_s - Resistance factor for steel (0.85)

φ_c - Resistance factor for concrete (0.65)

As the shear strength of the column is one of the most important parameters in the calculation of safe stand off distance it needs to be estimated as accurately as possible. To study the exactness of the above codes, the strength obtained using the codes is compared with that of experiments. Several experimental studies (Kokusho (1964), Kokusho and Fukuhara (1965), Ideda (1968), Li et al. (1995), Lynn et al (1996), Ohue et al (1985), Saatcioglu and Ozcebe (1989), Umemura and Endo (1970), Wight and Sozen (1975), Yalcin (1997) and Sezen (2002)) were carried out to develop the shear model. These experimental data were combined and presented in the form of a database by Sezen and Moehle (2004). The author used these data to develop his own shear model. The same experimental data is used to examine the accuracy of the various codes. Using experimental data, the shear strength of the columns are estimated using BSI 8110-1:1997, EN 1992-1-1:2004, ACI 318-2002 and CSA A23.3-04 and presented in Table 5.5. The curve, Fig 5.20 plots against the shear strengths obtained from experiments and code.

The mean ratio of measured to calculated strength, its coefficient of variation and 95% confidence interval are shown in Table 5.6. ACI 318-2002 predicted the shear strength relatively accurately, but it underestimated significantly for few samples. The lower limit of confidence interval for most of the codes falls below 1.0 except for BS code. The estimation of shear strength based on BSI 8110-1:1997 is conservative and safe; hence, the code is used hereafter to estimate the shear strength of column section which is an important parameter in a safe stand off distance approach, discussed in chapter 6.

Table 5. 5 Shear strength of columns, obtained from different experiments

Investigator	Material Properties			Section Properties					P (kN)	Vu(exp) In kN	Vu (est) in kN			
	fc' (N/mm^2)	fck (N/mm^2)	fy (N/mm^2)	b (mm)	d (mm)	a (mm)	p_l(%)	p_t(%)			BSI	ACI	EC2	CSA
Sezen (2002)	21.1	16.88	469	457	394	1473	1.25	0.17	667	315	397	318	383	294
	21.1	16.88	469	457	394	1473	1.25	0.17	2669	359	754	428	683	378
	20.9	16.72	469	457	394	1473	1.25	0.17	2224	301	675	403	616	357
	21.8	17.44	469	457	394	1473	1.25	0.17	667	294	399	321	384	295
Lynn et al. (1996)	25.6	20.48	400	457	381	1473	1.50	0.10	503	271	306	247	307	240
	25.6	20.48	400	457	381	1473	1.50	0.10	503	267	306	247	307	240
	33.1	26.48	400	457	381	1473	1.00	0.10	503	240	298	271	299	222
	33.1	26.48	400	457	381	1473	1.00	0.10	503	231	298	271	299	222
	25.7	20.56	400	457	381	1473	1.00	0.10	1512	316	461	308	438	255
	27.6	22.08	400	457	381	1473	1.50	0.10	1512	338	483	317	463	282
	27.6	22.08	400	457	381	1473	1.50	0.17	1512	356	532	366	507	322
	25.7	20.56	400	457	381	1473	1.50	0.17	1512	378	528	357	503	319
Ohue et al. (1985)	32.1	25.68	322	200	175	400	1.00	0.57	183	102	151	110	124	95
	29.9	23.92	322	200	175	400	1.35	0.57	183	111	154	108	127	103
Esaki (1996)	23	18.4	370	200	175	400	1.25	0.52	161	103	147	104	122	100
	20.2	16.16	370	200	175	400	1.25	0.52	161	102	145	102	120	100
	23	18.4	370	200	175	400	1.25	0.65	269	121	184	128	153	118
	20.2	16.16	370	200	175	400	1.25	0.65	236	112	176	123	147	116
Li et al. (1995)	29	23.2	382	400	375	1000	1.20	0.47	464	328	510	433	454	389
	33.5	26.8	382	400	375	1000	1.20	0.52	1072	393	695	517	578	443
	34.1	27.28	382	400	375	1000	1.20	0.57	1637	430	809	587	689	493
Saatcioglu and Ozceb (1989)	43.6	34.88	470	350	305	1000	1.65	0.30	0	275	270	268	270	255
	30.2	24.16	470	350	305	1000	1.65	0.30	600	270	378	288	344	268
	34.8	27.84	470	350	305	1000	1.65	0.60	600	268	534	448	485	379
Kokusho (1964)	19.9	15.92	352	200	170	500	0.50	0.31	156	74	95	71	82	53
	20.4	16.32	352	200	170	500	1.00	0.31	156	88	101	71	89	65

Table 5. 5 Shear strength of columns, obtained from different experiments (cont...)

Investigator	Material Properties			Section Properties					P (kN)	Vu(exp) In kN	Vu (est) In kN			
	fc' (N/mm^2)	fck (N/mm^2)	fy (N/mm^2)	b (mm)	d (mm)	a (mm)	p_l(%)	p_t(%)			BSI	ACI	EC2	CSA
Yelcin (1997)	45	36	425	550	482	1485	1.00	0.10	1800	578	739	553	630	441
Ikeda (1968)	19.6	15.68	558	200	173	500	1.00	0.28	78	74	101	84	93	74
	19.6	15.68	558	200	173	500	1.00	0.28	78	77	101	84	93	74
	19.6	15.68	558	200	173	500	1.00	0.28	156	82	119	88	104	78
	19.6	15.68	558	200	173	500	1.00	0.28	156	81	119	88	104	78
	19.6	15.68	476	200	173	500	1.00	0.28	78	58	93	76	86	68
	19.6	15.68	476	200	173	500	1.00	0.28	156	69	111	80	97	72
	19.6	15.68	476	200	173	500	1.00	0.28	156	69	111	80	97	72
Umemura and Endo (1970)	17.7	14.16	324	200	180	600	1.00	0.28	156	71	93	66	85	60
	17.7	14.16	324	200	180	400	1.00	0.28	156	106	106	66	85	67
	17.7	14.16	324	200	180	400	1.00	0.28	392	135	143	78	120	82
	17.7	14.16	324	200	180	600	1.00	0.14	392	83	123	61	106	547
	32.9	26.32	648	200	180	400	0.50	0.11	156	78	97	71	78	55
	14.8	11.84	524	200	180	400	0.50	0.13	156	51	86	55	70	50
	13.1	10.48	524	200	180	400	0.50	0.13	156	58	85	53	69	49
	13.9	11.12	524	200	180	400	0.50	0.13	156	69	86	54	69	49
	13.1	10.48	524	200	180	400	0.50	0.13	156	67	85	53	69	49
Kokusho and Fukuharo (1965)	21.9	17.52	317	200	170	500	1.50	0.31	392	110	153	82	127	80
	21.9	17.52	317	200	170	500	2.00	0.31	392	110	159	82	131	84
Wight and Sozen (1995)	34.7	27.76	344	152	254	876	1.20	0.33	189	96	118	95	110	80
	33.6	26.88	344	152	254	876	1.20	0.33	178	97	115	93	108	79
	33.6	26.88	344	152	254	876	1.20	0.33	111	87	102	89	98	76
	32	25.6	344	152	254	876	1.20	0.33	0	81	80	80	81	72
	26.1	20.88	344	152	254	876	1.20	0.48	178	95	132	107	122	91
	25.9	20.72	344	152	254	876	1.20	0.48	0	86	98	96	96	84

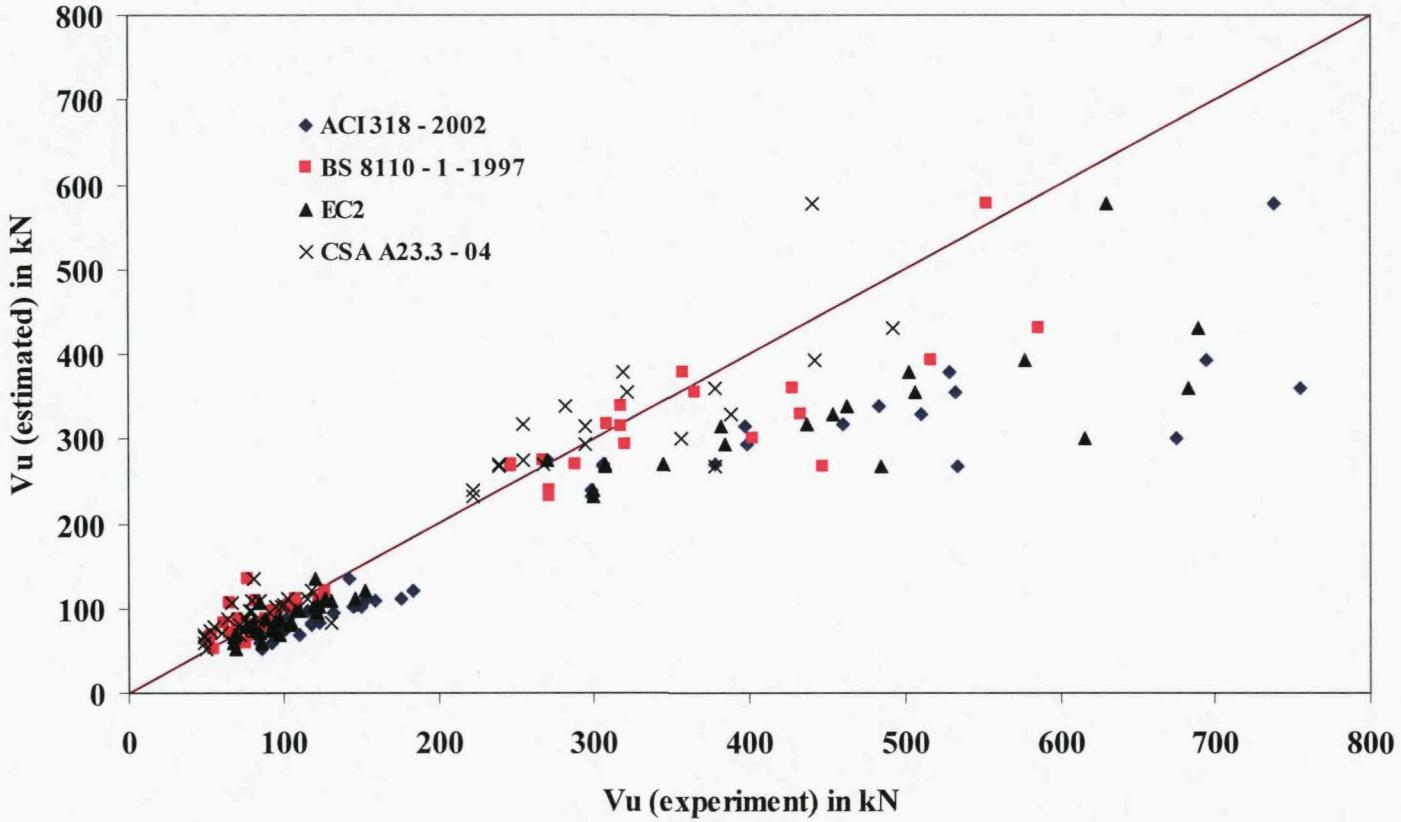

Fig. 5. 20 Comparison of shear strength of column obtained from experiments and code

Table 5. 6 Comparison of shear strength obtained using different codes

Standards	$V_{u\_experiment}/V_{u\_estimated}$		
	Mean	**Standard Deviation**	**95 % confidence interval**
ACI 318-2002	1.03	0.20	0.70 to 1.36
BSI 8110-1:1997	1.41	0.25	1.00 to 1.82
EN 1992-1-1:2004	1.25	0.23	0.87 to 1.63
CSA A23.3-04	0.93	0.18	0.63 to 1.23

5.6. Section properties

The cracking of concrete is a dominant phenomenon in RC members subjected to bending. It reduces stiffness of the member and results in increased deflections. In the case of dynamic effects it extends the natural time period of vibration which results in the reduction of blast effects on the column. It is complicated to estimate the cracked stiffness of the members because (i) the effective moment of inertia is not constant along the member; (ii) the modulus of elasticity of the concrete changes as the stress increases. TM 5 – 1300 (1990) recommends the average moment of inertia, given by,

$$I_{eff} = \frac{I_g + I_{cr}}{2} \tag{5.44}$$

Where,

I_{eff} - Effective moment of inertia

I_g - Gross moment of inertia, which is equal to $\frac{bD^3}{12}$

I_{cr} - Cracked moment of inertia, which is equal to FI_g, obtained from Fig. 5.26.

The ACI, EC and CSA suggested effective moment of inertia for finite element modelling purposes are summarized in Table 5.7. The presence of axial compression and steel reinforcement reduce tension cracking. The ACI and EC do not consider the effects of axial force and percentage of reinforcement in the calculation of

effective moment of inertia. Similarly the CSA does not consider the effect of the percentage of reinforcement. Hence, the charts are prepared to estimate the cracked moment of inertia considering the effect of axial force and the percentage of reinforcement.

Table 5. 7 Effective moment if inertia, adopted in different countries

Country Standards	Beam	Column
ACI 318-2000	$0.35I_g$	$0.7I_g$
EC 8: 1994-2003	$0.5I_g$	$0.5I_g$
CSA A23.3-04	$0.4I_g$	$\alpha_c I_g$ $\alpha_c = 0.5 + 0.6\frac{P_s}{f_c' A_g} \leq 1.0$

To estimate the cracked moment of inertia of the section,

= The neutral axis is estimated as explained in section 5.4.

= The reinforcement is replaced with equivalent concrete area.

= The concrete in tension zone is ignored.

= The CG of the transformed section is calculated and the moment of inertia about this CG is estimated and is termed as 'cracked moment of inertia'.

As the estimation of cracked moment of inertia is laborious and time consuming, the I_{cr} charts are developed (without considering the material partial safety factor) and are presented in Fig 5.21 for C25 concrete and the reinforcement on two opposite faces. The I_{cr} charts for other grade of concrete and arrangement of reinforcement are given in Appendix, A3.3.

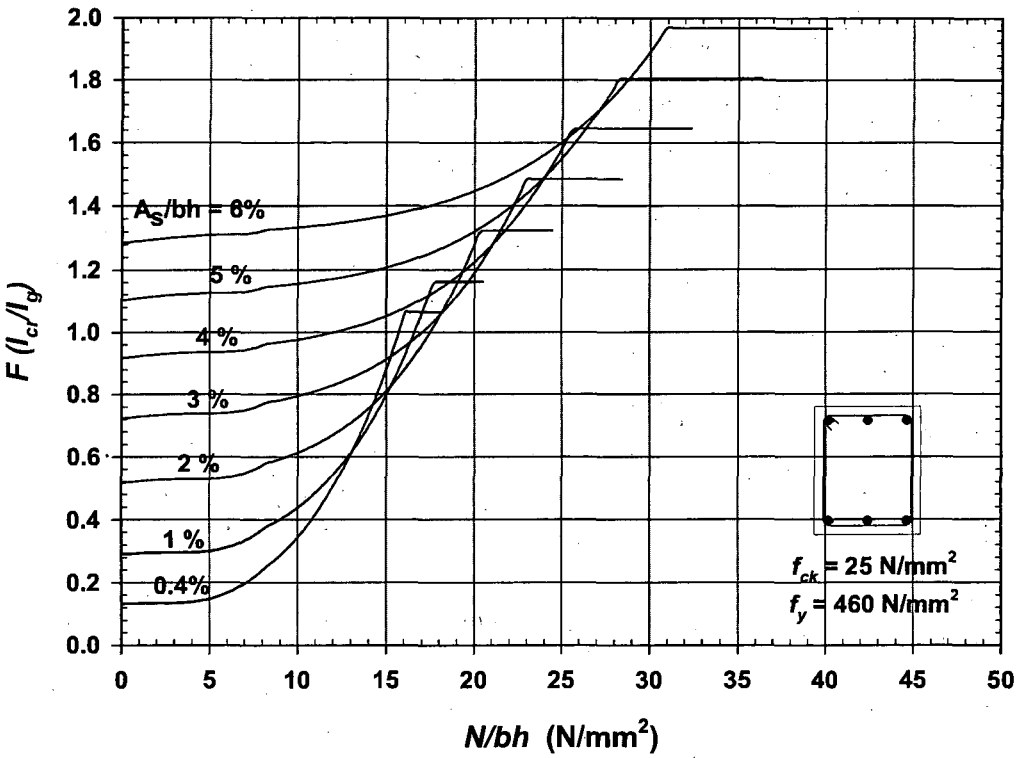

Fig. 5. 21 Cracked moment of inertia for C25 concrete columns

The blast load causes the high strain rate on column, hence considering the dynamic strength of concrete and steel (adopted in TM 5-1300) is very important. Furthermore, the occurrence of the events has very low probability, so it is not necessary to consider any partial material safety factors for concrete and steel in the design of the column. The flexural design charts for column based on British Standards, without considering any partial material safety factors, were developed and presented here. Subsequently, the shear design of column was discussed. The shear strength of the column is one of the most important parameters in the calculation of safe stand off distance and its estimation is highly empirical in nature. Hence, the exactness of the shear strength, obtained from different countries, was studied by comparing with experimental results.

Another important parameter is effective moment of inertia of the column, as it influence the column's natural time period. In dynamic analysis, it extends the natural time period of vibration which results in the reduction of blast effects on the

column. As all the codes are silent about the effect of axial compression and percentage of reinforcement on cracked moment of inertia of column, the charts are developed to estimate the cracked moment of inertia considering those effects.

5.7. Brisance effect

When a blast pressure wave impinges on the front face of an object, part of the wave reflects and other part propagates through the object and then reflects back from rear face in the form of a tensile wave. If the dynamic tensile strength of the material is exceeded then the material will crack. As a result momentum is imparted to the cracked off portion in the direction away from the structural elements in a process called spalling, which continues until the strength of propagating waves is less than that needed to cause spalling. If the initial blast wave is sufficiently strong, spalling can completely breach the structural element and this is called a *brisance failure* (Fig. 5.22).

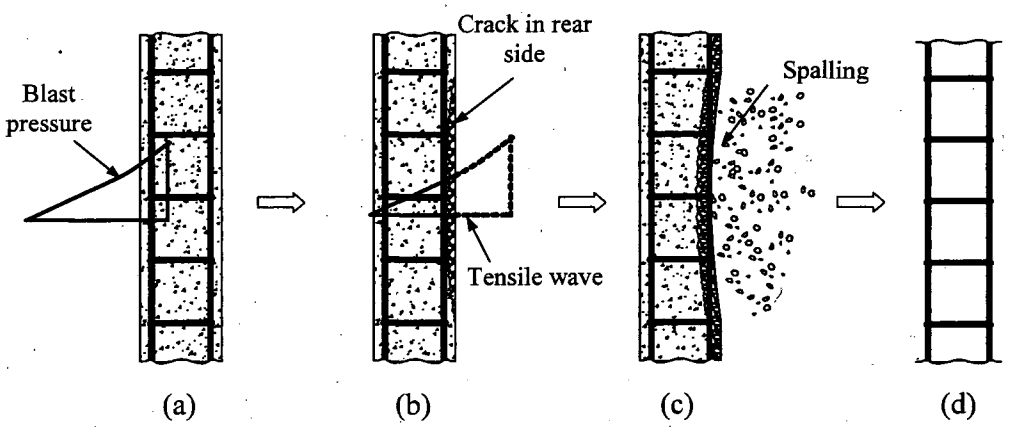

Fig. 5. 22 Spall damage of concrete walls

McVay (1988) conducted several experiments to study the influence of scaled stand off distances, charge weight, concrete wall thickness, etc., on spalling damage. Based on this research the empirical relationship shown in Fig. 5.23 was developed that can be used to estimate the potential for brisance failure. This was developed for panels but has been used herein for the assessment of columns.

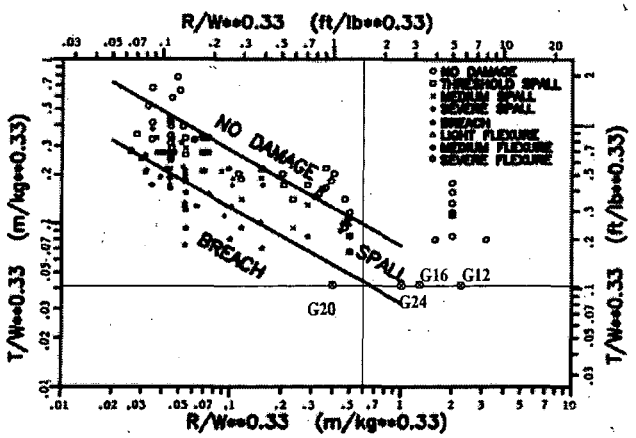

T – Depth of the column or Thickness of the wall
R – Stand off distance
W – Size of the charge weight

Fig. 5. 23 Failure of columns against brisance, (McVay, 1988)

5.8. Comparison between theoretical predictions and real behaviour using the Murrah Building as case study

A truck bomb loaded with the equivalent of 1800 kg of TNT was exploded about 2.1 m east and 4.3 m north of column G20 (FEMA, 1996). In this incident, one column was destroyed by brisance effect and another two columns by shear. The failure of these columns brought down the transfer girders which were supported by these columns, resulting in a progressive collapse. To study the behaviour of the building under direct blast and the influence of the transfer girder, this study was carried out considering two cases: first case concerning the collapse of original building; second with the building modified so that the transfer girder was removed and intermediate columns as well as second floor beams introduced as shown in Fig. 5.24.

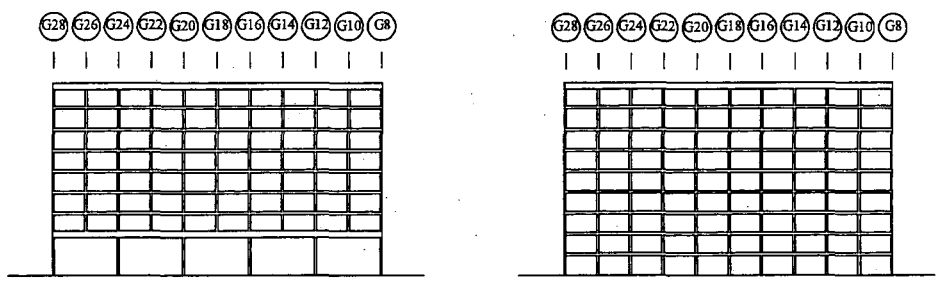

Case: 1 Building with transfer girder

Case: 2 Building without transfer girder

Fig. 5. 24 Case study on the collapse of the Murrah Building

Column failure due to brisance was assessed using the chart (Fig 5.23) provided by McVay (1980). The scaled range for the survival of reinforced concrete columns (G24, G20, G16 and G12 etc) against brisance is estimated to be more than 0.6 $m/kg^{1/3}$ (see, Fig 5.25). As the scaled distance of G20 is less than the above limiting value, this column is expected to have failed in brisance. G24, G16 and G12 columns were safe against brisance, as the scaled distance is more than the above limiting value. The intact portion of column G20 was not seen in the debris (FEMA 277, 1996), which shows the brisance failure of G20 column. One column, G20 is removed by spalling of concrete in the 1st case and two columns G22 and G20 are removed in 2nd case (Fig. 5.26). The blast loads on columns G12, G16 and G24 are calculated as per the procedure, given in section 5.2 and the profile of its blast load is shown in Fig 5.25. In the calculation of shear resistance of the columns, the enhancement in shear resistance due to the axial compression from the accidental load is also considered. Similarly, the flexural capacity of the column is calculated in the presence of axial compression from the accidental load. As mentioned in Section 5.5, the shear failure is brittle in nature, hence shear force due to blast are calculated based on elastic analysis using MDOF system modelling. At the same time, the flexural failure is ductile in nature, hence the dynamic bending moment is calculated considering nonlinear elasto-plastic analysis using SDOF system (SDOF system modelling yields the satisfactory results for moments) and the results are presented in tables 5.8 and 5.9 with the calculations for one row of the table presented in Appendix A3.4 for example purposes. The columns are assumed to be fixed at both ends in the analysis because of (i) continuity on either sides of the column; and (ii) presence of floor beams. The failure due to blast is shown in Fig 5.26 which resulted in collapse of half of the floor area as shown in Fig. 5.27.

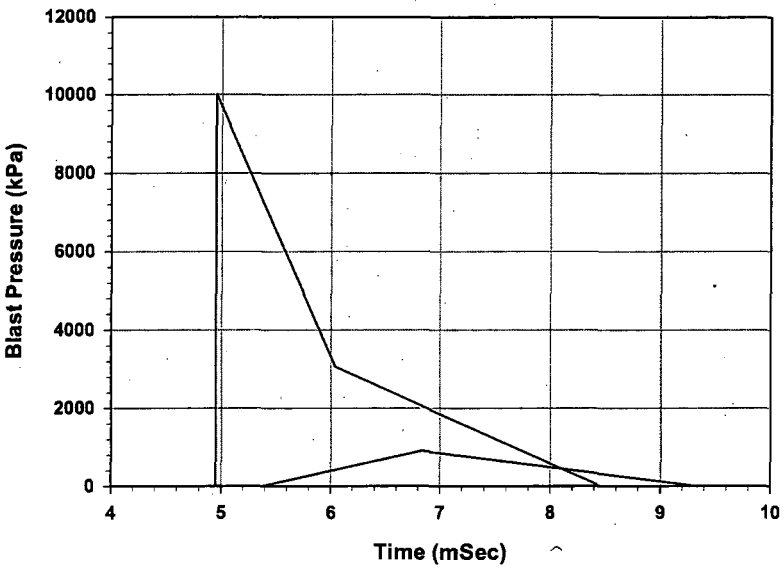

(a) Column G24

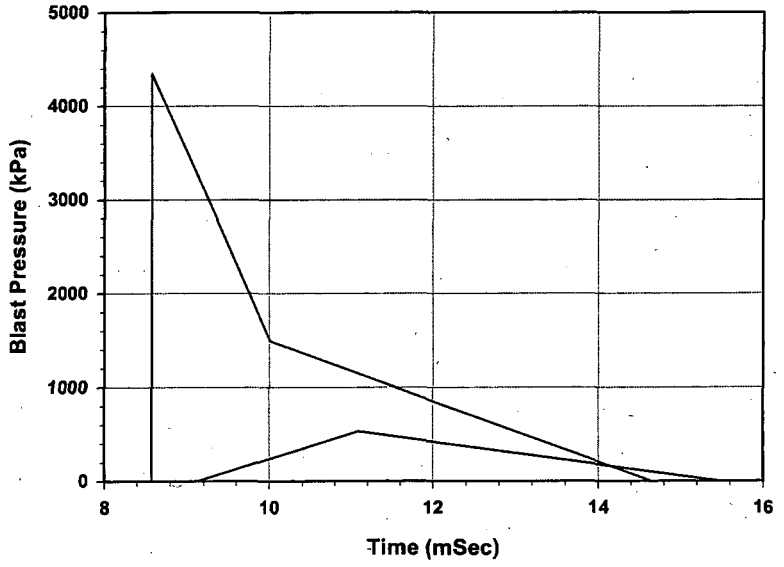

(b) Column G16

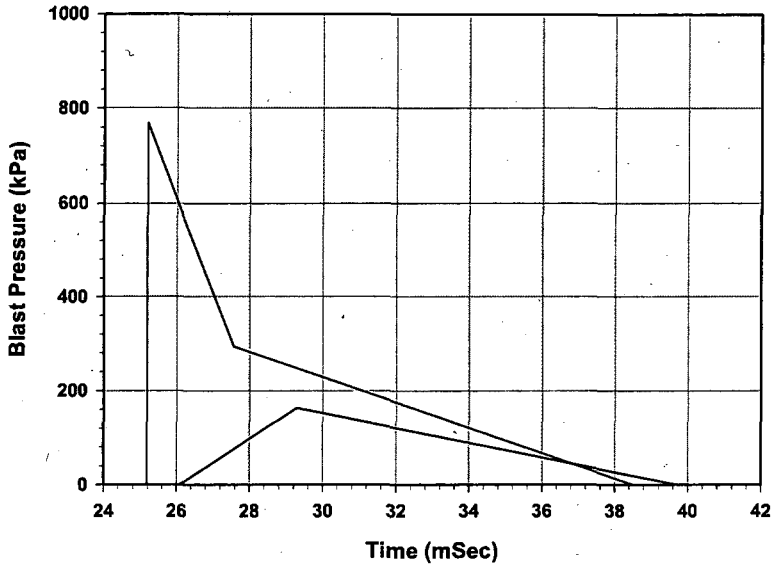

(c) Column G12

Fig. 5. 25 Blast Loadings on Columns

Table 5. 8 Blast loading and its effect on the columns (case 1)

Column No	Stand off Distance (m)	Blast Pressure (kN/m^2)	Duration of Blast Loading (mSec)	Shear Force (kN)	Bending Moment (kN-m)	Shear Capacity / Shear Force	Moment Capacity / Bending Moment	Comments
G28	22.86	1286	4.31	1896	737	1.05	1.90	Survived
G24	11.28	10023	1.80	11550	3214	0.16	0.75	Failed
G16	15.24	4354	2.73	6294	2140	0.30	1.13	Failed
G12	27.13	769	4.57	1293	603	1.46	4.01	Survived

Table 5. 9 Blast loading and its effect on the columns (case 2)

Column No	Stand off Distance (m)	Blast Pressure (kN/m^2)	Duration of Blast Loading (mSec)	Shear Force (kN)	Bending Moment (kN-m)	Shear Capacity / Shear Force	Moment Capacity / Bending Moment	Comments
G28	22.71	1312	3.39	923	335	1.17	2.71	Survived
G26	16.76	3287	2.59	1902	676	0.56	1.34	Failed
G24	10.97	10759	1.43	3725	1335	0.30	0.68	Failed
G18	9.45	15576	1.06	4025	1435	0.28	0.63	Failed
G16	14.94	4539	2.30	2388	853	0.47	1.06	Failed
G14	21.03	1684	3.18	1127	406	1.01	2.23	Survived
G12	26.82	789	3.80	721	215	1.54	4.21	Survived

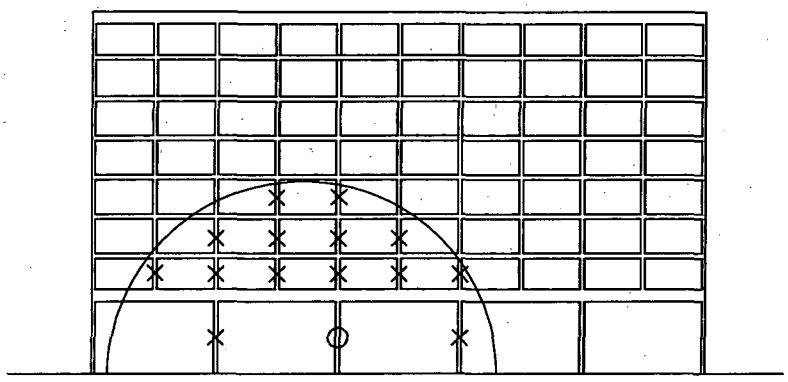

(a) Case 1

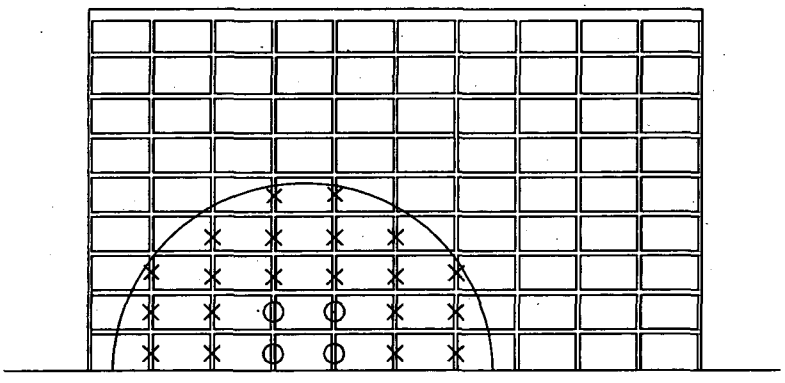

(b) Case 2

×— Shear or Flexural Failures ○ — Failure due to brisance effect

Fig. 5. 26 Failure due to direct blast effect

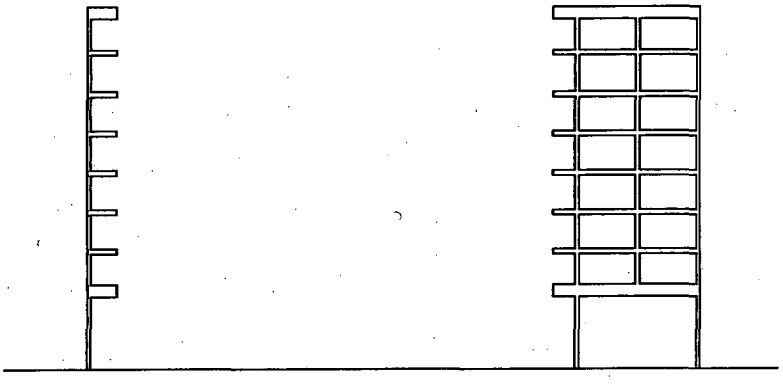

(a) Case 1

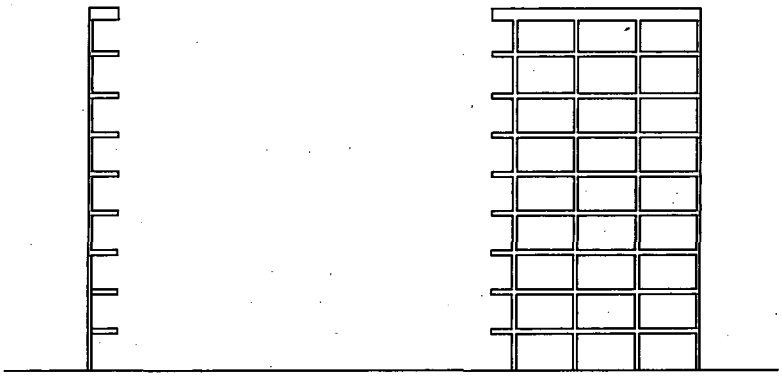

(b) Case 2

Fig. 5. 27 Failure of the Murrah Building

As the explosive is exploded in close proximity (2.1 m) to the building, most of the columns were removed by direct blast wave. In case 1, the column G20 failed by brisance and the columns G16 and G24 failed by shear. In case 2, the columns G22 and G20 were failed by brisance and the columns G26, G24, G18 and G16 failed by shear. There is little change in the subsequent failure patterns between cases 1 and 2; hence the transfer girder is not a main reason for the progressive collapse. To protect the building from a terrorist attack, the safe stand off distance for different threats such as truck, large to small vehicle, briefcase bombs needs to be maintained by providing check points.

5.9. Conclusions

Protective design against disproportionate collapse can be carried by several methods namely safe standoff distance approach, outrigger truss, double span, key element, specific local resistance and indirect design methods. The cons and pros of these methods were compared and it was concluded that design based on the safe stand off distance has probably the highest level of protection. This protective design of column against blast mainly consists of three phases: (i) estimation of blast load; (ii) dynamic analysis of column and (iii) design for the maximum shear and flexural responses.

A method to estimate blast load on columns was proposed. The load was represented in the form of a pressure-time history which includes two profiles, one represents the

load on front face and other represents the load on rear face. This complex blast profile results in complex dynamic analysis for the column. Hence, it was converted into a simple triangular impulse of equivalent area. To study the inaccuracy resulting from this simplification, a parametric study was carried out. This showed that the response is conservative and the error in column response for the triangular impulse is less than ten percent. Since, the column is subjected to high strain rates, therefore the dynamic strength of concrete and steel (adopted in TM 5-1300) was used in the analysis. The partial material safety factors for concrete and steel in the design of the column were not included, as the occurrence of the events has very low probability. The flexural design charts for columns were based on British Standards, without considering any partial material safety factors. Subsequently, the shear strength of column was discussed. Its estimation is highly empirical in nature; hence the exactness of the shear strength, obtained from different countries, was studied by comparing with experimental results. The study concluded that the strength obtained using BS 8110-1:1997 provides a sensible margin of safety, however CSA and ACI underestimated the shear strength for few samples. Anyway, this underestimation can be managed by introducing the factor of safety. The charts (Fig. 5.21) were developed to estimate the cracked moment of inertia of column considering the effect of axial compression and percentage of reinforcement.

Subsequently, a case study of the Murrah building was carried out. In the case study the building was considered with and without considering the use of the transfer girder. In both cases, columns failed by either brisance or shear, due to the blasts of blast pressure. Consequently, this local failure led to the disproportionate collapse in which half of the floor area of the building destroyed. The results of case 1 state that the predicted behaviour corresponded well to that determined from the forensic investigation namely, two columns failed by shear and one by brisance as predicted from McVay. The results of case 2 show that the provision of the transfer girder is not a primary reason for the progressive collapse. Even if the building were designed as per GSA guidelines, it could not have survived.

Chapter 6.

Protective Design for RC Framed Structures: The Safe Stand off Distance Approach

6.1. Introduction

In the safe stand off distance (SSD) approach, safety against blast is ensured by providing sufficient distance between potential devices and the structure to avoid failure. In the case of buildings in which ground floor columns are exposed to the outside environment the reflected pressure on the front face 'clears' quickly; subsequently the blast wave reaches the rear face and the pressure on the rear face rises to the incident pressure, as explained in chapter 5. This phenomenon is termed as 'clearing'. In the case of columns whose space between is infilled with load bearing elements, such as brick and sandwich panels, the blast wave takes time to breach the infilled wall; in that case the clearing of reflected pressure will not occur quickly enough and the reflected pressure takes time t_r to decay to zero. This condition is termed as 'no clearing' and it represents the worst case scenario. The typical pressure-time histories for clearing and no clearing are shown in Fig. 6.1. In this chapter, the method to estimate the safe scaled distance is proposed considering both clearing and no clearing and corresponding design charts are developed.

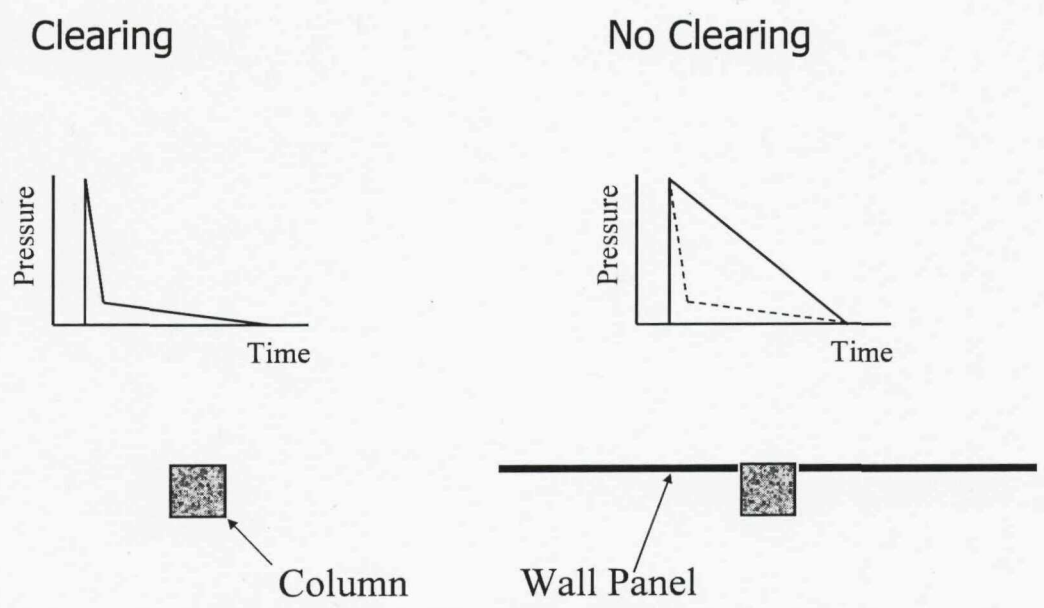

Fig. 6. 1 Typical Pressure time histories for clearing and non clearing

6.2. Calculation of Blast Load

In the calculation of safe stand off distance, the duration of blast load is an important parameter. The blast load profile for clearing is complex; hence it is simplified in the present analysis into a triangular impulse by adopting the same reflected pressure and with the time duration adjusted to give an equivalent impulse, as explained in chapter 5.

The blast load profile, shown in Fig 5.5 has many variables consisting of (i) the blast wave parameters (such as reflected and incident pressures, the duration of incident pressure and wave front velocity) at both the front and rear faces and (ii) the column dimension such as breadth and depth. These variables make the calculation of safe stand off distance complex. This was acceptable for assessing the behaviour of a single structure such as the Murrah Building. However, for development of SSD design charts covering a very wide range of variables a more simplified blast pressure time history is required for the clearing case. In view of this two simplifications to the full pressure-time profile are investigated herein, with their impulses compared with those of the full (unsimplified) pressure-time history profile.

Simplified Pressure Time Profile – 1

Assumption: the effect of static overpressure on the front face is assumed to be fully nullified by that on the rear face. This leaves only the drag pressure remaining up until time t_d, static over pressure is ignored. The simplified profile is shown Fig. 6.2.

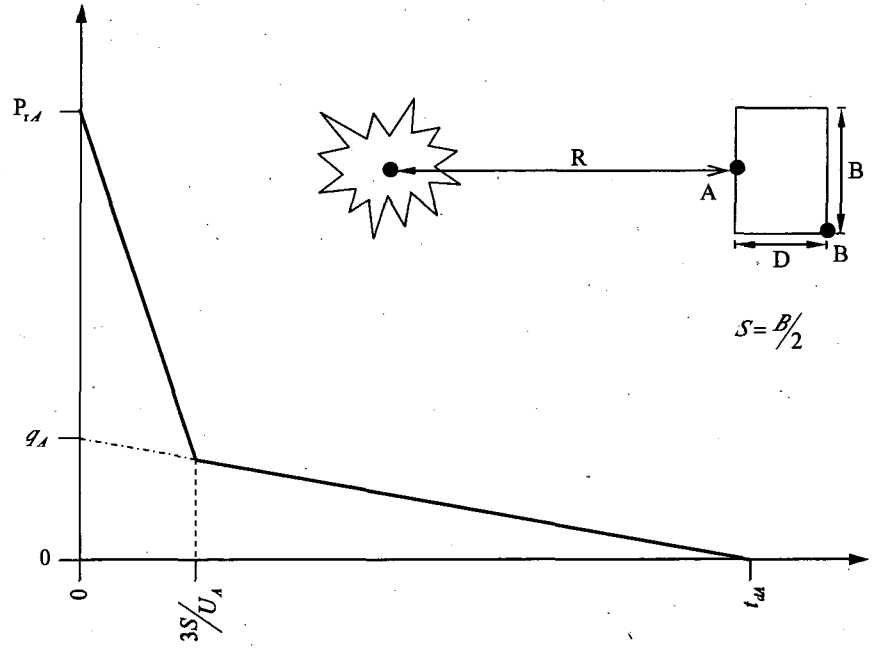

Fig. 6. 2 Pressure Time Profile – 1

Simplified Pressure Time Profile – 2

Assumption: as with the simplified profile 1 we assume the static overpressures are equal on both the front and rear faces. The difference in the approach is that the time for the rear face over pressure to rise is included. Based on this assumption, the complex pressure-time history is converted into the profile shown in Fig. 6.3.

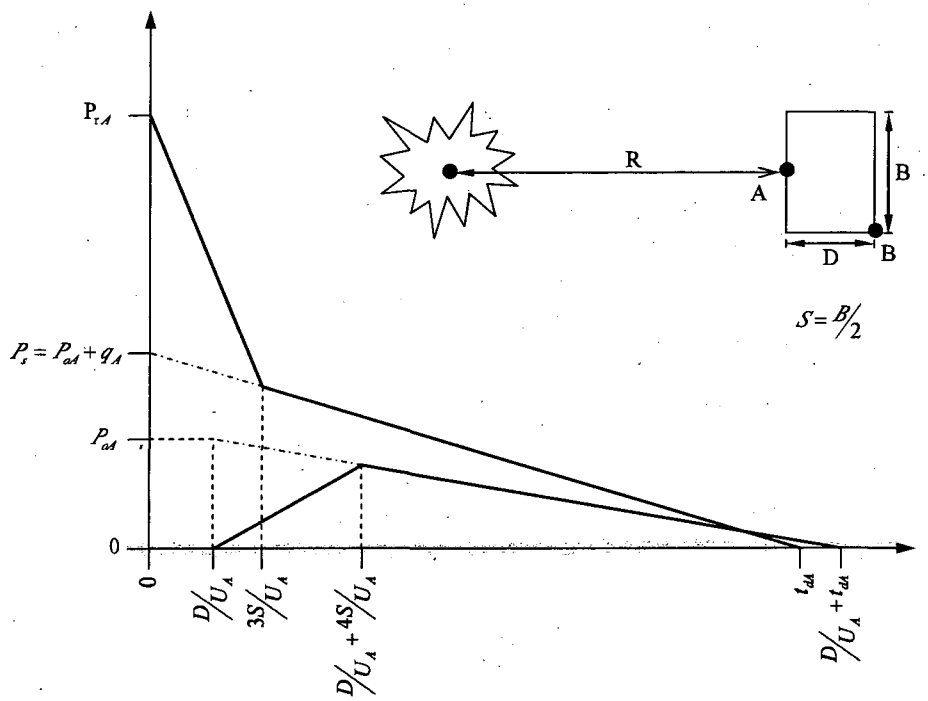

Fig. 6. 3 Pressure Time Profile – 2

The parametric study presented in section 5.2.1 is extended to check the degree of inaccuracy inherent in these two approaches. The simplified pressure-time histories for the typical columns are shown in Tables 6.1 and 6.2. The impulses of these profiles are compared with those of the complex profile (Table. 5. 3). The impulse of profile 1 differs by 4 to 9 percent and the profile-2 differs by less than 2 percent (Fig. 6.4), hence profile 2 is used in developing the SSD design charts in the case of clearing.

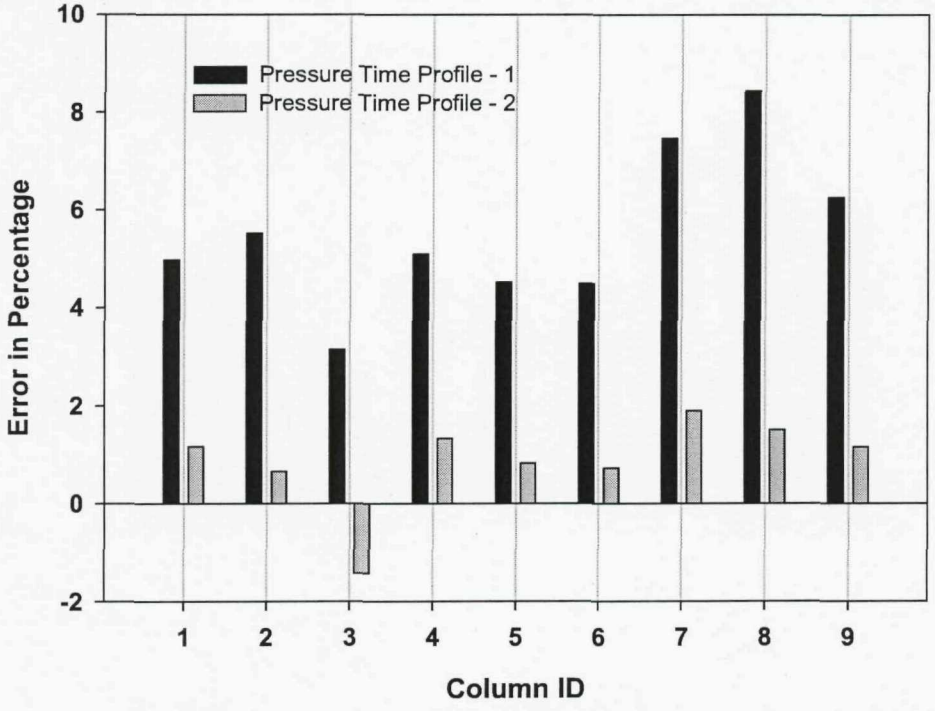

Fig. 6. 4 Percentage error in the impulses of different pressure-time profiles

Table 6. 1Pressure Time Profile - 1

Column ID	Charge Weight	Breadth	Depth	Stand off distance	Scaled distance	Front face loading				Net Impulse	Duration of Blast Load	% error in estimation of Impulse or duration of blast load
						Pressure		Time				
						P_r	$P_s(t_c)$	t_c	t_d	I	t_{dI}	
	(kg)	(mm)	(mm)	(m)	($m/kg^{1/3}$)	(kN/m^2)	(kN/m^2)	(mSec)	(mSec)	(kN/m^2-mSec)	(mSec)	
1	230	300	300	12	1.96	1125.09	193.07	0.71	5.65	942.35	1.68	4.98
2	230	450	300	12	1.96	1125.09	179.27	1.06	5.65	1102.07	1.96	5.52
3	230	600	450	6	0.98	8608.66	1541.95	0.74	2.06	4762.12	1.11	3.15
4	1000	300	300	30	3.00	330.74	38.97	0.94	16.03	467.94	2.83	5.10
5	1000	450	300	21	2.10	912.59	150.09	1.12	10.12	1269.58	2.78	4.53
6	1000	600	450	16	1.60	2080.56	391.58	1.19	7.02	2607.70	2.51	4.50
7	1800	300	300	73	6.00	71.29	3.18	1.17	38.54	102.96	2.89	7.47
8	1800	450	300	73	6.00	71.29	3.13	1.76	38.54	122.88	3.45	8.44
9	1800	600	450	36	2.96	342.95	39.47	1.87	19.19	699.11	4.08	6.25

Table 6. 2 Pressure Time Profile - 2

Column ID	Charge Weight	Breadth	Depth	Stand off distance	Scaled distance	Front face loading				Rear face loading			Net Impulse	Duration of Blast Load	% error in estimation of Impulse or duration of blast load
						Pressure		Time		Pressure	Time				
						P_r	$P_s(t_c)$	t_c	t_d	$P_s(t_r)$	t_r	t_d	I	t_{dI}	
	(kg)	(mm)	(mm)	(m)	($m/kg^{1/3}$)	(kN/m^2)	(kN/m^2)	(mSec)	(mSec)	(kN/m^2)	(mSec)	(mSec)	(kN/m^2-mSec)	(mSec)	
1	230	300	300	12	1.96	1125.09	453.54	0.71	5.65	247.07	0.96	5.65	980.14	1.74	1.17
2	230	450	300	12	1.96	1125.09	421.10	1.06	5.65	221.75	1.44	5.65	1158.75	2.06	0.66
3	230	600	450	6	0.98	8608.66	2450.11	0.74	2.06	689.40	1.06	2.06	4986.94	1.16	-1.42
4	1000	300	300	30	3.00	330.74	147.88	0.94	16.03	106.59	1.26	16.03	486.54	2.94	1.33
5	1000	450	300	21	2.10	912.59	375.83	1.12	10.12	216.00	1.51	10.12	1318.82	2.89	0.82
6	1000	600	450	16	1.60	2080.56	786.19	1.19	7.02	365.22	1.62	7.02	2710.82	2.61	0.73
7	1800	300	300	73	6.00	71.29	33.93	1.17	38.54	30.43	1.56	38.54	109.15	3.06	1.90
8	1800	450	300	73	6.00	71.29	33.40	1.76	38.54	29.79	2.34	38.54	132.17	3.71	1.51
9	1800	600	450	36	2.96	342.95	146.88	1.87	19.19	103.45	2.51	19.19	737.12	4.30	1.15

The net impulse acting on the column is equal to the net area under the pressure-time history, shown in Fig 6.2 and is calculated using Eq. 6.1.

$$I_{approx.} = \frac{1}{2}\left(p_s\left(\frac{3.5B}{U_A}\right) + q_A\left(t_{dA} + \frac{2.1B}{U_A}\right)\right) \tag{6.1}$$

The duration of the blast is assumed to be equal to the minimum of the fictitious duration, obtained using Eq. 6.2 or the duration obtained based on Eq. 6.3. The Eq. 6.2 yields a minimum value where the reflected pressure takes more time to clear, i.e., the width of the column is large. Similarly, Eq. 6.3 yields a minimum value where the reflected pressure takes much less time to clear, i.e., the width of the column is very small.

$$t_d = \frac{2I_r}{p_r} \tag{6.2}$$

$$t_d = \frac{2I_{approx.}}{p_r} \tag{6.3}$$

This equation can be simplified to,

$$t_d = \frac{7}{8}\left(\frac{B}{U_A}\right)\left(1 + \frac{2P_s}{P_r}\right) + \frac{5}{12}t_{dA}\left(1 - \frac{2P_s}{P_r}\right) \tag{6.4}$$

Where,

B - Width of the face which experience the blast pressure

I_r - Reflected impulse

I_{approx} - Area under the pressure-time history of Fig. 6.2

P_r - Reflected pressure on the front face

P_s - Incident pressure on the front face

q_A - Dynamic pressure on the front face;

t_d - Duration of blast load

t_{dA} - Duration of incident pressure on the front face

U_A - Blast wave front velocity for the front face

6.3. Calculation of SSD

The safe scaled distance is calculated considering both shear and flexural failure, with the minimum of these values taken as the safe scaled distance. As discussed in chapter 4, an elastic MDOF analysis is carried out for estimating the dynamic shear forces with the uncracked transformed section moment of inertia is used in the calculation of the natural time period ($I_g + I_s$), where I_g is the gross moment of inertia and I_s is the second moment of transformed area of steel about the CG of the section. This is because shear failures are associated with small displacements. In this situation it is also possible but less accurate to use just the gross moment of inertia for the concrete section, which is typically 20% lower than the transformed section value. Including the contribution of the rebars, it yields a conservative result as the increased moment of inertia reduces the natural time period of the column, resulting in greater dynamic shear force.

Analysing flexural we use a SDOF analysis because Chapter 4 demonstrated this to be within a reasonable degree of accuracy. Since flexural failure is ductile elasto-plastic behaviour of the column is assumed when selecting the equivalent stiffness factors for use in the solution of the equation of motion. In accordance with TM 5-1300 standard practice the moment of inertia was taken as the average of moment of inertia for the uncracked concrete section and the cracked section, $(I_g + I_c)/2$, where I_c is the cracked moment of inertia in which the concrete in compression zone and the transformed area of steel are considered.

6.3.1 SSD considering shear failure

The estimation of a SSD for a given column and charge weight is by a trial and error procedure. Initially, a close range is assumed and the blast wave parameters for the charge weight estimated. From these parameters, the blast load on the column is assessed and the dynamic analysis performed to estimate the shear force. If the dynamic shear force is greater than the shear strength then the column is not safe against blast and the stand off distance increased. This procedure is repeated until the strength of the column is exactly equal to the dynamic shear force. As described in Chapter 5 the shear capacity is in fact taken as a dynamic shear capacity, using

dynamic strength enhancement factors for both rebar and concrete strengths, with safety factors on material properties removed. However, the conventional design shear strength can also be used and this will yield a larger SSD.

It is assumed that the column survives only if the shear capacity is greater than the dynamic shear force (at the support). The dynamic shear force due to blast load is calculated based on the methods, presented in chapter 4. Mathematically, the failure of the column by shear can be expressed as follows.

$$Shear\ coefficient,\ \alpha_s \leq \frac{Shear\ capacity}{Total\ load} \tag{6.5}$$

$$Total\ load,\ W = p_r BL \tag{6.6}$$

This relationship is explained graphically in Fig 6.5. The dynamic shear force and shear capacity are made non dimensional by dividing by the total load. The total load depends on charge weight and stand off distance. The charge weight is held as a constant, hence the stand off distance is varied and its corresponding total load, shear force and t_d/t_n are estimated. The normalised dynamic shear force and shear capacity are plotted against t_d/t_n. The column is considered to be failed when the normalised shear force is less than the normalised shear capacity. The corresponding t_d/t_n value provides the SSD since t_n is constant.

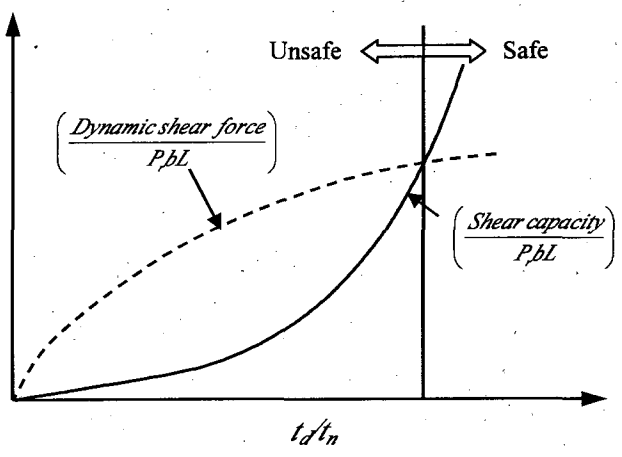

Fig. 6. 5 Safe stand off distance considering shear failure

The method of estimating the SSD is explained step by step as follows:

Step: 1 Calculate the natural time period (t_n) for the column, duration of blast load (t_d) and t_d/t_n for a range of different stand off distances (SD).

Step: 2 Calculate the total load (W) using Eq. 6.6, the shear capacity (V_c) of column section and $V_c/(P_r bL)$.

Step: 3 Calculate shear coefficients (α_s) for different t_d/t_n based on dynamic analysis.

Step: 4 Plot the curves (i) α_s Vs t_d/t_n (ii) $V_c/(P_r bL)$ Vs t_d/t_n and (iii) SD Vs t_d/t_n.

Step: 5 Obtain the intersecting point of the curves: α_sVs t_d/t_n and V_c/WVs t_d/t_n

Step: 6 Finally, obtain the stand off distance corresponding to the intersecting point.

6.3.2 SSD considering flexural failure

Mathematically the failure of the column by flexure can be expressed as follows:

$$\textit{Dynamic bending moment} \le \textit{Moment capacity}$$

$$\textit{Bending moment coefficient} \cdot \left(\textit{Total load} \cdot \textit{Span}\right) \le \textit{Moment capacity}$$

$$\textit{Bending moment coefficient} \le \frac{\textit{Moment capacity}}{\textit{Total load x Span}} \qquad (6.7)$$

Eq. 6.7 is explained graphically in Fig 6.6. The dynamic bending moment and moment capacity are non-dimensionalised by dividing though by total load x length. The total load depends on a charge weight and stand off distance. For different stand off distances the total load, bending moment and t_d/t_n are estimated. The normalised dynamic bending moment and moment capacity are plotted against t_d/t_n. The SSD is determined thereafter in the same manner as for shear.

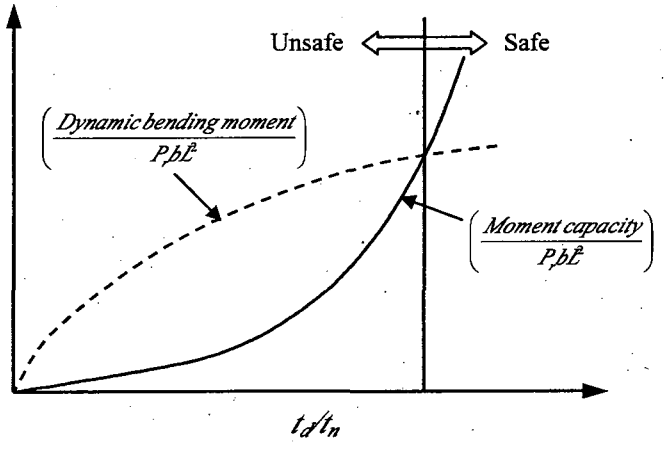

Fig. 6. 6 Safe stand off distance considering flexural failure

The method of estimating the SSD is explained step by step as follows:

Step: 1 Calculate the natural time period (t_n) for the column, duration of blast load (t_d) and t_d/t_n for different stand off distance (SD).

Step: 2 Calculate the total load x span ($P_r bL^2$), the moment capacity (M_c) of column section and $M_c/(P_r bL^2)$.

Step: 3 Calculate bending moment coefficients (α_m) for different t_d/t_n based on dynamic analysis.

Step: 4 Plot the curves (i) α_m Vs t_d/t_n (ii) $M_c/(P_r bL^2)$ Vs t_d/t_n and (iii) SD Vs t_d/t_n.

Step: 5 Obtain the intersecting point of the curves: α_m Vs t_d/t_n and $M_c/(P_r bL^2)$ Vs t_d/t_n

Step: 6 Obtain the SSD corresponding to the intersecting point.

6.4. A case study on the Murrah Building

At this stage it is worth reviewing the Murrah Building using this method. The blast load (W) and its duration (t_d) are estimated for varies stand off distances (3 to 50 m) and a charge weight of 1800 kg. From the column dimensions and the reinforcement details, the natural time period (t_n) and the shear strength of the column (V_c) are estimated. Based on the dynamic analysis, the shear coefficient of the column is estimated for different (t_d/t_n) ratio. The curves, similar to Fig 6.6 are plotted and shown in Fig. 6.7 (a). The intersecting point yields the safe stand off distance (Fig. 6.7(b)) of 23.75 m. The forensic investigation showed column G16 was 15.24 m away from the blast and failed in shear, whereas the next closest column (G12) was 27.13 m away and survived. The SSD charts demonstrated that shear was critical, with the SSD of 23.75m, lying as would be expected between G12 and 16. Thus the expected response corresponds with that observed.

For case 2 the SSD was reduced to 21.8m. This figure remains high because t_n reduces due to the shortened length. This creates a lower t_d/t_n value, thus attracting higher dynamic shear forces to the column. This and the reduced shear strength offsets the advantages of lower load due to reduced length and width. Therefore the SSD remains largely unchanged. The result is that the columns introduced into G14 would survive, although columns G16 to 26 would all fail. This would result in only a slight reduction in the extent of the progressive collapse.

It is of interest to consider the probable response of this building to a range of bomb sizes. Using this approach safe stand off distances of 33.5, 23.75, 11.64 and 5.15 m should be maintained for the case 1 building to protect it from the threat of truck, large and small vehicles, and briefcase bombs respectively, see Tables 6.3. Similarly, safe stand off distances of 29.0, 20.80, 9.80 and 4.30 m should be maintained for case 2 to protect from truck, large and small vehicles, and briefcase bombs respectively. The safe stand off distance increases gradually with increase in charge weight (Figs. 6.8).

The safe scaled distance provides a quick and simple means for developing a SSD. The US DoD (DoD, 2005) provides a range of safe scaled distances for different types of structure and recommends a safe scaled distance of 4.36 m/kg$^{1/3}$ (11 ft/lb$^{1/3}$) for unstrengthed framed structures. This US DoD value is obtained from the observations in field blast tests on structural models and low rise structures irrespective of the type of structure, the configurations, and the behaviour of structural elements. Recent work finite element modelling using LS DYNA3D by Wu and Hao (2007) has indicated that this value may be conservative, with a safe scaled distance of 1.8 m/kg$^{1/3}$ where column axial forces are low and 1.18 m/kg$^{1/3}$ where column axial forces are high. The reason for the different scaled distance is, the axial compression enhances the shear strength of the column section considerably and this enhancement leads to a reduced safe stand off distance.

Under accidental limit state load (1.0 DL + 1/3 of IL) the axial compression in the columns is of the 10 to 25 % of $A_g f_c'$. Hence the scaled distance of 1.8 m/kg$^{1/3}$ is considered for the comparison. Fig 6.9 shows that the safe scaled distances are nearly same (2.0 m/kg$^{1/3}$) for all the charge weights, even for the truck bomb. The scaled distance of 2.0 m/kg$^{1/3}$ is considered as a safe scaled distance for the Murrah building and it compares with that from Wu and Hao.

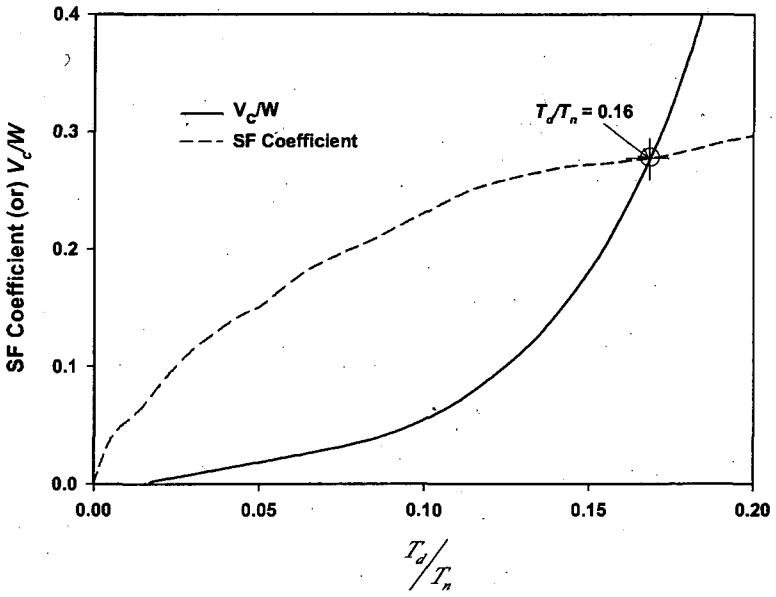

(a) α_s Vs T_d/T_n and V_c/W Vs T_d/T_n

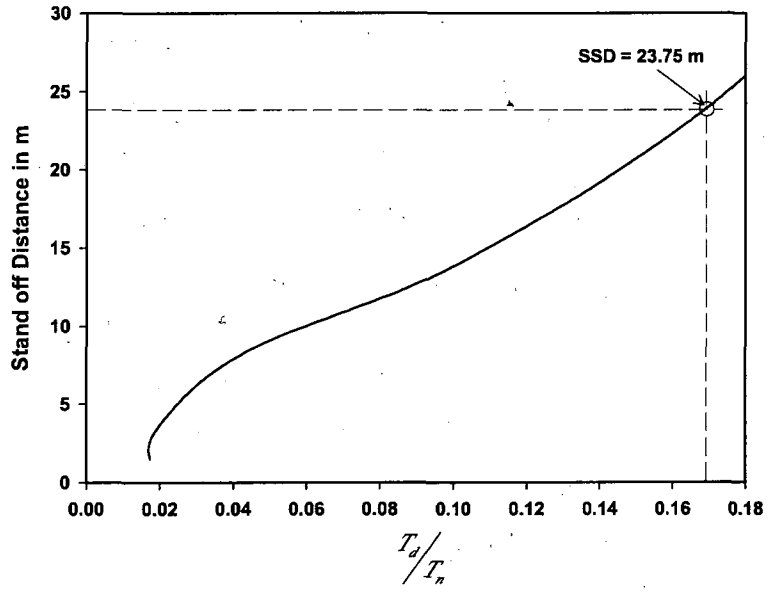

(b) Stand off distance Vs T_d/T_n

Fig. 6. 7 Safe Stand off Distance for the Murrah building in case of vehicle (van) bomb considering shear failure of the column

Table 6. 3 Safe scaled distance considering shear failure of columns

Charge Weight (kg)	Safe Stand off Distance (m)		Safe Scaled Stand off Distance ($m/kg^{1/3}$)	
	case 1	case 2	case 1	case 2
Truck Bomb - 4500	33.50	29.00	2.03	1.76
Vehicle Bomb (van-US) - 1800	23.75	20.80	1.95	1.71
Vehicle Bomb (van-UK) - 1800	19.50	16.80	1.95	1.68
Vehicle Bomb (car-UK) - 1800	15.40	13.00	1.94	1.64
Vehicle Bomb (car-US) - 230	11.64	9.80	1.90	1.60
Briefcase Bomb - 25	5.15	4.30	1.76	1.47

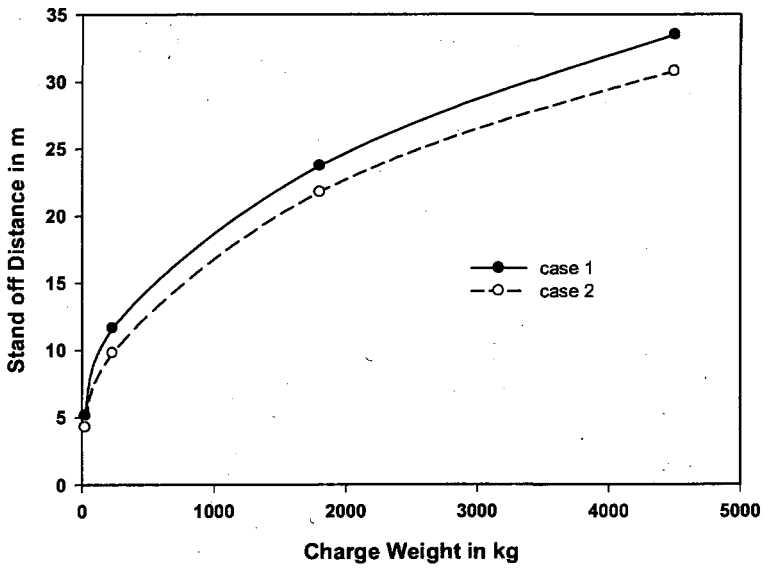

Fig. 6. 8 Safe stand of distance for the Murrah building

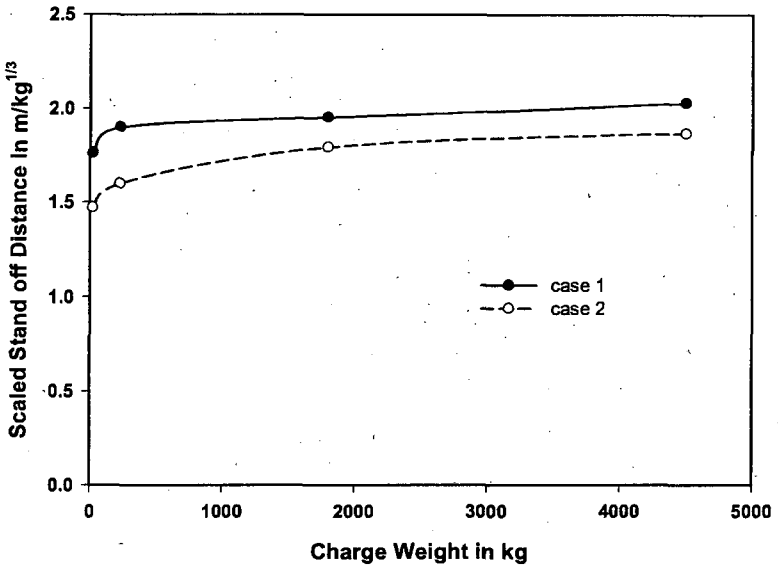

Fig. 6. 9 Safe scaled distance for the Murrah building

6.5. Development of Design Charts

We have a system for calculating SSD for a given set of parameters. The analysis is complex and therefore to create a usable approach for use by engineers, it is necessary to create a set of design charts for used by hand or interpolation functions that can be programmed into a spread sheet. This section describes how these design aids are developed using the method described in section 6.3. Because these functions and charts are sensitive in nature they are contained in an accompanying document called "Charts for estimating safe stand off distances". These charts fall into the following broad categories: those with and without clearing, and those for shear and those for flexure. Within these categories the end conditions create additional subcategories.

The creation of these charts is not as simple as fixing all parameters (e.g. charge weight, concrete grade, etc) and adjusting only a single parameter to create a relationship between lets say the D/L ratio with SSD. This is because the safe stand off distance may not be a linear function. The first step in developing an expression for SSD is to identify the influencing parameters. This is achieved through the following mathematical models.

6.5.1 Identifying the influencing parameters of SSD

The dynamic shear force can be mathematically represented as follows (the derivation of these equations is given in Appendix A.4.1),

$$V = f_1\left[W, B/L, D/L, L, I_t/I_g, f_{ck}, SD\right] \qquad \text{(Clearing)} \qquad (6.8)$$

$$V = f_1\left[W, D/L, L, I_t/I_g, f_{ck}, SD\right] \qquad \text{(Non clearing)} \qquad (6.9)$$

Where I_t is the second moment of area for the transformed section. For simplicity this is not broken down into sub parameters such as area of compression steel, cover thickness etc. Instead a chart is developed; see Fig. 5.21, in which the effect of axial compression and the reinforcements on cracking is included. In accordance with previous analysis, this was created using $I_g + I_s$ where I_g is the gross moment of inertia and I_s is the second moment of area of steel reinforcement about the CG of the section.

The explanation for the decision to divide B by L and D by L in this list of influencing parameters was that it reduces the size of the number range to 0.05 to 0.3 for typical column sizes. This had numerical advantage in speed of calculation.

The shear strength is normalised by dividing by $\sqrt{f_{ck}}bD$ to create the shear strength factor that can be represented by Eq. 6.10.

$$K_s = V_u/\sqrt{f_{ck}}bD$$

Or $$V_u = K_s\sqrt{f_{ck}}bD = V_u = K_s\sqrt{f_{ck}}\left(B/L\right)\left(D/L\right)L^2 \qquad (6.10)$$

This can be represented as

$$V_u = f_2\left[B/L, D/L, L, f_{ck}, K_s\right] \qquad (6.11)$$

Since,

Dynamic shear force, $V \le$ *Shear capacity,* V_u

$$f_1\left[W, B/L, D/L, L, I_t/I_g, f_{ck}, SD\right] \le f_2\left[B/L, D/L, L, f_{ck}, K_s\right]$$

To solve this equation, the curves, f_1 and f_2 are plotted against stand off distance, hence the variables $W, B/L, D/L, L, I_r, f_{ck}$ and K_s are constant. Then, the intersection point, SD is obtained. SD is called as safe stand off distance against shear. The safe stand off distance is mathematically represented as follows:

$$SSD_{shear} = f\left[W, B/L, D/L, L, I_r/I_g, f_{ck}, K_s\right] \quad \text{for clearing} \qquad (6.12)$$

$$SSD_{shear} = f\left[W, D/L, L, I_r, f_{ck}, K_s\right] \quad \text{for non clearing} \qquad (6.13)$$

From Eqs 6.12 and 6.13, it is identified that the SSD considering shear failure mainly depends on charge weight, concrete strength, *B/L*, *D/L*, *L*, I_r and K_s. We now use a regression analysis to create the functions relating these parameters to the *SSD*. Using the above method, the data base for safe stand off distance charts for shear and flexure are generated for the following range of variables:

= charge weight {230, 500, 1000, 1500, 1800, 4500}

= (f_{ck}) ranging from 20 to 40 N/mm^2

= breadth to length ratio $\left(B/L\right)$ ranging from 0.05 to 0.3

= depth to length ratio $\left(D/L\right)$ ranging from 0.05 to 0.3,

= length ranging from 2.5 to 6 m,

= shear strength factor (K_s) ranging from 0.1 to 0.8

= flexural strength factor ranging from 0.1 to 0.8.

Using DO loops this created an array of approximately 300,000 data points upon which the regression analysis could be based.

Development of SSD estimation functions

The first step is to develop regression analysis functions and this is done through the parametric study in which one variable is kept as independent variable and rest remain constant. From this study, the approximate relationship between the independent variable and the safe stand off distance is established. Finally, the regression functions which take many forms are developed using the unknown

parameters. For example, to study the influence of B/L the safe stand off distances are estimated by considering shear failure, set of characteristic strength of concrete, depth to length ratio, length and shear strength factor as constants and breadth to length ratio as a variable. For each data group, the curve, SSD vs. b/L is plotted and fitted with different functions such as cubic, quadratic, linear, power, exponential and inverse etc. For each fit, the coefficient of determination (R^2) is estimated and ranked. The R^2 value provides a quantitative measure of how well the fitted model predicts the dependent variable. The values of R squared that are close to 1 imply that most of the variability in y is explained by the regression model (Montgomery, 2003). The fundamentals of linear and nonlinear regression analysis are explained in Appendix 4.2. Table 6.5 shows the best three fits and their ranks. This table helps to identify the relationship between safe stand off distance and breadth to length ratio. The R-squared values are very close to 1, hence the polynomial and power ($y = ax^b$) functions can be used to correlate the variables.

Table 6. 4 Influence of *B/L* on Safe Scaled Distance

W (kg)	fck (N/mm^2)	D/L	L	$V_c/\sqrt{f_{ck}}BD$	Best Fits in Order (Higher to Lower)	respective R^2
1000	20	0.1	3	0.2	C, Q, L	1.000, 0.994, 0.994
1000	20	0.2	4	0.4	C, Q, L	0.999, 0.998, 0.994
1000	20	0.3	5	0.6	C, Q, P	0.998, 0.998, 0.987
1000	25	0.1	3	0.2	C, Q, L	0.998, 0.995, 0.994
1000	25	0.2	4	0.4	C, Q, L	0.999, 0.998, 0.994
1000	25	0.3	5	0.6	C, Q, P	0.998, 0.998, 0.989
1000	30	0.1	3	0.2	C, Q, L	0.999, 0.997, 0.994
1000	30	0.2	4	0.4	C, Q, L	0.998, 0.998, 0.993
1000	30	0.3	5	0.6	C, Q, P	0.998, 0.997, 0.990

Note: C – Cubic function; Q – Quadratic function; L Linear function and P – Power function.

A similar study was carried out to find out the correlation function for other variables, such as W, f_{ck}, D/L, L, I_t and K_s. From the study, the many possible empirical equations, shown in Appendix 4.3, were developed with the unknown

coefficients. The following three forms were considered here and these are shown with their corresponding R^2 value.

The first one was the power function:

$$SSD = AW^B f_{ck}^C \left(\frac{b}{L}\right)^D \left(\frac{D}{L}\right)^E L^F K_s^G \left(\frac{I_t}{I_g}\right)^H \qquad R^2 = 0.999$$

The second one was the polynomial function:

$$SSD = AW^B (f_{ck})^C \left(D\left(B/L\right) + E\left(B/L\right) + F\left(B/L\right)^2 + G\left(B/L\right)^3 \right) \left(D/L\right)^H L^I K_s^J \left(I_t/I_g\right)^K$$

$$R^2 = 0.998$$

The third one was the inverse function:

$$SSD = AW^B (f_{ck})^C \left(B/L\right)^D \left(E + \frac{F}{\left(D/L\right)} \right) L^G K_s^H \left(I_t/I_g\right)^I \qquad R^2 = 0.997$$

Where A, to K are constants that are determined using the software package, Statistical Package for Social Science (SPSS) that is specifically designed for this type of problem. The SPSS also gives the R^2 value for the model. Using R^2, the best solution was selected among the possible solutions. Finally, the regression analysis demonstrated that the functions of the form (Eqs. 6.21 and 6.22) below was the most accurate and also the simplest of the tried. In fact the accuracy was consistently shown to be greater than 0.99 when using the R^2 test.

$$SSD = AW^B f_{ck}^C \left(\frac{b}{L}\right)^D \left(\frac{D}{L}\right)^E L^F K_s^G \left(\frac{I_t}{I_g}\right)^H \qquad \text{for clearing} \quad (6.21)$$

$$SSD = AW^B f_{ck}^C \left(\frac{D}{L}\right)^E L^F K_s^G \left(\frac{I_t}{I_g}\right)^H \qquad \text{for no clearing} \quad (6.22)$$

The corresponding process to identify the influencing parameters for flexure is essentially the same as this. For simplicity the full details are located in Appendix A4.4. Similar to the estimation of SSD of shear failure, the empirical equations, given in Appendix A4.4 were developed based on the parametric study with the unknown coefficients. These coefficients were calculated for each empirical equation

through nonlinear regression analysis and the hypotheses were compared with R-squared values. Eqs. 6.23 and 6.24 yield maximum R-squared values of 0.996, 0.994 to estimate the SSD of a column for clearing and no clearing respectively.

$$\text{SSD} = \text{A}W^{B} f_{ck}^{C}\left(\frac{b}{L}\right)^{D}\left(\frac{D}{L}\right)^{C} K_m^{D}\left(\begin{array}{l} 1+E\ln(f_{ck})+F\ln\left(\frac{b}{L}\right)+G\ln\left(\frac{D}{L}\right)+ \\ H\ln(L)+I\ln(K_m)+J\ln\left(\frac{I_{eff}}{I_g}\right) \end{array}\right) \quad (6.23)$$

$$\text{SSD} = \text{A}W^{B} f_{ck}^{C}\left(\frac{D}{L}\right)^{D} L^{E} K_m^{F}\left(\frac{I_{eff}}{I_g}\right)^{G}\left(\begin{array}{l} 1+H\ln(f_{ck})+I\ln\left(\frac{b}{L}\right)+J\ln\left(\frac{D}{L}\right)+ \\ K\ln(L)+L\ln(K_m)+M\ln\left(\frac{I_{eff}}{I_g}\right) \end{array}\right) \quad (6.24)$$

b - Breadth of section

D - Depth of section

f_{ck} - Characteristic compressive strength of concrete in MPa

I_g - Gross moment of inertia

I_{eff} - Effective Moment of inertia

I_t - Moment of inertia of transformed section

K_m - Flexural strength factor

K_s - Shear strength factor

L - Length of column

Development of the design charts

Whilst the functions presented in the previous chapter are ideally suited to programming into a spreadsheet, it is also useful to create design charts from which the SSD can be estimated without use of a computer. Using Eq. 6.21, the design charts (Fig 6.10) are developed. For security reason the x and y axis labels are removed from the charts and these charts are provided in full in the supplementary document to this thesis. Fig 6.10 was prepared for the charge weight (W) of 1000 kg, concrete strength (f_{ck}) of 25 N/mm^2, length of 3 m, gross moment of inertia and the shear strength factor (K_s) of 0.4. For other W, f_{ck}, L, K_s and moment of inertia of transformed section, the safe stand off should be modified by multiplying with modification factors for charge weight (α_w), concrete strength (α_f), length (α_L)

and moment of inertia (α_i) and as given in Eq. 6.25. The method of obtaining safe stand off distance for a column using these charts was explained with an example in the supplementary.

$$SSD = SSD_{chart}\alpha_w\alpha_f\alpha_L\alpha_i\alpha_s \quad (6.25)$$

SSD_{chart} - Safe stand off distance of a column considering length of 3 m, concrete strength of 25 N/mm^2, shear strength factor of 0.4 gross moment of inertia and a charge weight of 1000 kg

α_f - Modification factor for concrete strength (obtained from Fig. 6.12)

α_i - - Modification factor for moment of inertia (obtained from Fig. 6.14)

α_L - - Modification factor for length of the column (obtained from Fig. 6.13)

α_s - - Modification factor for shear strength (obtained from Fig. 6.15)

α_w - Modification factor for charge weight (obtained from Fig. 6.11)

Similarly, Using Eq. 6.23, the design charts (Fig 6.16) are developed for SSD considering flexural failure. They are prepared for the charge weight (W) of 1000 kg of TNT, concrete strength (f_{ck}) of 25 N/mm^2, length of 3 m, gross moment of inertia and the flexural strength factor (K_m) of 0.2. For other W, f_{ck}, L, K_m and effective moment of inertia, the safe stand off should be modified using Eq. 6.26. The method of obtaining the safe stand off distance for a column using these charts explained with an example in the supplementary. The chart results are compared with that of expression. The comparison showed that these charts provide an exact correlation with the functions.

$$SSD = SSD_{chart}\alpha_w\alpha_f\alpha_m\left(\frac{\alpha_1+\alpha_2+\alpha_3}{\alpha_2+\alpha_4}\right) \quad \text{for clearing} \quad (6.26)$$

Where,

SSD - Safe stand off distance for a column

SSD_{chart} - Safe stand off distance of a column considering length of 3 m, concrete strength of 25 N/mm2, flexural strength factor of 0.2, gross moment of inertia and a charge weight of 1000 kg

$\alpha_1, \alpha_2, \alpha_3$ and α_4 -Modification factor for charge weight (From Figs 6.20 to 6.22)

α_f - Modification factor for concrete strength (From Fig. 6.18)

α_m - - Modification factor for flexural strength (From Fig. 6.19)

α_w - Modification factor for charge weight (From Fig 6.17)

Similarly, the charts and expressions for safe stand off distance for a column (fixed at both ends, fixed at one end and pinned at other end, and pinned at both ends) considering (i) both flexural and shear failures and (ii) with and without clearing are developed and presented in the supplementary.

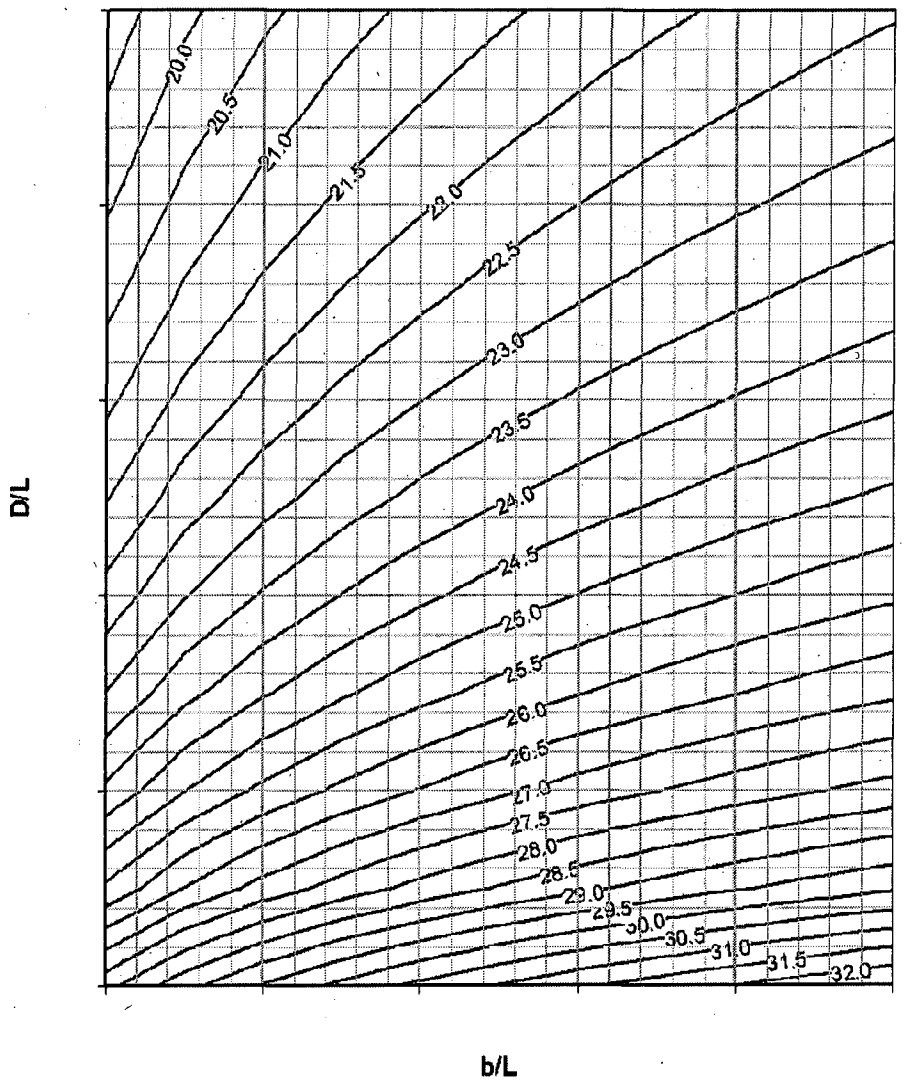

Fig. 6. 10 Safe stand off distance for a column considering its shear failure and clearing

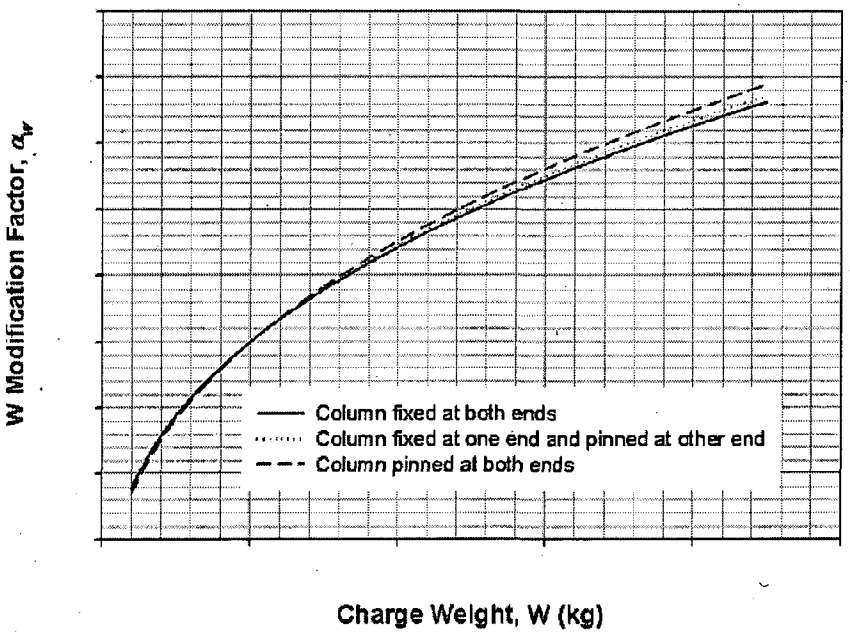

Fig. 6. 11 Charge weight modification factor considering shear failure and clearing

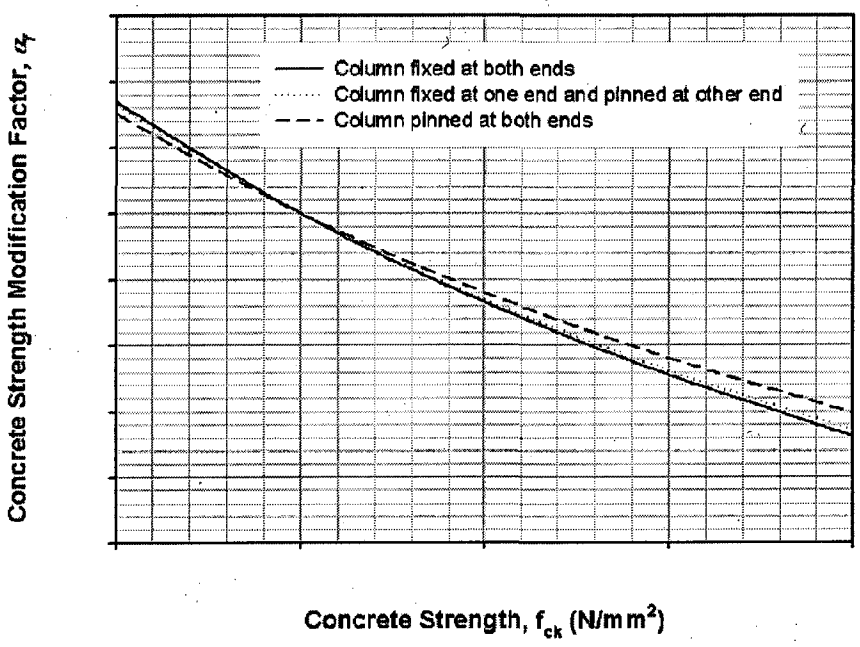

Fig. 6. 12 Concrete strength modification factor considering shear failure and clearing

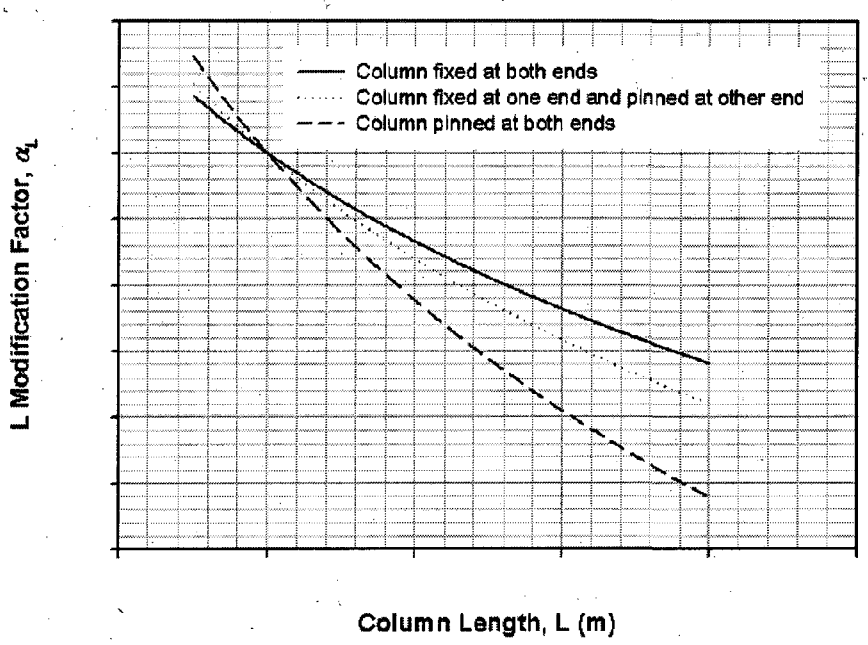

Fig. 6. 13 Column length modification factor considering shear failure and clearing

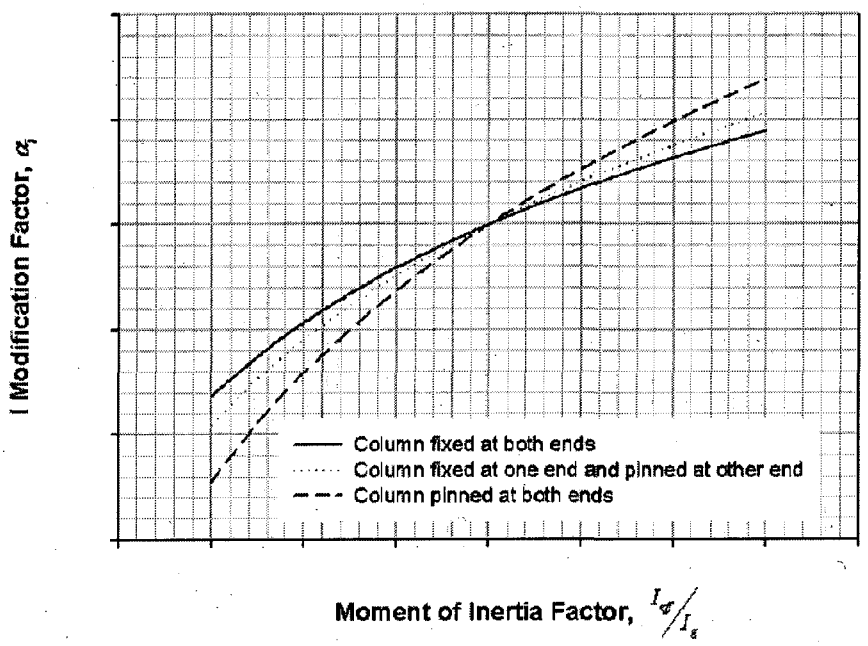

Fig. 6. 14 Moment of inertia modification factor considering shear failure and clearing

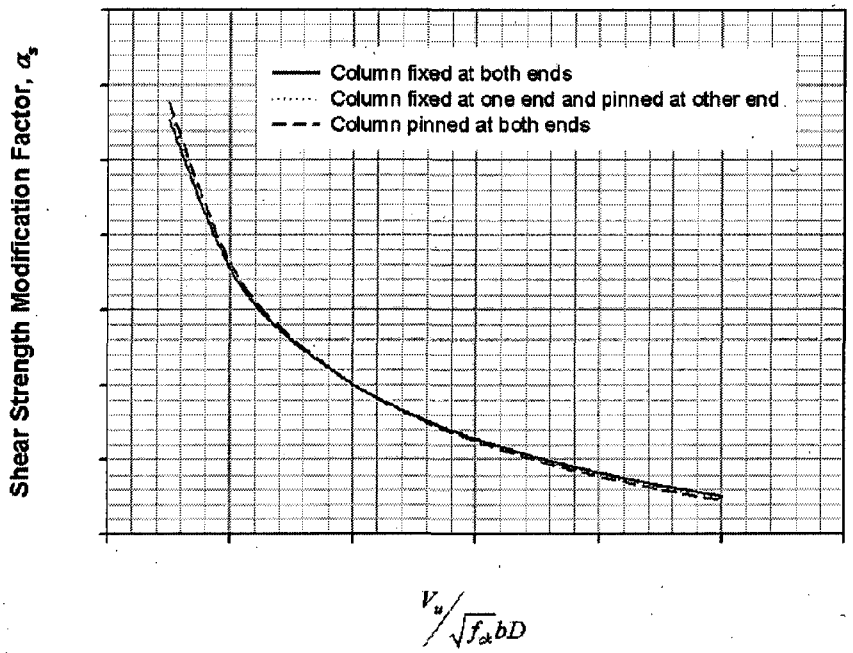

Fig. 6. 15 Shear strength modification factor considering shear failure and clearing

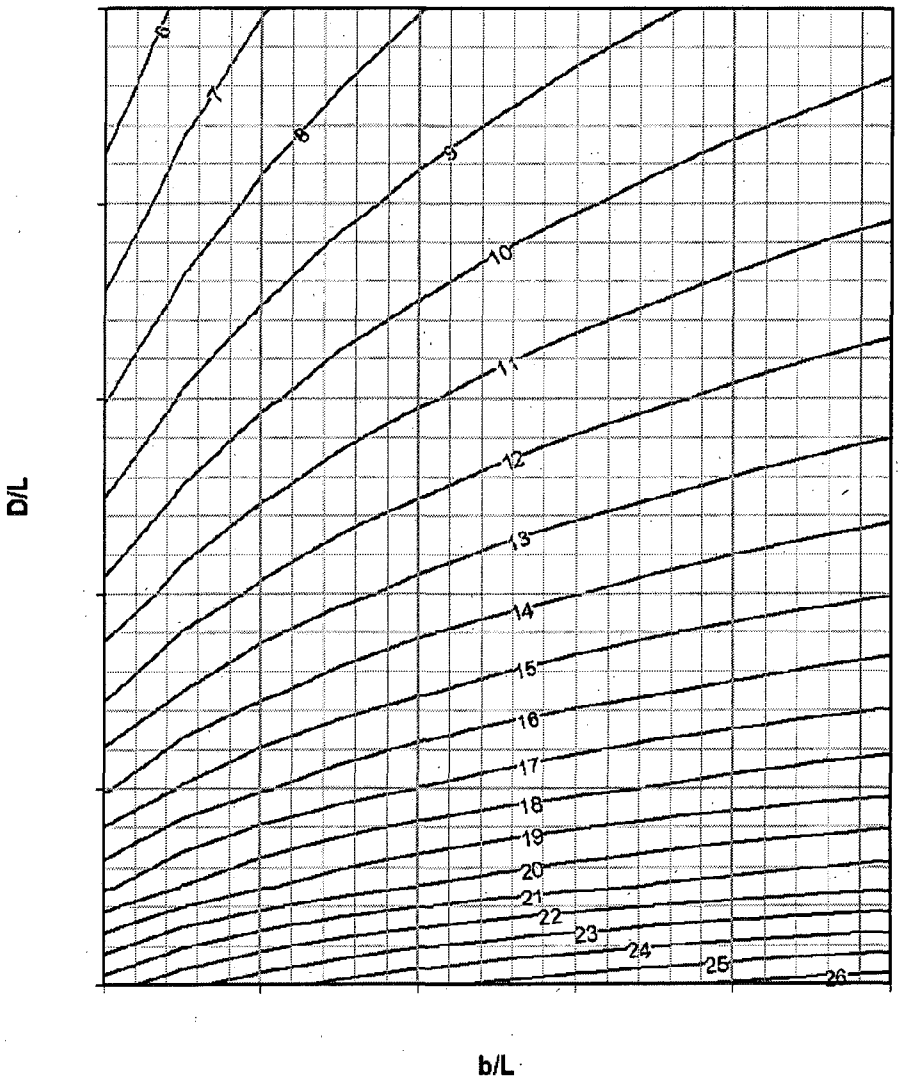

Fig. 6. 16 Safe stand off distance for a column, fixed at both ends considering its flexural failure and clearing

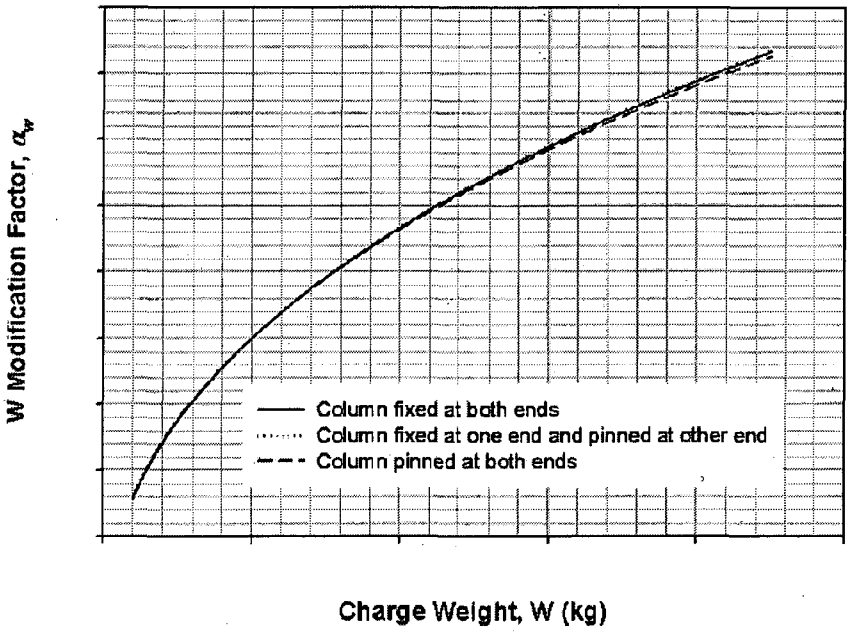

Fig. 6. 17 Charge weight modification factor considering flexural failure and clearing

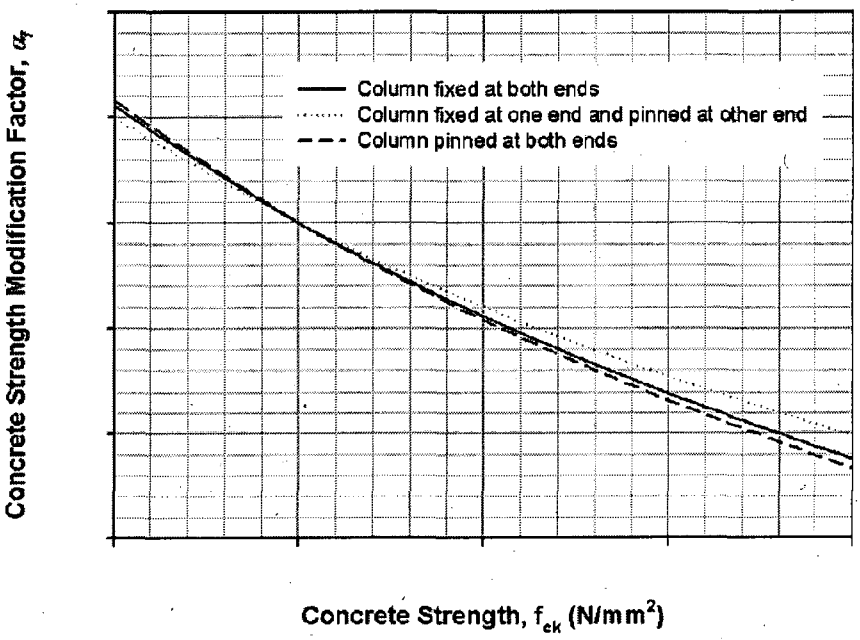

Fig. 6. 18 Concrete strength modification factor considering flexural failure and clearing

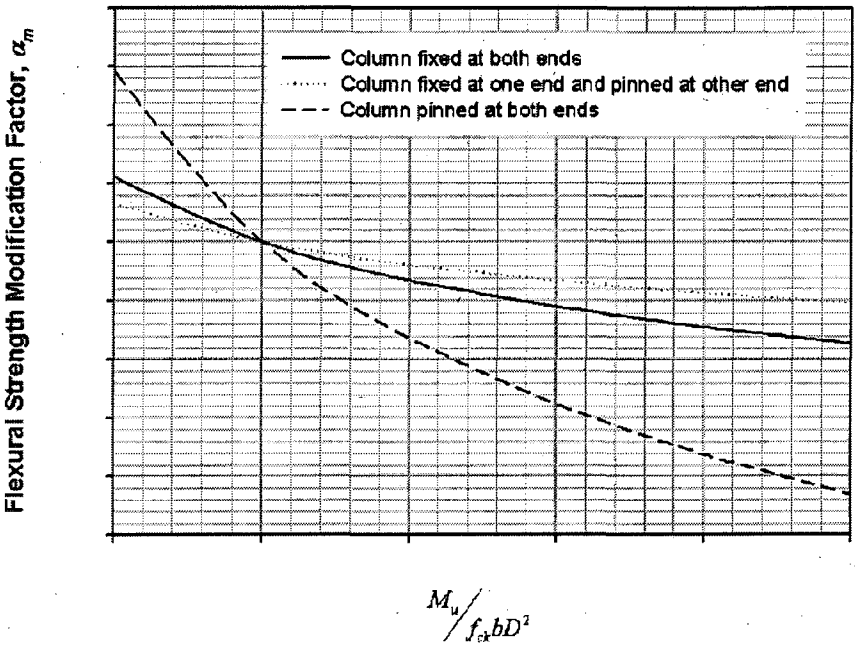

Fig. 6. 19 Flexural strength modification factor considering flexural failure and clearing

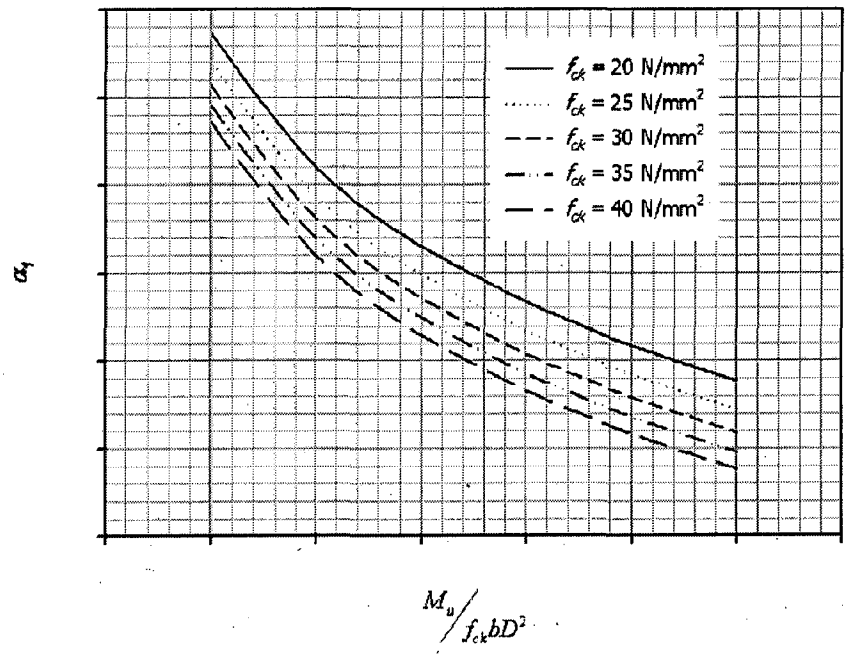

Fig. 6. 20 Modification factor, α_1 for flexural failure and clearing

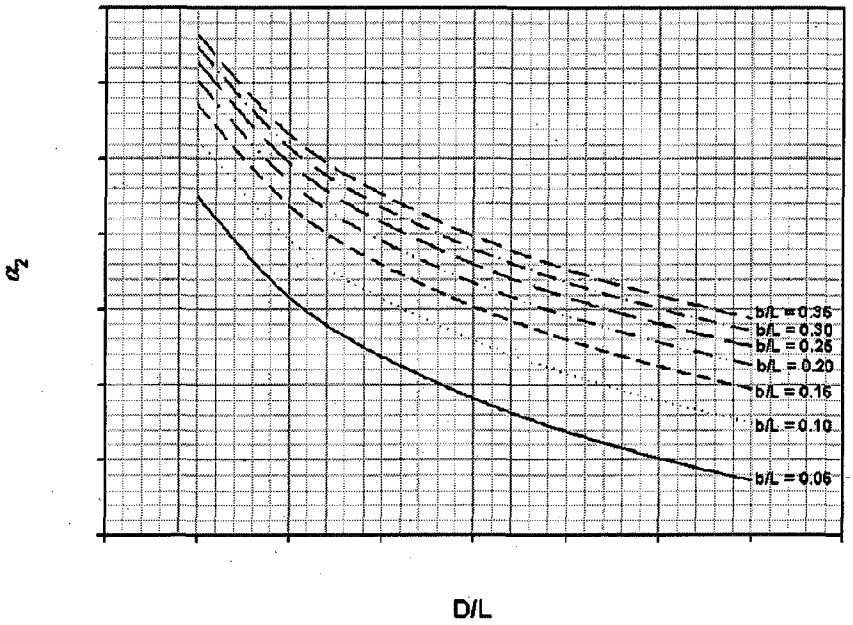

Fig. 6. 21 Modification factor, α_2 for flexural failure and clearing

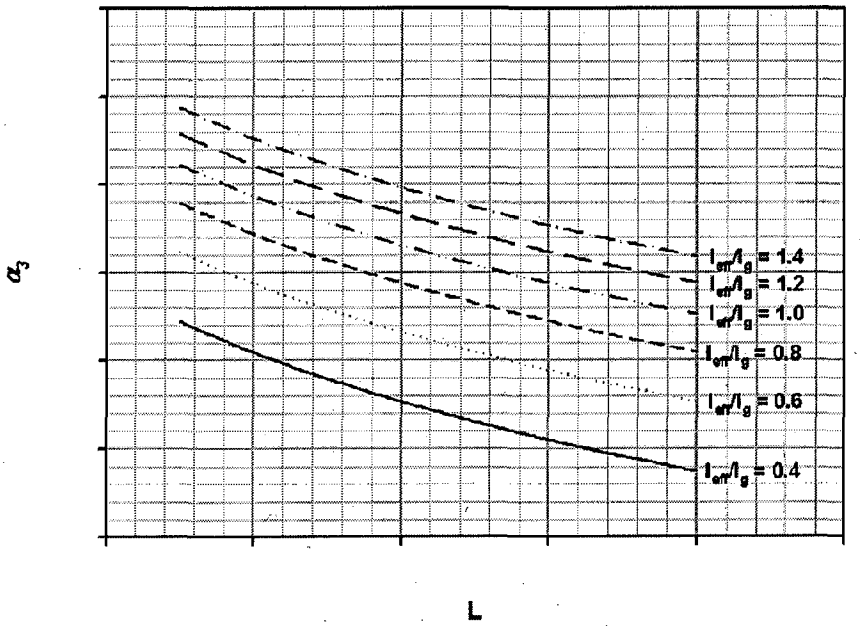

Fig. 6. 22 Modification factor, α_3 for flexural failure and clearing

6.6. Comparison between the chart predictions and those from WACOLUMMN

The charts were checked against results (called WACOLUMN), obtained from Weidlinger Associates (WA) proprietary code called FLEX, which is an explicit, nonlinear, large deformation transient analysis finite element code, developed in house. Using this it is possible to model RC members in detail, including cover and rebars (both compression and shear) explicitly for air blast and ground shock loading. WA provided the SSD for 16 columns considering different charge weights, column sizes, axial compressions, longitudinal and lateral (shear link) reinforcements. These are obtained from the detailed finite element modelling which considers all the parameters such as shear reinforcement, axial compression and the effect of high strain rate etc. Fig 6.23 shows the finite element modelling of a WACOLUMN.

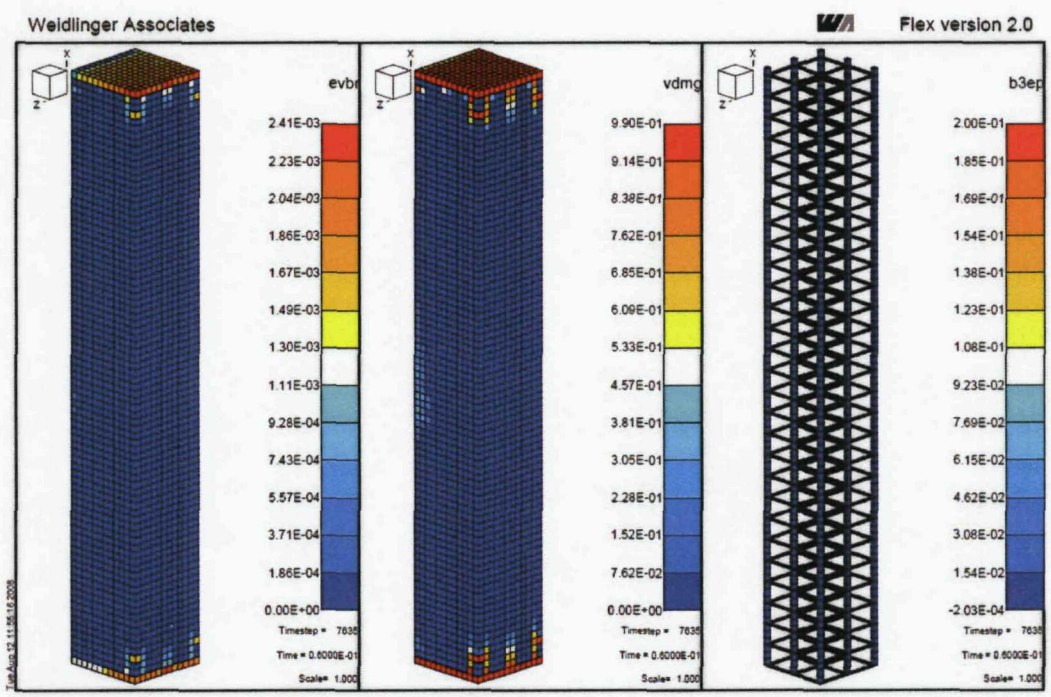

Fig. 6. 23 Column modelling in FLEX (Source:Weidlinger Associates)

These types of models are the computationally demanding and take considerable time to obtain solutions. Under typical working loads, columns can be expected to experience an axial compression of 10 to 25 % of $A_g f_c^{'}$. A total of 8 columns were reviewed, each with axial loads of 10 % of $A_g f_c^{'}$ and 25 % of $A_g f_c^{'}$. These axial loads were selected because they correspond to those values that a column would be likely

to be loaded under typical working conditions. This axial load is important, as it enhances the shear strength of column considerably, leading to shorter SSD's. Also, the dynamic strength enhancement (due to the effect of high strain rate) for both rebar and concrete are included and the partial safety factors are removed. The shear and flexural strengths of the column sections were estimated based on BS 8110 and these are presented in Tables 6.5 and 6.7. Finally, the SSD, considering both shear and flexural failures of column were estimated using the design charts (presented in the supplementary) and presented in Table 6.6 and 6.8. The maximum of these is considered as the safe stand off distance and it also shows mode of column failure. All the eight columns failed by shear. Table 6.9 is the main output from this analysis and includes the comparison between these chart predictions and the results of WACOLUMN. These column results are compared with WACOLUMN and this shows that the safe stand off distance approach has good correlation with WACOLUMN and it is conservative. The presence of axial compression enhances the shear strength of the column and leads to a reduced SSD, for example column 1 requires a safe stand off distances of 23.08 and 19.60 for the axial compression of 10 % and 25 % of $A_g f_c'$ respectively, see Table 6.9.

Table 6. 5 Dynamic shear strength of column

Column ID	f_{cd} (N/mm^2)	f_{yd} (N/mm^2)	b (mm)	d (mm)	p_l (%)	p_t (%)	P (kN)	v_c (N/mm^2)	v_c' (N/mm^2)	V_c (kN)	V_s (kN)	V_u (kN)	$V_u / (\sqrt{f_{ck}}bD)$
1	33	455.4	406.4	406.4	0.62	0.25	494	0.75	1.78	266	170	437	0.46
							1235	0.75	3.32	497	170	667	0.70
2	33	455.4	406.4	406.4	0.71	0.25	494	0.79	1.81	271	170	442	0.47
							1235	0.79	3.35	502	170	672	0.71
3	33	455.4	457.2	457.2	0.41	0.55	627	0.64	1.80	345	480	825	0.69
							1568	0.64	3.54	677	480	1157	0.96
4	33	455.4	609.6	609.6	0.64	0.31	1117	0.75	2.29	798	492	1290	0.60
							2793	0.75	4.61	1606	492	2098	0.98
5	33	455.4	609.6	609.6	0.64	0.42	1117	0.75	2.29	798	666	1465	0.69
							2793	0.75	4.61	1606	666	2273	1.06
6	33	455.4	304.8	304.8	1.09	0.42	280	0.99	1.59	129	155	285	0.53
							700	0.99	2.49	94	155	250	0.47
7	33	455.4	812.8	812.8	0.68	0.31	1979	0.76	2.36	1485	889	2374	0.63
							4948	0.76	4.76	2994	889	3883	1.02
8	52.8	455.4	355.6	355.6	0.80	0.28	609	1.00	2.27	257	144	401	0.44
							1523	1.00	4.19	473	144	617	0.67

Table 6. 6 Safe stand off distance of columns, fixed at both ends considering shear failure and clearing

Column ID	Charge Weight		f_{cd}	b/L	D/L	L	shear strength factor, K_s	I_{eff}/I_g	Safe Stand off Distance	
	(kg)	(lb)	(N/mm^2)			(m)			(m)	(ft)
1	998	2200	33	0.10	0.10	4.27	0.46	1.23	23.08	75.71
							0.70	1.23	19.60	64.30
2	1814	4000	33	0.10	0.10	4.27	0.47	1.27	28.61	93.87
							0.71	1.27	26.33	86.39
3	1814	4000	33	0.11	0.11	4.27	0.69	1.16	24.08	78.99
							0.96	1.16	23.13	75.89
4	454	1000	33	0.14	0.14	4.27	0.60	1.26	14.89	48.87
							0.98	1.26	12.35	40.51
5	454	1000	33	0.14	0.14	4.27	0.69	1.26	14.18	46.53
							1.06	1.26	11.97	39.28
6	408	900	33	0.06	0.06	5.49	0.53	1.38	19.64	64.39
							0.47	1.38	17.44	67.22
7	1814	4000	33	0.15	0.15	5.49	0.63	1.29	23.67	77.66
							1.02	1.29	19.58	64.23
8	998	2200	52.8	0.07	0.07	4.83	0.44	1.23	22.39	73.45
							0.67	1.23	18.95	62.18

Table 6. 7 Dynamic flexural strength of column

Column ID	f_{cd} (N/mm^2)	f_{yd} (N/mm^2)	b (mm)	D (mm)	p_t (%)	P (kN)	P/bD (N/mm^2)	M_u/bD^2 (N/mm^2)	M_u (kN-m)	I_c/I_g	I_{eff}/I_g	$M_u/(f_{ck}bD^2)$
1	36.9	517.5	406.4	406.4	1.23	494	3.00	3.81	256	0.30	0.65	0.10
						1235	7.50	5.13	344	0.30	0.65	0.15
2	36.9	517.5	406.4	406.4	1.88	494	3.00	4.96	333	0.36	0.68	0.13
						1235	7.50	5.70	383	0.37	0.68	0.17
3	36.9	517.5	457.2	457.2	1.09	627	3.00	3.45	330	0.23	0.62	0.09
						1568	7.50	4.41	422	0.24	0.62	0.13
4	36.9	517.5	609.6	609.6	1.70	1117	3.00	4.62	1047	0.34	0.67	0.13
						2793	7.50	5.41	1225	0.34	0.67	0.16
5	36.9	517.5	609.6	609.6	1.70	1117	3.00	4.62	1047	0.33	0.67	0.13
						2793	7.50	5.41	1225	0.34	0.67	0.16
6	36.9	517.5	304.8	304.8	2.18	280	3.00	5.74	162	0.48	0.74	0.16
						700	7.50	7.08	200	0.48	0.74	0.21
7	36.9	517.5	812.8	812.8	1.55	1979	3.00	4.34	2328	0.31	0.65	0.12
						4948	7.50	5.16	2773	0.32	0.66	0.15
8	59.04	517.5	355.6	355.6	1.60	609	4.82	4.69	211	0.30	0.65	0.08
						1523	12.04	7.46	335	0.31	0.66	0.14

Table 6. 8 Safe stand off distance of columns, fixed at both ends considering flexural failure and clearing

Column ID	Charge Weight		f_{cd}	b/L	D/L	L	Flexural strength factor, K_m	I_{ef}/I_g	Safe Stand off Distance	
	(kg)	(lb)	(N/mm^2)			(m)			(m)	(ft)
1	998	2200	36.9	0.10	0.10	4.27	0.10	0.65	15.66	51.37
							0.15	0.67	10.74	35.23
2	1814	4000	36.9	0.10	0.10	4.27	0.13	0.68	17.71	58.12
							0.17	0.71	13.05	42.82
3	1814	4000	36.9	0.11	0.11	4.27	0.09	0.62	19.74	64.78
							0.13	0.63	14.40	47.24
4	454	1000	36.9	0.14	0.14	4.27	0.13	0.67	8.53	27.98
							0.16	0.69	5.86	19.24
5	454	1000	36.9	0.14	0.14	4.27	0.13	0.67	8.52	27.96
							0.16	0.69	5.86	19.24
6	408	900	36.9	0.06	0.06	5.49	0.16	0.74	10.91	35.80
							0.21	0.78	7.27	23.85
7	1814	4000	36.9	0.15	0.15	5.49	0.12	0.65	14.43	47.35
							0.15	0.68	9.93	32.57
8	998	2200	59.04	0.07	0.07	4.83	0.08	0.65	16.04	52.62
							0.14	0.72	9.83	32.24

Table 6. 9 Comparison of WACOLUMN and the safe stand off distance approach

Column ID	Charge Weight, W	Collapse Prevention Stand off (WACOLUMN), SSD_{FEM}	SSD based on Shear, SSD_s	SSD based on Flexure, SSD_f	SSD	SSD/SSD_{FEM}	Scaled Distance (estimated)
	(kg)	(m)	(m)	(m)	(m)		$m/kg^{1/3}$
1	998	18.6	23.08	15.66	23.08	1.24	2.31
		18.0	19.60	10.74	19.60	1.09	1.96
2	1814	28.7	28.61	17.71	28.61	1.00	2.35
		26.8	26.33	13.05	26.33	0.98	2.16
3	1814	23.8	24.08	19.74	24.08	1.01	1.97
		20.4	23.13	14.40	23.13	1.13	1.90
4	454	10.1	14.89	8.53	14.89	1.48	1.94
		10.1	12.35	5.86	12.35	1.23	1.61
5	454	9.8	14.18	8.52	14.18	1.45	1.85
		8.5	11.97	5.86	11.97	1.40	1.56
6	408	21.4	19.64	10.91	19.64	0.92	2.65
		15.3	17.44	7.27	17.44	1.14	2.35
7	1814	19.2	23.67	14.43	23.67	1.23	1.94
		18.0	19.58	9.93	19.58	1.09	1.61
8	998	20.7	22.39	16.04	22.39	1.08	2.24
		19.2	18.95	9.83	18.95	0.99	1.90

The safe scaled distance of columns (Table 6.9) showed that it varies significantly from 1.60 to 2.65 depending on W, b/L, D/L, L, K_s and K_m. The safe scaled distance of Wu and Hao (2007), 1.8 $m/kg^{1/3}$ lies within the above mentioned range. It also showed good agreement between the present work and their work. Interestingly, the recommendation suggested by US DoD (4.36 $m/kg^{1/3}$) is much higher than the value indicated by this research.

6.7. Parametric Study on Safe Scaled Distance

The previous section showed good agreement between the safe stand off distance approach and WACOLUMN. Subsequently, a parametric study was carried out to explore the range of the safe scaled distance for columns adopted in practice. The following parameters (used in the practise) are considered for this study:

- Breadth of the column {300, 450, 600}
- Depth of the column {300, 450, 600}
- Length of the column {3, 4, 5, 6}
- Diameter of main reinforcement {20, 25, 32}
- Number of main reinforcement {4, 8}
- 2 and 4 legged ties-with 12 mm rebars
- Spacing of ties {150, 200, 250}
- Axial compression of 10, 20 and 30 % of $A_g f_c'$

From these parameters, 396 columns are developed and shown in Appendix A4. 4. The shear and flexural strength of these columns are estimated using BS 8110 without any material safety factor. Using the SSD equations the safe scaled distances are estimated for these columns (fixed at both ends) considering clearing and presented in Table A4.3. Fig 6.24 shows the range of scaled distances. The scaled distance varies from 1.31 m/kg$^{1/3}$ to 2.63 m/kg$^{1/3}$ with the mean and standard deviation of 1.84 m/kg$^{1/3}$ and 0.28 m/kg$^{1/3}$ respectively and the 95% confidence level of 2.3 m/kg$^{1/3}$ was estimated from this sample. This is very close with that of the Murrah building. Though it is crude, the scaled distance of 2.3 m/kg$^{1/3}$ can be used approximately to evaluate the safety of unstrengthened buildings against blast. Figs 6.25 to 6.29 show the variation of safe scaled distance against b/L, D/L, L, K_s and K_m. There are no trends in the curves, it is difficult to say exactly how these factors affect the safe scaled distance, i.e., the parameters are not separable. We can see a small trend in K_s curve (Fig. 6.28) and it shows that safe scaled distance decreases with increasing shear strength. Considering the partial safety factor underestimates the shear strength (safe in design), resulting in greater safe stand off distance. This leads to conservative design.

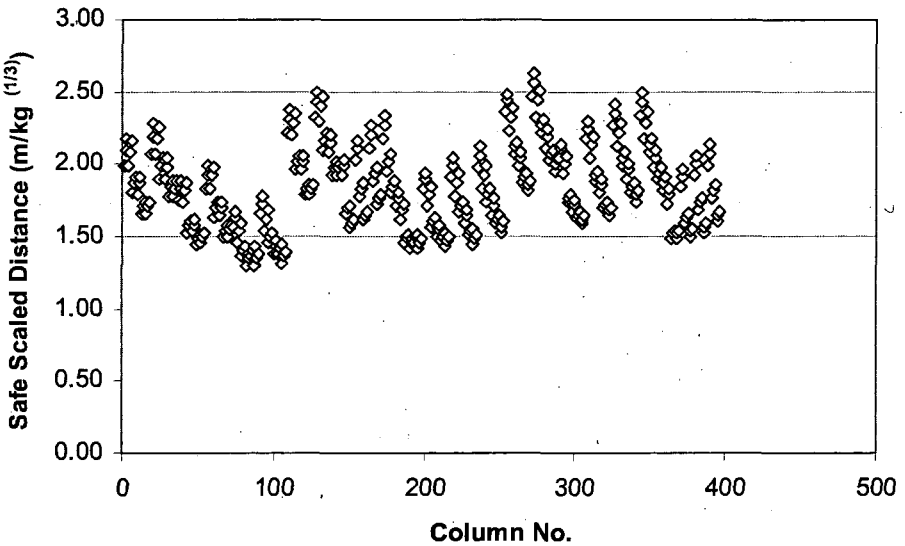

Fig. 6. 24 Variation of scaled distance for the practical columns

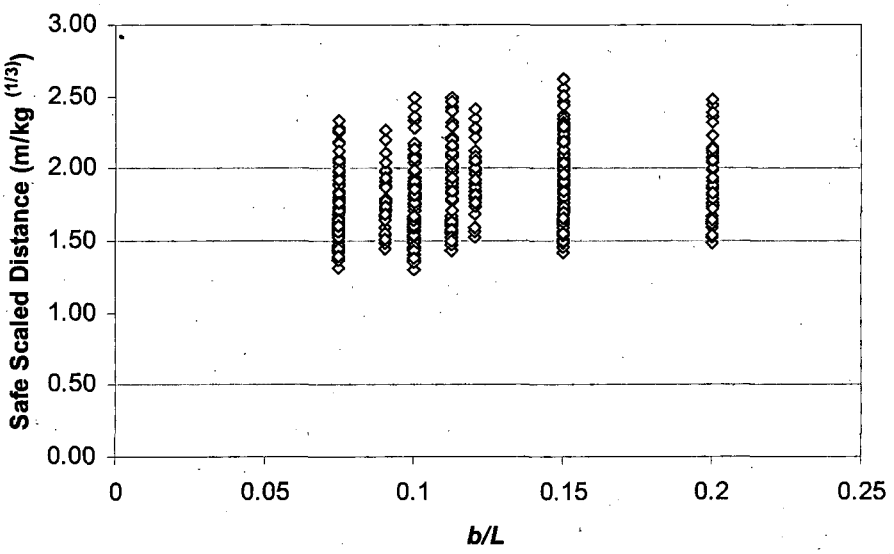

Fig. 6. 25 *b/L* vs. Safe scaled distance

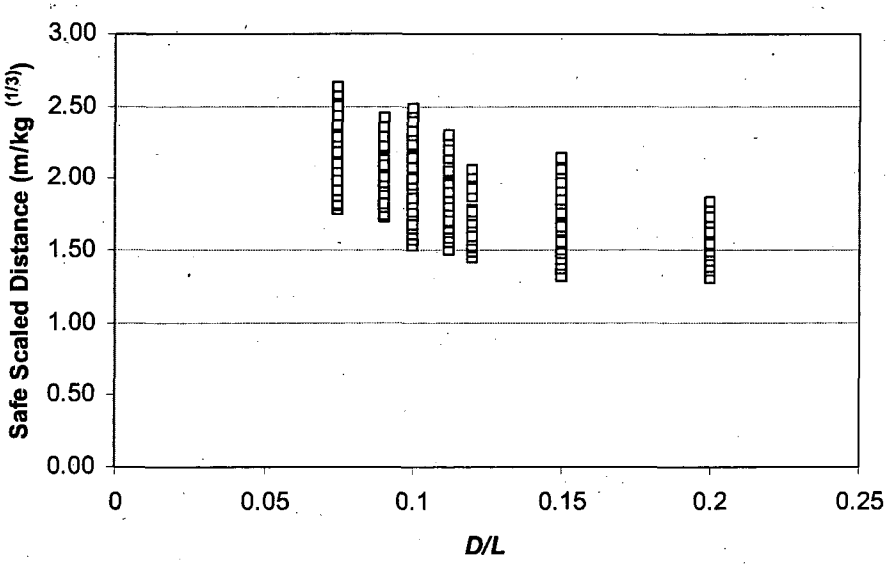

Fig. 6. 26 *D/L* vs. Safe scaled distance

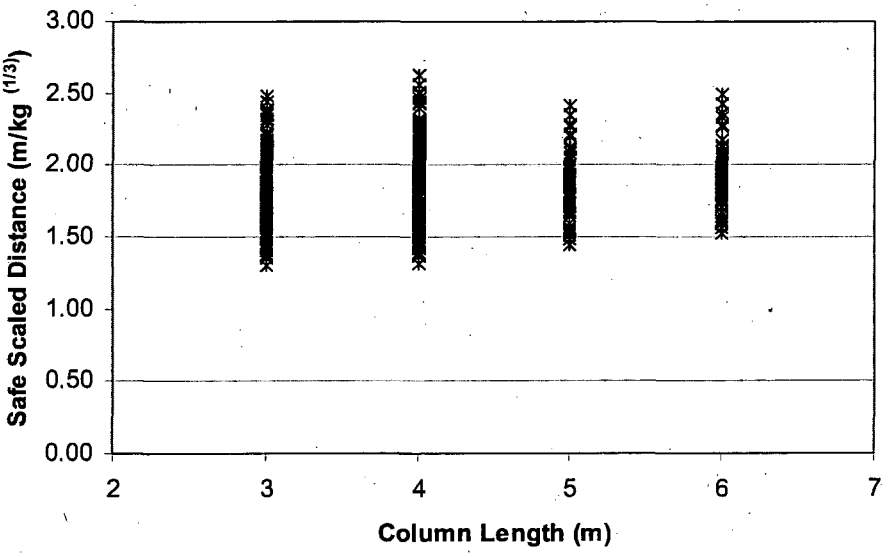

Fig. 6. 27 Columns length vs. Safe scaled distance

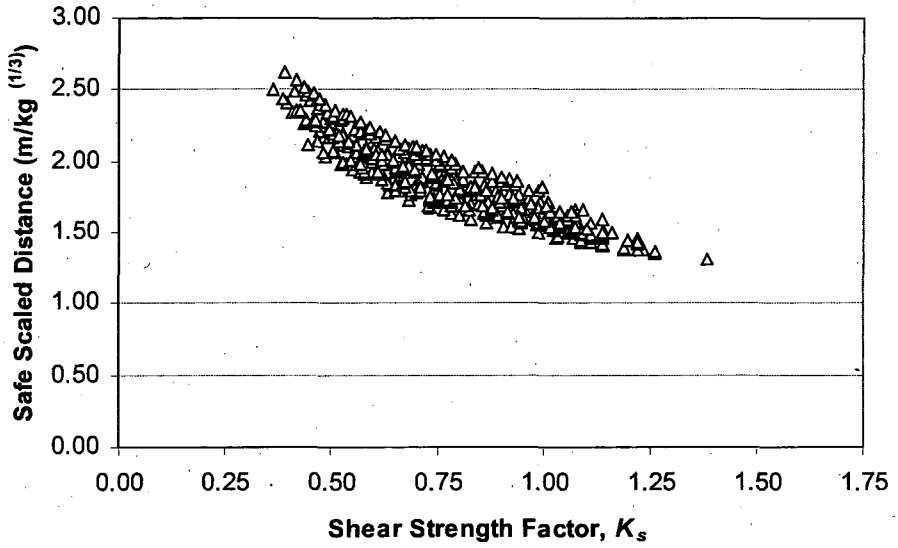

Fig. 6. 28 Shear strength factor vs. Safe scaled distance

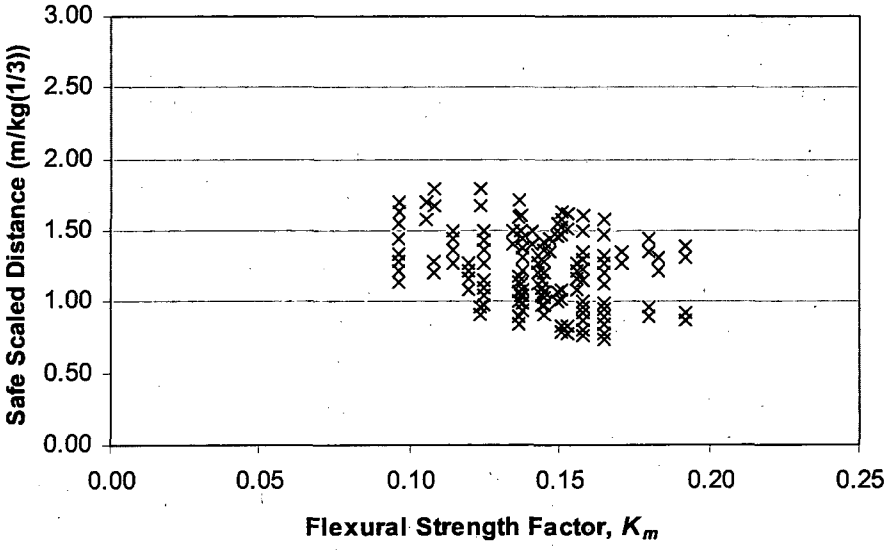

Fig. 6. 29 Flexural strength factor vs. Safe scaled distance

These calculations considered the case with clearing. However, columns without clearing presents the worst case scenario. Therefore safe scaled distances were estimated for the otherwise identical 396 columns. These scaled distances varied from 1.44 m/kg$^{1/3}$ to 3.30 m/kg$^{1/3}$ with the mean and standard deviation of 2.20 m/kg$^{1/3}$ and 0.42 m/kg$^{1/3}$ respectively and a 95% confidence level of 2.9 m/kg$^{1/3}$. This represents a 25% increase.

6.8. Conclusions

The methodology to estimate safe stand off distance was developed and tested using the results from the Murrah building. The forensic investigation showed column G16 was 15.24 m away from the detonation and failed in shear. This was the furthest column away from the charge. The SSD charts also demonstrated that shear was critical for this column and provided a SSD of 23.75 m, thus they confirm the findings from the forensic investigation. The method also confirmed that the next closest column (G12) should have survived intact. A safe scaled distance of 2.0 $m/kg^{1/3}$ was estimated for the Murrah Building and this compared well with the recent work by Wu and Hao (2007). Using the proposed method, a data base of safe stand off distances was generated for different influencing parameters, such as charge weight, compressive strength of the concrete, column breadth to length ratio, depth to length ratio, length, shear strength factor and flexural strength factor. The interpolation functions were derived to estimate the SSD for idealized columns by performing a regression analysis on the database. Design charts were also developed which provided SSD output that corresponded exactly with the output from the interpolation functions. These charts were checked against results from Weidlinger Associates proprietary code called FLEX (named WACOLUMN), which is an explicit, nonlinear, large deformation transient analysis finite element code, developed in house. The comparison showed a good agreement between the methods, with the charts most frequently providing conservative stand off distances. The safe scaled distance varies significantly from 1.6 to 2.8 depending on W, b/L, D/L, L, K_s and K_m. Interestingly, the recommendation suggested by US DoD (4.36 $m/kg^{1/3}$) is much higher than the value indicated by this research. One can get the safe stand off distance for a particular charge weight and column using these design charts. A parametric study was then carried out considering 396 practical columns with and without clearing, in order to established the range of safe scaled distances. The study showed that for columns with clearing the mean value for safe scaled distance was 1.8$m/kg^{1/3}$ with a 95% confidence level of 2.3 $m/kg^{1/3}$. Without clearing this increased to 2.2 $m/kg^{1/3}$ and 2.9 $m/kg^{1/3}$ for mean and 95% confidence limit respectively. Though it is crude, the scaled distances of 2.3 and 2.9 $m/kg^{1/3}$ can be used to evaluate the safety of the building approximately against blast.

Chapter 7.
Conclusions

An extensive literature review has been undertaken (i) to explore the previous incidents such as the Ronan Point, the Khobar Tower and the Murrah Building incidents; (ii) to examine current design guidelines and codal provisions adopted in the different countries namely USA, UK, Europe and Canada and (iii) to investigate available protective design methods for steel and RC framed structures. In the course of this review it was realized that most of the codes, such as British Standards and European Union regulations, suggest the tying approach to ensure adequate robustness against disproportionate collapse of steel framed building. This approach did not have any clear scientific base; hence research was carried out to quantify the strength of the steel frame against disproportionate collapse.

In the UK the general view amongst practitioners has been that compliance with the tying force method provides an alternative load path for damaged columns via the catenary action mechanism. The design tying capacity of the connection should be at least equal to the ULS shear force. It is very simple to comply with this requirement in practice and most of the industrial connections meet this requirement without costly modifications. Importantly, the tying force method sets no requirements for a minimum joint ductility. During this load redistribution the accidental load is assumed to be equal to 1.05 of the dead load plus $1/3^{rd}$ of the imposed load. Since the design tying capacity is equal to only the ULS shear force, substantial beam end rotation is required to redistribute column loads using catenary action. In addition, the accidental loads should also include a dynamic amplification factor to account for effects due to the sudden removal of column support, as could be the case if damage were to occur due to a blast. To transfer the accidental load, the beam-column joints need to have sufficient rotation capacity. This can be problematic because most high rise buildings built in the UK are designed with low cost nominally pinned joints. Since the beams would remain elastic during the

catenary action, all rotation demands would be placed on these simple connections which have limited ductility before prying action leads to fracture.

With an apparent potential for catenary action to exceed both the strength and ductility of many commonly occurring steelwork joints, it was decided to estimate the factor of safety against (FoS) collapse. The FoS was defined as equal to the ratio between the tying capacity of the joint and the tying force acting in the joint at the point when the rotation limit was reached. At this instance the connections are assumed to remain nominally pinned and to be resisting a catenary force limited to the design tying force. Beyond this rotation and force combination the joints are assumed to have failed. This assumption of failure was justified because analysis demonstrated that the moment capacity of the connections when subjected to large rotations was only approximately $1/10^{th}$ of that needed to redistribute loads by vierendeel action. Given the assumption that joints remain pinned and that columns remain in line because of lateral restraint from floor slabs, this catenary mechanism was analysed as an inverted three hinged arch. In this analysis, the loads supported by catenary action in the slab were accounted for. However, due to lack of confidence in the ability of the slab to maintain a tensile load at large deflection the FoS was estimated with and without the load carrying contribution of slab.

Complexity in quantifying the energy dissipation mechanisms such as, cracking in the concrete and yielding steelwork and reinforcement makes the estimation of the dynamic amplification factor (DAF) impractical without experimental testing. Hence, the FoS was estimated for three scenarios: (i) the best case scenario in which the full strength of the slab was considered to be mobilised and the dynamic effect ignored (i.e., DAF is equal to 1.0); (ii) the worst case scenario in which the tensile strength of slab was ignored and the likely maximum undamped factor of 2.0 was assumed; and (iii) a best guess scenario in which the catenary action in slab was included and damping reduced the DAF to 1.50. The investigation considered a medium rise office building as a case study comprising a 9m by 12 m column grid and 4 m storey height. The frame was designed with a range of industry standard simple connections, which included fin plate connections, as well as flexible end plate and double angle web cleat connections.

The results were startling and showed that the relatively simplistic analysis was sufficient to confirm the doubts concerning the ability of the tying force method to

successfully redistribute column loads. The frame with fin plate connections proved the least able to redistribute column loads, with the FoS estimated at ranging from 0.08 to 0.19. Insufficient ductility is the primary reason for the low FoS, although this analysis assumed the maximum limiting rotation of 4° was possible, whereas the predictions based on the Liu et al (2004) model predicted a rotation limit of just over 2 degrees. When the joint reaches its rotation capacity, the bottom flange of the beam touches the column. Thereafter, a prying action develops, leading to reduction in tying capacity of joint and leading ultimately to fracture of the joint. This study indicates that connection would need to rotate by the order of 24 degrees to the horizontal in order to support the damaged column by catenary action alone, involving a central deflection nearly equal to the storey height.

To study the response of other simple connections, the fin plate joints were replaced with flexible end plate and double angle web cleat connections. Using the component method, the limiting rotation of 4.3° and 2.5° were estimated for flexible end plate and double angle web cleat connections respectively. The factor of safety for these connections was estimated and it was again found to be less than 0.2.

Since these factors of safety are significantly less than unity it is unlikely that a more advanced method of analysis would have altered the main conclusion, namely that the tying force method is unable to guarantee robustness of steel framed buildings. Given this firm conclusion the focus of the research was transferred to investigating the vulnerability of concrete framed buildings to blast loads.

Protective design against disproportionate collapse can be carried out using several methods, such as the safe standoff distance approach, the provision of alternative load paths such as outrigger trusses, the double span method, through specific local resistance and indirect design methods such as the tying force approach. The pros and cons of these methods were compared and it was concluded that design based on safe stand off distances provides the highest level of protection. Since it is column failure that generally triggers progressive collapses, it was decided to investigate the vulnerability of RC columns to blast and thereafter to investigate a means for estimating the safe stand-off distance for columns.

The subsequent analysis involved three separate phases: (i) estimation of the loads, (ii) the dynamic analysis and (iii) the comparison between the dynamic shear

forces and moments with the static strengths, in order to determine if failure is or is not likely. The maximum response of the column occurs after the load diminishes therefore a dynamic analysis is essential. In RC columns, shear or compression dominated failures lead to brittle modes of failure and the flexural failure leads to a ductile failure mode. For this reason linear dynamic analysis was carried out examine shear failure, whereas the nonlinear dynamic analysis was carried out to predict flexural failure.

Columns were idealised as beams with a range of end support conditions, namely (i) pinned at both ends, (ii) fixed at both ends (iii) pinned at one end and fixed at another, and (iv) fixed at one end and free at the other (i.e. cantilever). As the column has an infinite number of dynamic degrees of freedom, a differential element of the column was considered. Using the force equilibrium, (in which inertia force was also included) a partial differential equation was formulated and solved using modal superposition theory. This distributed mass system is converted into a SDOF system by equating respective energy such as kinetic energy, potential energy and work done by the load. In the SDOF system models, the contributions from the higher modes of vibration are neglected. In the case of columns pinned at supports there is no redistribution of the mid span moment; hence the elastic analysis was used in the estimation of safe stand off distance. In the case of columns fixed at both ends, and fixed at one end and pinned at other end, the detailed elasto-plastic analysis was carried out as the fixed end moment can be redistributed to the mid span region.

The investigation compared the predictions of deflection, moment and shear using both single degree of freedom (SDOF) and multi-degrees of freedom (MDOF) system models. This showed that when the ratio between the duration of blast load (T_d) to the natural vibration period (T_n) is greater than 0.1, the contribution from the higher modes can be neglected to simplify the analysis, hence SDOF models are sufficiently accurate. However, when T_d/T_n is less than 0.1, the SDOF systems were shown to underestimate shear force by approximately 50%. For most practical columns when blast occurs at a distance close to that required for shear failure, T_d/T_n will be in the 0.05 to 0.15 region. For example T_d/T_n for the columns that failed in shear in the Murrah Building (columns G16 and G24), T_d/T_n was approximately 0.11

and 0.07 respectively. Therefore, this lack of conservation inherent in SDOF analysis does have design implications, with most of the design guidelines such as TM 5-1300 based on SDOF system analysis. Therefore one might consider increasing shear force by 50% to account for the higher modes if analysis is based on SDoF system models. This approximation is crude but likely to be safe.

A method to simplify the blast on columns with clearing was proposed. When the shock front strikes the front face of a column the pressure immediately rises from zero to the reflected pressure. The reflected pressure clears in the clearing time and reaches the stagnation pressure which is equal to the sum of incident over pressure and the drag pressure. The sum of incident and drag pressures decays to atmospheric pressure after the duration of the incident pressure. At the same time, the pressure wave reaches the rear side and suddenly rises from zero to the incident pressure and then decays to zero within the duration of the incident pressure. This blast load on the column was represented in the form of a pressure-time history which includes two profiles, one on the front face and the other on the rear face. This creates a complex load profile, resulting in problems in the dynamic analysis. This was overcome by simplifying the pressure time history to form an equivalent triangular impulse with the same reflected pressure, but with the duration adjusted to provide an identical impulse. Inaccuracy caused by this simplification was studied through a parametric study and was found to be conservative by less than 10%. Hence the columns were thereafter analyzed for clearing using this triangular impulse simplification.

Using the method, the Murrah building was analysed and the results corresponded closely with the failure pattern observed during the forensic analysis of the collapse. Both columns G16 and G24 were shown to have failed in shear (as was found in the forensic investigation) and column G20 was expected to have failed in brisance when assessed using a reinforced concrete panel design chart developed by McVay.

The design of the Murrah Building has been criticised because of the use of transfer girders. The building was therefore reanalysed by replacing these with a more conventional arrangement of beams and columns. The reanalysis showed that the girder was not a primary reason for the progressive collapse, with extensive shear failures of columns still resulting in a progressive collapse that would have

consumed approximately 40% of the building floor area. Therefore, even if the building had have designed as per GSA guidelines, it may not have survived, as the guidelines consider the removal of only one column at any one time.

Shear strength is one of the most important parameters in the calculation of SSD and its estimation is empirical in nature. Hence, the exactness of the methods adopted in different countries to estimate shear strength was studied by comparing predictions with experimental data. The study revealed that strength obtained using BS 8110-1:1997 is conservative but safe. However, lack of conservatism was observed for some tests in both the ACI and CSA methods. The Eurocode was found to have similar reliability to the British Standard although the British Standard was found to be the most reliable of the four codes and was therefore used for the analysis. Another important parameter is the selection of the moment of inertia of the column in the dynamic analysis because it affects T_d and therefore the T_d/T_n ratio. Charts were developed to estimate the cracked moment of inertia of columns considering the effects of axial compression and percentage of reinforcement, as codes provide no equivalent design resource.

A regression analysis was carried out and the influencing parameters for SSD were identified as: charge weight, compressive strength of the concrete, column breadth to length ratio, depth to length ratio, length, shear strength factor and flexural strength factor. Using the proposed method, a data base of safe stand off distances was generated for the following these parameters within the following ranges:

- charge weights of 230, 500, 1000, 1500 and 1800 kg of TNT
- compressive strength of concrete ranging from 20 to 40 N/mm^2
- breadth to length ratio ranging from 0.05 to 0.3
- depth to span ratio ranging from 0.05 to 0.3
- span ranging from 2.5 to 6 m
- shear capacity factor ranging from 0.1 to 0.8
- flexural strength factor ranging from 0.1 to 0.6.

By performing a regression analysis on the database, interpolation functions were derived to estimate the SSD for idealized columns. Design charts were also developed which provided SSD output that corresponded exactly with the output from the interpolation functions.

These charts were checked against results from Weidlinger Associates proprietary code called FLEX (named WACOLUMN), which is an explicit, nonlinear, large deformation transient analysis finite element code, developed in house. In the FLEX code, the blast effect on whole building or individual members can be modelled and the shear and compression reinforcement is modelled explicitly. In the validation, the columns with axial compression of 10 and 25% of $A_g f_c'$ were considered. The shear and flexural strengths of column sections were estimated in the SSD approach using dynamic strength enhancement factors for both rebar and concrete and all the material safety factors were removed. Finally, the safe stand off distance was estimated using the design charts. The comparison showed a good agreement between the methods, with the charts most frequently providing conservative stand off distances. A safe scaled distance of 2.0 m/kg$^{1/3}$ was estimated for the Murrah Building and this compared well with the recent work by Wu and Hao (2007).

Finally in order to define a suitable design value for the safe scaled distance, a parametric study was carried out considering 396 practical columns with and without clearing. The study showed that for columns with clearing the mean value for safe scaled distance was 1.8m/kg$^{1/3}$ with the 95% confidence level was 2.3 m/kg$^{1/3}$. Without clearing this increased to 2.2 m/kg$^{1/3}$ and 2.9 m/kg$^{1/3}$ for mean and 95% confidence limit respectively. These values provide an alternative to the US DoD safe scaled distances, which may be conservative.

Recommendation for future work

During the course of this research, the following future works have been identified:

1. In the case of steel framed buildings with rigid connections, the accidental load from a damaged column is transferred through either beam or catenary actions or in a combination of these. The methodology, presented in this research can be extended to quantify strength against disproportionate collapse of this form of building.

2. Steel framed buildings with simple connection can be strengthened by providing emergence bracing systems, or by strengthening connections. The feasibility of these retrofitting techniques can be explored.

3. The feasibility of arching action in transferring accidental loads from damaged columns requires further study.

4. The feasibility of load redistribution via catenary action in the concrete framed buildings merits further study.

5. The safe stand off distance approach would benefit from validation with field tests.

6. The safe stand off distance approach can be extended for steel columns and brick masonry.

REFERENCES

AMERICAN CONCRETE INSTITUTE (2002). *Building code requirements for structural concrete.* ACI 318-02, Farmington Hills, Mich, USA.

AMERICAN SOCIETY OF CIVIL ENGINEERS (2002), *Minimum Design Loads for Buildings and Other Structures,* ASCE 7-02, Reston, USA.

ASTANEH-ASL, A. (2003) Progressive collapse prevention in new and existing buildings. *Emerging Technologies in Structural Engineering, Proc. of the 9th Arab Engineering Conf,* Abu Dhabi, UAE, Nov 29-Dec.1, (1001-1008).

ASTANEH-ASL, A. et al (2001), *Floor Catenary Action to Prevent Progressive Collapse of Steel Structures.* Report No. UCB/CE-Steel-03/2001, Department of Civil and Environmental Engineering, University of California, Berkeley.

ASTANEH-ASL, A. et al (2001), *Use of Catenary Cables to Prevent Progressive Collapse of Buildings,* Final Report. Department of Civil and Environmental Engineering, University of California, Berkeley.

BAKER J. F., WILLIAMS E. L. and LAX D (1948). The Design of Framed Buildings against High-Explosive Bombs. *The Civil Engineer In War, Vol. III – Properties of Materials, Structures, Hydraulics, Tunnelling and Surveying* (BAKER J. F. (eds)). Institution of Civil Engineers, London, 80-113.

BIGGS, M. (1964), Introduction to Structural Dynamics, McGraw-Hill, Inc., New York, USA.

BSI, Eurocode 0 – Basis of structural design, EN 1990, 2002.

BSI, Eurocode 1 – Actions on structures, Part 1-7: *General actions – Accidental actions,* EN 1991-1-7, 2004.

BSI, Eurocode 4 – Design of composite steel and concrete structures, Part 1: *General rules and rules for buildings,* EN 1994-1, 2005.

BSI, Loadings for buildings, Part1: *Code of Practise for dead and imposed loads*, BS 6399-1, 1996.

BSI, Structural use of steelwork in building, Part1: *Code of Practise for design – rolled and welded sections*, BS 5950-1, 2000.

BSI, Structural use of steelwork in building, Part5: *Code of Practise for design of cold formed thin gauge sections*, BS 5950-5, 2000.

BYFIELD, M. P., DHANALAKSHMI, M., AND COUCHMAN, G. H (2004). Assessment of the use of composite connections with unpropped composite beams. *J. Const. Steel Research.*, 60, 1369-1386.

CHOPRA, A. K. (2001), Dynamics of Structures: Theory and Applications to Earthquake Engineering, Prentice Hall, NJ, USA.

CLOUGH, R. W., AND PENZIEN, J. (1995) Dynamics of Structures, Computers and Structures Inc., Berkeley, USA.

COLLINS, A. R. (1969) The implications of the report of the inquiry into the collapse of flats at Ronan Point, Canning Town. *The Structural Engineer*, 47(7), 255-284.

COREL, W.G. (2002) *World Trade Center building performance study: Data collection, preliminary observations, and recommendations.* Washington, D. C.: Federal Emergency Management Agency Mitigation Directorate. FEMA-403.

CORLEY, W. G. et al (1998) The Oklahoma City bombing: Summary and recommendations for multi-hazard mitigation. *J. Perf. Constr. Fac.*, ASCE, 12(3), 100-112.

CRAIG, R. R. (1981) Structural Dynamics: An Introduction to Computer Methods, John Wiley and Sons, New York, USA.

DEPARTMENT OF ARMY (1990) *Structures to Resist the Effects of Accidental Explosions.* Publication No. TM5-1300., Washington, D.C.

DEPARTMENT OF DEFENSE (2002) *Unified facilities criteria (UFC) - DoD minimum antiterrorism standards for buildings.* Department of Defence, *UFC 4-010-01,* U.S. Army Corps of Engineering, Washington, D.C.

DEPARTMENT OF DEFENSE (2005) *Unified facilities criteria (UFC) – Structural Design Criteria for Buildings.* Department of Defence, *UFC 3-310-02A,* U.S. Army Corps of Engineering, Washington, D.C.

DEPARTMENT OF THE ARMY (1986) Fundamentals of protective design for conventional weapons effects. Publication. No. TM5-855-1. Washington, D.C.

FAELLA C., PILUSO V. and RIZZANO G. (2000) *Structural Steel Semirigid Connections,* CRC Press, London.

FEDERAL EMERGENCY MANAGEMENT AGENCY MITIGATION DIRECTORATE. (1996) *The Oklahoma City Bombing: Improving Building Performance through Multi-Hazard Mitigation- Report, FEMA-227,* Washington, D. C: ASCE press

FEDERAL EMERGENCY MANAGEMENT AGENCY MITIGATION DIRECTORATE. (2003) *Primer for Design of Commercial Buildings to Mitigate Terrorist Attacks – Risk Management Series, FEMA-427,* Jessup, USA

GENERAL SERVICES ADMINISTRATION (2003) *Progressive collapse analysis and design guidelines for new federal office buildings and major modernization projects.* Office of Chief Architect, Washington, D.C.

GIBBONS C. (2003) Making sense of tall: the design of high rise buildings in a post 9/11 world. *Joint Institution of Structural Engineers / IABSE Lecture,* London.

GILMOUR. J. R. and VIRDI. K. S. (1998) Numerical Modelling of the progressive collapse of framed structures as a result of impact explosion. IN: 2nd *Int. PhD symposium in Civil Engg.* Budapest, 289-296.

GRANT, R. (1998) Khobar Towers. *Journal of Air Force Association* [online], 81 (6), Available from: http://afa.org/magazine/june1998/0698khobar.asp [Accessed 24 November 2005].

GUO, W. AND GILSANZ, R (2003) *Nonlinear Static Analysis Procedure – Progressive Collapse Evaluation.* Gilsanz Murray Steficek, LLP. Available from: www.arche.psu.edu/thesis/2004/mxf277/mxf277Research.htm [Accessed 12 May 2006]

GUO, W. AND GILSANZ, R. (2004) Simple Nonlinear Static Analysis Procedure for progressive collapse evaluation. *Proceedings*, National Steel Construction Conference, American Institute of Steel Construction, Long Beach, CA, 97-106.

HOUSE ARMED SERVICES COMMITTEE (1996) *The khobar Towers Bombing Incident, Chairman's Statement and Staff Report.* Washington, D. C: Press Releases, Available from: http://armedservices.house.gov/Publications/104thCongress/Reports/saudi.pdf [Accessed 24 November 2005]

IKEDA, A. (1968). *Rep.*, Training Institute for Engineering Teachers, Yokohama National Univ., Japan, also in, Masaya, H. (1973). *A list of past experimental results of reinforced concrete columns*, Building Research Inst., Ministry of Construction, Japan.

KAEWKULCHAI, G. AND WILLIAMSON, E. B. (2003) Dynamic Behavior of Planar Frames during Progressive Collapse. IN: *16th ASCE Engineering Mechanics Conference*, July 16-18, University of Washington, Washington, D. C.

KATO, B., AOKI, H., AND YAMANOUCHI, H. (1990) Standardized mathematical expression for stress-strain relations of structural steel under monotonic and uniaxial tension loading. *Materials and Structures,* 23(1), 47-58.

KOKUSHO, S. (1964). *Rep.*, Building Research Inst., Tsukuba, Japan, also in Masaya, H. (1973). *A list of past experimental results of reinforced concrete columns*, Building Research Inst., Ministry of Construction, Japan.

KOKUSHO, S., AND FUKUHARA, M. (1965). *Rep.*, Kokusho Lab., Tokyo Industrial Univ., also in Masaya, H. (1973). *A list of past experimental results of reinforced concrete columns*, Building Research Inst., Ministry of Construction, Japan.

KUHLMANN, U. JASPART, J.-P. VASSART, O. WEYNAND, K. AND ZANDONINI, R. (2007). Robust structures by joint ductility. IN: *COST Action C26:*

Urban Habitat Constructions under Catastrophic Events, March 30-31, Prague, 380-381.

LI, X., PARK, R., AND TANAKA, H. (1995). Reinforced concrete columns under seismic lateral force and varying axial load. *Research Rep. 95-5*, Dept. of Civil Engineering, Univ. of Canterbury, Christchurch, New Zealand.

LIU, J. AND ASTANEH-ASL, A. (2004) Moment–Rotation Parameters for Composite Shear Tab Connections. *Journal of Structural Engineering*, 130(9), 1371-1380.

LIU, R., DAVISON, J. B., AND TYAS, A. (2005) Is catenary action sufficient to resist progressive collapse in a steel framed building. *In:* HOFFMEISTER, B., HECHLER, O., ed. *4th European Conference on Steel and Composite Structures*, 8 - 10 June 2005, Maastricht, the Netherlands, 155-162.

LYNN, A. C., MOEHLE, J. P., MAHIN, S. A., AND HOLMES, W. T. (1996). Seismic evaluation of existing reinforced concrete building columns. *Earthquake Spectra*, 12(4), 715–739.

MARJANISHVILI. S. M. (2004) Progressive Analysis Procedure for Progressive Collapse. *J. Perform. Constr. Facil.*, 18(2), 79-85.

MAYS, G. C., AND SMITH, P. D. (2004), Blast and ballistic loading of structures, Elsevier Science and Technology Books., Oxford, UK.

MCVAY, M. K. (1988). Spall damage of concrete structures. *U.S Army Engr. Wtrwy. Experiment Station Tech. Rep. SL-88-22.* U.S Army Engineer Waterways Experiment Station, Vicksburg, Miss.

MENZIES, J. B. AND NETHERCOT, D. A. (1998) Progressive Collapse – Preventive Measures in the United Kingdom. *Structural Engineering World Wide, Elsevier Science Ltd,* ISBN: 0-08-042845-2, Paper Reference: P 312-1.

MLAKAR, P. F. et all (1998) The Oklahoma City bombing: Analysis of blast damage to the Murrah building. *J. Perf. Constr. Fac.*, ASCE, 12(3), 113-119.

MOORE. D. B. (2002) The UK and European Regulations for Accidental Actions. IN: *National Institute of Building Sciences Workshop on Prevention of Progressive Collapse*, Rosemont, IL.

NAIR, R. (2004) Progressive Collapse Basics. *Proceedings*, National Steel Construction Conference, American Institute of Steel Construction, Long Beach, CA, 1-11.

NATIONAL BUILDING CODE OF CANADA (1995) Part 4 and Commentary C, National Research Council of Canada, Ottawa, Ontario.

NGO, T., MENDIS, P., GUPTA, A., AND RAMSAY, J. (2007) Blast Loading and Blast Effects on Structures – An Overview. *Electronic Journal of Structural Engineering, Special Issue: Loading on Structures,* 76-91.

OHUE, M., MORIMOTO, H., FUJII, S., AND MORITA, S. (1985). The behaviour of R. C. short columns failing in splitting bond-shear under dynamic lateral loading. *Trans. Jpn. Concr. Inst.*, 7, 293–300.

PEARSON, C. AND DELATTE, N. (2005) Ronan point apartment tower collapse and its effects on building codes. *J. Perf. Constr. Fac.*, ASCE, 19(2), 172-177.

PUGSLEY, A. G. *et al* (1968). *Report of the Inquiry into the Collapse of Flats at Ronan Point, Canning Town.* Her Majesty's Stationery Office, London.

RAHIMIAN, A. AND MOAZAMI, K. (2004) Non-linear structural integrity analysis. *Proceedings*, National Steel Construction Conference, American Institute of Steel Construction, Long Beach, CA, 107-114.

SAATCIOGLU, M., AND OZCEBE, G. (1989). Response of reinforced concrete columns to simulated seismic loading. *ACI Struct. J.*, 86(1), 3–12.

SABUWALA. T. et al (2005) Finite element analysis of steel beam to column connections subjected to blast loads. *Int. J Impact Eng,* 31, 861-876.

SEZEN, H. (2002). *Seismic behavior and modeling of reinforced concrete building columns.* Thesis (PhD), Univ. of California at Berkeley, Berkeley.

SMITH, P. D., AND HEINEMANN, G. J. (2003), Blast and ballistic loading of structures, Elsevier Science and Technology Books., Oxford, UK.

SOZEN, M. A. et al (1998) The Oklahoma City bombing: Structure and mechanisms of the Murrah buildings. *J. Perf. Constr. Fac.*, ASCE, 12(3), 120-136.

STEEL CONSTRUCTION INSTITUTE (1989) Design of Composite Slabs and Beams with Steel Decking, SCI, Publication No. P055, Berkshire.

THE BUILDING REGULATIONS (2004) *Structure, Approved Document-A,* Her Majesty's Stationery Office, London

THE STEEL CONSTRUCTION INSTITUTE (2002) Joints in Steel Construction: Simple Connections, SCI, Publication No. P206, Berkshire.

UMEMURA, H., AND ENDO, T. (1970). *Rep.*, Umemura Laboratory, Tokyo University, also in Masaya, H. (1973). "*A list of past experimental results of reinforced concrete columns.*" Building Research Inst., Ministry of Construction, Japan.

WAY, A. G. J. (2004) *Guidance on meeting the Robustness Requirements in Approved Documents 'A'*, The steel Construction Institute, London: SCI publications.

WIGHT, J. K., AND SOZEN, M. A. (1975). Strength decay of RC columns under shear reversals. *J. Struct. Div. ASCE*, 101(5), 1053–1065.

WU, C. AND HAO, H. (2007) Safe Scaled Distance for Masonry Infilled RC Frame Structures subjected to Airblast Loads. *J. Perf. Constr. Fac.*, ASCE, 21(6), 422-431.

YALCIN, C. (1997). *Seismic evaluation and retrofit of existing reinforced concrete bridge columns.* Thesis (PhD). Univ. of Ottawa, Ottawa.

YEE Y. L. and MELCHERS R. E. (1986) Moment Rotation Curves for Bolted Connections. *J. Struct. Eng.*, ASCE, 112(3), 615-635.

APPENDIX

A. 1 DIRECT DESIGN METHODS: PROTECTIVE DESIGN FOR STEEL FRAMED STRUCTURES

A. 1.1. STRENGTH AND STIFFNESS OF THE JOINT COMPONENTS

Table A1. 1 Strength and stiffness of the joint components

Components	Strength	Stiffness
Column web in shear	$K_{cws} = \frac{0.38EA_{vc}}{h_1}$	$V_{cwc.Rd} = \frac{f_{y.cw}A_{vc}}{\sqrt{3}}$
Column web in compression = Crashing failure	$K_{cwc} = E\frac{b_{eff.cwc}t_{wc}}{d_{wc}}$	$F_{cwc.Rd} = f_{y.cw}t_{wc}b_{eff.cwc}\rho$ Where, $\rho = \frac{1}{\sqrt{1+1.92\beta^2\left(\frac{b_{eff.cwc}t_{wc}}{A_{vc}}\right)^2}}$
= Buckling failure		$F_{cwc.Rd} = F_{cwc.Rd}\left[\frac{1}{\bar{\lambda}}\left(1-\frac{0.22}{\bar{\lambda}}\right)\right] \le F_{cwc.Rd}$ Where, $\bar{\lambda} = \sqrt{\frac{b_{eff.cwc}t_{wc}f_{y.cw}}{F_{cr}}}$ $F_{cr} = \frac{\pi Et_{wc}^3}{3(1-\nu^2)d_{wc}}$
Column web in tension	$K_{cwt} = E\frac{b_{eff.cwt}t_{wc}}{d_{wc}}$	$F_{cwc.Rd} = f_{y.cw}t_{wc}b_{eff.cwt}\rho$
Beam flange and web in compression	-	$F_{bfc.Rd} = \frac{f_{y.bfw}Z_b}{h_b - t_{fb}}$
Beam web in tension	-	$F_{bwt.Rd} = f_{y.bfw}t_{wb}b_{eff.cwt}$

Where,

$$b_{eff.cwc} = t_{fb} + 2\sqrt{2}a_b + 5\left(t_{fc} + r_c\right)$$

$$b'_{eff.cwc} = t_{fb} + 2\sqrt{2}a_b + 2\left(t_{fc} + r_c\right)$$

$$b^*_{eff.cwc} = t_{fb} + 2\sqrt{2}a_b + 2\left[0.75\left(\frac{d_{wc}b_{fc}}{3t_{wc}t_{fc}}\right)^{1/4}\right]\left(t_{fc} + r_c\right)$$

$$b'_{eff.cwt} = \min of\left\{d_h + 2m; p; \frac{d_h}{2} + m + \frac{p}{2}\right\}$$

$$b_{eff.cwt} = p$$

A_{vc} - Shear area of the column web

a_b - Throat thickness of the weld between beam flange and the end plate

$b_{eff.cwc}$ - Effective width of column web in compression for strength calculation

$b_{eff.cwt}$ - Effective width of column web in tension for strength calculation

$b'_{eff.cwc}$ - Effective width of column web in compression for stiffness calculation

$b'_{eff.cwt}$ - Effective width of column web in tension for stiffness calculation

$b^*_{eff.cwc}$ - Effective width of column web in compression considering buckling failure

b_{fc} - Width of column flanges

d_{wc} - Clear depth of the column web

d_h - Washer diameter

E - Young's modulus of steel

F_{cr} - Elastic critical load of the column web in compression

$F_{bwt.Rd}$ - Resistance of the beam web in tension

$F_{bfc.Rd}$ - Resistance of the beam flange and web in compression

$F_{cwc.Rd}$ - Resistance of the column web in compression (crushing failure)

$F_{cwc.Rd}$ - Resistance of the column web in compression (buckling failure)

$f_{y.cw}$ - Yield stress of the column web

$f_{y.bfw}$ - Yield stress of the beam

h - Column length or inter storey height

h_b - Beam height

h_t - Lever arm, approximately equal to the distance between extreme bolts

K_{cwc} - Stiffness of the spring element, modelling the column web in compression

K_{cws} - Stiffness of the spring element, modelling the column web in shear

K_{cwt} - Stiffness of the spring element, modelling the column web in tension

m - Distance between the bolt axis and the face of the web

p - Pitch of the bolt row

r_c - Radius of fillet of the web to flange connection of the column

t_{fb} - Thickness of beam flanges

t_{fc} - Thickness of column flanges

t_{wc} - Thickness of column web

t_{wb} - Thickness of beam web

$V_{cwc.Rd}$ - Resistance of the column web in shear

Z_b - Plastic modulus of beam section

β - Coefficient related to the panel zone internal action, which is equal to $1-{}^{h_t}/_{h}$

ρ - Coefficient for shear compression interaction in the column web in compression

$\overline{\lambda}$ - Nondimensional slenderness

ν - Poisson's ratio

A. 1.2. FORCE-DEFORMATION RELATIONSHIP FOR T-STUB

Table A1. 2 Force deformation relationship for T Stub

Mechanism	Characteristic Points	Force	Displacements
Type 1 (Flange yielding) $\beta_u \le \frac{2(n/m)}{1+2(n/m)}$	First Yielding	$F_y = \alpha_1 M_y$	$\delta_y = \frac{F_y}{K}$
	Beginning of strain hardening	$F_h = \alpha_1 \xi_h M_y$	$\delta_h = \frac{F_h}{K} + \frac{m^2}{2t_f} C_h$
	Maximum load	$F_m = \alpha_1 \xi_m M_y$	$\delta_m = \frac{F_m}{K} + \frac{m^2}{2t_f} C_m$
	Fracture Point	$F_u = \alpha_1 \xi_u M_y$	$\delta_h = \frac{F_h}{K} + \frac{m^2}{2t_f} C$
Type 2 (Flange yielding with bolt failure) $\frac{2(n/m)}{1+2(n/m)} < \beta_u \le 2$	First Yielding	$F_y = \alpha_2 M_y$	$\delta_y = \frac{F_y}{K}$
	Beginning of strain hardening	$F_h = \alpha_2 \xi_h M_y$	$\delta_h = \frac{m(m+n)}{t_f(1+\xi_2)} C_h - \frac{mn}{t_f}\left(\frac{\xi_2}{1+\xi_2} + \frac{n}{m}\right) C[\xi^*]$, *where* $\xi^* = \xi\xi_2$
	Maximum load	$F_m = \alpha_2 \xi_m M_y$	$\delta_m = \frac{m(m+n)}{t_f(1+\xi_3)} C_m - \frac{mn}{t_f}\left(\frac{\xi_3}{1+\xi_3} + \frac{n}{m}\right) C[\xi^*]$, *where* $\xi^* = \xi\xi_3$
	Fracture Point	$F_u = \alpha_2 \xi_u M_y$	$\delta_h = \frac{F_h}{K} + \frac{m^2}{2t_f} C$

Type 3 (Bolt failure) $\beta_u > 2$	Case 1: T-stub flange in elastic region: $(\xi \le \xi_1)$		
	T-stub flange in elastic region	$F = 2B_u$	$\delta = \frac{F}{K}$
	Case 2: T-stub flange in yielding plateau: $(\xi_1 \le \xi \le \xi_2)$		
	First yielding point	$F_y = \frac{2M_y}{m}$	$\delta_y = \frac{F_y}{K}$
	Yielding plateau region	$F_u = 2B_u$	$\delta_h = \frac{F_u}{K} + \frac{m^2}{t_f} C[\xi]$
	Case 3: T-stub flange in strain hardening region: $(\xi_2 \le \xi \le \xi_3)$		
	First yielding point	$F_y = \frac{2M_y}{m}$	$\delta_y = \frac{F_y}{K}$
	Beginning of strain hardening	$F_h = \frac{2\xi_h M_y}{m}$	$\delta_h = \frac{F_h}{K} + \frac{m^2}{t_f} C[\xi_2]$
	Strain hardening region	$F_u = 2B_u$	$\delta_u = \frac{F_u}{K} + \frac{m^2}{t_f} C[\xi]$
	Case 4: T-stub flange in softening region: $(\xi \ge \xi_3)$		
	First yielding point	$F_y = \frac{2M_y}{m}$	$\delta_y = \frac{F_y}{K}$
	Beginning of strain hardening	$F_h = \frac{2\xi_h M_y}{m}$	$\delta_h = \frac{F_h}{K} + \frac{m^2}{t_f} C[\xi_2]$
	Maximum load	$F_m = \frac{2\xi_m M_y}{m}$	$\delta_m = \frac{F_m}{K} + \frac{m^2}{t_f} C[\xi_3]$

	Softening region	$F_u = 2B_u$	$\delta_u = \frac{F_u}{K} + \frac{m^2}{t_f} C[\xi]$

Where,

$$K = 0.5E\frac{b'_{eff}t_f^3}{m^3}$$

$$\alpha_1 = \frac{(32n - 2d_w)}{8mn - (m+n)d_w}$$

$$\alpha_2 = \frac{2}{m}(1+\xi)$$

$$\beta_u = \frac{2\xi_u M_y}{B_u m}$$

$$\xi = \frac{(2-\beta_u)(n/m)}{\beta_u(1+(n/m))} \quad \text{for Type 2 failure}$$

$$\xi = \frac{2}{\beta_u} \quad \text{for Type 3 failure}$$

C_h - 0.0012 and 0.0015 for S275 and S355 respectively

C_m - 0.0155 and 0.0148 for S275 and S355 respectively

C - 0.1951 and 0.3315 for S275 and S355 respectively

$C[\xi]$ - Coefficient provides displacement corresponding to section moment, which is obtained from Fig. A1.1

m - Distance between the bolt axis and the face of the web

n - Distance between the bolt axis and the prying force (or flange edge)

ξ - Coefficient providing the bending moment in a section where ultimate conditions are not reached

ξ_h - 1.50

ξ_m - 1.95 and 1.84 for S275 and S355 respectively

ξ_u - 3.18 and 3.29 for S275 and S355 respectively

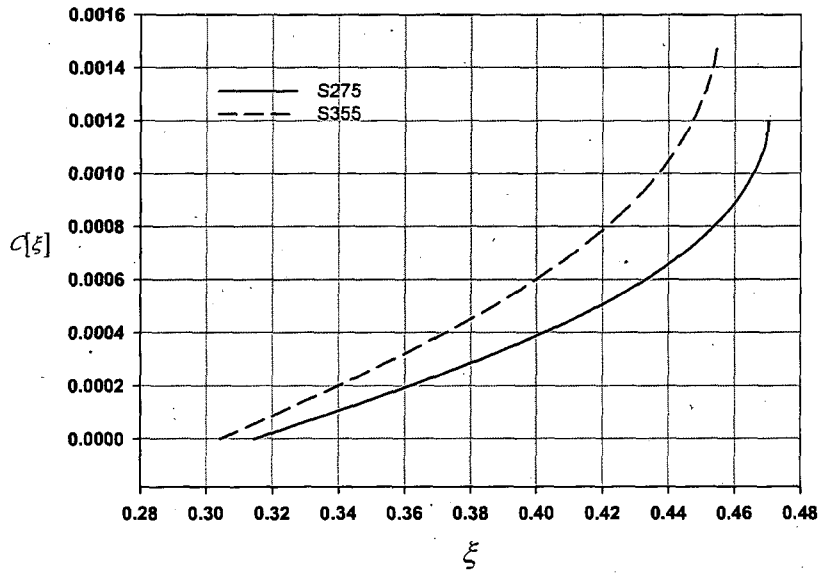

(a) T-stub flange in yielding plateau

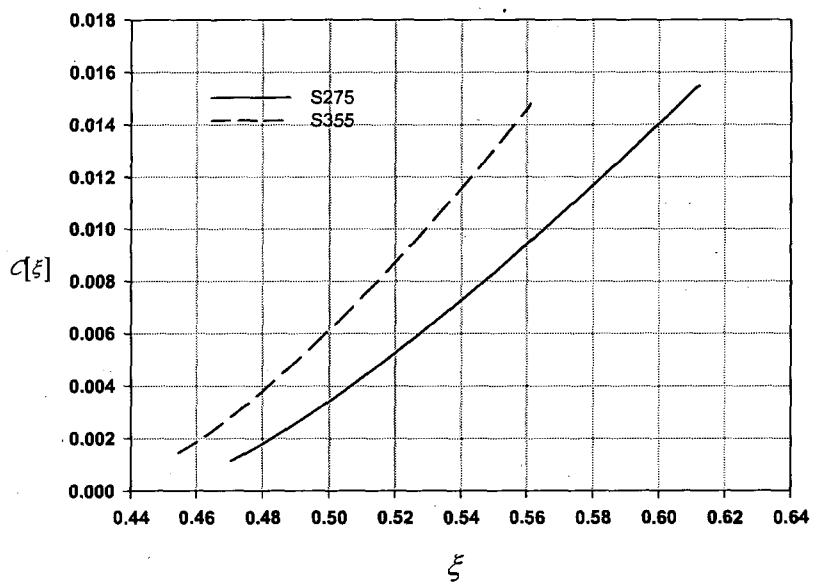

(b) T-stub flange in strain hardening region

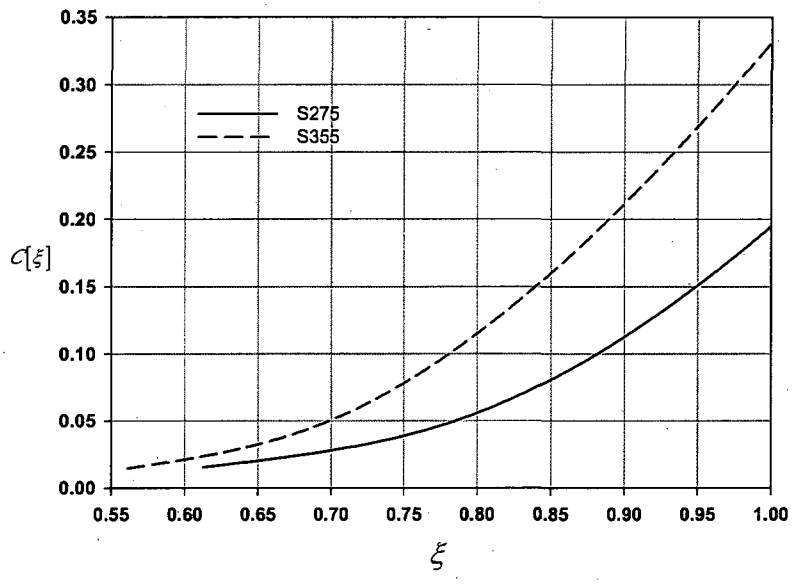

(c) T-stub flange in softening region

Fig. A1. 1 $C[\xi]$ for different ξ

A. 1.3. ROTATION CAPACITY OF FLEXIBLE END PLATE CONNECTIONS

Bending of End Plate:

Thickness of flange, t_f= 12 mm

Weld size, s= 6 mm

$m = \frac{(140-9.6)}{2} - 0.8 \cdot 1.414 \cdot 6 = 58.41$ mm

n = 30 mm

D_b = 20 mm

D_h = 22 mm

D_w = 30 mm

$A_b = \pi D_b^2 / 4 = 314.1\,\text{mm}^2$

b_{eff} = Min of $\{b_{eff1}, b_{eff2}, b_{eff3}\}$

$b_{eff1} = D_h + 2m = 138.82$ mm

b_{eff2} = *pitch* (p = 70 mm) = 70 mm

$b_{eff3} = \frac{D_h}{2} + \frac{p}{2} + m = 104.41$ mm

Hence, b_{eff1} = 70 mm

For bolt grade 8.8, f_{ub} = 800 N/mm^2

$B_u = f_{ub} A_b = 251.28$ kN

$M_y = \frac{b_{eff} t_f^2}{6} f_y = 0.462$ kN-m

$M_h = 1.50 M_y = 0.691$ kN-m

$M_m = 1.95 M_y = 0.900$ kN-m

$M_u = 3.18 M_y = 1.469$ kN-m

$\beta_u = \frac{4M_u}{2B_u m} = 0.2$

$\lambda = n/m = 0.514$

$\beta_1 = \frac{2\lambda}{1+2\lambda} = 0.507$

$\beta_u < \beta_1$, Hence Angle fails by 1st mechanisms

$F = \left(\frac{32n - 2d_w}{8mn - (m+n)d_w} \right) M$

$F = 0.07918M$

$F_y = 0.07918 M_y = 36.58$ kN

$F_h = 0.07918 M_h = 54.721$ kN

$F_m = 0.07918 M_m = 71.23$ kN

$F_u = 0.07918 M_u = 116.33$ kN

$$K = 0.5E\frac{b_{eff}t_f^3}{m^3} = 63733.74 \text{ kN/m}$$

$$\delta_y = \frac{F_y}{K} = 0.574 \text{ mm}$$

$$\delta_{eh} = \frac{F_h}{K} = 0.8585 \text{ mm}$$

$$C_h = 0.0012$$

$$\delta_{ph} = \frac{m^2}{2t_f}C_h = 0.1705 \text{ mm}$$

$$\delta_h = \delta_{eh} + \delta_{ph} = 1.029 \text{ mm}$$

$$\delta_{em} = \frac{F_m}{K} = 1.1176 \text{ mm}$$

$$C_m = 0.0148$$

$$\delta_{pm} = \frac{m^2}{2t_f}C_m = 2.1038 \text{ mm}$$

$$\delta_m = \delta_{em} + \delta_{pm} = 3.2215 \text{ mm}$$

$$\delta_{eu} = \frac{F_u}{K} = 1.825 \text{ mm}$$

$$C = 0.1951$$

$$\delta_{pu} = \frac{m^2}{2t_f}C = 27.73 \text{ mm}$$

$$\delta_u = \delta_{eu} + \delta_{pu} = 29.56 \text{ mm}$$

Bending of Column Flange:

Thickness of web, t_w = 18.4 mm

Thickness of flange, t_f = 30.2 mm

Root radius, r_c = 15.2 mm

$$m = \frac{(140-18.4)}{2} - 0.8 \cdot 15.2 = 48.64 \text{ mm}$$

$$n = 127.4 \text{ mm}$$

Effective Width, b_{eff} = Pitch, p = 70 mm

$$M_y = \frac{b_{eff}t_f^2}{6}f_y = 3.78 \text{ kN-m}$$

$$M_h = 1.50M_y = 5.65 \text{ kN-m}$$

$$M_m = 1.95M_y = 7.36 \text{ kN-m}$$

$$M_u = 3.18M_y = 12.01 \text{ kN-m}$$

$$\beta_u = \frac{4M_u}{2B_u m} = 1.966 < 2.0$$

$$\lambda = n/m = 2.619$$

$$\beta_1 = \frac{2\lambda}{1+2\lambda} = 0.839$$

$\beta_u > \beta_1$ and $\beta_u < 2$, Hence Column flange fails by 2nd mechanisms

$$\xi = \frac{(2-\beta_u)\lambda}{\beta_u(1+\lambda)} = 0.0125$$

$$\xi_1 = \frac{M_y}{M_u} = 0.3143$$

$$\xi_2 = \frac{M_m}{M_u} = 0.6122$$

$$C_m = 0.0148$$

$\xi < \xi_1$, $\theta_{p2} = 0$

$$F = \frac{2M}{m}(1+\xi) = 0.0416\ M$$

$$F_y = 0.0416\ M_y = 157.26 \text{ kN}$$

$$F_h = 0.0416\ M_h = 235.06 \text{ kN}$$

$$F_m = 0.0416\ M_m = 306.00 \text{ kN}$$

$$F_u = 0.0416\ M_u = 499.81 \text{ kN}$$

$$K = \frac{0.5 E b_{eff} t_f^3}{m^3} = 1759250 \text{ kN/m}$$

$$\delta_y = \frac{F_y}{K} = 0.089 \text{ mm}$$

$$\theta_{p1h} = \frac{m}{t_f(1+\xi)} C_h = 1.91 \times 10^{-3}$$

$\xi < \xi_2$, $\theta_{p2h} = 0$

$$\delta_{eh} = \frac{F_h}{K} = 0.1336 \text{ mm}$$

$$\delta_{ph} = \theta_{p1h}(1+\lambda)m - \theta_{p2h}\lambda m = 0.3360 \text{ mm}$$

$$\delta_h = \delta_{eh} + \delta_{ph} = 0.4696 \text{ mm}$$

$$\theta_{p1m} = \frac{m}{t_f(1+\xi)} C_m = 23.54 \times 10^{-3}$$

$$\theta_{p2m} = 0$$

$$\delta_{em} = \frac{F_m}{K} = 0.1739 \text{ mm}$$

$$\delta_{ph} = \theta_{p1m}(1+\lambda)m - \theta_{p2m}\lambda m = 4.1437 \text{ mm}$$

$$\delta_m = \delta_{em} + \delta_{pm} = 4.3176 \text{ mm}$$

$$\theta_{p1u} = \frac{m}{t_f(1+\xi)} C = 0.310$$

$$\theta_{p2u} = 0$$

$$\delta_{eu} = \frac{F_u}{K} = 0.2841 \text{ mm}$$

$$\delta_{pu} = \theta_{p1u}(1+\lambda)m - \theta_{p2u}\lambda m = 54.62 \text{ mm}$$

$$\delta_u = \delta_{em} + \delta_{pm} = 54.9 \text{ mm}$$

Shear Deformation of Column Web:

$A_c =$ 300 x 10^2 mm^2

$b_{fc} =$ 394.8 mm

$t_{fc} =$ 30.2 mm

$t_{wc} =$ 18.4 mm

$r_c =$ 15.2 mm

$\gamma_{mo} =$ 1.0

$A_{vc} = A_c - 2b_{fc}t_{fc} + (t_{wc} + 2r_c)t_{fc} =$ 7628 mm^2

$V_{cwc.Rd} = \frac{f_y}{\sqrt{3}} A_{vc} =$ 1563.4 kN

$A_{vc1k} = t_{wc}(h_c - 2t_{fc}) + (t_{wc} + 2r_c)t_{fc} + (2r_c)^2 - \pi r_c^2$

$A_{vc1k} =$ 7571 mm^2

$K_{cws} = \frac{0.38EA_{vc1k}}{h_t}$

$K_{cws1} = \frac{0.38 \cdot 2.1 \cdot 10^5 \cdot 7571}{(528.3 - 90 - 13.2/2)} =$ 1399552 kN/m

$K_{cws2} = \frac{0.38 \cdot 2.1 \cdot 10^5 \cdot 7571}{(430 - 90)} =$ 1777019 kN/m

$\delta_{cws1} = \frac{V_{cwc.Rd}}{K_{cws1}} =$ 1.12 mm

$\delta_{cws2} = \frac{V_{cwc.Rd}}{K_{cws2}} =$ 0.88 mm

Bolt Deformation:

$t_{fu} =$ 30.2 mm

$t_{fl} =$ 10.0 mm

$t_{wh} =$ 3.0 mm

$t_h =$ 13.9 mm

$t_n =$ 16.0 mm

For bolt grade 8.8, $f_u = 800$ N/mm^2, $f_y = 640$ N/mm^2

$L_b = t_{fu} + t_{fl} + 2t_{wh} + \frac{t_h + t_n}{2} =$ 63.15 mm

$\varepsilon_y = \frac{f_y}{E} =$ 3.047 x 10^{-3}

$\delta_y = l\varepsilon_y =$ 0.1924 mm

Table A1. 3 Deformation of flexible end plate joint components

Description		Bending of End Plate	Bending of Column Flange	Shear Deformation of Column Web	Deformation of Bolt
F (kN)	F_y	36.58	157.26	1563.40	402.05
	F_h	54.72	235.06	-	-
	F_m	71.23	306.00	-	-
	F_u	116.33	499.80	-	-
δ (mm)	δ_y	0.57	0.09	1.12	0.19
	δ_h	1.03	0.47	-	-
	δ_m	3.22	4.32	-	-
	δ_u	29.55	54.90	-	-

$$\delta_{ult} = \quad 29.55 \text{ mm}$$

$$\theta_{ult} = \quad \frac{\delta_{ult}}{h_t} = 4.33^{\circ}$$

The rotation capacity of flexible end plate connection is 4.33 degree.

A. 1.4. ROTATION CAPACITY OF DOUBLE ANGLE WEB CLEAT CONNECTIONS

Bending of Angle:

Effective Width, b_{eff}= Pitch, p= 70 mm

Thickness of flange, t_f= 10 mm

Distance between plastic hinges in a thin flange of a bolted T-stubs, m= 50-10-0.8x11 = 31.2 mm

Distance between the bolt axis and the prying force, n = 40 mm

Bolt diameter, D_b= 20 mm

Washer diameter, D_w= 30 mm

Bolt shank area, A_b= $\pi D_b^2/4 = 314.1\,\text{mm}^2$

For bolt grade 8.8, f_{ub}= 800 N/mm^2

Ultimate axial resistance of bolts, B_u= $f_{ub}A_b$ = 251.28 kN

Bending moment corresponding to first yielding, M_y= $\frac{b_{eff}t_f^2}{6}f_y$ = 0.414 kN-m

Bending moment corresponding to the beginning of strain-hardening, M_h= $1.4948M_y$ = 0.619 kN-m

Bending moment corresponding to the maximum load point, M_m= $1.8447M_y$ = 0.764 kN-m

Ultimate bending moment , M_u= $3.2879M_y$ = 1.361 kN-m

Parameter governing the plastic mechanism typology of a bolted T-stubs with reference to ultimate conditions, β_u = $\frac{4M_u}{2B_u m}$ = 0.347

λ = n/m = 1.282

β_1= $\frac{2\lambda}{1+2\lambda}$ = 0.7194

$\beta_u < \beta_1$, Hence Angle fails by 1st mechanisms

F= $\left(\frac{32n-2d_w}{8mn-(m+n)d_w}\right)M$

F= $0.15545M$

First yielding lateral force, F_y= $0.15545M_y$ = 64.38 kN

Force corresponding to the beginning of strain hardening, F_h= $0.15545M_h$ = 96.24 kN

Force corresponding to the attainment of the ultimate true stress (f_u), F_m= $0.15545M_m$ = 118.77 kN

Ultimate Resistance, F_u= $0.15545M_u$ = 211.68 kN

K= $0.5E\frac{b_{eff}t_f^3}{m^3}$ = 242004.56 kN/m

First yielding displacement, δ_y = $\frac{F_y}{K}$ = 0.266 mm

$$\delta_{eh} = \frac{F_h}{K} = 0.398 \text{ mm}$$

$$C_h = 0.0015$$

$$\delta_{ph} = \frac{m^2}{2t_f} C_h = 0.073 \text{ mm}$$

Displacement corresponding to the beginning of strain hardening, $\delta_h = \delta_{eh} + \delta_{ph} = 0.471$ mm

$$\delta_{em} = \frac{F_m}{K} = 0.491 \text{ mm}$$

$$C_m = 0.0148$$

$$\delta_{pm} = \frac{m^2}{2t_f} C_m = 0.720 \text{ mm}$$

Displacement corresponding to the attainment of the ultimate true stress (f_u),

$$\delta_m = \delta_{em} + \delta_{pm} = 1.211 \text{ mm}$$

$$\delta_{eu} = \frac{F_u}{K} = 0.875 \text{ mm}$$

$$C = 0.3315$$

$$\delta_{pu} = \frac{m^2}{2t_f} C = 16.134 \text{ mm}$$

Ultimate Displacement, $\delta_u = \delta_{eu} + \delta_{pu} = 17.0$ mm

Bending of Column Flange:

Thickness of web, t_w = 18.4 mm

Thickness of flange, t_f = 30.2 mm

Root radius, r_c = 15.2 mm

$$m = \frac{(100 - 18.4)}{2} - 0.8 \cdot 15.2 = 28.64 \text{ mm}$$

$$n = 147.4 \text{ mm}$$

b_{eff} = Pitch, p = 70 mm

$$M_y = \frac{b_{eff} t_f^2}{6} f_y = 3.78 \text{ kN-m}$$

$$M_h = 1.4959 M_y = 5.65 \text{ kN-m}$$

$$M_m = 1.9473 M_y = 7.36 \text{ kN-m}$$

$$M_u = 3.1807 M_y = 12.01 \text{ kN-m}$$

$$\beta_u = \frac{4M_u}{2B_u m} = 3.333 > 2.0$$

$$\lambda = n/m = 5.1466$$

$$\beta_f = \frac{2\lambda}{1+2\lambda} = 0.91145$$

$\beta_u > 2$, Hence Column flange fails by 3rd mechanisms

Coefficient providing the bending moment in a section where ultimate conditions are not reached, $\xi = \frac{2}{\beta_u} = 0.6$

$\xi_1 = \frac{M_y}{M_u} = 0.3143$

$\xi_2 = \frac{M_m}{M_u} = 0.6122$

$C_m = 0.0148$

Ultimate plastic rotation, $\theta_p = \frac{(m+n)}{t_f} C_m = 0.0863$

$\delta_p = \theta_p \cdot m = 2.471$ mm

$F_y = \frac{2M_y}{m} = 263.78$ kN

$K = \frac{0.5 E b_{eff} t_f^3}{m^3} = 8617655$ kN/m

$\delta_y = \frac{F_y}{K} = 0.031$ mm

$F_h = \frac{2M_h}{m} = 394.59$ kN

$\delta_{eh} = \frac{F_h}{K} = 0.0458$ mm

$\delta_{ph} = \frac{m^2}{2t_f} C_h = 0.0204$ mm

$\delta_h = \delta_{eh} + \delta_{ph} = 0.066$ mm

$\delta_{eu} = \frac{2B_u}{K} = 0.0583$ mm

$\delta_u = \delta_{eu} + \delta_p = 2.529$ mm

Shear Deformation of Column Web:

$A_c = 300 \times 10^2$ mm^2

$b_{fc} = 394.8$ mm

$t_{fc} = 30.2$ mm

$t_{wc} = 18.4$ mm

$r_c = 15.2$ mm

$\gamma_{mo} = 1.0$

shear resistant area of the column, $A_{vc} = A_c - 2b_{fc}t_{fc} + (t_{wc} + 2r_c)t_{fc} = 7628$ mm^2

Design resistance of the column web in shear, $V_{cwc.Rd} = \frac{f_y}{\sqrt{3}} \frac{A_{vc}}{\gamma_{mo}} = 1563.4$ kN

$A_{vclk} = t_{wc}(h_c - 2t_{fc}) + (t_{wc} + 2r_c)t_{fc} + (2r_c)^2 - \pi r_c^2$

$A_{vclk} = 7571$ mm^2

$$K_{cws} = \frac{0.38EA_{vc}k}{h_t}$$

$$K_{cws1} = \frac{0.38 \cdot 2.1 \cdot 10^5 \cdot 7571}{(528.3-90-13.2/2)} = 1399552 \text{ kN/m}$$

$$K_{cws2} = \frac{0.38 \cdot 2.1 \cdot 10^5 \cdot 7571}{(360-90)} = 2237728 \text{ kN/m}$$

$$\delta_{cws1} = \frac{V_{cwc.Rd}}{K_{cws1}} = 1.12 \text{ mm}$$

$$\delta_{cws2} = \frac{V_{cwc.Rd}}{K_{cws2}} = 0.70 \text{ mm}$$

Bolt Deformation:

Upper flange thickness, t_{fu} = 30.2 mm

Lower flange thickness, t_{fl} = 10.0 mm

Washer thickness, t_{wh} = 3.0 mm

Bolt head thickness, t_h = 13.9 mm

Bolt nut thickness, t_n = 16.0 mm

For bolt grade 8.8, $f_u = 800$ N/mm^2, $f_y = 640$ N/mm^2

Conventional bolt length, $L_b = t_{fu} + t_{fl} + 2t_{wh} + \frac{t_h + t_n}{2} = 61.15$ mm

$$\varepsilon_y = \frac{f_y}{E} = 3.047 \text{ x } 10^{-3}$$

$$\delta_y = l\varepsilon_y = 0.186 \text{ mm}$$

Table A1. 4 Deformation of double angle web cleat joint components

Description		Bending of Angle Section	Bending of Column Flange	Shear Deformation of Column Web	Deformation of Bolt
F (kN)	F_y	64.58	263.78	1563.40	402.05
	F_h	96.24	394.59	-	-
	F_m	118.77	-	-	-
	F_u	211.68	502.56	-	-
δ (mm)	δ_y	0.27	0.03	1.12	0.19
	δ_h	0.47	0.07	-	-
	δ_m	1.21	-	-	-
	δ_u	17.00	2.53	-	-

$$\delta_{ult} = 17.00 \text{ mm}$$

$$\theta_{ult} = \frac{\delta_{ult}}{h_t} = 2.5^o$$

The rotation capacity of double angle web cleat connection is **2.5** degree.

A. 1.5. CASE STUDY ON CATENARY ACTION IN SIMPLE CONNECTION FRAMES

Calculation of maximum joint ductility and tensile strength

It has been assumed that rotation occurs about the CG of the bolt group, with a total plastic deformation of the upper bolt hole in the fin-plate of 10mm (corresponding to half a bolt diameter).

Rotation capacity = 10/140 = 0.0714 rad or 4°

Tension capacity of fin plate = $K_e p_y A_{net}$

$K_e = 1.1$; $A_{net} = A - n D_h t = 360 \times 10 - 5 \times 22 \times 9.6 = 2544$ mm^2

Tension capacity of fin plate = $1.1 \times 355 \times 2544 \times 10^{-3} = 993.43$ kN

Bearing capacity of fin plate $= 1.5n\ d\ t_f p_{bs} \leq 0.5n\ e_2\ t_f\ p_{bs}$

$0.5n\ e_2\ t_f\ p_{bs} = 0.5 \times 5 \times 50 \times 10 \times 550 \times 10^{-3} = 687.5$ kN

$1.5n\ d\ t_f p_{bs} = 1.5 \times 5 \times 20 \times 10 \times 550 \times 10^{-3} = 825$ kN

Hence, Bearing capacity of fin plate = 687.5 kN

Tension capacity of beam web at the connection = $L_e\ t_w\ p_y$

$L_e = 2\ e_e + (n-1)\ p_e - n\ p_h = 2 \times 40 + (5-1) \times 70 - 5 \times 22 = 250$ mm

Tension capacity of beam web at the connection = $250 \times 9.6 \times 355 \times 10^{-3} = 852$ kN

Bearing capacity of beam web at the connection $= 1.5n\ d\ t_w p_{bs} \leq 0.5n\ e_3\ t_w\ p_{bs}$

$0.5n\ e_3\ t_w\ p_{bs} = 0.5 \times 5 \times 40 \times 9.6 \times 550 \times 10^{-3} = 528$ kN

$1.5n\ d\ t_w p_{bs} = 1.5 \times 5 \times 20 \times 9.6 \times 550 \times 10^{-3} = 792$ kN

Hence, Bearing capacity of supported beam web at the connection = 528 kN

Tying capacity of the connection, the minimum of above values is 528 kN

Calculation of slab tensile strength

Tying capacity of reinforcement mesh per metre = $142 \times 460 \times 10^{-3} = 65.32$ kN

Tying capacity of profiled sheet per metre = $40 \times 1.2 \times 19 \times 550 \times 10^{-3}/12 = 41.8$ kN

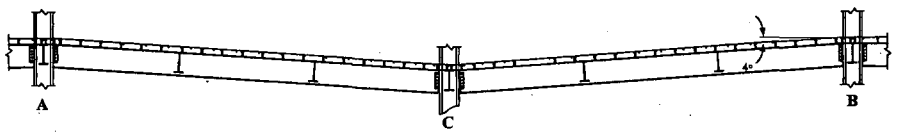

Fig. A1. 2 Deflected shape of beam at maximum rotation capacity of 4 °

Calculation of factor of safety against collapse

To explain the calculation, a one metre strip XZY (Fig. A. 8), located 6m from beam '$A_1C_1B_1$' is taken. This strip is idealised as beam, having pinned support at X and Y, and internal hinge at Z since there is no top reinforcement to resist hogging moment. The average rotation at X is 2.17° and the tying capacity of slab is 107 kN (Fig. A. 8). This rotation and tying capacity of slab causes the upward force of 8.10 kN on the beam CC_1 at Z that will be helpful in resisting downward accidental load. The loading on main beam CC_1 is shown in Fig. A. 9. There will not be any reduction in the accidental load on the secondary beam as no change in angles of tying force occurs on either side. The reactions from this beam and secondary beams are calculated and transferred on the main beam as shown in Fig. A. 10. To understand the influence of steel reinforcement, profile sheet and steel beam on catenary action, the analysis is carried out with and without considering the tying capacity of slab. For these cases, the slopes of the inverted three hinged arch at 'A and B' are considered to be the rotation capacity. In addition, the analysis for each case is carried out with and without dynamic amplification factor (DAF). Consequently, the maximum tying force acting on this beam and the factor of safety for the joint which is defined as the ratio between the tying capacity and the tying force acting on the beam are calculated.

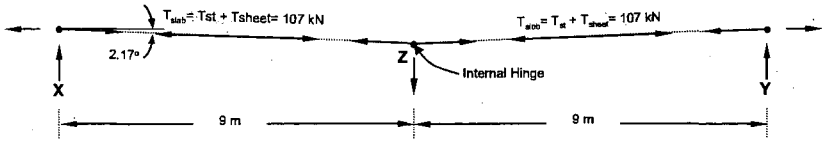

Fig. A1. 3 Tying force carried by beam 'XZY'

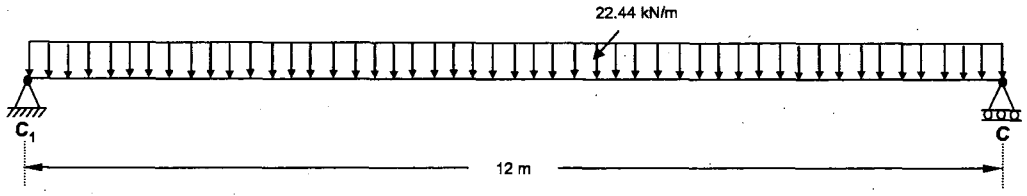

(a) Accidental load

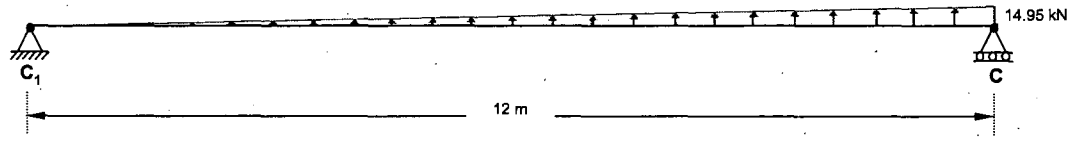

(b) Resisting force by catenary action

Fig. A1. 4 Load on main beam 'CC$_1$'

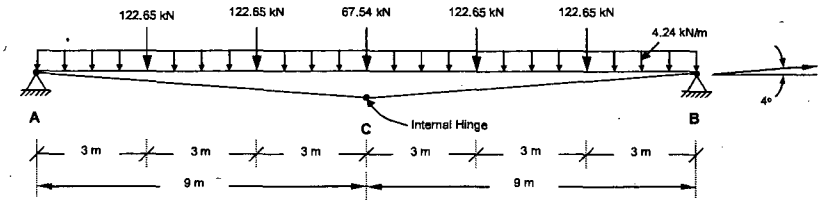

Fig. A1. 5 Accidental load on main beam 'ACB'

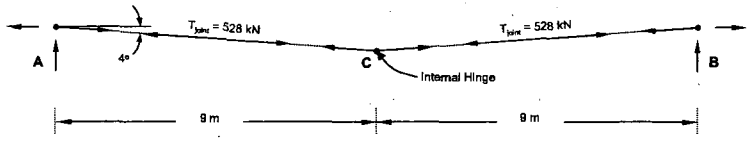

Fig. A1. 6 Tying force carried by main beam 'ACB'

Case 1: Without dynamic amplification

Tying capacity of reinforcement mesh per metre = 65.32 kN

Tying capacity of profiled sheet per metre = 41.8 kN

Tying capacity of slab per metre, T = 65.32 + 41.8 = 107.12 kN

Upward reactive force resulting from slab tying capacity per metre = 2 $T \sin \theta$

Upward reactive force caused by 1 m strip located 6 m from $A_1C_1B_1$ = 2 x 107.12 x sin *2.17° = 8.10 kN*

Reaction at C due to accidental load acting on beam CC_1 =0.5 x 12 x 20.44 = 122.65 kN

Reaction at C due to the upward reactive force acting on beam CC1 = 0.5 x 14.95 x 12 x (2/3) = 59.8 kN

Force transferred on the main beam ACB from the secondary beam SS_1 = 0.5 x 12 x 20.44 = 122.65 kN

(a) if the contribution of slab is considered in resisting accidental load

Force transferred on the main beam ACB from beam CC_1 = 122.65 – 59.8 = 62.85 kN

Horizontal thrust at A, $H_A = \frac{1}{9\tan 4^o}\left[122.65x9 + \frac{67.54x9}{2} + \frac{4.24x9^2}{2}\right]$ =2509.8 kN

Vertical reaction at A, V_A = 0.5 x [4 x 122.65 + 67.54 + 2 x 9 x 4.24] = 317.23 kN

Resultant force (Tying force) = $\sqrt{H_A^2 + V_A^2} = \sqrt{2509.8^2 + 317.23^2}$ = 2530 kN

Factor of safety for the joint = $\frac{\text{Tying capacity of the joint}}{\text{Tying force acting in the joint}} = \frac{528}{2530}$ =0.21

(b) if the contribution of slab is neglected in resisting accidental load

Force transferred on the main beam ACB from beam CC_1 = 122.65 kN

Horizontal thrust at A, $H_A = \frac{1}{9\tan 4^o}\left[122.65x9 + \frac{127.25x9}{2} + \frac{4.24x9^2}{2}\right]$ =2936.7 kN

Vertical reaction at A, V_A = 0.5 x [4 x 122.65 + 127.25 + 2 x 9 x 4.24] = 347.10 kN

Resultant force (Tying force) = $\sqrt{2936.7^2 + 347.10^2}$ = 2957 kN

Factor of safety for the joint = $\frac{528}{2957}$ =0.18

Case 2: With dynamic amplification of 1.5

Reaction at C due to accidental load acting on beam CC_1 = 1.5 x 0.5 x 12 x 20.44 = 184 kN

Reaction at C due to the upward reactive force acting on beam CC1 = 0.5 x 14.95 x 12 x (2/3) = 59.8 kN

Force transferred on the main beam ACB from the secondary beam SS_1 = 1.5 x 0.5 x 12 x 20.44 = 184 kN

(a) if the contribution of slab is considered in resisting accidental load

Force transferred on the main beam ACB from beam CC_1 = 184 – 59.8 = 124.2 kN

Horizontal thrust at A, $H_A = \frac{1}{9\tan 4^o}\left[184x9 + \frac{131.2x9}{2} + \frac{6.36x9^2}{2}\right]$ =3979 kN

Vertical reaction at A, V_A = 0.5 x [4 x 184 + 131.2 + 2 x 9 x 6.36] = 490.8 kN

Resultant force (Tying force) = $\sqrt{3979^2 + 490.8^2}$ = 4009 kN

Factor of safety for the joint = $\frac{528}{4009}$ =0.13

(b) if the contribution of slab is neglected in resisting accidental load

Force transferred on the main beam ACB from beam CC_1, if the contribution of slab is neglected in resisting accidental load = 184 kN

Horizontal thrust at A, $H_A = \frac{1}{9\tan 4^o}\left[184x9 + \frac{191x9}{2} + \frac{6.36x9^2}{2}\right]$ =4406 kN

Vertical reaction at A, V_A = 0.5 x [4 x 184 + 191 + 2 x 9 x 6.36] = 521 kN

Resultant force (Tying force) = $\sqrt{4406^2 + 521^2}$ = 4437 kN

Factor of safety for the joint = $\frac{528}{4437}$ =0.12

At rotation capacity of joints, the tying force on the connection is much higher than that of the tying capacity. At the same time, bottom flange of beam touches the flange of the column at joints 'A & B' (Fig. A. 12). Due to insufficient joint ductility, couple can develop between beam flange and column. The resulting prying action causes early joint fracture and subsequent failure of catenary action as shown in Fig. A. 13.

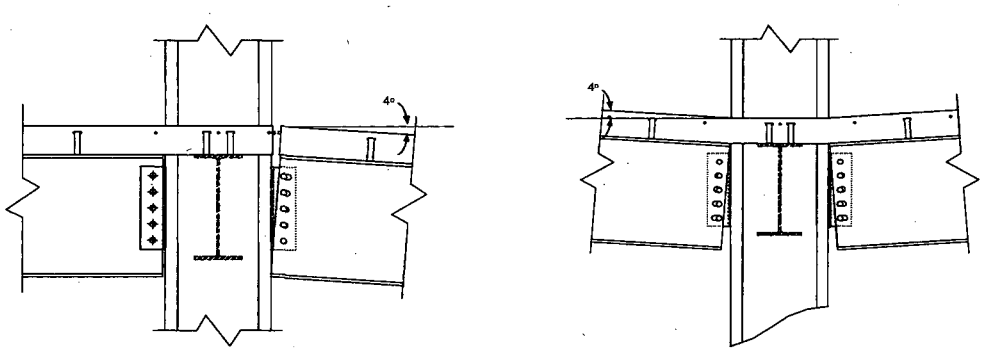

(a) Joint **(b) Joint**

Fig. A1. 7 Beam-column joint when it reaches maximum rotation capacity

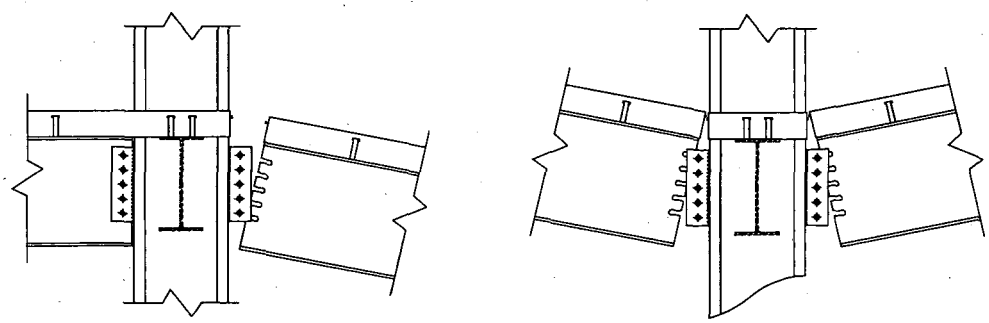

(a) Joint 'A' (b) Joint

Fig. A1. 8 Failure of beam-column joint

Calculation of displacement required to achieve equilibrium

To obtain the required rotation capacity, the equation is formed through the analysis, considering the rotation as a variable. This equation is solved by trial and error procedure.

Case 1: Without dynamic amplification

(a) if the contribution of slab is considered in resisting accidental load

The trial rotation is assumed as 13.1°.

Upward reactive force at C resulting from slab tying capacity per metre = 2 $T \sin\theta$ = 2 x 107.12 x sin 13.1° = 48.56 kN

Reaction at C due to the upward reactive force acting on beam CC_1 = 0.5 x 48.56 x 12 x (2/3) = 194.24 kN

Force transferred on the main beam ACB from beam CC_1 = 122.65 – 194.24 = -71.6 kN

Horizontal thrust at A, $H_A = \frac{1}{9\tan 13.1^{o}}\left[122.65x9 + \frac{(-67)x9}{2} + \frac{4.24x9^2}{2}\right] = 465$ kN

Vertical reaction at A, V_A = 0.5 x [4 x 122.65 - 67 + 2 x 9 x 4.24] = 250 kN

Resultant force (Tying force) = $\sqrt{465^2 + 250^2} = 528$ kN

Factor of safety for the joint = $\frac{528}{528} = 1$

Hence, the required rotation capacity is 13.1° which is calculated considering the contribution of slab and neglecting dynamic effects.

(b) if the contribution of slab is neglected in resisting accidental load

The trial rotation is assumed as 27.3°.

Force transferred on the main beam ACB from beam CC_1 = 122.65 kN

Horizontal thrust at A, $H_A = \frac{1}{9\tan 27.3^o}\left[122.65x9 + \frac{127.25x9}{2} + \frac{4.24x9^2}{2}\right] = 398$ kN

Vertical reaction at A, V_A = 0.5 x [4 x 122.65 + 127.25 + 2 x 9 x 4.24] = 347 kN

Resultant force (Tying force) = $\sqrt{398^2 + 347^2}$ = 528 kN

Factor of safety for the joint = $\frac{528}{528} = 1.0$

Hence, the required rotation capacity is 27.3° which is calculated neglecting both the contribution of slab and dynamic effects.

Case 2: With dynamic amplification of 1.5

(a) if the contribution of slab is considered in resisting accidental load

The trial rotation is assumed as 21.4°.

Upward reactive force at C resulting from slab tying capacity per metre = 2 T sin θ = 2 x 107.12 x sin 21.4° = 78.2 kN

Reaction at C due to the upward reactive force acting on beam CC_1 = 0.5 x 78.2 x 12 x (2/3) = 312.8 kN

Force transferred on the main beam ACB from beam CC_1 = 184 – 312.8 = -128.8 kN

Horizontal thrust at A, $H_A = \frac{1}{9\tan 21.4^o}\left[184x9 + \frac{(-124.2)x9}{2} + \frac{6.36x9^2}{2}\right] = 384$ kN

Vertical reaction at A, V_A = 0.5 x [4 x 184 -124.2 + 2 x 9 x 6.36] = 363 kN

Resultant force (Tying force) = $\sqrt{384^2 + 363^2}$ = 528 kN

Factor of safety for the joint = $\frac{528}{528} = 1$

Hence, the required rotation capacity is 21.4° which is calculated considering both the contribution of slab and dynamic effects.

(b) if the contribution of slab is neglected in resisting accidental load

Vertical reaction at A, V_A = 0.5 x [4 x 184 + 191 + 2 x 9 x 6.36] = 521 kN

As the vertical reaction is nearly equal to the tying capacity of the connections, the connections need huge rotation capacity (more than 45°) to sustain this accidental load.

A. 2 DYNAMIC ANALYSIS FOR COLUMNS SUBJECTED TO BLAST LOAD

A. 2.1. MATHEMATICA PROGRAMMES FOR DYNAMIC ANALYSIS OF COLUMNS

A. 2.1.1. RESPONSE OF A COLUMN, PINNED AT BOTH ENDS

```
Clear[L, n, MI, EL, x, kn, u, ul, qn, ωn, MaxDefCoeff, DefCoeff, td, tn, Dis1, Dis2];
P[t_] = 1 * (td - t)/td;
u[x_] = Sin[n * π * x/L];
Ml = m;
M2 = ∫_0^L m * (u[x])^2 dx;
Mn = Ml * M2;
Kl = EL * MI;
K2 = ∫_0^L u[x] * D[D[u[x], {x, 2}], {x, 2}] dx;
Kn = Kl * K2;
Pn = ∫_0^L u[x] dx;
ModalEq = D[qn[t], {t, 2}] + ωn^2 * qn[t] == P[t] * Pn * ωn^2 * 384 / (5 * K2 * L^4);
Soll = DSolve[{ModalEq, qn[0] == 0, qn'[0] == 0}, qn[t], t];
Shapel[t_] = Soll[[1, 1, 2]];
Disl[x_, t_] = (u[x] * Shapel[t]);
DeriDis[t_] = D[Shapel[t], {t, 1}];
uattd = Shapel[td];
Deriuattd = DeriDis[td];
Shape2[t_] = uattd * Cos[ωn * (t - td)] + Deriuattd/ωn * Sin[ωn * (t - td)];
Dis2[x_, t_] = (u[x] * Shape2[t]);
Moml[x_, t_] = (5/384) * L^2 * D[Disl[x, t], {x, 2}];
Mom2[x_, t_] = (5/384) * L^2 * D[Dis2[x, t], {x, 2}];
Shearl[x_, t_] = (5/384) * L^3 * D[Disl[x, t], {x, 3}];
Shear2[x_, t_] = (5/384) * L^3 * D[Dis2[x, t], {x, 3}];
tn = 0.01;
ωl = 2 * π/tn;
ωn = n^2 * ωl;
RatioFile = OpenWrite["D:\SpecificResistanceMethod\Response Simply Supported\Ratio.txt"];
DefFile = OpenWrite["D:\SpecificResistanceMethod\Response Simply Supported\Def.txt"];
BMFile = OpenWrite["D:\SpecificResistanceMethod\Response Simply Supported\BM.txt"];
SFFile = OpenWrite["D:\SpecificResistanceMethod\Response Simply Supported\SF.txt"];
```

```
Do[{
   MaxDefCoeff = 0.0;
   DefCoeff = 0;
   MaxMomCoeff = 0.0;
   MomCoeff = 0;
   MaxShearCoeff = 0.0;
   ShearCoeff = 0;
   td = tn / (10 * j);
   Do[{
     time = i / 10000.0;
     If[time ≤ td,
      {DefCoeff = Σ_{n=1}^{20} (Dis1[L/2, time]);
       MomCoeff = Σ_{n=1}^{20} (Mom1[L/2, time]);
       ShearCoeff = Σ_{n=1}^{20} (Shear1[L, time]);
      },
      {DefCoeff = Σ_{n=1}^{20} (Dis2[L/2, time]);
       MomCoeff = Σ_{n=1}^{20} (Mom2[L/2, time]);
       ShearCoeff = Σ_{n=1}^{20} (Shear2[L, time]);
      }
     ];
     If[MaxDefCoeff <= Abs[DefCoeff], {MaxDefCoeff = Abs[DefCoeff]}, {}];
     If[MaxMomCoeff <= Abs[MomCoeff], {MaxMomCoeff = Abs[MomCoeff]}, {}];
     If[MaxShearCoeff <= Abs[ShearCoeff], {MaxShearCoeff = Abs[ShearCoeff]}, {}];

    },
    {i, 1, 10000, 1}];

   PutAppend[td / tn, RatioFile];
   PutAppend[MaxDefCoeff, DefFile];
   PutAppend[MaxMomCoeff, BMFile];
   PutAppend[MaxShearCoeff, SFFile];

  },
  {j, 1, 5, 1}];
Close[RatioFile];
Close[DefFile];
Close[BMFile];
Close[SFFile];
```

A. 2.1.2. RESPONSE OF A COLUMN, FIXED AT BOTH ENDS

```
ClearAll[L, n, MI, EL, x, kn, u, ul, qn, ωn, MaxDefCoeff, DefCoeff, td, tn, Dis1, Dis2,
  Mom1, Mom2, Shear1, Shear2, MaxMidMomCoeff, MidMomCoeff, MaxEndMomCoeff,
  EndMomCoeff, MaxShearCoeff, ShearCoeff, βn, P, K2, K1, Pn, L, j];
P[t_] = 1 * (td - t) / td;
u[x_] = (Cos[βn * x] - Cosh[βn * x]) - kn * (Sin[βn * x] - Sinh[βn * x]);
Mn = ∫_0^L m * (u[x])^2 dx;
K1 = EL * MI;
K2 = ∫_0^L u[x] * D[D[u[x], {x, 2}], {x, 2}] dx;
Kn = K1 * K2;
Pn = ∫_0^L u[x] dx;
βn = π * (2 * n + 1) / (2 * L);
kn = (Cos[βn * L] - Cosh[βn * L]) / (Sin[βn * L] - Sinh[βn * L]);
ModalEq = D[qn[t], {t, 2}] + ωn^2 * qn[t] == P[t] * Pn * ωn^2 * 384 / (1 * K2 * L^4);
Sol1 = DSolve[{ModalEq, qn[0] == 0, qn'[0] == 0}, qn[t], t];
Shape1[t_] = Sol1[[1, 1, 2]];
Dis1[x_, t_] = (u[x] * Shape1[t]);
DeriDis[t_] = D[Shape1[t], {t, 1}];
uattd = Shape1[td];
Deriuattd = DeriDis[td];
Shape2[t_] = uattd * Cos[ωn * (t - td)] + Deriuattd / ωn * Sin[ωn * (t - td)];
Dis2[x_, t_] = (u[x] * Shape2[t]);
Mom1[x_, t_] = (1 / 384) * L^2 * D[Dis1[x, t], {x, 2}];
Mom2[x_, t_] = (1 / 384) * L^2 * D[Dis2[x, t], {x, 2}];
Shear1[x_, t_] = (1 / 384) * L^3 * D[Dis1[x, t], {x, 3}];
Shear2[x_, t_] = (1 / 384) * L^3 * D[Dis2[x, t], {x, 3}];
tn = 0.01;
ω1 = 2 * π / tn;
ωn = (2 * n + 1)^2 / 9 * ω1;
RatioFile = OpenWrite["C:\SpecificResistanceMethod\Response Fixed\Ratio.txt"];
DefFile = OpenWrite["C:\SpecificResistanceMethod\Response Fixed\Def.txt"];
MidBMFile = OpenWrite["C:\SpecificResistanceMethod\Response Fixed\MidBM.txt"];
EndBMFile = OpenWrite["C:\SpecificResistanceMethod\Response Fixed\EndBM.txt"];
SFFile = OpenWrite["C:\SpecificResistanceMethod\Response Fixed\SF.txt"];
```

```
j} 100;
Do[{
  MaxDefCoeff } 0.0;
  DefCoeff } 0;
  MaxMidMomCoeff } 0.0;
  MidMomCoeff } 0;
  MaxEndMomCoeff } 0.0;
  EndMomCoeff } 0;
  MaxShearCoeff } 0.0;
  ShearCoeff } 0;
  td } tn*0.005*j;
  i} 1;
  Do[{
    time} i/10000.0;
    If[time≤ td,
     {DefCoeff } ∑_{n}1^{20} (N[Dis1[L/2, time]]);
      MidMomCoeff} ∑_{n}1^{20} (N[Mom1[L/2, time]]);
      EndMomCoeff} ∑_{n}1^{20} (N[Mom1[0, time]]);
      ShearCoeff} ∑_{n}1^{20} (N[Shear1[0, time]]);
     },
     {DefCoeff } ∑_{n}1^{20} (N[Dis2[L/2, time]]);
      MidMomCoeff} ∑_{n}1^{20} (N[Mom2[L/2, time]]);
      EndMomCoeff} ∑_{n}1^{20} (N[Mom2[0, time]]);
      ShearCoeff} ∑_{n}1^{20} (N[Shear2[0, time]]);
     }
    ];
    If[MaxDefCoeff }} Abs[DefCoeff], {MaxDefCoeff } Abs[DefCoeff]}, {}];
    If[MaxMidMomCoeff }} Abs[MidMomCoeff], {MaxMidMomCoeff } Abs[MidMomCoeff]}, {}];
    If[MaxEndMomCoeff }} Abs[EndMomCoeff], {MaxEndMomCoeff } Abs[EndMomCoeff]}, {}];
    If[MaxShearCoeff }} Abs[ShearCoeff], {MaxShearCoeff } Abs[ShearCoeff]}, {}];
```

```
    },
    {i, 1, 10000, 1}];

  PutAppend[td/tn, RatioFile];
  PutAppend[MaxDefCoeff, DefFile];
  PutAppend[MaxMidMomCoeff, MidBMFile];
  PutAppend[MaxEndMomCoeff, EndBMFile];
  PutAppend[MaxShearCoeff, SFFile];

  },
 {j, 1, 100, 1}];
Close[RatioFile];
Close[DefFile];
Close[MidBMFile];
Close[EndBMFile];
Close[SFFile];
```

A. 2.1.3. RESPONSE OF A COLUMN, FIXED AT ONE END AND PINNED AT OTHER END

```
ClearAll[L, n, MI, EL, x, kn, u, u1, qn, ωn, MaxDefCoeff, DefCoeff, td, tn, Dis1,
  Dis2, Mom1, Mom2, Shear1, Shear2, MaxMidMomCoeff, MidMomCoeff, MaxEndMomCoeff,
  EndMomCoeff, MaxShear1Coeff, Shear1Coeff, MaxShear2Coeff,
  Shear2Coeff, βn, P, K2, K1, Pn, L];
P[t_] = 1 * (td - t) / td;
u[x_] = (Cos[βn * x] - Cosh[βn * x]) + kn * (Sinh[βn * x] - Sin[βn * x]);
Mn = ∫_0^L m * (u[x])^2 dx;
K1 = EL * MI;
K2 = ∫_0^L (u[x] * D[D[u[x], {x, 2}], {x, 2}]) dx;
Pn = ∫_0^L u[x] dx;
βn = π * (4 * n + 1) / (4 * L);
kn = (Cos[βn * L] - Cosh[βn * L]) / (Sin[βn * L] - Sinh[βn * L]);
ModalEq = D[qn[t], {t, 2}] + ωn^2 * qn[t] == P[t] * Pn * ωn^2 * 185 / (1 * K2 * L^4);
Sol1 = DSolve[{ModalEq, qn[0] == 0, qn'[0] == 0}, qn[t], t];
Shape1[t_] = Sol1[[1, 1, 2]];
Dis1[x_, t_] = (u[x] * Shape1[t]);
DeriDis[t_] = D[Shape1[t], {t, 1}];
uattd = Shape1[td];
Deriuattd = DeriDis[td];
Shape2[t_] = uattd * Cos[ωn * (t - td)] + Deriuattd / ωn * Sin[ωn * (t - td)];
Dis2[x_, t_] = (u[x] * Shape2[t]);
Mom1[x_, t_] = (1 / 185) * L^2 * D[Dis1[x, t], {x, 2}];
Mom2[x_, t_] = (1 / 185) * L^2 * D[Dis2[x, t], {x, 2}];
Shear1[x_, t_] = (1 / 185) * L^3 * D[Dis1[x, t], {x, 3}];
Shear2[x_, t_] = (1 / 185) * L^3 * D[Dis2[x, t], {x, 3}];
tn = 0.01;
ω1 = 2 * π / tn;
ωn = (4 * n + 1)^2 * ω1 / 25;

RatioFile = OpenWrite["C:\SpecificResistanceMethod\Response Propped\Ratio.txt"];
DefFile = OpenWrite["C:\SpecificResistanceMethod\Response Propped\Def.txt"];
EndBMFile = OpenWrite["C:\SpecificResistanceMethod\Response Propped\EndBM.txt"];
MidBMFile = OpenWrite["C:\SpecificResistanceMethod\Response Propped\MidBM.txt"];
SF1File = OpenWrite["C:\SpecificResistanceMethod\Response Propped\SF1.txt"];
SF2File = OpenWrite["C:\SpecificResistanceMethod\Response Propped\SF2.txt"];
```

```
Do[{
  MaxDefCoeff = 0.0;
  DefCoeff = 0;
  MaxMidMomCoeff = 0.0;
  MidMomCoeff = 0;
  MaxEndMomCoeff = 0.0;
  EndMomCoeff = 0;
  MaxShear1Coeff = 0.0;
  MaxShear2Coeff = 0.0;
  Shear1Coeff = 0.0;
  Shear2Coeff = 0.0;
  td = tn*0.005*j;
  i = 1;
  Do[{
    time = i / 10000.0;
    If[time ≤ td,
     {DefCoeff = Σ_{n=1}^{20} (N[Dis1[0.581*L, time]]);
      MidMomCoeff = Σ_{n=1}^{20} (N[Mom1[0.6167*L, time]]);
      EndMomCoeff = Σ_{n=1}^{20} (N[Mom1[0, time]]);
      Shear1Coeff = Σ_{n=1}^{20} (N[Shear1[0, time]]);
      Shear2Coeff = Σ_{n=1}^{15} (N[Shear1[L, time]]);
     },
     {DefCoeff = Σ_{n=1}^{20} (N[Dis2[0.581*L, time]]);
      MidMomCoeff = Σ_{n=1}^{20} (N[Mom2[0.6167*L, time]]);
      EndMomCoeff = Σ_{n=1}^{20} (N[Mom2[0, time]]);
      Shear1Coeff = Σ_{n=1}^{20} (N[Shear2[0, time]]);
      Shear2Coeff = Σ_{n=1}^{15} (N[Shear2[L, time]]);
     }
    ];
    If[MaxDefCoeff <= Abs[DefCoeff], {MaxDefCoeff = Abs[DefCoeff]}, {}];
    If[MaxMidMomCoeff <= Abs[MidMomCoeff], {MaxMidMomCoeff = Abs[MidMomCoeff]}, {}];
    If[MaxEndMomCoeff <= Abs[EndMomCoeff], {MaxEndMomCoeff = Abs[EndMomCoeff]}, {}];
    If[MaxShear1Coeff <= Abs[Shear1Coeff], {MaxShear1Coeff = Abs[Shear1Coeff]}, {}];
    If[MaxShear2Coeff <= Abs[Shear2Coeff], {MaxShear2Coeff = Abs[Shear2Coeff]}, {}];
```

```
    },
    {i, 1, 10000, 1}];

  PutAppend[td/tn, RatioFile];
  PutAppend[MaxDefCoeff, DefFile];
  PutAppend[MaxMidMomCoeff, MidBMFile];
  PutAppend[MaxEndMomCoeff, EndBMFile];
  PutAppend[MaxShear1Coeff, SF1File];
  PutAppend[MaxShear2Coeff, SF2File];

  },
 {j, 1, 100, 1}];
Close[RatioFile];
Close[DefFile];
Close[MidBMFile];
Close[EndBMFile];
Close[SF1File];
Close[SF2File];
```

A. 2.2. RESPONSE CHARTS FOR COLUMN FIXED AT BOTH ENDS

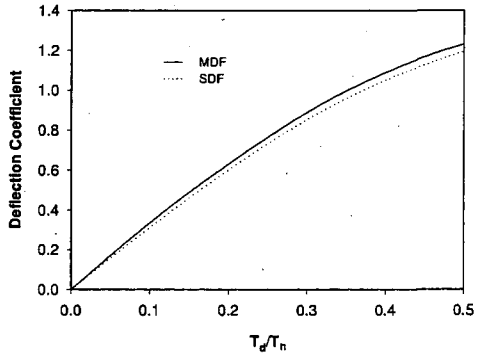

(a) Deflection

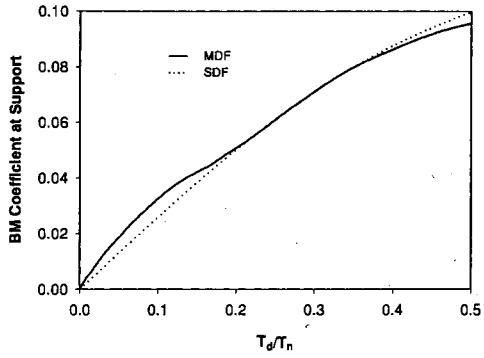

(b) Support moment

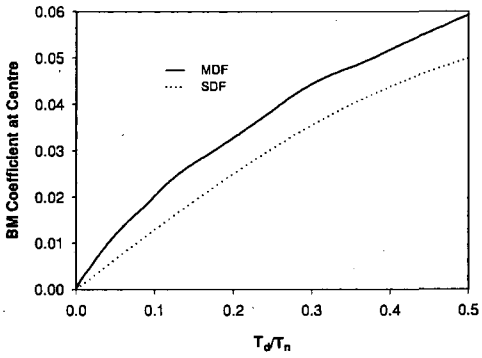

(c) Bending moment at mid span

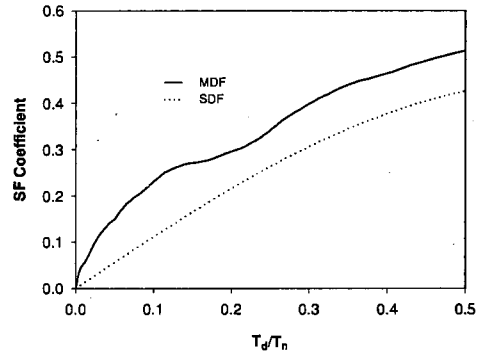

(d) Shear force at support

A. 2.3. RESPONSE CHARTS FOR COLUMN FIXED AT ONE END AND PINNED AT OTHER END

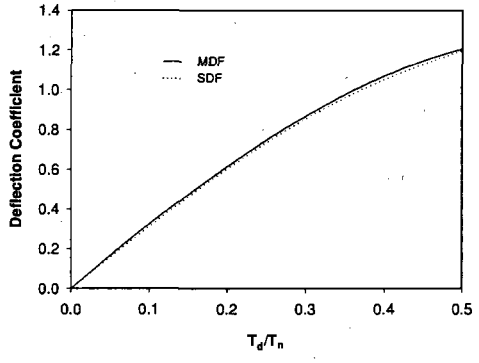

(a) Deflection at 0.62L from fixed end

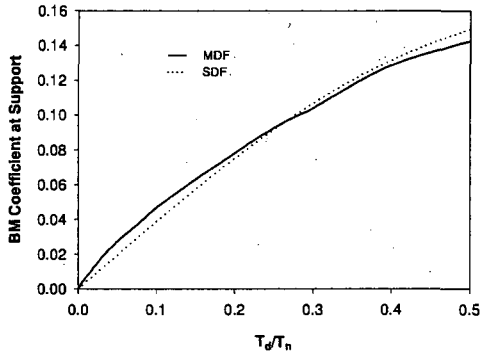

(b) Support moment

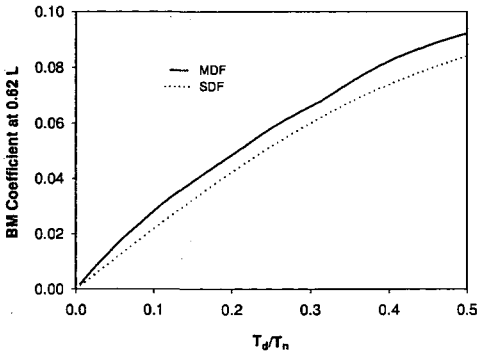

(c) Bending moment at 0.62L

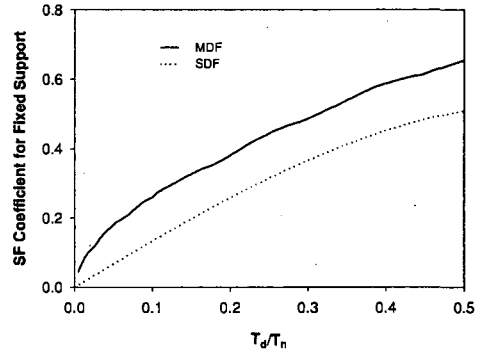

(d) Shear force at fixed support

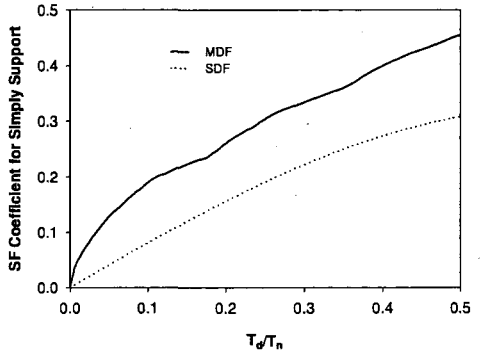

(d) Shear force at pinned support

A. 3 PROTECTIVE DESIGN FOR RC FRAMED STRUCTURES WITH A CASE STUDY OF THE MURRAH BUILDING

A. 3.1. FLOW CHART TO ESTIMATE COLUMN RESPONSE FOR COMPLEX PRESSURE TIME HISTORY PROFILE

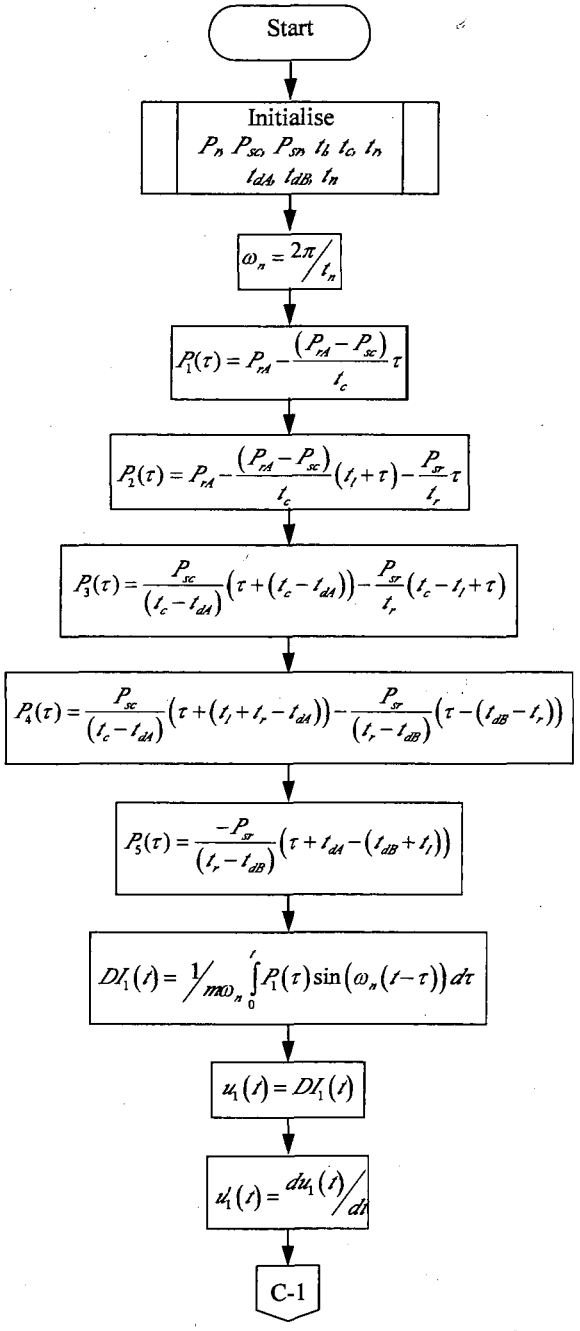

Fig. A3. 1 Flow chart to estimate the column response for complex pressure time history

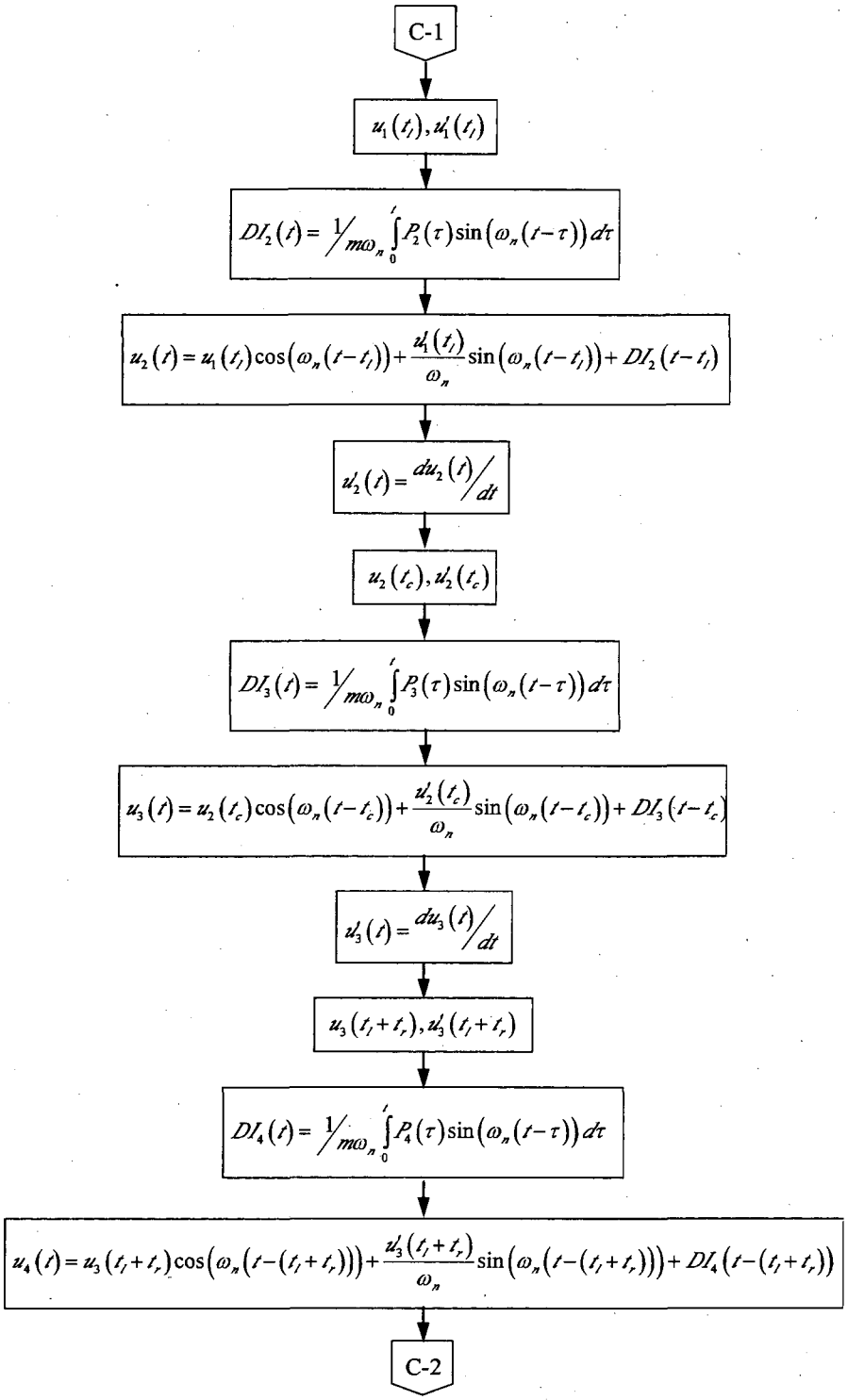

Fig. A3. 1 Flow chart to estimate the column response for complex pressure time history (cont...)

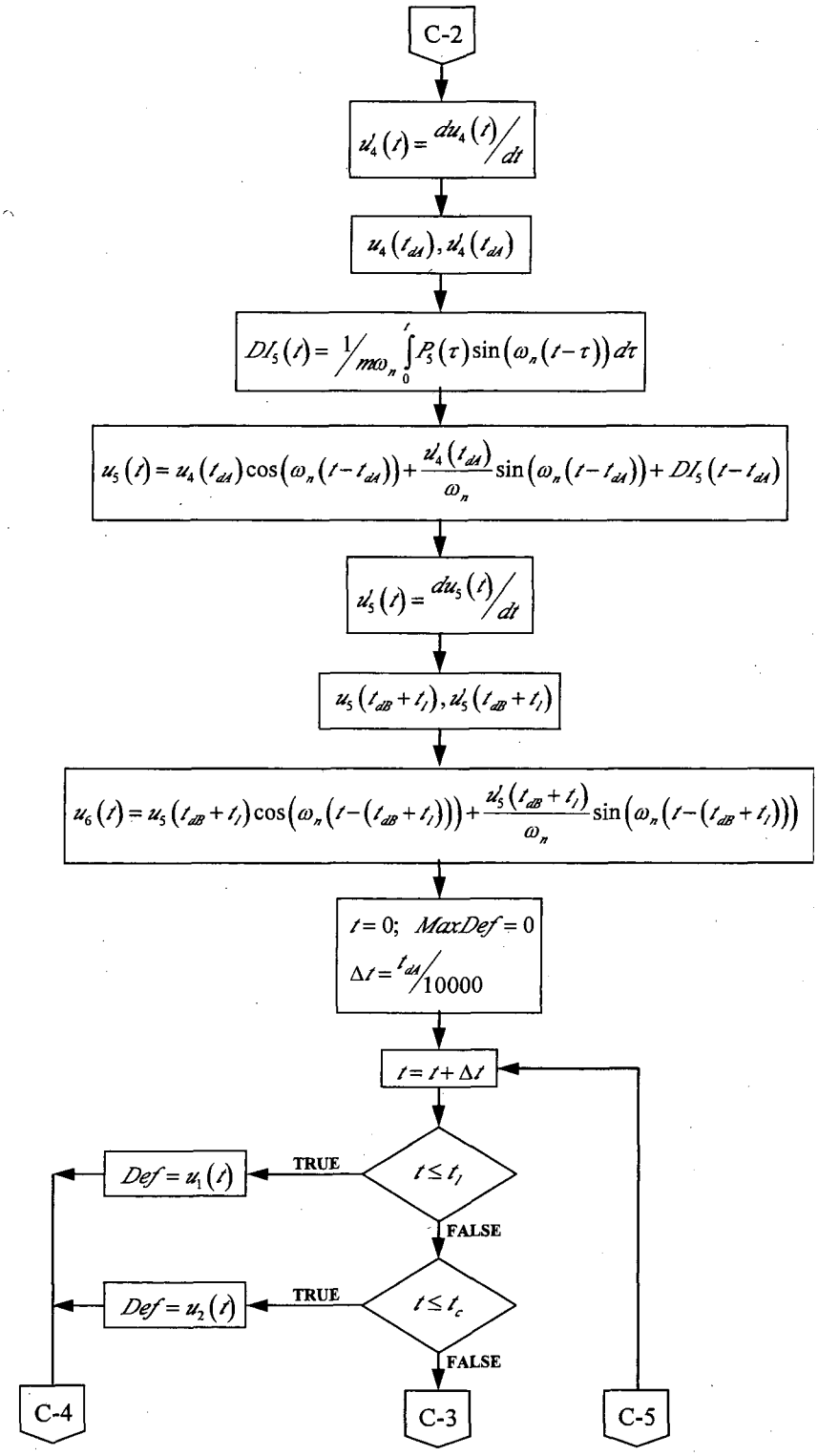

Fig. A3. 1 Flow chart to estimate the column response for complex pressure time history (cont...)

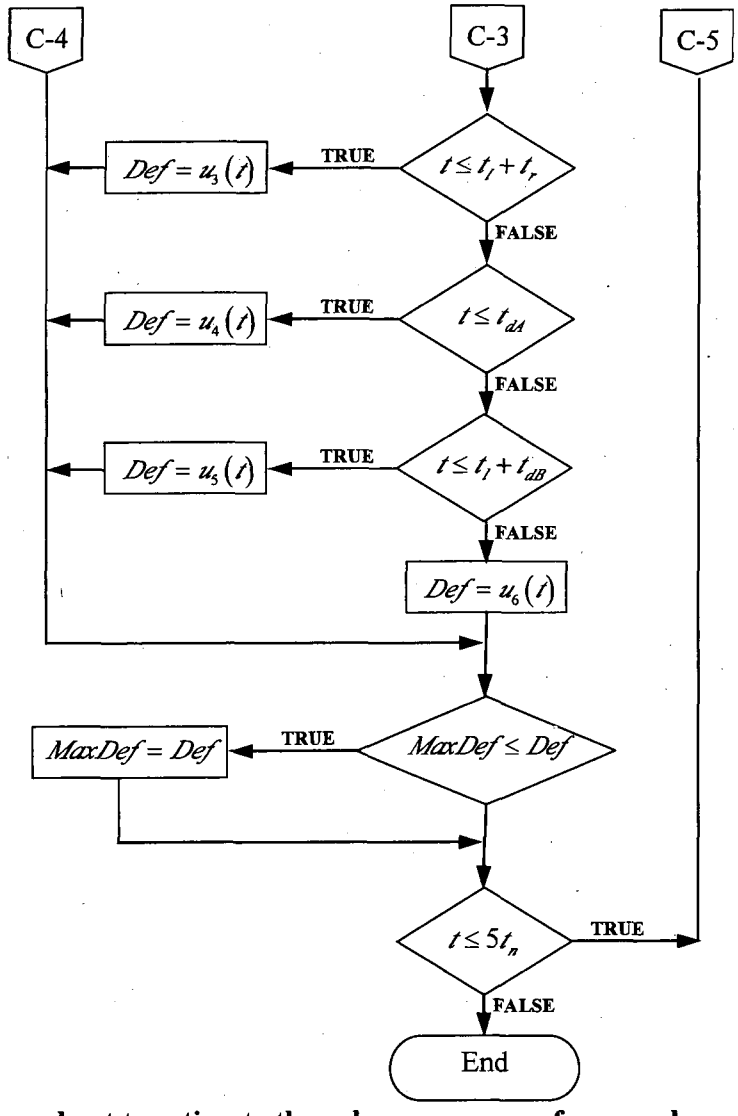

Fig.A3. 1 Flow chart to estimate the column response for complex pressure time history (cont...)

A. 3.2. DESIGN CHARTS FOR FLEXURAL STRENGTH OF COLUMNS

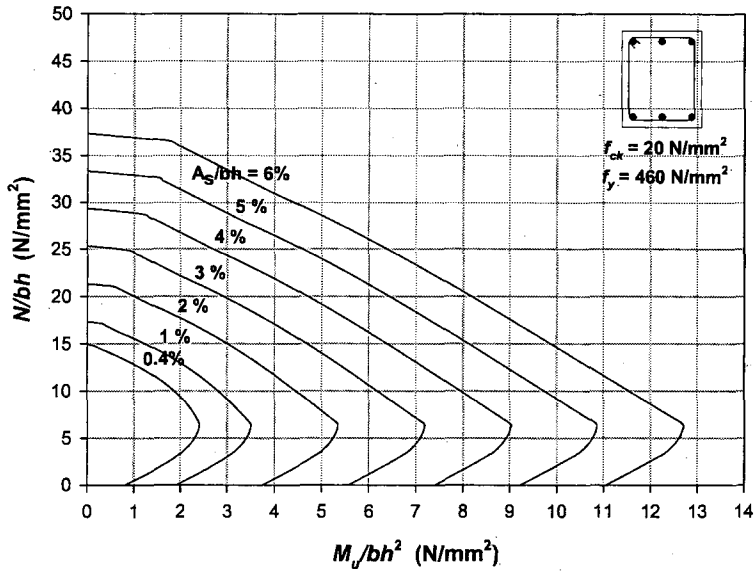

Fig. A3. 2 Design chart for C20 concrete column with reinforcement on two opposite faces

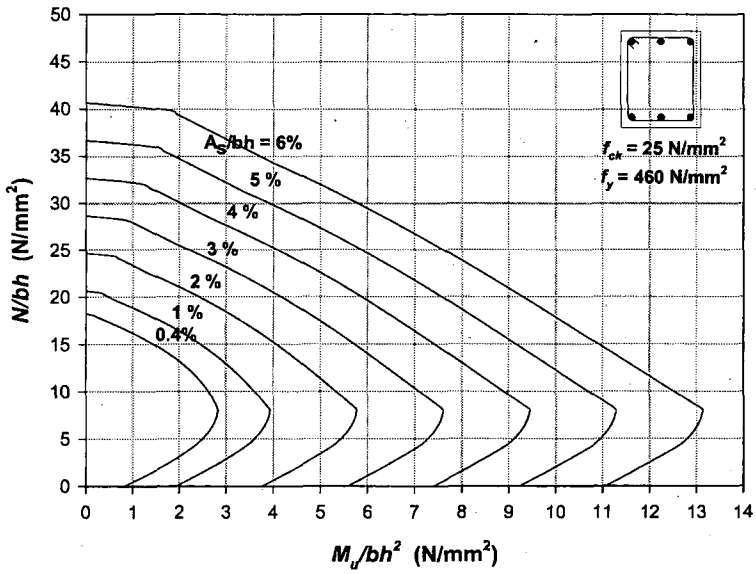

Fig. A3. 3 Design chart for C25 concrete column with reinforcement on two opposite faces

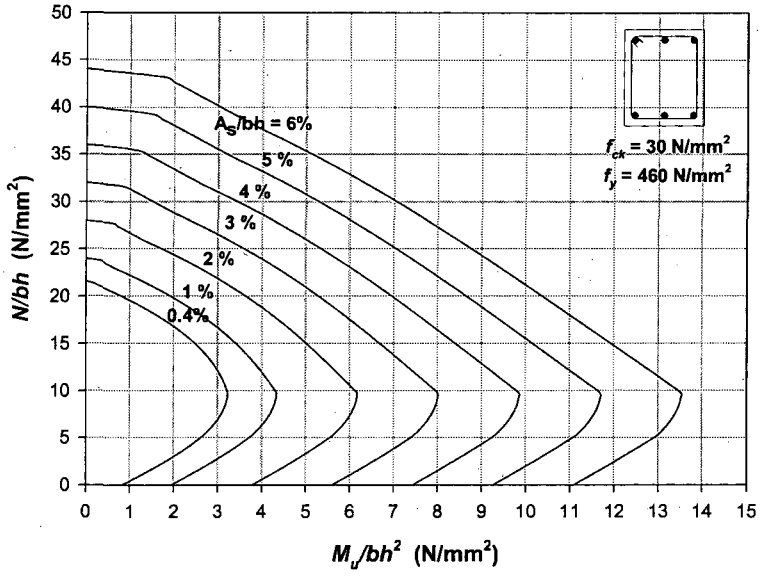

Fig. A3. 4 Design chart for C30 concrete column with reinforcement on two opposite faces

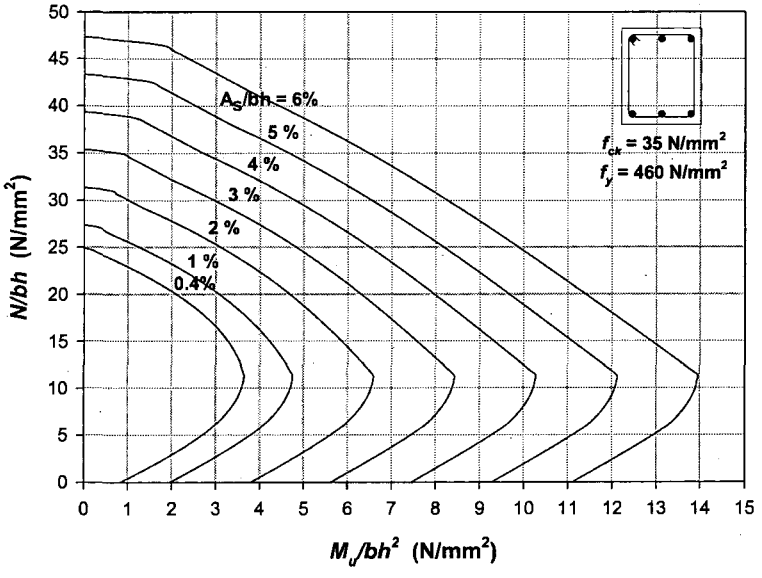

Fig. A3. 5 Design chart for C35 concrete column with reinforcement on two opposite faces

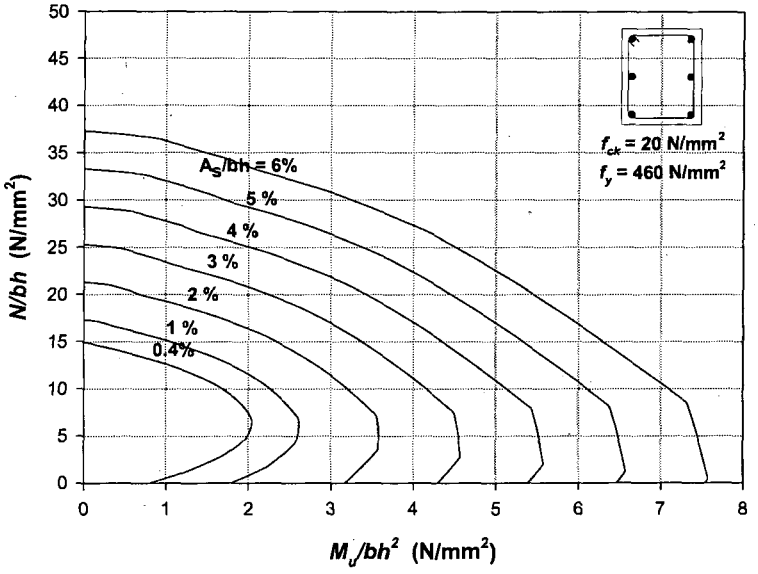

Fig. A3. 6 Design chart for C20 concrete column with reinforcement on two side faces

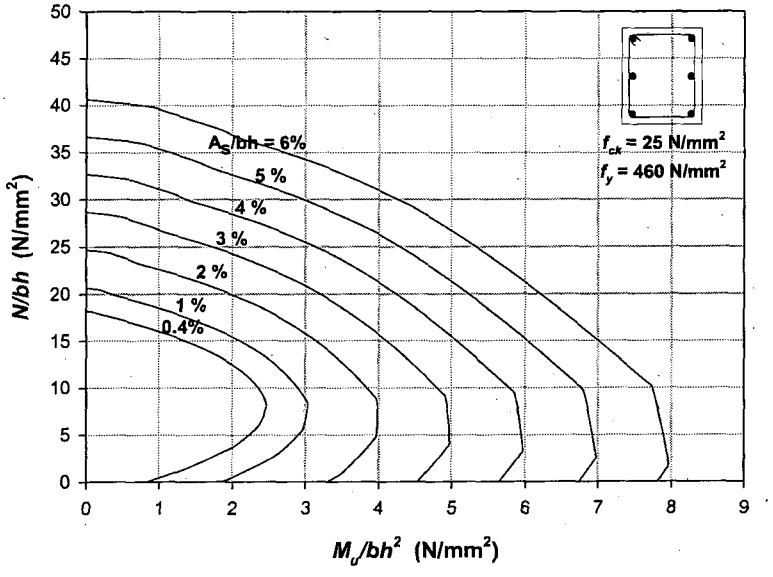

Fig. A3. 7 Design chart for C25 concrete column with reinforcement on two side faces

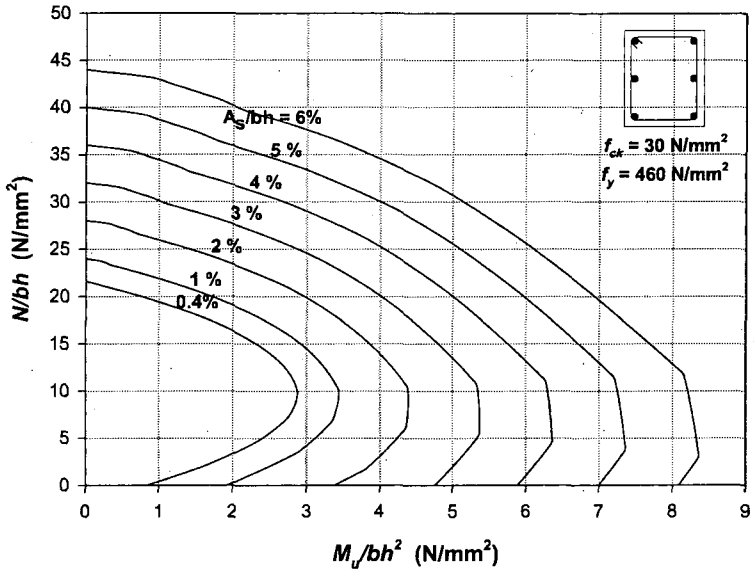

Fig. A3. 8 Design chart for C30 concrete column with reinforcement on two side faces

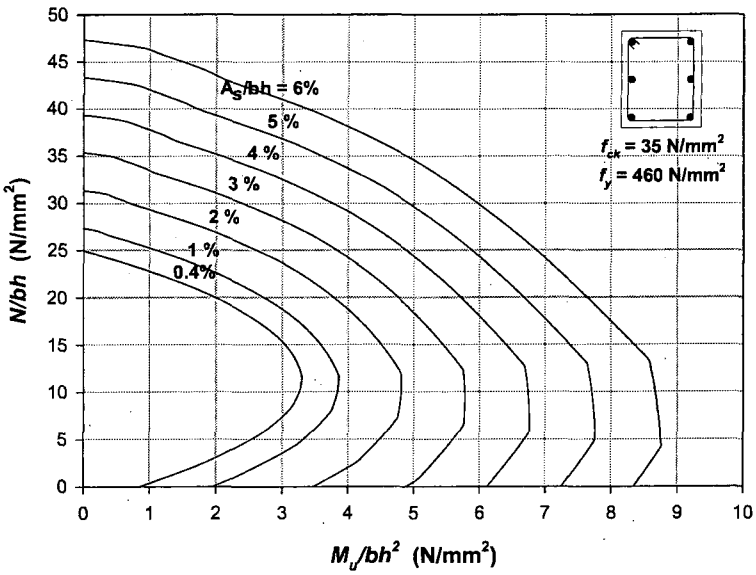

Fig. A3. 9 Design chart for C35 concrete column with reinforcement on two side faces

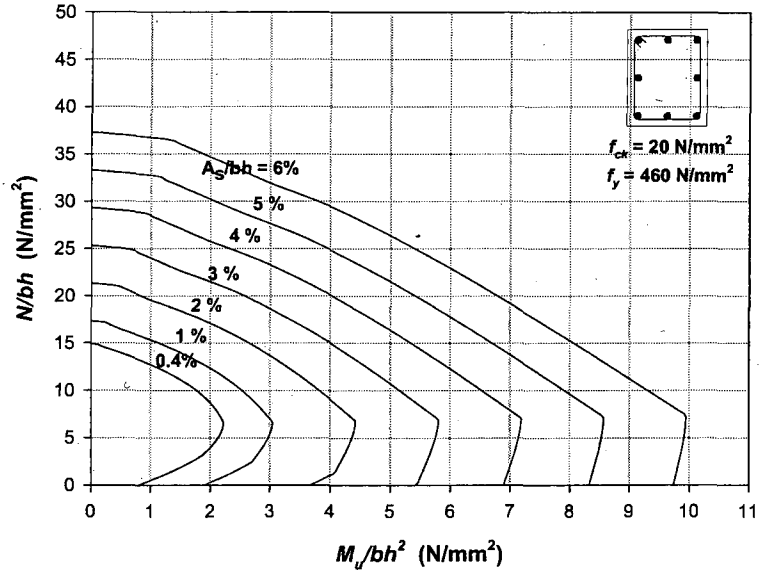

Fig. A3. 10 Design chart for C20 concrete column with reinforcement, distributed equally on all faces

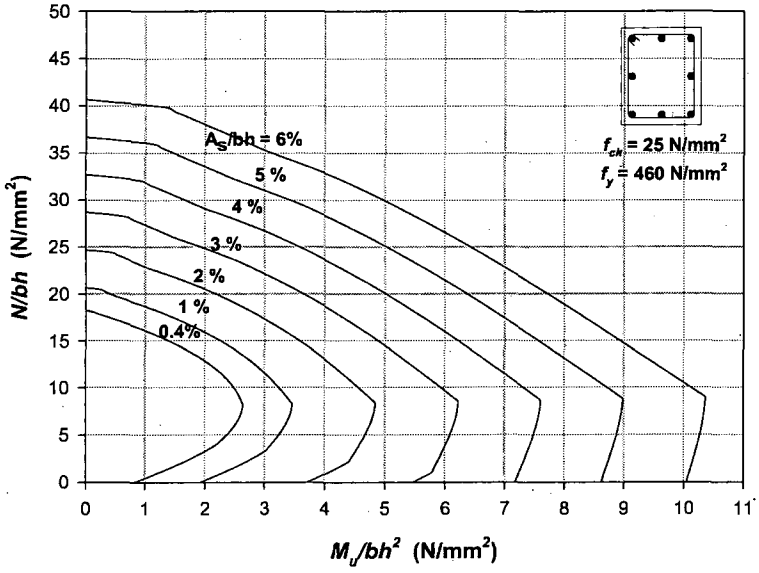

Fig. A3. 11 Design chart for C25 concrete column with reinforcement, distributed equally on all faces

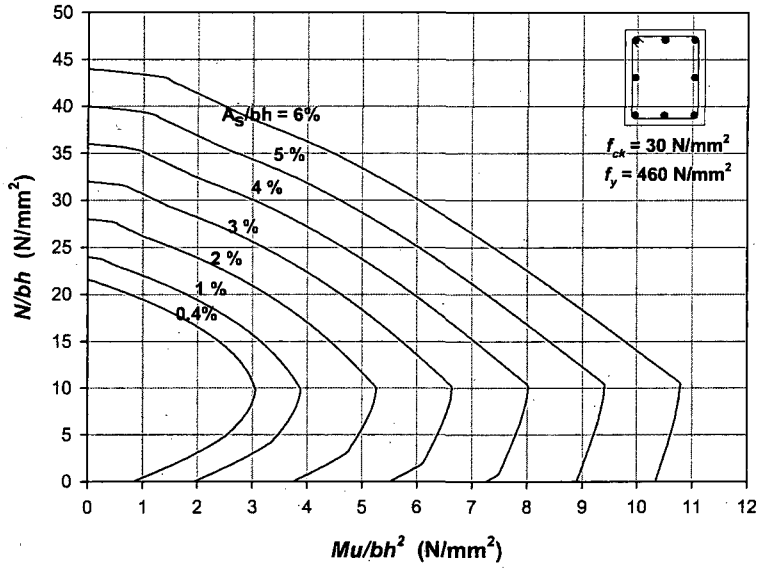

Fig. A3. 12 Design chart for C30 concrete column with reinforcement, distributed equally on all faces

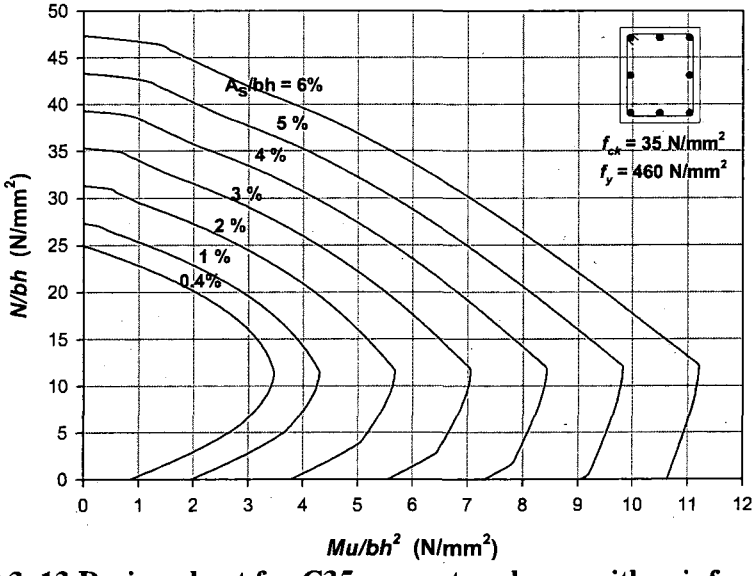

Fig. A3. 13 Design chart for C35 concrete column with reinforcement, distributed equally on all faces

A. 3.3. CRACKED MOMENT OF INERTIA FOR RC COLUMN

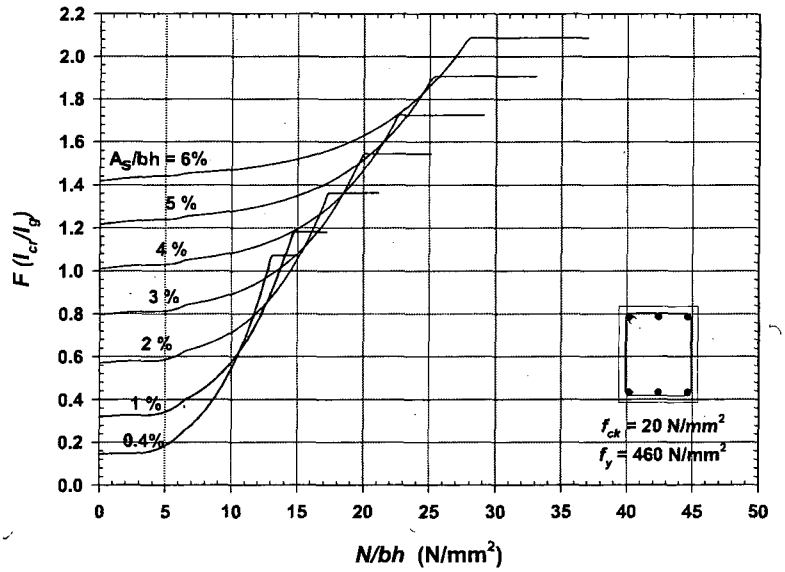

Fig. A3. 14 Cracked moment of inertia for C20 concrete column with reinforcement on two opposite faces

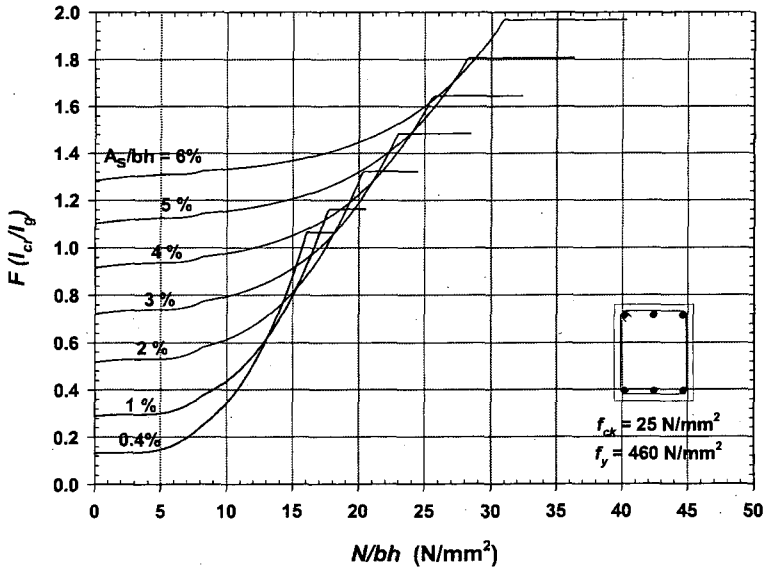

Fig. A3. 15 Cracked moment of inertia for C25 concrete column with reinforcement on two opposite faces

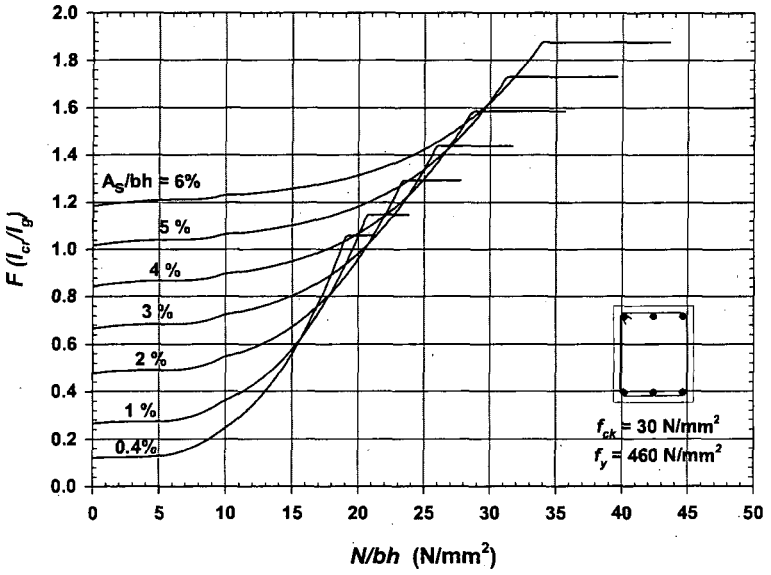

Fig. A3. 16 Cracked moment of inertia for C30 concrete column with reinforcement on two opposite faces

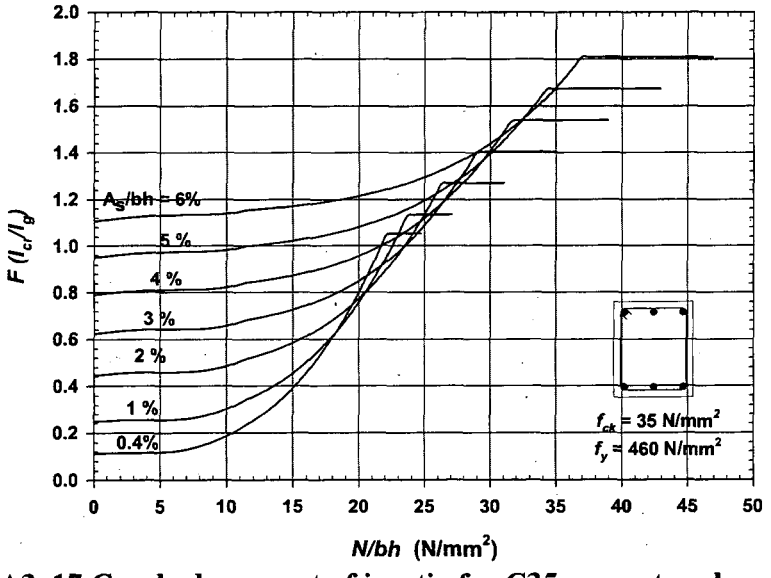

Fig. A3. 17 Cracked moment of inertia for C35 concrete column with reinforcement on two opposite faces

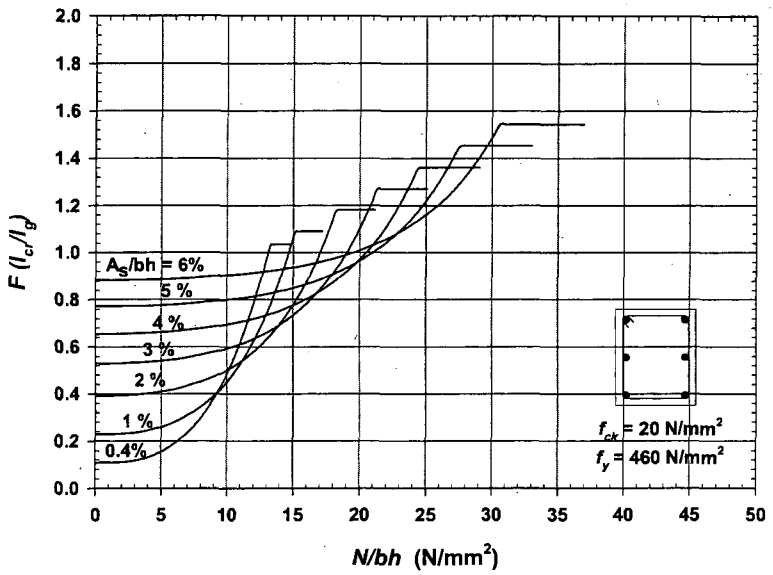

Fig. A3. 18 Cracked moment of inertia for C20 concrete column with reinforcement on two side faces

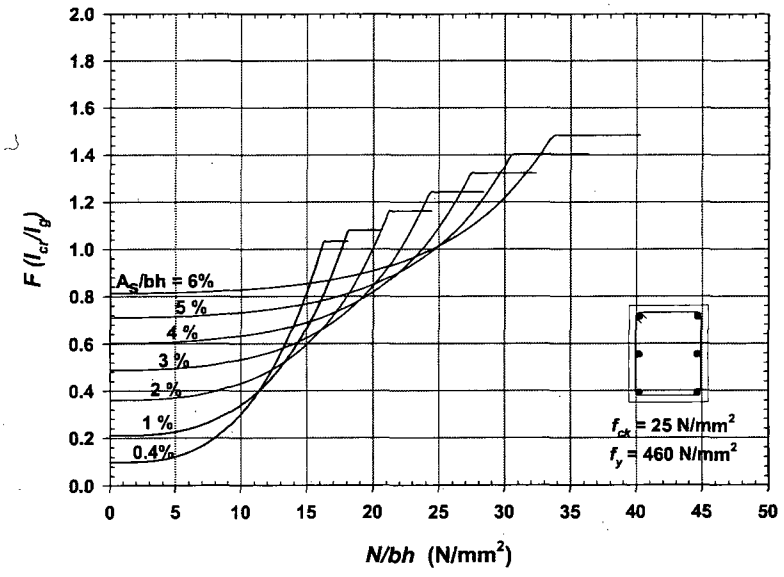

Fig. A3. 19 Cracked moment of inertia for C25 concrete column with reinforcement on two side faces

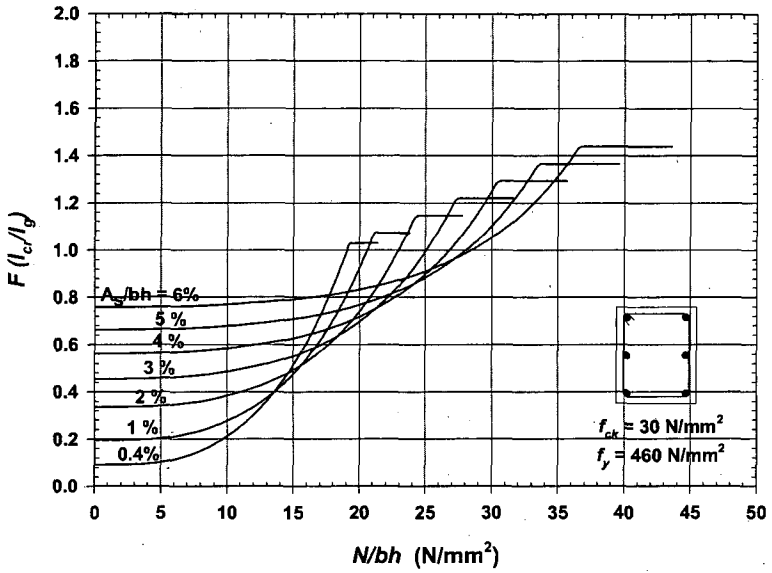

Fig. A3. 20 Cracked moment of inertia for C30 concrete column with reinforcement on two side faces

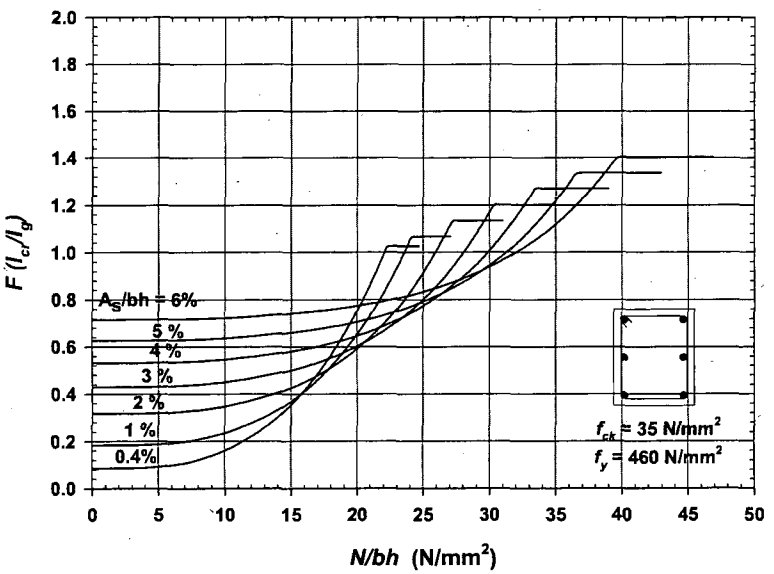

Fig. A3. 21 Cracked moment of inertia for C35 concrete column with reinforcement on two side faces

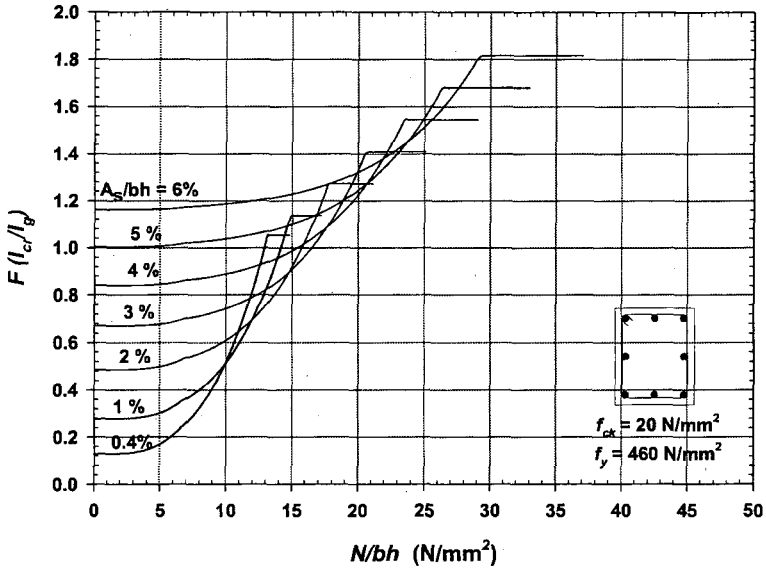

Fig. A3. 22 Cracked moment of inertia for C20 concrete column with reinforcement, distributed equally on all faces

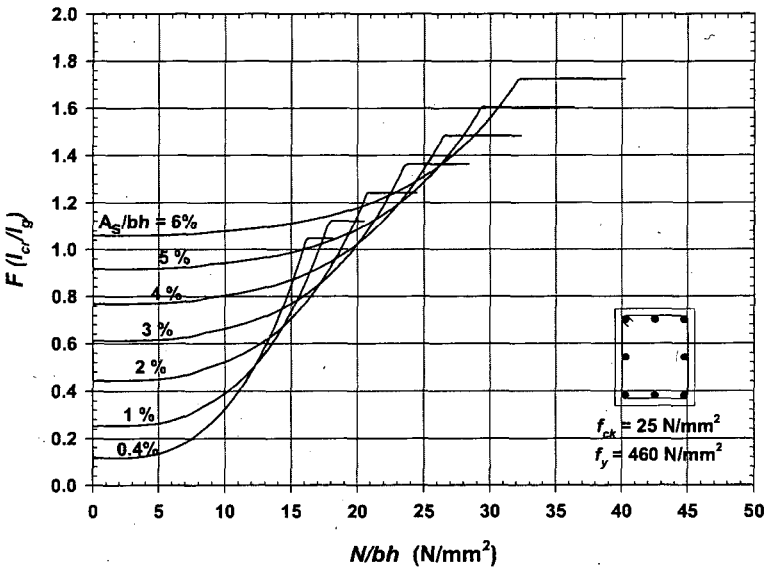

Fig. A3. 23 Cracked moment of inertia for C25 concrete column with reinforcement, distributed equally on all faces

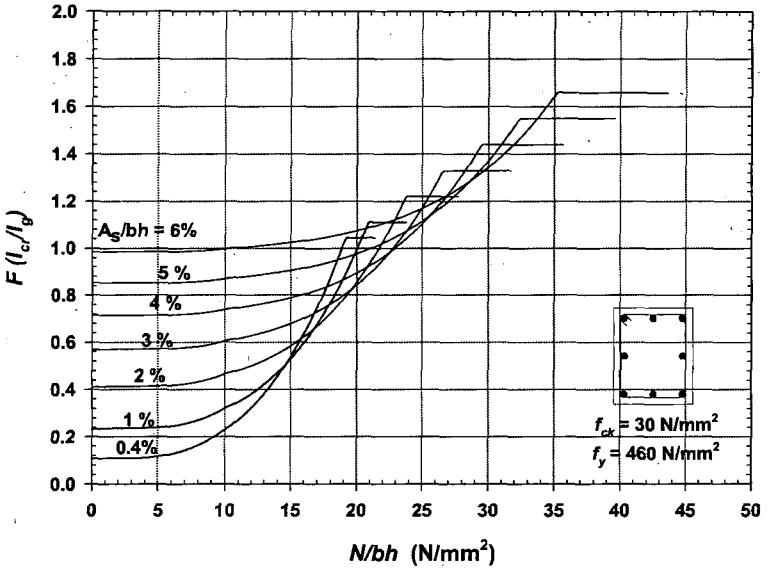

Fig. A3. 24 Cracked moment of inertia for C30 concrete column with reinforcement, distributed equally on all faces

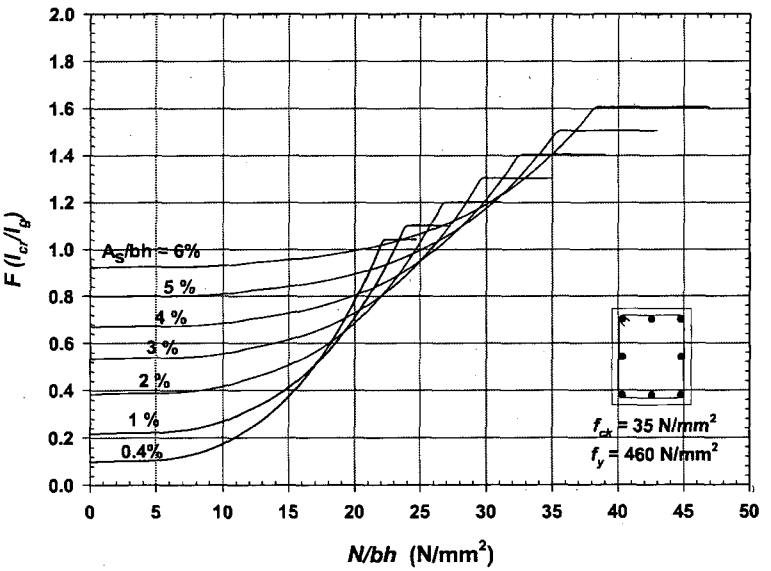

Fig. A3. 25 Cracked moment of inertia for C35 concrete column with reinforcement, distributed equally on all faces

A. 3.4. CALCULATION OF BLAST PRESSURE ON COLUMNS OF MURRAH BUILDING

Breadth, b = 914.4 mm or 36 in.

Depth, D = 508 mm or 20 in

Stand off Distance, SD = 15.24 m or 50 ft

Charge Weight, W = 1800 kg or 4000 lbs.

Scaled Stand off Distance, $SSD = SD/W^{1/3}$

SSD = 1.25 m/kg$^{1/3}$ or 3.15 ft/lbs$^{1/3}$

Blast wave parameters such as reflected pressure (P_r), static over pressure (P_s), blast wave front velocity (U), static impulse (I_s), reflected impulse (I_r) and time of arrival (t_a) of blast wave are obtained for a particular charge and scaled distance from Fig. A3.26.

Blast Wave Parameters at Point, A:

Static over pressure, P_{OA} = 120 psi or 830 kN/m^2

Reflected pressure, P_{rA} = 630 psi or 4350 kN/m^2

Blast wave front velocity, U_A = 3.15 ft/mSec or 0.96 m/mSec

$I_s/W^{1/3}$ = 23 psi-mSec/lbs$^{1/3}$

$I_r/W^{1/3}$ = 73 psi-mSec/lbs$^{1/3}$

$t_a/W^{1/3}$ = 0.56 mSec/lbs$^{1/3}$

Incident impulse, I_{sA} = 365 psi-mSec or 2530 kPa-mSec

Reflected impulse, I_{rA} = 1165 psi-mSec or 8030 kPa-mSec

Time of arrival for blast wave , t_{aA} = 8.9 mSec

Duration of blast pressure from incident impulse, t_{dA} = $2I_{sA}/P_{sA}$ = 26.85 mSec

Dynamic Pressure, $q_A = (p_{rA} - 2p_{sA})/2.4$ = 1120 kPa

Blast Wave Parameters at Point, B:

Static over pressure, P_{OB}= 112.4 psi or 775 kN/m^2

Blast wave front velocity, U_B= 3.05 ft/mSec or 0.93 m/mSec

$I_s/W^{\lambda/3}$ = 22.7 psi-mSec/lbs$^{1/3}$

Incident impulse, I_{sB}= 360 psi-mSec or 2470 kPa-mSec

Duration of blast pressure from incident impulse, t_{dB}= $2I_{sB}/P_{sB}$ = 6.4 mSec

Blast Loading:

Clearing time for reflected pressure on front face of column, t_c= $3S/U_A$ = 0.94 mSec

Stagnation pressure on front face at clearing, P_{sc}= $\frac{(P_{oA}+q_A)}{t_{dA}}(t_{dA}-t_c)$ = 1650 kPa

Time for blast wave to reach point, B from front face, t_l= D/U_A = 0.53 mSec

Rising time for pressure on rear face of column, t_r= $4S/U_B$ = 1.29 mSec

Stagnation pressure on rear face after rising (t_r), P_{sr}= $\frac{P_{oB}}{t_{dB}}(t_{dB}-t_r)$ = 620 kPa

Impulse on front face, I_1= $\frac{1}{2}(P_{rA}-P_{sc})t_c+P_{sc}t_c+\frac{1}{2}P_{sc}(t_{dA}-t_c)$

= 7058.25 kPa-mSec

Impulse on rear face, I_2= $\frac{1}{2}P_{sr}t_{dB}$ = 1967.76 kPa-mSec

Net Impulse, I= 5090.5 kPa-mSec

Duration of blast load, t_d= $2I/P_{rA}$ =2.34 mSec

Finally, the profile of the blast load on column, G16 is shown in Fig. A3.27.

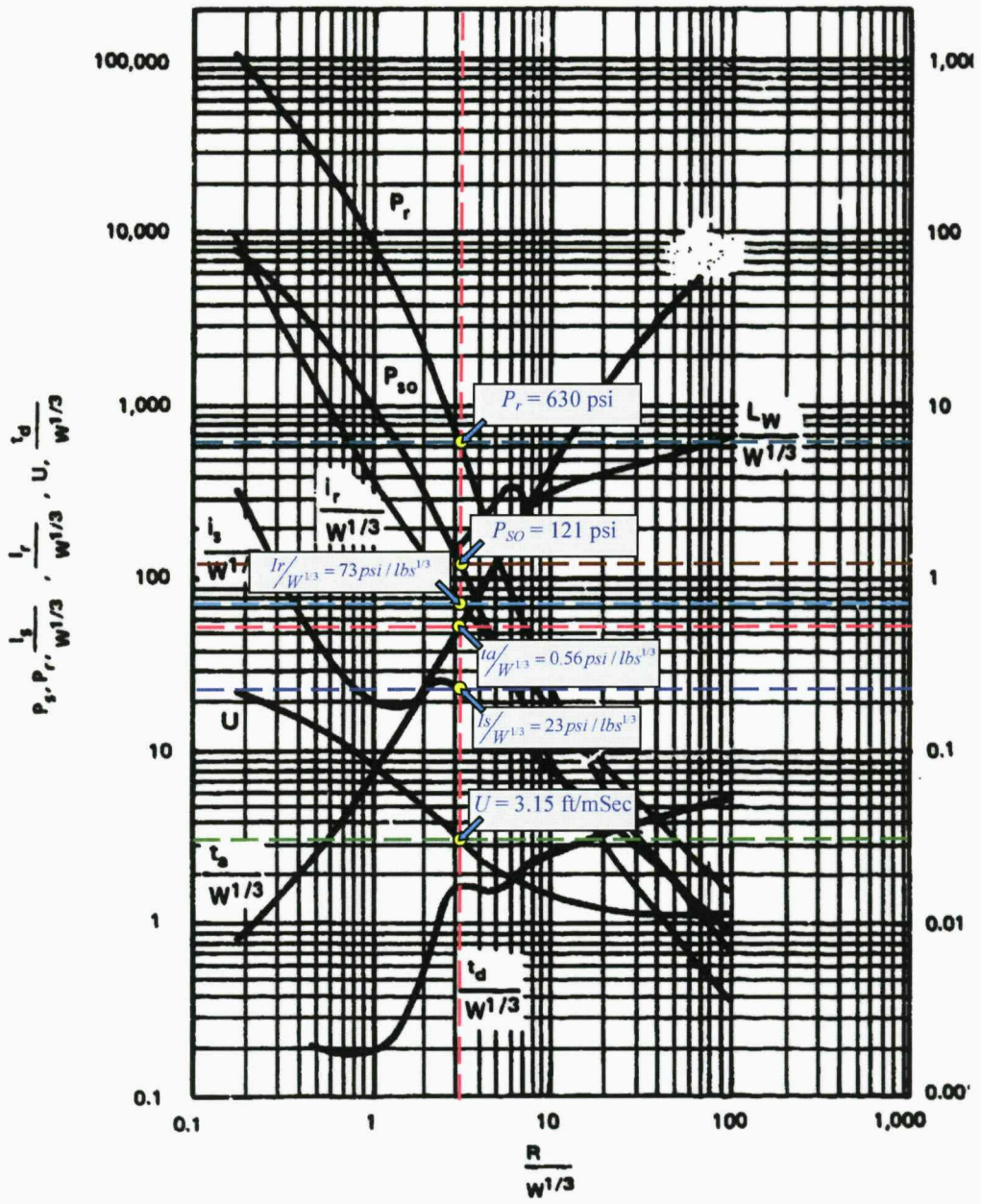

Fig. A3. 26 Blast wave parameters for surface blast

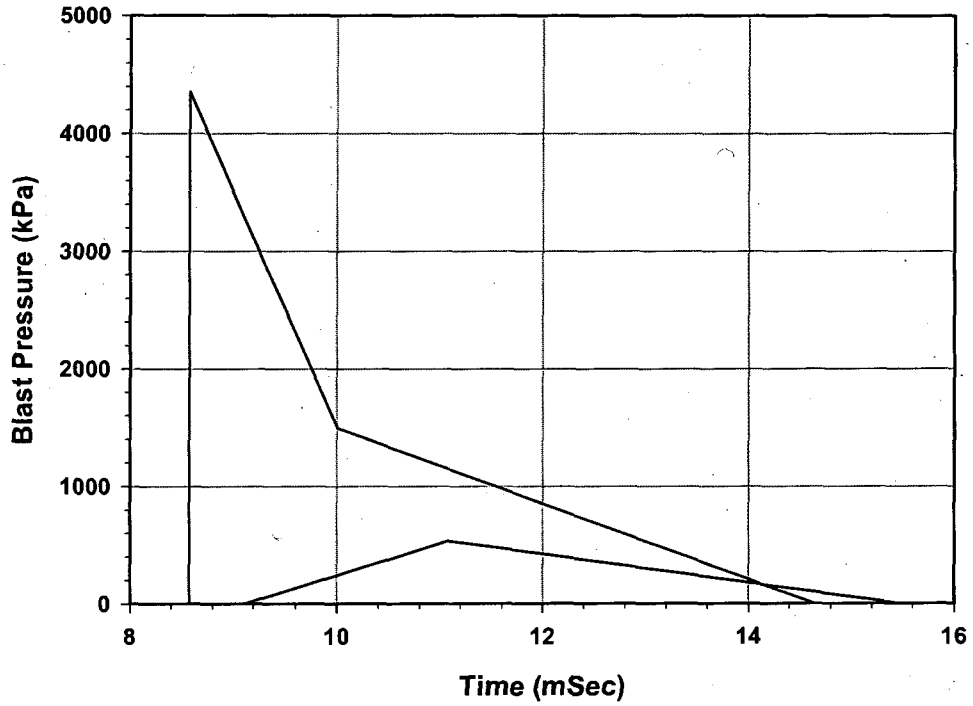

Fig. A3. 27 Blast Loadings on Columns, G16

A. 4 PROTECTIVE DESIGN FOR RC FRAMED STRUCTURES: THE SAFE STAND OFF DISTANCE APPROACH

A. 4.1. MATHEMATICAL MODELS FOR DYNAMIC SHEAR FORCE AND BENDING MOMENT

Safe stand off distance based on shear failure:

For linear dynamic analysis, the natural time period for the column, fixed at both ends is calculated using the following equation:

$$T_n = \frac{8L^2}{9\pi}\sqrt{\frac{m}{EI_{eff}}} \qquad \text{(A4.1)}$$

Where,

$$m = \frac{\gamma}{9.81}BD \qquad \text{(A4.2)}$$

$$I_{eff} = F_i I_g$$

$$I_g = \frac{bD^3}{12} \qquad \text{(A4.3)}$$

$$E \approx 4490\sqrt{f_{ck}} \qquad \text{(A4.4)}$$

γ - Unit weight of concrete (kN/m^3)

B - Breadth of column (m)

D - Depth of column (m)

m - Mass of column per metre (kg)

f_{ck} - Characteristic compressive strength of concrete (N/mm^2)

E - Modulus of elasticity of concrete (N/mm^2)

I_{eff} - Effective moment of inertia (mm^3)

I_g - Gross moment of inertia (mm^3)

F_i - Ratio of I_{eff} to I_g

By substituting Eq. A4.2, A4.3 and A4.4 into Eq. A4.1, the system's natural time period is simplified into Eq. A4.5.

$$T_n = 48\left(L^2/D\right)\sqrt{\frac{1}{EF_i}} \qquad \text{(A4.5)}$$

The ratio of the duration of the blast load to the natural time period is calculated using Eqs. 6.2, 6.4 and A4.5 and shown in Eq. A4.6 and A4.7.

$$\frac{T_d}{T_n}=\frac{\sqrt{EF_i}}{55}\left(\left(\frac{1}{U}\right)\left(\frac{B}{L}\right)\left(\frac{D}{L}\right)\left(1+\frac{2P_{oA}}{P_{rA}}\right)+0.475\left(\frac{D}{L}\right)\left(\frac{1}{L}\right)t_{dA}\left(1-\frac{2P_{oA}}{P_{rA}}\right)\right)$$

- for clearing (A4.6)

$$\frac{T_d}{T_n}=\frac{t_r}{\left(48\left(L^2/D\right)\sqrt{\frac{1}{EF_i}}\right)}$$

- for non clearing (A4.7)

The dynamic shear force is the function of T_d, T_n, W and SD. It is mathematically represented as follows,

$$V=f_1\left[W, B/L, D/L, L, F_c, f_{ck}, SD\right] \quad \text{(Clearing)} \quad \text{(A4.8)}$$

$$V=f_1\left[W, D/L, L, F_c, f_{ck}, SD\right] \quad \text{(Non clearing)} \quad \text{(A4.9)}$$

Safe stand off distance based on flexural failure:

The mathematical formulation for the estimation of safe stand off distance considering the flexural failure of column is same as that of shear failure and explained below.

For nonlinear dynamic analysis, the natural time period for the column, fixed at both ends is calculated using the following equation:

$$T_n=2\pi\sqrt{\frac{0.5(mL)}{0.64\left(\frac{307EI_{eff}}{L^3}\right)}} \quad \text{(A4.10)}$$

By substituting Eq. A4.2, A4.3 and A4.4 into Eq. A4.10, the system's natural time period is simplified into Eq. A4.11.

$$T_n=54\left(L^2/D\right)\sqrt{\frac{1}{EF_i}} \quad \text{(A4.11)}$$

The ratio of the duration of the blast load to the natural time period is calculated using Eqs. 6.2, 6.4 and A4.11 and shown in Eq. A4.12 and A4.13.

$$\frac{T_d}{T_n}=\frac{\sqrt{EF_i}}{63}\left(\left(\frac{1}{U}\right)\left(\frac{B}{L}\right)\left(\frac{D}{L}\right)\left(1+\frac{2P_{oA}}{P_{rA}}\right)+0.475\left(\frac{D}{L}\right)\left(\frac{1}{L}\right)t_{dA}\left(1-\frac{2P_{oA}}{P_{rA}}\right)\right)$$

- for clearing (A4.12)

$$\frac{T_d}{T_n} = \frac{t_r}{\left(54\left(L^2/D\right)\sqrt{\frac{1}{EF_i}}\right)}$$ - for non clearing (A4.13)

The dynamic bending moment is the function of T_d, T_n, W and SD. It is mathematically represented as follows,

$$M = g_1\left[W, B/L, D/L, L, F_c, f_{ck}, SD\right]$$ for clearing (A4.14)

$$M = g_1\left[W, D/L, L, F_c, f_{ck}, SD\right]$$ for non clearing (A4.15)

A. 4.2. LINEAR AND NONLINEAR REGRESSION MODELS

Regression analysis is a statistical technique for investigating and modelling the relationship between one or more independent variables and a continuous dependent variable. When the response (dependent) variable is related to the predictors (independent variables) through a nonlinear function, it leads to nonlinear regression model. In common practise, the residual sum of squares is minimized by an iterative procedure, when the method of least squares is applied (Montgomery et al., 2003). The linear regression model includes not only the first order relationships (Eq. A4.16), but also polynomial and other complex relationships (Eq. A4.17).

$$y = \beta_0 + \beta_1 x_1 + \beta_2 x_2 + \beta_3 x_3 + \ldots\ldots + \beta_n x_n + \varepsilon \qquad \text{(A4.16)}$$

$$y = \beta_0 + \beta_1 z_1 + \beta_2 z_2 + \beta_3 z_3 + \ldots\ldots + \beta_n z_n + \varepsilon \qquad \text{(A4.17)}$$

Where x_i - Independent variables

y - Independent variables

z_i - Any function of the original regressor $x_1, x_2, x_3 \ldots\ldots x_k$ including transformations such as e^{x_i}, $\sqrt{x_i}$, and $\sin(x_i)$.

ε - Error

β_i - Unknown parameters

The linear regression model can be written in general form as

$$\begin{aligned} y &= f(\beta, x) + \varepsilon \\ &= [x^T][\beta] + \varepsilon \end{aligned} \qquad \text{(A4.18)}$$

where

$$[\beta] = \begin{bmatrix} \beta_1 \\ \beta_2 \\ \beta_3 \\ . \\ . \\ . \\ \beta_k \end{bmatrix}; [x] = \begin{bmatrix} x_1 \\ x_2 \\ x_3 \\ . \\ . \\ . \\ x_k \end{bmatrix}; \text{and } [x^T] = [x_1 \quad x_2 \quad . \quad . \quad x_k]$$

In nonlinear problems, when the iterative method is used, the estimation of parameters may or may not work satisfactorily, depending on the form of the equation. Therefore, the parameter estimates are obtained by using several routine computer programmes. Some of the methods implemented are (Draper and Smith, 1966):

i) Linearization (or Taylor Series)
ii) Sequential Quadratic Programming
iii) Steepest Descent and
iv) Levenberg – Merquardt Compromise

The Statistical Package for Social Science (SPSS) provides two algorithms for analysis: i) Levenberg – Merquardt algorithm (ii) sequential quadratic programming algorithm. The Levenberg – Merquardt algorithm analyses unconstrained models where as sequential quadratic programming algorithm does not, instead they demand to specify the constraints on parametric estimates and they requires the user to specify the loss function.

Levenberg – Merquardt algorithm represents a compromise between the linearization (or Taylor series) and steepest descent methods. It also combines the best features of these methods to avoid serious limitations. It always converges but does not slow down as in two methods. The early iteration works well on linear descent method but when it goes close to the best fit value it works slowly. On the other hand, the Gauss-Newton method works badly in early iteration but for later iteration it works well. Therefore these two methods are combined as Levenberg – Merquardt method. The early iteration uses the linear descent method and then switches to Gauss-Newton approach.

Test for Hypotheses:

An overall summary of the results of any regression analysis can be provided by a table called an analysis of variance (ANOVA) table. ANOVA tables contain the sum of squares which is obtained from the source of regression, residual, total uncorrected and total corrected. In addition to this, they contain the mean squares of the above source. The corrected regression sum of squares ($SSR_{corrected}$) is the sum of the squares of deviations of the fitted regression line ($\hat{Y}$) from the mean ($\bar{Y}$). The

uncorrected regression sum of squares ($SSR_{uncorrected}$) is the sum of the squares of the fitted regression line ($\hat{Y}$). The residual sum of squares is the sum of the squares of deviations of the observed Y's from the fitted regression line ($\hat{Y}$). The total sum of squares is the sum of the sum of squares of regression and the sum of squares of residuals. The sum of squares are calculated using the following equations:

Regression sum of squares (corrected), $SSR_{corrected} = \sum_{1}^{n}\left(\hat{Y}_i - \bar{Y}\right)^2$ (A4.19)

Regression sum of squares (uncorrected), $SSR_{uncorrected} = \sum_{1}^{n}\hat{Y}_i^2$ (A4.20)

Residual sum of squares, $SSE = \sum_{1}^{n}\left(Y_i - \hat{Y}_i\right)^2$ (A4.21)

Total sum of squares (uncorrected), $SSY_{uncorrected} = \sum_{1}^{n}Y_i^2$ (A4.22)

Total sum of squares (corrected), $SSY_{corrected} = \sum_{1}^{n}\left(Y_i - \bar{Y}\right)^2$ (A4.23)

The F static is obtained by dividing the regression mean square by the residual mean square.

$$F_{static} = \frac{\text{Regression Mean Square}}{\text{Residual Mean Square}} \quad \text{(A4.24)}$$

The coefficient of determination (R^2) provides a quantitative measure of how well the fitted model predicts the dependent variable and is calculated using the following equation:

$$R^2 = 1 - \frac{SSE}{SSY_{corrected}} \quad \text{(A4.25)}$$

In regression analysis, the model needs to be tested for adequacy and certain tests of hypotheses such as F-test, partial F-test, t-test and coefficient of determination (R^2), are available. The linear model is tested using F-test and R^2. For a nonlinear model, the tests used for linear models are not appropriate. In this situation, the residual

mean square is not an unbiased estimate of the error variance, even if the model is correct. For practical purposes, the residual variance is still compared with an estimate of the total variance, but the usual F statistic cannot be used for testing hypotheses. R squared may be interpreted as the proportion of the total variation of the dependent variable around its mean that is explained by the fitted model (Norusis, 2005). The values of R squared that are close to 1 imply that most of the variability in y is explained by the regression model (Montgomery, 2003).

A. 4.3. REGRESSION MODELS FOR SSD

Table A4. 1 Nonlinear empirical equations governs safe stand off distance based on shear failure of column and clearing

Empirical Equations	R-squared value
$SSD = AW^{B} f_{ck}^{C} \left(B/L\right)^{D} \left(D/L\right)^{E} L^{F} K_s^{G} \left(I_t/I_g\right)^{H}$	0.999
$SSD = AW^{B} \left(f_{ck}\right)^{C} \left(D\left(B/L\right) + E\left(B/L\right) + F\left(B/L\right)^{2} + G\left(B/L\right)^{3} \right) \left(D/L\right)^{H} L^{I} K_s^{J} \left(I_t/I_g\right)^{K}$	0.998
$SSD = AW^{B} \left(f_{ck}\right)^{C} \left(B/L\right)^{D} \left(E + \frac{F}{\left(D/L\right)} \right) L^{G} K_s^{H} \left(I_t/I_g\right)^{I}$	0.997
$SSD = AW^{B} \left(f_{ck}\right)^{C} \left(B/L\right)^{D} \left(E + \frac{F}{\left(D/L\right)} \right) \left(G + HL + IL^{2} + JL^{3}\right) K_s^{M} \left(I_t/I_g\right)^{N}$	0.997

Table A4. 2 Nonlinear empirical equations governs safe stand off distance based on flexural failure of column and clearing

Empirical Equations	R-squared value
$SSD = AW^{B} f_{ck}^{C}\left(\frac{B}{L}\right)^{D}\left(\frac{D}{L}\right)^{E} L^{F} K_m^{G}\left(I_{eff}/I_g\right)^{H}$	0.983
$SSD = AW^{B} f_{ck}^{C}\left(\frac{B}{L}\right)^{\left(D+EK_m+FK_m^2\right)}\left(\frac{D}{L}\right)^{G} L^{H} K_m^{I}\left(I_{eff}/I_g\right)^{J}$	0.986
$SSD = AW^{B} f_{ck}^{C}\left(\frac{B}{L}\right)^{\left(D+EK_m+FK_m^2\right)}\left(\frac{D}{L}\right)^{\left(G+HK_m+IK_m^2\right)} L^{J} K_m^{K}\left(I_{eff}/I_g\right)^{L}$	0.990
$SSD = AW^{B} f_{ck}^{C}\left(\frac{B}{L}\right)^{\left(D+EK_m+FK_m^2\right)}\left(\frac{D}{L}\right)^{\left(G+HK_m+IK_m^2\right)}\left(1+\frac{J}{L}\right) K_m^{K}\left(I_{eff}/I_g\right)^{L}$	0.990
$SSD = AW^{B} f_{ck}^{C}\left(\frac{B}{L}\right)^{\left(D+EK_m+FK_m^2\right)}\left(\frac{D}{L}\right)^{\left(G+HK_m+IK_m^2\right)} L^{\left(J+KK_m+MK_m^2\right)} K_m^{N}\left(1+O\left(\frac{B}{L}\right)+P\left(\frac{D}{L}\right)+QL+RK_m\right)\left(I_{eff}/I_g\right)^{S}$	0.994
$SSD = AW^{B} f_{ck}^{C}\left(\frac{B}{L}\right)^{\left(D+EK_m+FK_m^2\right)}\left(\frac{D}{L}\right)^{\left(G+HK_m+IK_m^2\right)} L^{\left(J+KK_m+MK_m^2\right)} K_m^{N}\left(1+O\left(\frac{B}{L}\right)+P\left(\frac{D}{L}\right)+QK_m\right)\left(I_{eff}/I_g\right)^{R}$	0.994
$SSD = AW^{B} f_{ck}^{C}\left(\frac{B}{L}\right)^{D}\left(\frac{D}{L}\right)^{\left(E+FK_m+GK_m^2\right)} L^{H} K_m^{I}\left(I_t/I_g\right)^{J}\left(\begin{array}{l}1+K\ln\left(f_{ck}\right)+L\ln\left(\frac{B}{L}\right)+M\ln\left(\frac{D}{L}\right)\\ +N\ln\left(L\right)+O\ln\left(K_m\right)+P\ln\left(I_{eff}/I_g\right)\end{array}\right)$	0.995
$\mathrm{SSD} = AW^{B} f_{ck}^{C}\left(\frac{B}{L}\right)^{D}\left(\frac{D}{L}\right)^{C} K_m^{D}\left(\begin{array}{l}1+E\ln\left(f_{ck}\right)+F\ln\left(\frac{B}{L}\right)+G\ln\left(\frac{D}{L}\right)+\\ H\ln\left(L\right)+I\ln\left(K_m\right)+J\ln\left(\frac{I_{eff}}{I_g}\right)\end{array}\right)$	0.996

A. 4.4. SAFE SCALED DISTANCE FOR THE PRACTICAL COLUMNS

Table A4. 3 Safe scaled distance for the practical columns

Column ID	Column Dimensions			Main rebar details			Spacing of lateral ties	Shear strength, V_u	Flexural strength, M_u	SSD distance based on shear	SSD distance based on flexure	SSD	Safe Scaled Distance
	Breadth, b	Depth, D	Length, L	Dia of rebars	No of rebars	Rebars arrangment							
	(mm)	(mm)	(m)	(m)	(m)		(mm)	(kN)	(kN)	(m)	(m)	(m)	(m/kg$^{1/3}$)
1	300	300	3	20	4	R1	150	377	114	19.97	15.85	19.97	2.00
2	300	300	3	20	4	R1	200	330	114	21.02	15.85	21.02	2.10
3	300	300	3	20	4	R1	250	302	114	21.76	15.85	21.76	2.18
4	300	300	3	25	4	R1	150	389	152	19.90	14.03	19.90	1.99
5	300	300	3	25	4	R1	200	342	152	20.91	14.03	20.91	2.09
6	300	300	3	25	4	R1	250	314	152	21.61	14.03	21.61	2.16
7	300	300	3	20	4	R1	150	494	145	18.00	14.08	18.00	1.80
8	300	300	3	20	4	R1	200	447	145	18.71	14.08	18.71	1.87
9	300	300	3	20	4	R1	250	419	145	19.18	14.08	19.18	1.92
10	300	300	3	25	4	R1	150	506	184	17.98	12.67	17.98	1.80
11	300	300	3	25	4	R1	200	459	184	18.67	12.67	18.67	1.87
12	300	300	3	25	4	R1	250	431	184	19.13	12.67	19.13	1.91
13	300	300	3	20	4	R1	150	610	158	16.59	13.54	16.59	1.66
14	300	300	3	20	4	R1	200	564	158	17.10	13.54	17.10	1.71
15	300	300	3	20	4	R1	250	536	158	17.45	13.54	17.45	1.74
16	300	300	3	25	4	R1	150	622	198	16.60	12.23	16.60	1.66
17	300	300	3	25	4	R1	200	575	198	17.10	12.23	17.10	1.71
18	300	300	3	25	4	R1	250	547	198	17.44	12.23	17.44	1.74
19	300	300	4	20	4	R1	150	348	114	20.75	16.97	20.75	2.08
20	300	300	4	20	4	R1	200	301	114	21.94	16.97	21.94	2.19
21	300	300	4	20	4	R1	250	273	114	22.79	16.97	22.79	2.28
22	300	300	4	25	4	R1	150	360	152	20.65	15.01	20.65	2.07
23	300	300	4	25	4	R1	200	313	152	21.79	15.01	21.79	2.18
24	300	300	4	25	4	R1	250	285	152	22.60	15.01	22.60	2.26
25	300	300	4	20	4	R1	150	435	145	19.03	15.06	19.03	1.90
26	300	300	4	20	4	R1	200	389	145	19.89	15.06	19.89	1.99
27	300	300	4	20	4	R1	250	361	145	20.47	15.06	20.47	2.05
28	300	300	4	25	4	R1	150	447	184	18.99	13.54	18.99	1.90
29	300	300	4	25	4	R1	200	400	184	19.82	13.54	19.82	1.98
30	300	300	4	25	4	R1	250	372	184	20.38	13.54	20.38	2.04
31	300	300	4	20	4	R1	150	523	158	17.73	14.48	17.73	1.77
32	300	300	4	20	4	R1	200	476	158	18.39	14.48	18.39	1.84
33	300	300	4	20	4	R1	250	448	158	18.82	14.48	18.82	1.88
34	300	300	4	25	4	R1	150	535	198	17.72	13.07	17.72	1.77
35	300	300	4	25	4	R1	200	488	198	18.36	13.07	18.36	1.84
36	300	300	4	25	4	R1	250	460	198	18.79	13.07	18.79	1.88
37	300	450	3	25	4	R1	150	644	263	17.48	12.05	17.48	1.75
38	300	450	3	25	4	R1	200	574	263	18.27	12.05	18.27	1.83
39	300	450	3	25	4	R1	250	532	263	18.82	12.05	18.82	1.88
40	300	450	3	32	4	R1	150	662	365	17.45	10.20	17.45	1.75
41	300	450	3	32	4	R1	200	592	365	18.22	10.20	18.22	1.82
42	300	450	3	32	4	R1	250	550	365	18.75	10.20	18.75	1.88
43	300	450	3	25	4	R1	150	907	333	15.32	10.48	15.32	1.53
44	300	450	3	25	4	R1	200	836	333	15.80	10.48	15.80	1.58
45	300	450	3	25	4	R1	250	794	333	16.12	10.48	16.12	1.61
46	300	450	3	32	4	R1	150	925	436	15.34	9.03	15.34	1.53
47	300	450	3	32	4	R1	200	855	436	15.82	9.03	15.82	1.58
48	300	450	3	32	4	R1	250	812	436	16.13	9.03	16.13	1.61
49	300	450	3	25	4	R1	150	1040	363	14.53	10.00	14.53	1.45
50	300	450	3	25	4	R1	200	970	363	14.92	10.00	14.92	1.49
51	300	450	3	25	4	R1	250	928	363	15.18	10.00	15.18	1.52
52	300	450	3	32	4	R1	150	1040	467	14.66	8.65	14.66	1.47
53	300	450	3	32	4	R1	200	970	467	15.06	8.65	15.06	1.51
54	300	450	3	32	4	R1	250	928	467	15.32	8.65	15.32	1.53
55	300	450	4	25	4	R1	150	579	263	18.35	12.89	18.35	1.83
56	300	450	4	25	4	R1	200	508	263	19.29	12.89	19.29	1.93
57	300	450	4	25	4	R1	250	466	263	19.94	12.89	19.94	1.99
58	300	450	4	32	4	R1	150	597	365	18.30	10.89	18.30	1.83
59	300	450	4	32	4	R1	200	526	365	19.21	10.89	19.21	1.92
60	300	450	4	32	4	R1	250	484	365	19.84	10.89	19.84	1.98

Note: R1 indicates the arrangement of reinforcement, placed on two opposite faces and R2 indicates the arrangement of reinforcement, distributed equally on all faces

Table A4. 3 Safe scaled distance for the practical columns (cont...)

Column ID	Column Dimensions			Main rebar details			Spacing of lateral ties	Shear strength, V_u	Flexural strength, M_u	SSD distance based on shear	SSD distance based on flexure	SSD	Safe Scaled Distance
	Breadth, b	Depth, D	Length, L	Dia of rebars	No of rebars	Rebars arrangment							
	(mm)	(mm)	(m)	(m)	(m)		(mm)	(kN)	(kN)	(m)	(m)	(m)	(m/kg$^{1/3}$)
61	300	450	4	25	4	R1	150	775	333	16.39	11.19	16.39	1.64
62	300	450	4	25	4	R1	200	705	333	17.00	11.19	17.00	1.70
63	300	450	4	25	4	R1	250	663	333	17.41	11.19	17.41	1.74
64	300	450	4	32	4	R1	150	794	436	16.39	9.62	16.39	1.64
65	300	450	4	32	4	R1	200	723	436	16.99	9.62	16.99	1.70
66	300	450	4	32	4	R1	250	681	436	17.39	9.62	17.39	1.74
67	300	450	4	25	4	R1	150	972	363	15.02	10.67	15.02	1.50
68	300	450	4	25	4	R1	200	902	363	15.46	10.67	15.46	1.55
69	300	450	4	25	4	R1	250	860	363	15.75	10.67	15.75	1.57
70	300	450	4	32	4	R1	150	990	467	15.05	9.21	15.05	1.51
71	300	450	4	32	4	R1	200	920	467	15.48	9.21	15.48	1.55
72	300	450	4	32	4	R1	250	878	467	15.77	9.21	15.77	1.58
73	300	600	3	32	4	R1	150	985	532	15.67	9.08	15.67	1.57
74	300	600	3	32	4	R1	200	892	532	16.29	9.08	16.29	1.63
75	300	600	3	32	4	R1	250	835	532	16.70	9.08	16.70	1.67
76	300	600	3	25	8	R2	150	1168	589	14.65	8.44	14.65	1.47
77	300	600	3	25	8	R2	200	1028	589	15.39	8.44	15.39	1.54
78	300	600	3	25	8	R2	250	944	589	15.91	8.44	15.91	1.59
79	300	600	3	32	4	R1	150	1387	658	13.73	7.77	13.73	1.37
80	300	600	3	32	4	R1	200	1293	658	14.11	7.77	14.11	1.41
81	300	600	3	32	4	R1	250	1237	658	14.35	7.77	14.35	1.44
82	300	600	3	25	8	R2	150	1574	650	13.06	7.84	13.06	1.31
83	300	600	3	25	8	R2	200	1434	650	13.54	7.84	13.54	1.35
84	300	600	3	25	8	R2	250	1350	650	13.86	7.84	13.86	1.39
85	300	600	3	32	4	R1	150	1387	712	13.73	7.36	13.73	1.37
86	300	600	3	32	4	R1	200	1293	712	14.11	7.36	14.11	1.41
87	300	600	3	32	4	R1	250	1237	712	14.35	7.36	14.35	1.44
88	300	600	3	25	8	R2	150	1574	682	13.06	7.61	13.06	1.31
89	300	600	3	25	8	R2	200	1434	682	13.54	7.61	13.54	1.35
90	300	600	3	25	8	R2	250	1350	682	13.86	7.61	13.86	1.39
91	300	600	4	32	4	R1	150	869	532	16.57	9.68	16.57	1.66
92	300	600	4	32	4	R1	200	775	532	17.32	9.68	17.32	1.73
93	300	600	4	32	4	R1	250	719	532	17.83	9.68	17.83	1.78
94	300	600	4	25	8	R2	150	1052	589	15.37	9.00	15.37	1.54
95	300	600	4	25	8	R2	200	911	589	16.24	9.00	16.24	1.62
96	300	600	4	25	8	R2	250	827	589	16.86	9.00	16.86	1.69
97	300	600	4	32	4	R1	150	1219	658	14.54	8.27	14.54	1.45
98	300	600	4	32	4	R1	200	1125	658	15.00	8.27	15.00	1.50
99	300	600	4	32	4	R1	250	1069	658	15.30	8.27	15.30	1.53
100	300	600	4	25	8	R2	150	1402	650	13.76	8.35	13.76	1.38
101	300	600	4	25	8	R2	200	1261	650	14.33	8.35	14.33	1.43
102	300	600	4	25	8	R2	250	1177	650	14.72	8.35	14.72	1.47
103	300	600	4	32	4	R1	150	1387	712	13.83	7.83	13.83	1.38
104	300	600	4	32	4	R1	200	1293	712	14.21	7.83	14.21	1.42
105	300	600	4	32	4	R1	250	1237	712	14.46	7.83	14.46	1.45
106	300	600	4	25	8	R2	150	1574	682	13.15	8.10	13.15	1.32
107	300	600	4	25	8	R2	200	1434	682	13.64	8.10	13.64	1.36
108	300	600	4	25	8	R2	250	1350	682	13.96	8.10	13.96	1.40
109	450	300	3	25	4	R1	150	474	175	22.17	16.76	22.17	2.22
110	450	300	3	25	4	R1	200	427	175	23.08	16.76	23.08	2.31
111	450	300	3	25	4	R1	250	399	175	23.70	16.76	23.70	2.37
112	450	300	3	32	4	R1	150	494	243	22.03	14.75	22.03	2.20
113	450	300	3	32	4	R1	200	447	243	22.89	14.75	22.89	2.29
114	450	300	3	32	4	R1	250	419	243	23.47	14.75	23.47	2.35
115	450	300	3	25	4	R1	150	649	222	19.64	15.06	19.64	1.96
116	450	300	3	25	4	R1	200	602	222	20.22	15.06	20.22	2.02
117	450	300	3	25	4	R1	250	574	222	20.59	15.06	20.59	2.06
118	450	300	3	32	4	R1	150	668	291	19.59	13.48	19.59	1.96
119	450	300	3	32	4	R1	200	622	291	20.15	13.48	20.15	2.01
120	450	300	3	32	4	R1	250	594	291	20.51	13.48	20.51	2.05

Note: R1 indicates the arrangement of reinforcement, placed on two opposite faces and R2 indicates the arrangement of reinforcement, distributed equally on all faces

Table A4. 3 Safe scaled distance for the practical columns (cont...)

Column ID	Column Dimensions			Main rebar details			Spacing of lateral ties	Shear strength, V_u	Flexural strength, M_u	SSD distance based on shear	SSD distance based on flexure	SSD	Safe Scaled Distance
	Breadth, b	Depth, D	Length, L	Dia of rebars	No of rebars	Rebars arrangment							
	(mm)	(mm)	(m)	(m)	(m)		(mm)	(kN)	(kN)	(m)	(m)	(m)	(m/kg$^{1/3}$)
121	450	300	3	25	4	R1	150	824	242	17.91	14.53	17.91	1.79
122	450	300	3	25	4	R1	200	777	242	18.32	14.53	18.32	1.83
123	450	300	3	25	4	R1	250	749	242	18.58	14.53	18.58	1.86
124	450	300	3	32	4	R1	150	843	311	17.91	13.07	17.91	1.79
125	450	300	3	32	4	R1	200	797	311	18.31	13.07	18.31	1.83
126	450	300	3	32	4	R1	250	769	311	18.57	13.07	18.57	1.86
127	450	300	4	25	4	R1	150	430	175	23.19	17.96	23.19	2.32
128	450	300	4	25	4	R1	200	383	175	24.24	17.96	24.24	2.42
129	450	300	4	25	4	R1	250	355	175	24.96	17.96	24.96	2.50
130	450	300	4	32	4	R1	150	450	243	23.00	15.79	23.00	2.30
131	450	300	4	32	4	R1	200	403	243	23.99	15.79	23.99	2.40
132	450	300	4	32	4	R1	250	375	243	24.67	15.79	24.67	2.47
133	450	300	4	25	4	R1	150	561	222	20.92	16.12	20.92	2.09
134	450	300	4	25	4	R1	200	514	222	21.64	16.12	21.64	2.16
135	450	300	4	25	4	R1	250	486	222	22.11	16.12	22.11	2.21
136	450	300	4	32	4	R1	150	581	291	20.83	14.42	20.83	2.08
137	450	300	4	32	4	R1	200	534	291	21.52	14.42	21.52	2.15
138	450	300	4	32	4	R1	250	506	291	21.97	14.42	21.97	2.20
139	450	300	4	25	4	R1	150	692	242	19.29	15.56	19.29	1.93
140	450	300	4	25	4	R1	200	645	242	19.82	15.56	19.82	1.98
141	450	300	4	25	4	R1	250	617	242	20.16	15.56	20.16	2.02
142	450	300	4	32	4	R1	150	712	311	19.26	13.98	19.26	1.93
143	450	300	4	32	4	R1	200	665	311	19.77	13.98	19.77	1.98
144	450	300	4	32	4	R1	250	637	311	20.10	13.98	20.10	2.01
145	450	450	3	32	4	R1	150	830	416	19.22	12.78	19.22	1.92
146	450	450	3	32	4	R1	200	760	416	19.89	12.78	19.89	1.99
147	450	450	3	32	4	R1	250	718	416	20.33	12.78	20.33	2.03
148	450	450	3	32	4	R1	150	1224	522	16.55	11.31	16.55	1.65
149	450	450	3	32	4	R1	200	1154	522	16.93	11.31	16.93	1.69
150	450	450	3	32	4	R1	250	1112	522	17.18	11.31	17.18	1.72
151	450	450	3	32	4	R1	150	1420	567	15.63	10.85	15.63	1.56
152	450	450	3	32	4	R1	200	1350	567	15.94	10.85	15.94	1.59
153	450	450	3	32	4	R1	250	1308	567	16.13	10.85	16.13	1.61
154	450	450	4	32	4	R1	150	732	416	20.33	13.68	20.33	2.03
155	450	450	4	32	4	R1	200	662	416	21.13	13.68	21.13	2.11
156	450	450	4	32	4	R1	250	620	416	21.68	13.68	21.68	2.17
157	450	450	4	32	4	R1	150	1027	522	17.84	12.09	17.84	1.78
158	450	450	4	32	4	R1	200	957	522	18.33	12.09	18.33	1.83
159	450	450	4	32	4	R1	250	915	522	18.65	12.09	18.65	1.87
160	450	450	4	32	4	R1	150	1323	567	16.18	11.59	16.18	1.62
161	450	450	4	32	4	R1	200	1252	567	16.52	11.59	16.52	1.65
162	450	450	4	32	4	R1	250	1210	567	16.74	11.59	16.74	1.67
163	450	450	5	32	4	R1	150	673	416	21.12	14.41	21.12	2.11
164	450	450	5	32	4	R1	200	603	416	22.03	14.41	22.03	2.20
165	450	450	5	32	4	R1	250	561	416	22.66	14.41	22.66	2.27
166	450	450	5	32	4	R1	150	909	522	18.80	12.72	18.80	1.88
167	450	450	5	32	4	R1	200	839	522	19.39	12.72	19.39	1.94
168	450	450	5	32	4	R1	250	797	522	19.78	12.72	19.78	1.98
169	450	450	5	32	4	R1	150	1145	567	17.20	12.20	17.20	1.72
170	450	450	5	32	4	R1	200	1075	567	17.62	12.20	17.62	1.76
171	450	450	5	32	4	R1	250	1033	567	17.90	12.20	17.90	1.79
172	450	450	6	32	4	R1	150	634	416	21.71	15.04	21.71	2.17
173	450	450	6	32	4	R1	200	563	416	22.72	15.04	22.72	2.27
174	450	450	6	32	4	R1	250	521	416	23.41	15.04	23.41	2.34
175	450	450	6	32	4	R1	150	830	522	19.56	13.27	19.56	1.96
176	450	450	6	32	4	R1	200	760	522	20.24	13.27	20.24	2.02
177	450	450	6	32	4	R1	250	718	522	20.69	13.27	20.69	2.07
178	450	450	6	32	4	R1	150	1027	567	18.02	12.72	18.02	1.80
179	450	450	6	32	4	R1	200	957	567	18.52	12.72	18.52	1.85
180	450	450	6	32	4	R1	250	915	567	18.84	12.72	18.84	1.88

Note: R1 indicates the arrangement of reinforcement, placed on two opposite faces and R2 indicates the arrangement of reinforcement, distributed equally on all faces

Table A4. 3 Safe scaled distance for the practical columns (cont...)

Column ID	Column Dimensions			Main rebar details			Spacing of lateral ties	Shear strength, V_u	Flexural strength, M_u	SSD distance based on shear	SSD distance based on flexure	SSD	Safe Scaled Distance
	Breadth, b	Depth, D	Length, L	Dia of rebars	No of rebars	Rebars arrangment							
	(mm)	(mm)	(m)	(m)	(m)		(mm)	(kN)	(kN)	(m)	(m)	(m)	(m/kg$^{1/3}$)
181	450	600	3	32	4	R1	150	1263	623	17.14	11.40	17.14	1.71
182	450	600	3	32	4	R1	200	1170	623	17.66	11.40	17.66	1.77
183	450	600	3	32	4	R1	250	1113	623	18.00	11.40	18.00	1.80
184	450	600	3	32	8	R2	150	1478	939	16.23	9.16	16.23	1.62
185	450	600	3	32	8	R2	200	1337	939	16.87	9.16	16.87	1.69
186	450	600	3	32	8	R2	250	1253	939	17.30	9.16	17.30	1.73
187	450	600	3	32	4	R1	150	1893	809	14.66	9.80	14.66	1.47
188	450	600	3	32	4	R1	200	1800	809	14.95	9.80	14.95	1.50
189	450	600	3	32	4	R1	250	1743	809	15.14	9.80	15.14	1.51
190	450	600	3	32	8	R2	150	2081	1022	14.23	8.66	14.23	1.42
191	450	600	3	32	8	R2	200	1940	1022	14.62	8.66	14.62	1.46
192	450	600	3	32	8	R2	250	1856	1022	14.87	8.66	14.87	1.49
193	450	600	3	32	4	R1	150	1893	890	14.66	9.32	14.66	1.47
194	450	600	3	32	4	R1	200	1800	890	14.95	9.32	14.95	1.50
195	450	600	3	32	4	R1	250	1743	890	15.14	9.32	15.14	1.51
196	450	600	3	32	8	R2	150	2081	1067	14.23	8.44	14.23	1.42
197	450	600	3	32	8	R2	200	1940	1067	14.62	8.44	14.62	1.46
198	450	600	3	32	8	R2	250	1856	1067	14.87	8.44	14.87	1.49
199	450	600	4	32	4	R1	150	1088	623	18.29	12.19	18.29	1.83
200	450	600	4	32	4	R1	200	995	623	18.93	12.19	18.93	1.89
201	450	600	4	32	4	R1	250	938	623	19.36	12.19	19.36	1.94
202	450	600	4	32	8	R2	150	1303	939	17.17	9.77	17.17	1.72
203	450	600	4	32	8	R2	200	1162	939	17.94	9.77	17.94	1.79
204	450	600	4	32	8	R2	250	1078	939	18.47	9.77	18.47	1.85
205	450	600	4	32	4	R1	150	1613	809	15.71	10.47	15.71	1.57
206	450	600	4	32	4	R1	200	1520	809	16.08	10.47	16.08	1.61
207	450	600	4	32	4	R1	250	1463	809	16.31	10.47	16.31	1.63
208	450	600	4	32	8	R2	150	1828	1022	15.06	9.23	15.06	1.51
209	450	600	4	32	8	R2	200	1687	1022	15.54	9.23	15.54	1.55
210	450	600	4	32	8	R2	250	1603	1022	15.85	9.23	15.85	1.58
211	450	600	4	32	4	R1	150	1893	890	14.77	9.95	14.77	1.48
212	450	600	4	32	4	R1	200	1800	890	15.06	9.95	15.06	1.51
213	450	600	4	32	4	R1	250	1743	890	15.25	9.95	15.25	1.52
214	450	600	4	32	8	R2	150	2081	1067	14.33	9.00	14.33	1.43
215	450	600	4	32	8	R2	200	1940	1067	14.72	9.00	14.72	1.47
216	450	600	4	32	8	R2	250	1856	1067	14.98	9.00	14.98	1.50
217	450	600	5	32	4	R1	150	983	623	19.12	12.84	19.12	1.91
218	450	600	5	32	4	R1	200	890	623	19.88	12.84	19.88	1.99
219	450	600	5	32	4	R1	250	834	623	20.38	12.84	20.38	2.04
220	450	600	5	32	8	R2	150	1198	939	17.83	10.28	17.83	1.78
221	450	600	5	32	8	R2	200	1057	939	18.71	10.28	18.71	1.87
222	450	600	5	32	8	R2	250	973	939	19.32	10.28	19.32	1.93
223	450	600	5	32	4	R1	150	1403	809	16.67	11.01	16.67	1.67
224	450	600	5	32	4	R1	200	1310	809	17.12	11.01	17.12	1.71
225	450	600	5	32	4	R1	250	1253	809	17.41	11.01	17.41	1.74
226	450	600	5	32	8	R2	150	1618	1022	15.88	9.70	15.88	1.59
227	450	600	5	32	8	R2	200	1477	1022	16.45	9.70	16.45	1.64
228	450	600	5	32	8	R2	250	1393	1022	16.82	9.70	16.82	1.68
229	450	600	5	32	4	R1	150	1823	890	15.07	10.46	15.07	1.51
230	450	600	5	32	4	R1	200	1730	890	15.38	10.46	15.38	1.54
231	450	600	5	32	4	R1	250	1673	890	15.58	10.46	15.58	1.56
232	450	600	5	32	8	R2	150	2038	1067	14.53	9.46	14.53	1.45
233	450	600	5	32	8	R2	200	1897	1067	14.93	9.46	14.93	1.49
234	450	600	5	32	8	R2	250	1813	1067	15.20	9.46	15.20	1.52
235	450	600	6	32	4	R1	150	913	623	19.77	13.40	19.77	1.98
236	450	600	6	32	4	R1	200	820	623	20.61	13.40	20.61	2.06
237	450	600	6	32	4	R1	250	764	623	21.18	13.40	21.18	2.12
238	450	600	6	32	8	R2	150	1128	939	18.33	10.71	18.33	1.83
239	450	600	6	32	8	R2	200	987	939	19.30	10.71	19.30	1.93
240	450	600	6	32	8	R2	250	903	939	19.98	10.71	19.98	2.00

Note: R1 indicates the arrangement of reinforcement, placed on two opposite faces and R2 indicates the arrangement of reinforcement, distributed equally on all faces

Table A4. 3 Safe scaled distance for the practical columns (cont...)

Column ID	Column Dimensions			Main rebar details			Spacing of lateral ties	Shear strength, V_u	Flexural strength, M_u	SSD distance based on shear	SSD distance based on flexure	SSD	Safe Scaled Distance
	Breadth, b	Depth, D	Length, L	Dia of rebars	No of rebars	Rebars arrangment							
	(mm)	(mm)	(m)	(m)	(m)		(mm)	(kN)	(kN)	(m)	(m)	(m)	(m/kg$^{1/3}$)
241	450	600	6	32	4	R1	150	1263	809	17.44	11.48	17.44	1.74
242	450	600	6	32	4	R1	200	1170	809	17.97	11.48	17.97	1.80
243	450	600	6	32	4	R1	250	1113	809	18.31	11.48	18.31	1.83
244	450	600	6	32	8	R2	150	1478	1022	16.52	10.10	16.52	1.65
245	450	600	6	32	8	R2	200	1337	1022	17.17	10.10	17.17	1.72
246	450	600	6	32	8	R2	250	1253	1022	17.60	10.10	17.60	1.76
247	450	600	6	32	4	R1	150	1613	890	15.87	10.90	15.87	1.59
248	450	600	6	32	4	R1	200	1520	890	16.24	10.90	16.24	1.62
249	450	600	6	32	4	R1	250	1463	890	16.48	10.90	16.48	1.65
250	450	600	6	32	8	R2	150	1828	1067	15.22	9.85	15.22	1.52
251	450	600	6	32	8	R2	200	1687	1067	15.69	9.85	15.69	1.57
252	450	600	6	32	8	R2	250	1603	1067	16.01	9.85	16.01	1.60
253	600	300	3	32	4	R1	150	580	266	23.58	16.68	23.58	2.36
254	600	300	3	32	4	R1	200	533	266	24.36	16.68	24.36	2.44
255	600	300	3	32	4	R1	250	505	266	24.88	16.68	24.88	2.49
256	600	300	3	25	8	R2	150	669	295	22.28	15.96	22.28	2.23
257	600	300	3	25	8	R2	200	598	295	23.26	15.96	23.26	2.33
258	600	300	3	25	8	R2	250	556	295	23.92	15.96	23.92	2.39
259	600	300	3	32	4	R1	150	813	329	20.70	15.19	20.70	2.07
260	600	300	3	32	4	R1	200	766	329	21.17	15.19	21.17	2.12
261	600	300	3	32	4	R1	250	738	329	21.48	15.19	21.48	2.15
262	600	300	3	25	8	R2	150	902	325	19.85	15.27	19.85	1.99
263	600	300	3	25	8	R2	200	832	325	20.48	15.27	20.48	2.05
264	600	300	3	25	8	R2	250	790	325	20.90	15.27	20.90	2.09
265	600	300	3	32	4	R1	150	1046	356	18.77	14.72	18.77	1.88
266	600	300	3	32	4	R1	200	999	356	19.11	14.72	19.11	1.91
267	600	300	3	32	4	R1	250	971	356	19.32	14.72	19.32	1.93
268	600	300	3	25	8	R2	150	1135	341	18.16	15.00	18.16	1.82
269	600	300	3	25	8	R2	200	1065	341	18.62	15.00	18.62	1.86
270	600	300	3	25	8	R2	250	1023	341	18.91	15.00	18.91	1.89
271	600	300	4	32	4	R1	150	521	266	24.74	17.88	24.74	2.47
272	600	300	4	32	4	R1	200	474	266	25.66	17.88	25.66	2.57
273	600	300	4	32	4	R1	250	446	266	26.27	17.88	26.27	2.63
274	600	300	4	25	8	R2	150	610	295	23.25	17.10	23.25	2.32
275	600	300	4	25	8	R2	200	540	295	24.37	17.10	24.37	2.44
276	600	300	4	25	8	R2	250	498	295	25.15	17.10	25.15	2.51
277	600	300	4	32	4	R1	150	696	329	22.13	16.26	22.13	2.21
278	600	300	4	32	4	R1	200	649	329	22.73	16.26	22.73	2.27
279	600	300	4	32	4	R1	250	621	329	23.12	16.26	23.12	2.31
280	600	300	4	25	8	R2	150	785	325	21.09	16.35	21.09	2.11
281	600	300	4	25	8	R2	200	715	325	21.87	16.35	21.87	2.19
282	600	300	4	25	8	R2	250	673	325	22.39	16.35	22.39	2.24
283	600	300	4	32	4	R1	150	871	356	20.29	15.76	20.29	2.03
284	600	300	4	32	4	R1	200	824	356	20.73	15.76	20.73	2.07
285	600	300	4	32	4	R1	250	796	356	21.01	15.76	21.01	2.10
286	600	300	4	25	8	R2	150	960	341	19.52	16.06	19.52	1.95
287	600	300	4	25	8	R2	200	890	341	20.10	16.06	20.10	2.01
288	600	300	4	25	8	R2	250	848	341	20.48	16.06	20.48	2.05
289	600	450	3	32	4	R1	150	995	468	20.46	14.45	20.46	2.05
290	600	450	3	32	4	R1	200	924	468	21.04	14.45	21.04	2.10
291	600	450	3	32	4	R1	250	882	468	21.43	14.45	21.43	2.14
292	600	450	3	32	8	R2	150	1162	704	19.38	12.07	19.38	1.94
293	600	450	3	32	8	R2	200	1057	704	20.11	12.07	20.11	2.01
294	600	450	3	32	8	R2	250	994	704	20.59	12.07	20.59	2.06
295	600	450	3	32	4	R1	150	1520	607	17.37	12.76	17.37	1.74
296	600	450	3	32	4	R1	200	1449	607	17.69	12.76	17.69	1.77
297	600	450	3	32	4	R1	250	1407	607	17.89	12.76	17.89	1.79
298	600	450	3	32	8	R2	150	1687	766	16.79	11.54	16.79	1.68
299	600	450	3	32	8	R2	200	1582	766	17.21	11.54	17.21	1.72
300	600	450	3	32	8	R2	250	1519	766	17.48	11.54	17.48	1.75

Note: R1 indicates the arrangement of reinforcement, placed on two opposite faces and R2 indicates the arrangement of reinforcement, distributed equally on all faces

Table A4. 3 Safe scaled distance for the practical columns (cont...)

Column ID	Column Dimensions			Main rebar details			Spacing of lateral ties	Shear strength, V_u	Flexural strength, M_u	SSD distance based on shear	SSD distance based on flexure	SSD	Safe Scaled Distance
	Breadth, b	Depth, D	Length, L	Dia of rebars	No of rebars	Rebars arrangment							
	(mm)	(mm)	(m)	(m)	(m)		(mm)	(kN)	(kN)	(m)	(m)	(m)	(m/kg$^{1/3}$)
301	600	450	3	32	4	R1	150	1800	667	16.27	12.25	16.27	1.63
302	600	450	3	32	4	R1	200	1729	667	16.52	12.25	16.52	1.65
303	600	450	3	32	4	R1	250	1687	667	16.68	12.25	16.68	1.67
304	600	450	3	32	8	R2	150	1940	801	15.91	11.32	15.91	1.59
305	600	450	3	32	8	R2	200	1835	801	16.25	11.32	16.25	1.63
306	600	450	3	32	8	R2	250	1772	801	16.47	11.32	16.47	1.65
307	600	450	4	32	4	R1	150	863	468	21.76	15.47	21.76	2.18
308	600	450	4	32	4	R1	200	793	468	22.49	15.47	22.49	2.25
309	600	450	4	32	4	R1	250	751	468	22.96	15.47	22.96	2.30
310	600	450	4	32	8	R2	150	1031	704	20.45	12.91	20.45	2.04
311	600	450	4	32	8	R2	200	926	704	21.32	12.91	21.32	2.13
312	600	450	4	32	8	R2	250	863	704	21.90	12.91	21.90	2.19
313	600	450	4	32	4	R1	150	1257	607	18.82	13.65	18.82	1.88
314	600	450	4	32	4	R1	200	1187	607	19.25	13.65	19.25	1.92
315	600	450	4	32	4	R1	250	1145	607	19.52	13.65	19.52	1.95
316	600	450	4	32	8	R2	150	1425	766	18.05	12.34	18.05	1.80
317	600	450	4	32	8	R2	200	1320	766	18.59	12.34	18.59	1.86
318	600	450	4	32	8	R2	250	1256	766	18.95	12.34	18.95	1.89
319	600	450	4	32	4	R1	150	1651	667	16.95	13.10	16.95	1.69
320	600	450	4	32	4	R1	200	1581	667	17.23	13.10	17.23	1.72
321	600	450	4	32	4	R1	250	1538	667	17.41	13.10	17.41	1.74
322	600	450	4	32	8	R2	150	1819	801	16.43	12.10	16.43	1.64
323	600	450	4	32	8	R2	200	1713	801	16.81	12.10	16.81	1.68
324	600	450	4	32	8	R2	250	1650	801	17.05	12.10	17.05	1.71
325	600	450	5	32	4	R1	150	785	468	22.71	16.32	22.71	2.27
326	600	450	5	32	4	R1	200	715	468	23.54	16.32	23.54	2.35
327	600	450	5	32	4	R1	250	672	468	24.10	16.32	24.10	2.41
328	600	450	5	32	8	R2	150	953	704	21.20	13.61	21.20	2.12
329	600	450	5	32	8	R2	200	847	704	22.18	13.61	22.18	2.22
330	600	450	5	32	8	R2	250	784	704	22.86	13.61	22.86	2.29
331	600	450	5	32	4	R1	150	1100	607	19.93	14.39	19.93	1.99
332	600	450	5	32	4	R1	200	1029	607	20.45	14.39	20.45	2.04
333	600	450	5	32	4	R1	250	987	607	20.78	14.39	20.78	2.08
334	600	450	5	32	8	R2	150	1267	766	18.99	12.99	18.99	1.90
335	600	450	5	32	8	R2	200	1162	766	19.63	12.99	19.63	1.96
336	600	450	5	32	8	R2	250	1099	766	20.06	12.99	20.06	2.01
337	600	450	5	32	4	R1	150	1415	667	18.09	13.80	18.09	1.81
338	600	450	5	32	4	R1	200	1344	667	18.45	13.80	18.45	1.84
339	600	450	5	32	4	R1	250	1302	667	18.67	13.80	18.67	1.87
340	600	450	5	32	8	R2	150	1582	801	17.43	12.74	17.43	1.74
341	600	450	5	32	8	R2	200	1477	801	17.90	12.74	17.90	1.79
342	600	450	5	32	8	R2	250	1414	801	18.20	12.74	18.20	1.82
343	600	450	6	32	4	R1	150	732	468	23.43	17.05	23.43	2.34
344	600	450	6	32	4	R1	200	662	468	24.36	17.05	24.36	2.44
345	600	450	6	32	4	R1	250	620	468	24.98	17.05	24.98	2.50
346	600	450	6	32	8	R2	150	900	704	21.77	14.20	21.77	2.18
347	600	450	6	32	8	R2	200	795	704	22.84	14.20	22.84	2.28
348	600	450	6	32	8	R2	250	731	704	23.58	14.20	23.58	2.36
349	600	450	6	32	4	R1	150	995	607	20.81	15.02	20.81	2.08
350	600	450	6	32	4	R1	200	924	607	21.41	15.02	21.41	2.14

Note: R1 indicates the arrangement of reinforcement, placed on two opposite faces and R2 indicates the arrangement of reinforcement, distributed equally on all faces

Table A4. 3 Safe scaled distance for the practical columns (cont...)

Column ID	Column Dimensions			Main rebar details			Spacing of lateral ties	Shear strength, V_u	Flexural strength, M_u	SSD distance based on shear	SSD distance based on flexure	SSD	Safe Scaled Distance
	Breadth, b	Depth, D	Length, L	Dia of rebars	No of rebars	Rebars arrangment							
	(mm)	(mm)	(m)	(m)	(m)		(mm)	(kN)	(kN)	(m)	(m)	(m)	(m/kg$^{1/3}$)
351	600	450	6	32	4	R1	250	882	607	21.80	15.02	21.80	2.18
352	600	450	6	32	8	R2	150	1162	766	19.72	13.55	19.72	1.97
353	600	450	6	32	8	R2	200	1057	766	20.46	13.55	20.46	2.05
354	600	450	6	32	8	R2	250	994	766	20.95	13.55	20.95	2.10
355	600	450	6	32	4	R1	150	1257	667	19.02	14.40	19.02	1.90
356	600	450	6	32	4	R1	200	1187	667	19.44	14.40	19.44	1.94
357	600	450	6	32	4	R1	250	1145	667	19.72	14.40	19.72	1.97
358	600	450	6	32	8	R2	150	1425	801	18.23	13.29	18.23	1.82
359	600	450	6	32	8	R2	200	1320	801	18.78	13.29	18.78	1.88
360	600	450	6	32	8	R2	250	1256	801	19.14	13.29	19.14	1.91
361	600	600	3	32	8	R2	150	1757	1033	17.32	10.87	17.32	1.73
362	600	600	3	32	8	R2	200	1616	1033	17.89	10.87	17.89	1.79
363	600	600	3	32	8	R2	250	1532	1033	18.26	10.87	18.26	1.83
364	600	600	3	32	8	R2	150	2587	1178	14.92	10.08	14.92	1.49
365	600	600	3	32	8	R2	200	2446	1178	15.24	10.08	15.24	1.52
366	600	600	3	32	8	R2	250	2362	1178	15.45	10.08	15.45	1.54
367	600	600	3	32	8	R2	150	2587	1246	14.92	9.81	14.92	1.49
368	600	600	3	32	8	R2	200	2446	1246	15.24	9.81	15.24	1.52
369	600	600	3	32	8	R2	250	2362	1246	15.45	9.81	15.45	1.54
370	600	600	4	32	8	R2	150	1524	1033	18.43	11.62	18.43	1.84
371	600	600	4	32	8	R2	200	1383	1033	19.13	11.62	19.13	1.91
372	600	600	4	32	8	R2	250	1299	1033	19.60	11.62	19.60	1.96
373	600	600	4	32	8	R2	150	2223	1178	15.93	10.77	15.93	1.59
374	600	600	4	32	8	R2	200	2083	1178	16.33	10.77	16.33	1.63
375	600	600	4	32	8	R2	250	1999	1178	16.60	10.77	16.60	1.66
376	600	600	4	32	8	R2	150	2587	1246	15.02	10.48	15.02	1.50
377	600	600	4	32	8	R2	200	2446	1246	15.35	10.48	15.35	1.54
378	600	600	4	32	8	R2	250	2362	1246	15.56	10.48	15.56	1.56
379	600	600	5	32	8	R2	150	1384	1033	19.24	12.23	19.24	1.92
380	600	600	5	32	8	R2	200	1243	1033	20.05	12.23	20.05	2.00
381	600	600	5	32	8	R2	250	1159	1033	20.60	12.23	20.60	2.06
382	600	600	5	32	8	R2	150	1943	1178	16.87	11.34	16.87	1.69
383	600	600	5	32	8	R2	200	1803	1178	17.37	11.34	17.37	1.74
384	600	600	5	32	8	R2	250	1719	1178	17.69	11.34	17.69	1.77
385	600	600	5	32	8	R2	150	2503	1246	15.30	11.03	15.30	1.53
386	600	600	5	32	8	R2	200	2363	1246	15.65	11.03	15.65	1.56
387	600	600	5	32	8	R2	250	2279	1246	15.87	11.03	15.87	1.59
388	600	600	6	32	8	R2	150	1290	1033	19.85	12.76	19.85	1.99
389	600	600	6	32	8	R2	200	1150	1033	20.76	12.76	20.76	2.08
390	600	600	6	32	8	R2	250	1066	1033	21.37	12.76	21.37	2.14
391	600	600	6	32	8	R2	150	1757	1178	17.62	11.82	17.62	1.76
392	600	600	6	32	8	R2	200	1616	1178	18.20	11.82	18.20	1.82
393	600	600	6	32	8	R2	250	1532	1178	18.58	11.82	18.58	1.86
394	600	600	6	32	8	R2	150	2223	1246	16.09	11.50	16.09	1.61
395	600	600	6	32	8	R2	200	2083	1246	16.50	11.50	16.50	1.65
396	600	600	6	32	8	R2	250	1999	1246	16.77	11.50	16.77	1.68

Note: R1 indicates the arrangement of reinforcement, placed on two opposite faces and R2 indicates the arrangement of reinforcement, distributed equally on all faces